ECOPHYSIOLOGICAL MODELING OF METABOLIC OXYGEN SUPPLY IN SUPPORT OF GROWTH FOR THE SOUTHERN FLOUNDER *Paralichthys lethostigma*

A Dissertation

by

TODD STEPHEN DART

Submitted to the Office of Graduate and Professional Studies of
Texas A&M University
in partial fulfillment of the requirements for the degree of

DOCTOR OF PHILOSOPHY

Chair of Committee,	William H. Neill
Co-Chair of Committee,	Delbert M. Gatlin III
Committee Members,	Robert R. Vega
	Bradford Wilcox G.
Head of Department,	Cliff Lamb

May 2021

Major Subject: Wildlife and Fisheries Sciences

ABSTRACT

A dynamic growth model for Southern Flounder (SFL) *Paralichthys lethostigma* was developed and evaluated, to promote understanding of this species' ecophysiology in the cause of its improved management. The new model, labeled E.F-RMD, and parameterized specifically for SFL, was based on the Stella® model Ecophys.Fish (E.F); but, E.F-RMD included a more mechanistic representation of tissue oxygen-delivery called the "respiratory model, dynamic" (RMD). The integrated model E.F-RMD uses simulation of cardio-respiratory processes to estimate oxygen availability in support of bioenergetic growth for SFL. A unique feature of E.F-RMD is the inclusion of cutaneous-sourced oxygen supplementation.

The combined model was evaluated by comparing E.F-RMD estimated juvenile SFL growth, expressed as weight-over-time (Wt) and percent weight change per day (%Wtchg/day), to growth data collected by the Texas Parks and Wildlife Department's Coastal Fisheries Division for juvenile SFL raised in cool (17 – 22°C) and warm (20 – 26°C) recirculating systems indoors, and in outdoor ponds. For the indoor growth trials, routine respirometry also was performed, to measure metabolic responses. Published data on SFL growth also were used in E.F-RMD evaluation.

Correlation (R^2) and Consilience (*C*, a provisional measure of holistic goodness-of-fit) analyses compared modeled to observed values for Wt and %Wtchg/day. For Wt, all *C* values were significant ($\alpha = 0.05$). For %Wtchg/day, *C* values varied from

significant to marginally significant. *JointC* values (all datasets considered together) were significant both for Wt and %Wtchg/day.

From these evaluations, the following conclusions were drawn: 1) E.F-RMD can reliably simulate juvenile SFL growth as measured by Wt and %Wtchg/day. 2) Growth results suggest $\dot{M}O_2$ via cutaneous respiration in flounder is significant for juvenile fish, but declines exponentially as the SFL grows. Rather than being a set percentage, cutaneous $\dot{M}O_2$ declines as weight and skin thickness increase with age. 3) Growth comparison to literature data indicates E.F-RMD accommodates well to changes in temperature and O_2, but less so to salinity.

DEDICATION

To my wife Anna Lux, for her love, understanding, lots of patience, and encouragement.

And to Dr. William Neill, for being willing to mentor and teach an old war horse.

ACKNOWLEDGEMENTS

Much gratitude and thanks are owed to my committee chair, Dr. William Neill, and my committee members, Dr. Delbert Gatlin III, Dr. Robert Vega, and Dr. Bradford Wilcox, for their guidance and support throughout the course of this effort and to the Wildlife and Fisheries Department faculty and staff at Texas A&M University for their guidance and support.

My extreme gratitude goes to Herschiel Tuley, Dr. Ivonne Blandon, Paul Cason, and to the graduate students of Dr. Robert Vega at Texas A&M University – Corpus Christi for their support in providing respirometry and pond feed data; without whom this dissertation would not have been possible.

Thanks to the staff of the Marine Development Center, Texas Parks and Wildlife Department, Corpus Christi, TX for their scientific acumen, hard work and dedication in sustaining Texas fisheries.

Finally, thanks to my co-workers and friends for their continuous support and encouragement.

CONTRIBUTORS AND FUNDING SOURCES

Contributors

This work was supported by a dissertation committee consisting of co-chairs Dr. William H. Neill (Professor Emeritus, Texas A&M University) and Dr. Delbert M. Gatlin III (Professor, Department of Ecology and Conservation Biology), and Dr. Bradford Wilcox (Professor, Department of Ecology and Conservation Biology) and Dr. Robert R. Vega (Associate Faculty and former director of the Texas Parks and Wildlife Department's Coastal Fish Hatcheries).

The data analyzed for Chapter VIII were from TPWD's Marine Development Center in Corpus Christi, TX, and were provided by volunteer researcher Mr. Herschiel Tuley, and by Dr. Ivonne Blandon and Dr. Vega. Data on pond studies at Sea Center Texas were provided by Dr. Vega and Mr. Paul Cason. The analyses presented in Chapter VII were conducted by the candidate using spreadsheets developed by himself, Dr. Neill and Dr. Ray H. Kamps of the Department of Science and Mathematics, Texas A&M University – San Antonio.

All other work conducted for the dissertation was completed by the candidate independently.

Funding Sources

There are no outside funding contributions to acknowledge related to the research and compilation of this document. However, the candidate gratefully acknowledges the indirect support provided by Texas Parks and Wildlife Department and by Texas A&M University System.

TABLE OF CONTENTS

Page

LIST OF FIGURES

Page

LIST OF TABLES

Page

CHAPTER I

OVERVIEW

Southern Flounder (SFL; Figure 1) *Paralichthys lethostigma* is an important commercial and sport fish in sub-temperate waters of the western Atlantic Ocean and the Gulf of Mexico. Primarily a euryhaline species of coastal habitats, SFL occurs in the Atlantic from the Carolinas southward to middle-Florida and in the Gulf of Mexico (GoM) from northern Florida, then westward, with greatest abundance along the Louisiana and Texas coasts (Wenner and Archambault 2005, VanderKooy 2015). Mature individuals of SFL are found primarily near shore and in estuaries (Wenner and Archambault 2005), which often places the management of this flatfish species under State control. In Texas, this responsibility rests with Texas Parks and Wildlife Department's Coastal Fisheries Division (TPWD-CF). TPWD-CF is actively engaged in ecosystem-based management of Texas coastal fishes and fisheries. In partnership with the Coastal Conservation Association (CCA) and the American Electric Power company, TPWD-CF operates the CCA Marine Development Center (MDC) in Corpus Christi, Texas. The MDC is one of three TPWD-CF facilities dedicated to marine stock enhancement and associated research, education, and public outreach. SFL is a current focus of TPWD-CF and its marine stock enhancement program because of the apparent decline of SFL in the South Atlantic (Flowers et al. 2019) and GoM (Froeschke et al. 2011) during the past several decades.

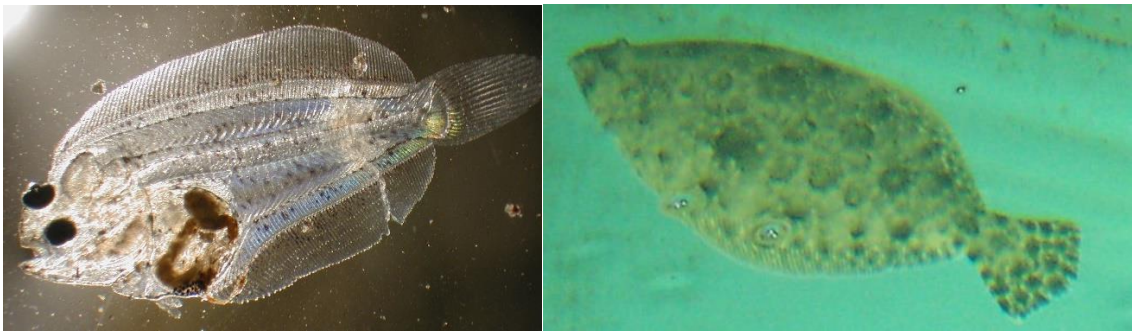

Figure 1. Southern Flounder *Paralichthys lethostigma*.
Left: 38 days post-hatch. Right: Adult. Source: CCA Marine Development Center, Corpus Christi, Texas

An essential part of ecosystem-based fisheries management is bioenergetic modeling, which enables estimation of the size of cultured-fish optimal for release into the wild (Latour et al. 2003) and the estimation of consequent numbers of released fish needed for effective stock enhancement. The Stella® model "Ecophys.Fish" (E.F), developed by Neill et al. (2004), has proven useful for simulating bioenergetics and growth of Red Drum *Sciaenops ocellatus*, which is another euryhaline fish prominent in the efforts of TPWD-CF to enhance stocks of marine fish in Texas waters. E.F was deemed appropriate for adaptation to SFL. However, a recognized deficiency of E.F in its original form, is that it utilizes a strictly-empirical respiratory sub-model for calculating active metabolic rate (AMR), which is the oxycaloric equivalent of maximal rate of oxygen uptake available to support growth, locomotion and other aerobic activities. To afford E.F a more mechanistic basis for estimating maximal oxygen-uptake rate consistent with AMR, development of a Stella®-based dynamic respiratory model was undertaken for simulating maximal rates of oxygen (O_2) uptake specifically for the SFL, with the ultimate objective of integrating the dynamic model into a SFL

version of the E.F model. A mechanism-based dynamic model of SFL cardiac and respiratory processes seemed especially appropriate for SFL, given the prominent role of cutaneous respiration in flatfishes (Kirsch and Nonnotte 1977, Nonnotte and Kirsch 1978, Steffensen et al. 1981, Steffensen and Lomholt 1985).

This dissertation focuses on developing a SFL respiratory model, called the "respiratory model, dynamic" or RMD. The approach starts by providing a natural history of the SFL in Chapter II, followed in Chapter III by introducing physiological ecology and bioenergetics of fishes with particular emphasis on the SFL. The computer-modeling process is a critical aspect of this investigation and is explored in Chapter IV. Special emphasis is given to computer modeling basics and also to the history of bioenergetics models, and simple versus dynamic modeling. Considered are standard model programs used by ecologists with special emphasis on fisheries modeling, and flounder modeling as applicable to E.F. Chapter V provides a more in-depth discussion of the physiological principles that RMD is intended to simulate. Investigation of RMD, including the rationale and analysis of the components that constitute the model, will be the subject of chapter VI. The integration of RMD into a more expansive SFL growth model will be the subject of Chapter VII. Chapter VIII will present the processes and data used to validate RMD as a reliable simulator of maximal O_2 uptake by the modeled SFL via analysis and discussion of a respirometry experiment used to collect data from live flounder, validation of methodology and results. Finally, interpretation and discussion of the modeling results and implications for ecosystem-based management efforts with a SFL focus are presented in Chapter IX.

CHAPTER II

NATURAL HISTORY OF THE SOUTHERN FLOUNDER

Southern Flounder is a euryhaline species that frequents coastal waters of eastern North America and Central America, ranging from the Carolinas down to mid-Florida in the Atlantic (Wenner and Archambault 2005) and around the GoM from middle Florida to northern Mexico (VanderKooy 2015), Figure 2. SFL does not occur within the Florida keys (Froese and Pauly 2016). This geographic separation likely began during the Pleistocene when sea levels were lower due to glaciation and resulted in allopatric sub-speciation as determined by mitochondrial DNA analysis. Thus, it has been proposed that the Atlantic and GoM populations of SFL be classified as taxonomic sub-species. However, small percentages of Atlantic haplotypes have been detected in the GoM population and vice versa (Anderson et al. 2012).

Figure 2. Computer generated distribution map of Southern Flounder.
Reprinted from Aquamaps (Accessed March 25, 2016).

The Southern Flounder Life Cycle

The life cycle of the SFL begins in the late fall or early winter with spawning activities of mature adults, two years of age or older, after they have migrated to offshore waters from estuaries, bays, and even rivers (Wenner and Archambault 2005, VanderKooy 2015). Fertilized SFL eggs are buoyant and hatch into ~2.5-mm larvae in about 48 hours at 21.1° C (Wenner and Archambault 2005). Early larvae are pelagic, growing best in higher salinity water (VanderKooy 2015), and retaining the bilateral eye morphology of their phylogenetic ancestors (Friedman 2008) until they are about 40 days old when metamorphosis begins with the migration of the right eye to what will become the head's upper surface, a process taking approximately 10 days to complete (Reagan and Wingo 1985).

In the winter months of January and February, the now-juvenile flounder, aided by ocean currents (Wenner and Archambault 2005), begin migrating inshore towards estuaries (VanderKooy 2015). Following migration inshore, the young SFL settle in estuaries that optimally are brackish or of low salinity. Upon completion of metamorphosis and adoption of definitive flatfish morphology, SFL juveniles assume a primarily demersal, ambush-predator lifestyle, feeding primarily at night on small crustaceans such as mysids until they approach adulthood when they become piscivorous (Reagan and Wingo 1985, Wenner and Archambault 2005, VanderKooy 2015). SFL remain in estuarine waters, growing until reaching sexual maturity when they may engage in the annual late-fall, seaward migration to spawn and then return to the estuary,

repeating this phase of their life cycle for the remainder of their estimated life span of 4 years for males and 8 years for females (Fischer and Thompson 2004).

Sexual Determination and Dimorphism

Sexual determination in the SFL is a complex process. Genotypic males, based on all observations to date, develop only into phenotypic males; whereas, a genotypic female may develop into a phenotypic female or male, depending upon ambient environmental temperature when the individual is 75 to 120 mm in total length (TL) and has a mass of 3.3 to 11.25 g. (Luckenbach 2005). If the ambient temperature is above or below the temperature interval of 18-28°C during this development stage, genotypic females tend to develop into phenotypic males (Luckenbach 2005). This sexual-determination mechanism is likely an important factor in causing the approximately 6:1 female to male ratio observed in Texas waters (VanderKooy 2015). The evolutionary determinants for this selection process are currently unknown, but a clue may be that females appear to live twice as long as males and can grow to be much larger (Fischer and Thompson 2004). Greater longevity increases the females' temporal fecundity, and a larger body size equates to greater gonadal size and thus greater fecundity as more eggs are produced, both of which increase the viability of the species (Futuyma 1998).

Threats and Conservation

As a target of commercial and sport fishing, SFL became more popular in the 1960s resulting in significant over-fishing of the species in the early1970s (Martine 2008, VanderKooy 2015). In response, federal- and state-legislated restrictions of fishing equipment and catch were initiated, both for commercial and sport fishing.

These management actions led to reduced flounder landings, which placed less stress on GoM flounder populations (VanderKooy 2015). However, as welcome as these changes have been, flounder populations still face two significant anthropogenic pressures—the first being the continuing effects of overharvesting, either from directed fishing or as bycatch (Martine 2008), and the second being the more pervasive consequence of increasing mean global temperatures which decreases egg viability while increasing larval and juvenile predation (Martine 2008). Furthermore, higher temperature affects sex determination within the SFL population, skewing the male to female numbers ratio towards more phenotypic males, thereby affecting the species' overall fecundity (Martine 2008, Ospina-Alvarez and Piferrer 2008).

Exacerbating threats to recruitment within, and survival of, SFL populations has increased the need to supplement the wild population with hatchery-reared juveniles (VanderKooy 2015). Concurrently, this has increased the need for increased knowledge of SFL autecology and consequent computer-modeling to facilitate management of SFL stocks.

CHAPTER III

PHYSIOLOGICAL ECOLOGY OF THE SOUTHERN FLOUNDER

According to F. E. J. Fry, the study of animal function within its environment can be grouped under just three mechanistic headings; "what it can do, how it works, and what makes it go." Fry associated these headings with the biological disciplines of autecology, physiology, and biochemistry (Fry 1971); all three disciplines are encompassed, for the most part, within physiological ecology (PE). It was Fry's seminal paper, "Effects of the Environment on Animal Activity," (Fry 1947), that has helped guide research in PE, especially that of fishes.

While there is a growing body of data and literature on the PE of the SFL, prominent gaps exist. Therefore, to comprehensively consider the PE of the SFL, these gaps must be filled by casting a broader net to include data from other species within the order Pleuronectiformes, i.e., other flounder species, such as plaice, sole, turbot, and halibut (Friedman 2008), as appropriate. My analysis will consider environmental factors outlined by F.E.J. Fry as they apply to the context of metabolic scope (MS), in conjunction with the phenotypic adaptations associated with SFL existence as a generally solitary, euryhaline, and demersal predator (Wenner and Archambault 2005, VanderKooy 2015).

Energy, Environmental, and Evolution

Jorgensen (1983) observed that the study of energy dynamics, i.e., bioenergetics, within the organism, is important for understanding the union of physiology with

ecology. This view reflects Fry's concept of activity as the "manifestations of the energy that is released by metabolism" (Fry 1947); activity, in Fry's view, includes not only locomotion and other aspects of "rapid" movement typical of animals, but also non-overtly-mechanical energy expenditures such as those for growth and excretion which are characteristic of all living organisms. Fry further clarified the distinction between metabolism and activity by categorizing the components of metabolism, emphasizing metabolic scope (MS) and, erecting a complementary "physiological classification of environment." This ecophysiological structure has had a significant impact on the field of fisheries ecology (Kerr 1990). These autecology concepts about Pleuronectiformes need to be delved into in more detail.

Metabolic Scope

Fry's paradigms of metabolism vs. activity, and his physiological classification of environment, provide a cognitive structure for relating the chaotic external environment and the ordered internal one of the organism. Although Fry's ideas can and have been applied to homeotherms, especially concerning altitude-induced hypoxia (Hochachka 1985), the greater application has been found in the study of poikilotherm autecology, particularly about the concept of MS in relation to the limiting effects of environmental O_2 on metabolic rate (Boddington 1978, Chabot et al. 2016, Claireaux and Chabot 2016). This application has been due in no small part to the strength of the conceptual framework of MS and environmental-factor classification perfected over many decades. Applying Fry's paradigm to the MS of various fish species (Neill et al. 1994, Neill et al. 2004, Fonseca et al. 2010) has proven beneficial, and shall be used

herein as the basis for an analysis of the PE of flounders in general and the SFL in particular.

The effects of environmental factors on MS form the basis of Fry's theory (Kerr 1990, Neill et al. 1994, Del Toro-Silva et al. 2008, Claireaux and Chabot 2016). The basic concept underlying MS is shown in Figure 3, related to metabolic-rate components to O_2 concentration. Still, MS can also be represented in relation to other factors such as temperature. Measures analogous to MS also can be developed for responses beyond metabolism per se, such as animal and population growth and community development (Neill et al. 1994). Nonetheless, metabolic rate as a function of environmental O_2 availability is the key relationship on which my work has focused. In this regard, the standard metabolic rate (SMR) is the amount of O_2 consumed to produce adenosine triphosphate (ATP) for the maintenance of an organism's basic physiological processes (Claireaux and Chabot 2016). That is, SMR is the minimum amount of O_2 needed to keep the resting organism alive and to sustain the basal physiological performance of the whole organism, for a key tenant of Fry's paradigm is that an organism needs to be considered in its totality as the emergent property of all lower organizational levels (Claireaux and Chabot 2016). While SMR represents the basal metabolism necessary for sustaining life, organisms seldom operate at this minimum level. They typically sustain metabolic rates commensurate with maintaining routine locomotion and other activities (i.e., RMR).

As metabolic rate increases, physical and physiological constraints such as limitations in chemical reaction rates and availability of substrates (e.g., O_2 or food) for

obtaining free energy and resources, and the inherent inefficiency of these reactions due to heat loss imposed by the second law of thermodynamics (Haynie 2001), set a theoretical maximum metabolic rate (MMR). As a result, an active animal's achievable metabolic rate will be restricted when available environmental O_2 concentrations decline (Figure 3).

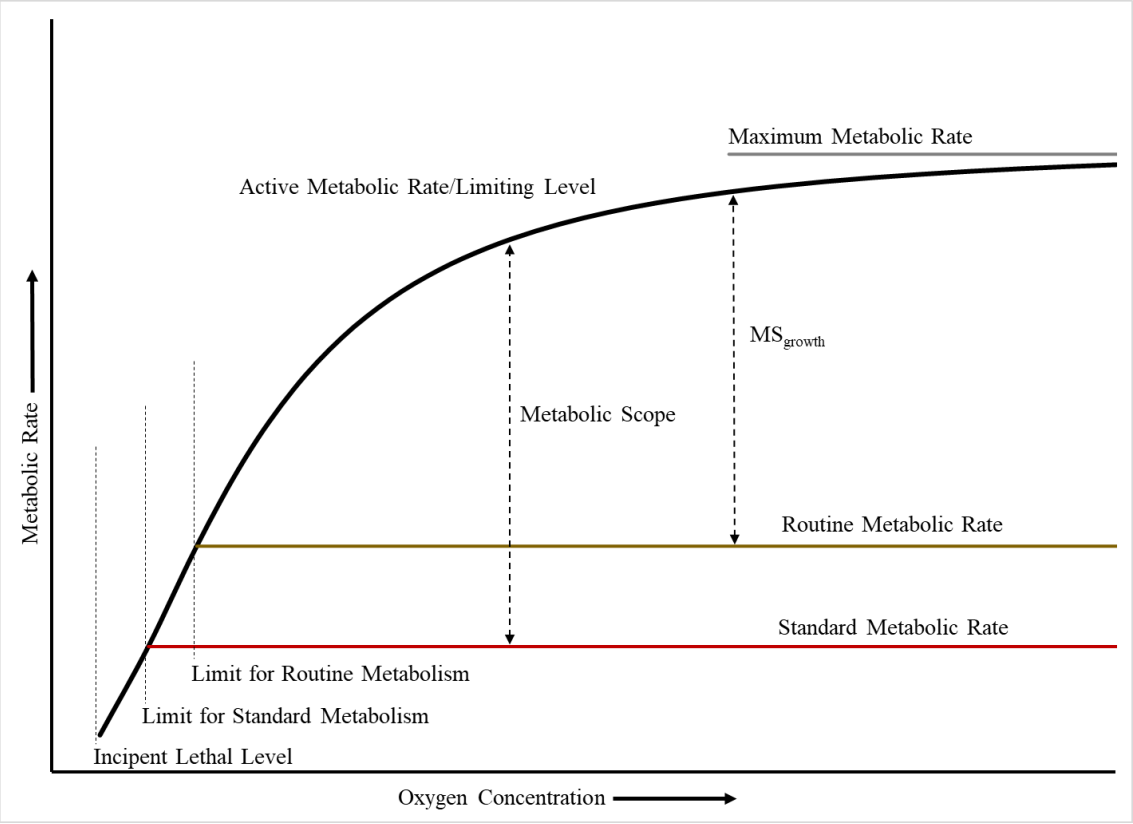

Figure 3. Idealized representation of active, routine, and standard metabolic rates in relation to oxygen concentration.
Metabolic scope is defined as the value difference between standard and active rates, with metabolic scope for growth (MS_{growth}) being the energy difference between routine and active rates as the energy available for growth as described by Fry (1947) and Neill et al. (1994).

Whereas the active metabolic rate (AMR) places an upper and somewhat variable ceiling on metabolic rate, the SMR represents a minimum below which energy flow through the organism is insufficient to maintain homeostatic conditions for long-term survival.

Metabolic scope thus represents the potential dynamic energy range, given existing environmental conditions and physiological-maintenance demands, available to an organism to support its engagement in other activities such as swimming, growth, and reproduction (Boddington 1978, Neill et al. 1994, Neill et al. 2004, Claireaux and Lefrancois 2007, Fonseca et al. 2010, Claireaux and Chabot 2016, Farrell 2016). In practice, MS_{growth} provides a useful measure for evaluating the MS of individual organisms or their populations by analyzing environmental effects on growth rate over time (Neill et al. 2004, Del Toro-Silva et al. 2008, Fonseca et al. 2010). Identities of these environmental factors and how they impact MS are central to Fry's classification of the environment.

Environmental Factors

Ecologists before F.E.J. Fry recognized the effects of the environment on an organism's performance, but Fry's categorization of the environment into classes of factors by their impacts on metabolism was an important paradigm shift (Claireaux and Chabot 2016). In his 1947 paper, Fry identified these factors as lethal, masking, directive, controlling, limiting, and accessory. Over the years, he refined his concepts by clarifying those environmental factors making up each class, and dropping the "accessory" class, leaving the five-factor classes remaining in use today (Fry 1947,

1971, Claireaux and Chabot 2016). These five-factor classes are characterized and discussed below. Examples will be provided for Pleuronectiformes as a group, with more detail for SFL in cases where specific factor-effects have been studied.

Lethal Factors

Lethal factors, such as toxic substances, can "…destroy the integration of the organism." (Fry 1971). Lethal factors have two components: The first is the *incipient lethal level* "beyond which the organism can no longer live for an indefinite period of time." The second component is the *effective time* "… required to bring about a lethal effect at a given level…" of the environmental factor once past the incipient lethal level. These interacting components are often encapsulated by LD_{50}, the median (50%) lethal dose of a particular factor (Fry 1971). Essentially any environmental factor or combination of factors that can lead to unrecoverable disruption of the organism's biochemical and physiological integrity may be considered lethal, with common examples being extreme temperature (Fry 1947, 1971, Neill et al. 1994) and toxins (Fry 1971). Other authors, expanding on Fry's original examples, have added low O_2 (e.g., anoxia) to the lethal category (Claireaux and Chabot 2016).

Organisms are capable of some physiologic adaption called "acclimation," a phenomenon that Fry addressed concerning fish that demonstrate different lethal-temperature limits depending on the temperature at which the fish previously had been maintained (Fry 1971). Consequently, a fish's upper incipient-lethal temperature limit will be lower for a low-temperature acclimated fish than for one acclimated to a higher temperature, as shown in Figure 4.

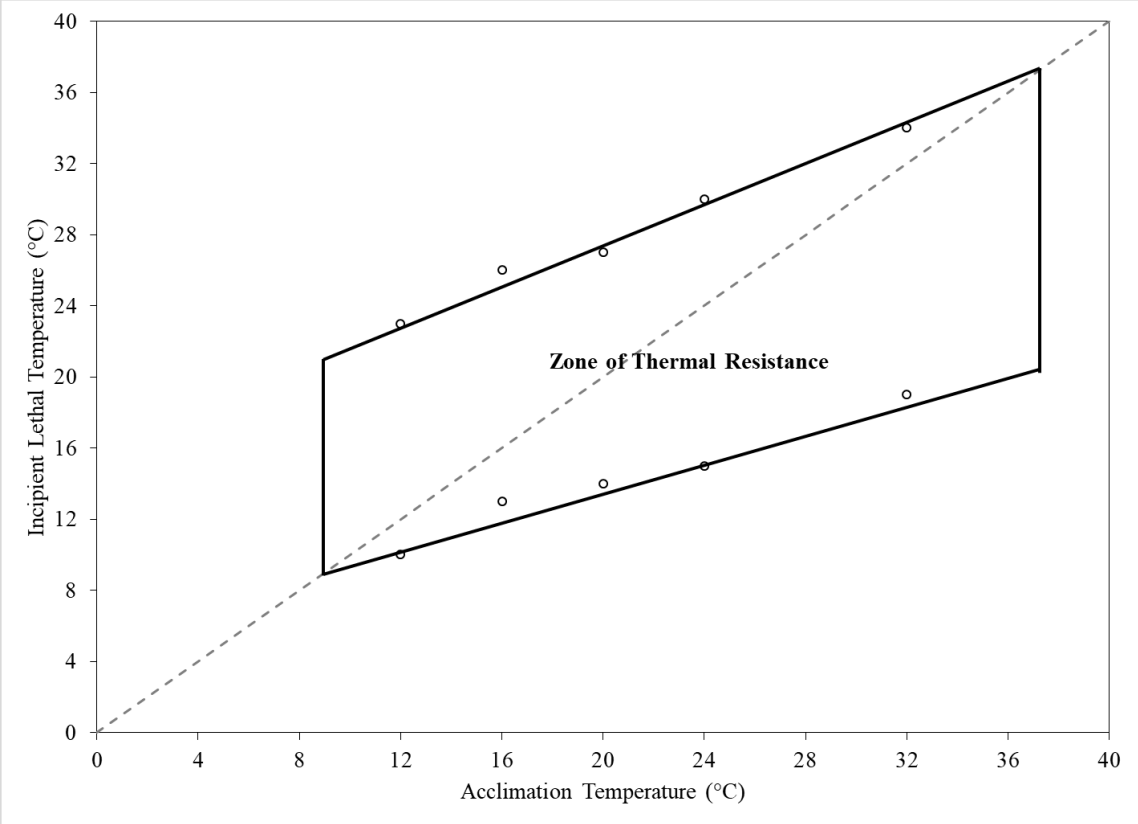

Figure 4. Representational thermal tolerance diagram.
Adapted from data on Pufferfish *Spheroides maculatus*, presented by Fry (1971).

Lethal factors also include predation and dissolved gases (Neill et al. 1994). The literature on lethal effects of toxins, particularly the effects of crude oil on SFL is available (Miller 1987, Park et al. 2013, Brown-Peterson et al. 2015, Bayha et al. 2017). While relevant, a thorough analysis would result in a departure from the intended objective concerning more ordinary environmental factors pertinent to SFL growth modeling. Therefore, focus here will be restricted to salinity, temperature and DO.

Of the three factors under discussion, lethal salinity is least documented. Mature individuals of euryhaline species can acclimate to a wide range of salinities, based on

studies by Daniels et al. (1996), SFL do not tolerate low salinity levels during larval development. The survival of SFL larvae is greater than 50 % at salinities above 20 parts per thousand (ppt). Below 20 ppt, survival appears to decline, falling to 29 % at 10 ppt with total mortality at 0 ppt, consistent with other findings that physiological adaption to lower salinities by SFL occurs only in post-larval stages (VanderKooy 2015).

Lethal Factors in Plueronectiformes

A literature review of thermal limits within the Plueronectiformes can be somewhat conflicted as the criteria for "lethal" may vary by source or simply not be well defined. Furthermore, limits may shift over the lifespan of the species. Nonetheless, literature exists on the lethal limits of temperature, and oxygen for Plueronectiformes. References have been consolidated within the table found in Appendix A.

In many of the studies cited, a thermal maximum is specified, but the values are not necessarily the incipient upper-lethal limit; some are simply the point at which the organism exhibits or begins exhibiting a negative behavioral response, such as kinetic avoidance (Deubler and Posner 1963). Minimum temperature limits are less well documented, but of those available, the lower limits given are reported specifically as lower-lethal limits.

For references in which acclimation temperatures are given, the tolerance limits are graphically represented by species in Figure 5. Fortunately, thermal limits for SFL are better represented, particularly with respect to maximal temperature limits derived from juvenile SFL data by van Maaren et al. (2000). Upper temperature limits for other

species of flatfishes are reported for Winter Flounder *Pseudopleuronectes americanus* (Grimes et al. 1989), Deep Flounder *Pseudorhombus elevates* and Ovate Sole *Solea ovata* (Menasveta 1981), and Summer Flounder *Paralichthys dentatus* (Stierhoff et al. 2006), while lower limits are available for SFL (Prentice 1989) and Winter Flounder (Grimes et al. 1989).

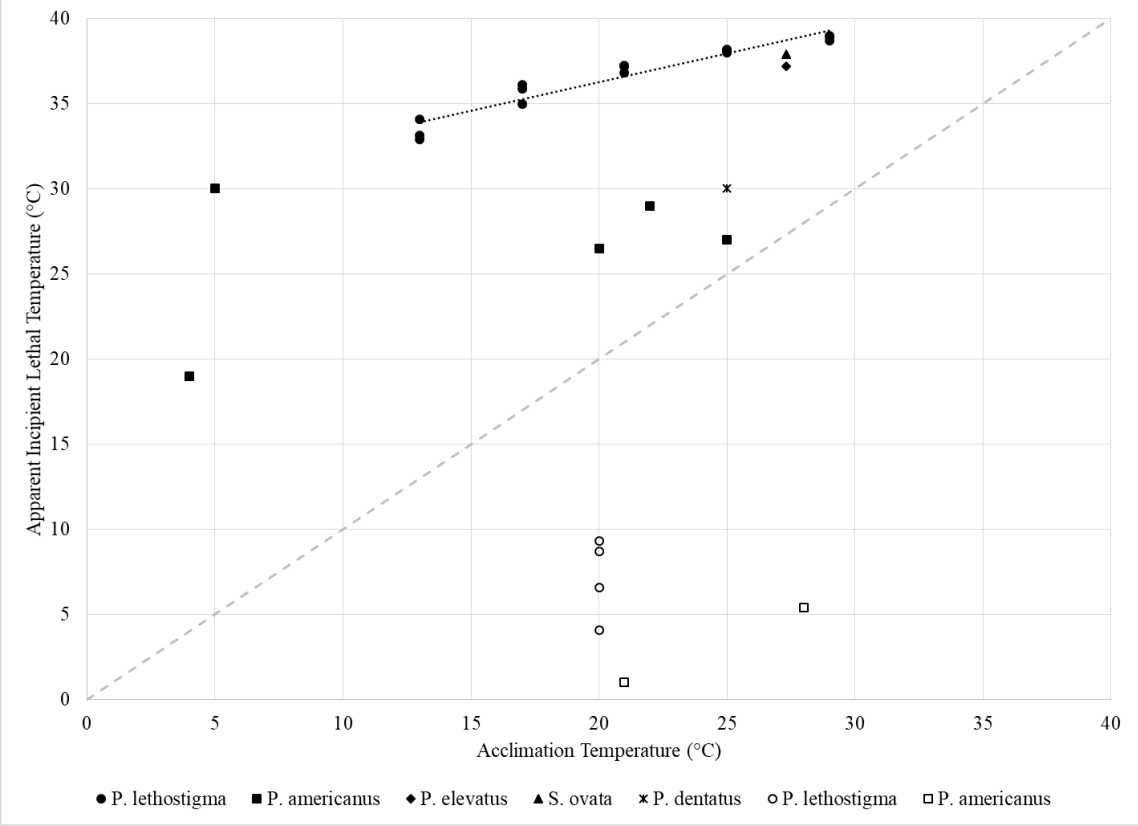

Figure 5. Thermal tolerance limits.
Data for five species of flatfishes. The trend-line is for SFL data only. Upper thermal limits, solid markers; lower thermal limits, open markers. Data obtained from literature sources listed in Appendix A. See text for the full discussion.

With respect to upper temperature limits, there is an observable difference in the upper lethal (or near lethal) temperatures for Winter and Summer Flounders, which are found in cooler waters of more northerly latitudes (Grimes et al. 1989). The data suggest that the upper lethal limit for Winter and Summer Flounders is near 30°C; whereas, SFL and other more southerly distributed species appear to have an upper temperature limit near 39°C for individuals acclimated to temperatures above 25°C.

Malloy and Targett (1991) do not provide an acclimation temperature (thus, their data are not presented in Figure 5) but indicate the lower temperature limit for the Summer Flounder to be approximately 3°C, well below the lower-limit range of 4.1 up to 9.3°C for SFL acclimated to 20°C as reported by Prentice (1989). Field observations by Moore (1976) of fish mortality in the bays, estuaries, and channels of Port Aransas, TX following an overnight freeze in February 1973, provide some support for these lower temperature limits in flounder. Among the individuals of 35 fish species reported by Moore (1976) as victims of the freeze, two Gulf Flounder *Paralichthys albiguttata* were found moribund in channel waters at 7°C where average winter temperatures range between 13 to 14°C. Thus, it is not unreasonable to presume that the lower temperature limit of SFL falls between 5 and 10°C, depending upon acclimation temperature.

Returning to the issue of upper lethal-temperature levels for SFL, the effects of acclimation are demonstrated by the SFL trend-line in Figure 5, indicating that SFL exhibits a decline in the upper thermal tolerance limit with a decline in acclimation temperature. Using data from van Maaren et al. (2000), the difference between the

upper lethal limit and acclimation temperatures (i.e., $T_{UL} - T_{accl}$) are plotted (see Figure 6) against the measured acclimation temperatures.

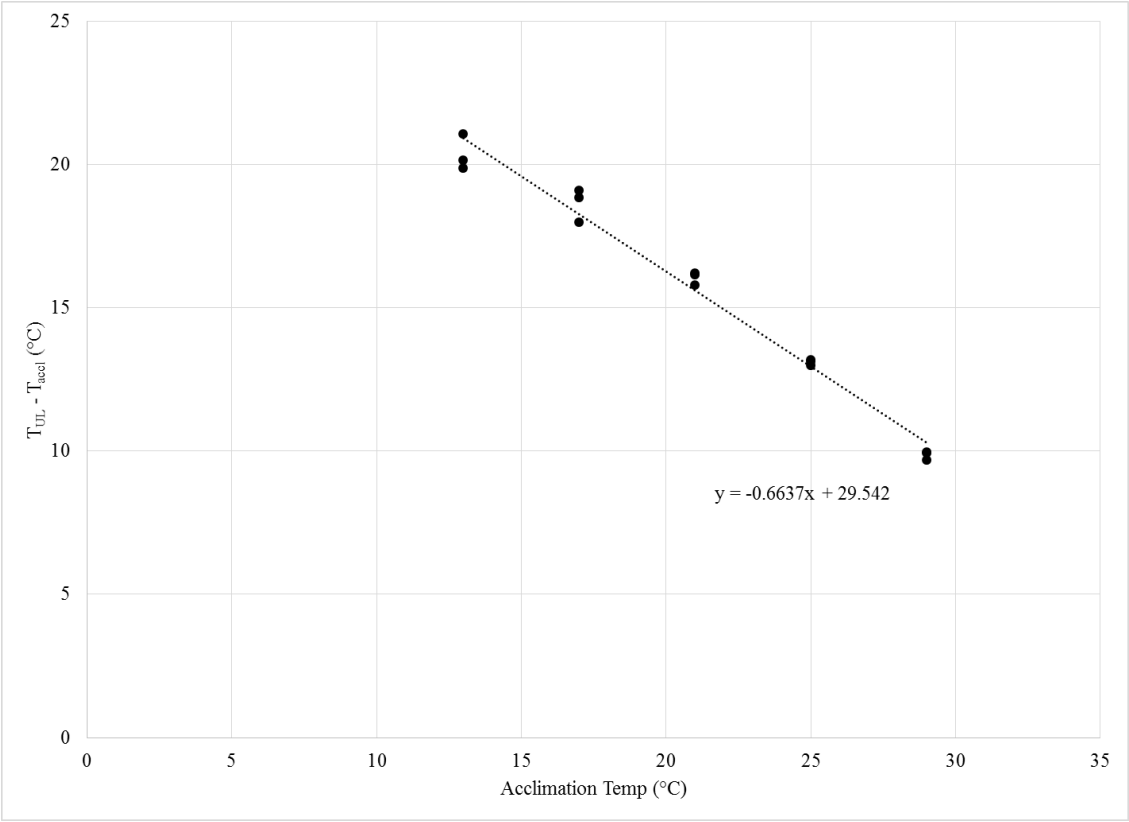

Figure 6. Trend in SFL upper temperature limit and acclimation temperature difference relative to acclimation temperature.

Based on this figure, the following linear trend-line may be derived:

$$T_{UL-accl} = -0.664 \times T_{accl} + 29.542 \quad (1)$$

The resultant slope indicates that the difference between the upper lethal temperature and acclimation temperature declines at a rate of approximately 0.7°C for

every 1°C increase in acclimation temperature until linearity begins to fail as Tul converges with Taccl.

Because metabolic rate is tied to temperature in poikilotherms, in many fish an increase in ambient temperature places a greater demand on the respiratory and cardiovascular systems to supply O_2, via blood, to more active tissues. As cardiac output ($\dot{Q}$)[1] demands increase, the heart muscle requires additional O_2. Eventually, these demands exceed the heart's capacity to acquire sufficient O_2 to perform the work, thus $\dot{Q}$ reaches its maximum, then abruptly declines (Eddy and Handy 2012). This limit has been observed in flounder (Mendonca and Gamperl 2010). Based on van Maaren et al. (2000) data, the T_{UL} for juvenile SFL acclimated to 29°C is approximately 39°C. Although van Maaren et al. (2000) do not provide any $\dot{Q}$ data, they show that SFL O_2 consumption begins to plateau at 39°C suggesting that this temperature may represent the maximum thermal limit.

Unlike temperature, which has upper and lower boundaries, the same is not practically valid concerning dissolved oxygen (DO) limits. While O_2 is toxic to fish as it is with mammals at very high concentrations (D'Aoust 1969), the levels necessary for O_2 toxicity are not naturally encountered; on the contrary, given low solubility of O_2 in water, low DO (hypoxia) or no DO (anoxia) are almost daily concerns for many fish,

[1] $\dot{Q}$ is defined as heart rate (HR, beats per minute) multiplied by stroke volume (SV, mL of blood expelled per heartbeat). See Chapter V for more discussion.

including SFL (Steffensen et al. 1982, Tallqvist et al. 1999, Stierhoff et al. 2006, Ishibashi et al. 2007, Mandic et al. 2009, Davidson et al. 2016).

Flounder appear moderately well adapted to hypoxia, with a lower DO limit typically below 2 mg O_2/L water as shown in the DO Lower Limit column of the table in Appendix A.

In a study by Deubler and Posner (1963), post-larval SFL were acclimated to various temperatures, then exposed to increasingly hypoxic water, then observed to determine when 100% avoidance kinesis occurred. They reported that at an acclimation temperature of 6.1°C, SFL withdrawal was complete after 23 minutes at a DO of 1.09 mg/L. For the 14.4°C acclimated group, withdrawal was complete after 13 minutes when DO reached 0.68 mg/L, while at an acclimation temperature of 25.3°C, it took 7 minutes for complete withdrawal at a DO of 1.03 mg/L. The observation of reduced time-to-avoidance with increased ambient temperature is consistent with increased metabolic rate, which has also been shown to negatively influence survival time for poikilotherms under hypoxic conditions (Nilsson 2010).

Kinetic avoidance provides a useful mechanism to determine when DO becomes sufficient to trigger adaptive neurophysiological feedback mechanisms. That hypoxia-induced kinesis occurs is also indicative of a species lack of capacity to withstand anoxia. In anoxia-tolerant species such as the crucian Carp *Carassius carassius,* and freshwater turtles of the genera *Trachemys* and *Chrysemys*, brain activity is suppressed by the release of the inhibitory neurotransmitter gamma aminobutyric acid (GABA) which decreases behavioral response and, via inaction, metabolic rate (Vornanen et al.

2009, Nilsson 2010). The Common Sole, while being relatively hypoxia tolerant, does not appear to be anoxia tolerant as Dalla Via et al. (1997) report that the Sole exhibits signs of panic, characterized by burst swimming upward into the water column, as DO falls below 5% air saturation at 20°C. SFL, while hypoxia tolerant, enter the zone of respiratory dependence as DO nears 1.1 mg/L (Deubler and Posner (1963). However, avoidance is not the same as reaching the limiting oxygen concentration (LOC) which is the point at which oxygen concentration ($[O_2]$) begins to limit either standard (LOCs) or routine (LOCr) metabolic rates, but should SMR be limited by DO then that condition is ultimately lethal (Neill et al. 1994, Neill et al. 2004).

Further evidence for a tolerance of hypoxia, but not anoxia, within flounder species is provided by Poupa (1991) and Ostadal (2014), who compared the capacity of strips of cardiac muscle excised from various species to maintain contractility over time after the tissue was made anoxic by cyanide inhibition of aerobic ATP production (Figure 7). In Ostadal's report of Johansen's analysis, each cardiac muscle strip's initial contractility following mounting to a force meter was set, and the decay in tension over time measured as a percentage decline from baseline at 12°C. The rate of contractile decay across time varied between species, with Hagfish and *Varanus* (monitor lizards) cardiac tissue possessing a dramatic anoxic capacity. For flounder, a decline to 50% of the initial measured force required approximately 40 minutes, indicating that while flounders are not as anoxia resistant as the Hagfish, they appear to have a greater anoxia-coping capacity than Cod. Contrast this to human cardiac tissue at 24°C, which has a 50% reduction in contractility in only a few minutes.

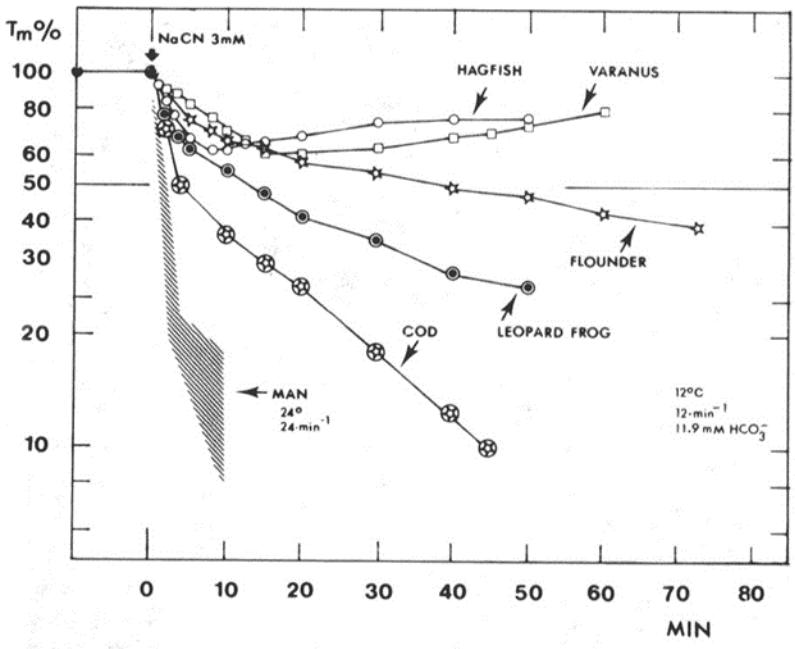

Figure 7. Anoxia tolerance of cardiac muscle in vertebrates.
Percent decline from maximal muscle tension (T_m %) over time in muscle with cyanide-inhibited (NaCN at 3 mM) mitochondrial ATP production. Reprinted with permission from Poupa (1991).

Controlling Factors

As defined by Fry (1971), controlling factors are those "which govern the metabolic rate by their influence on the state of molecular activation of the components of the metabolic chain." Here Fry's primary consideration was the importance of temperature with respect to maximum and minimum metabolic rates (Fry 1971). In essence, then, Fry's controlling factor is the reaction kinetics of metabolic molecules with respect to temperature (Haynie 2001), which can be expressed graphically using an Arrhenius plot, a representative example is shown in Figure 8 below.

In Figure 8, two hypothetical metabolic pathways (A and B) are presumed to occur in, and influence, a hypothetical organism as a whole. The slope of metabolic pathway B indicates this pathway has a lower activation energy requirement than pathway A. Each pathway's maximum metabolic rate is likely to become initially limited by thermodynamic regulation of molecular activity, availability of substrates, and activation energies (Haynie 2001). The eukaryotic cell's ultimate upper temperature limitations are due to the thermal denaturing of cellular proteins and membranes (Tansey and Brock 1972). The minimum metabolic rate is when the metabolic process is simply too slow to "keep the organism in being" (Fry 1971). For example, the Deubler and Posner (1963) data, in which the latency of low-DO avoidance in SFL decreased as temperature increased, is consistent with the role of temperature as a controlling factor of metabolic rate (Fry 1947, 1958, 1971).

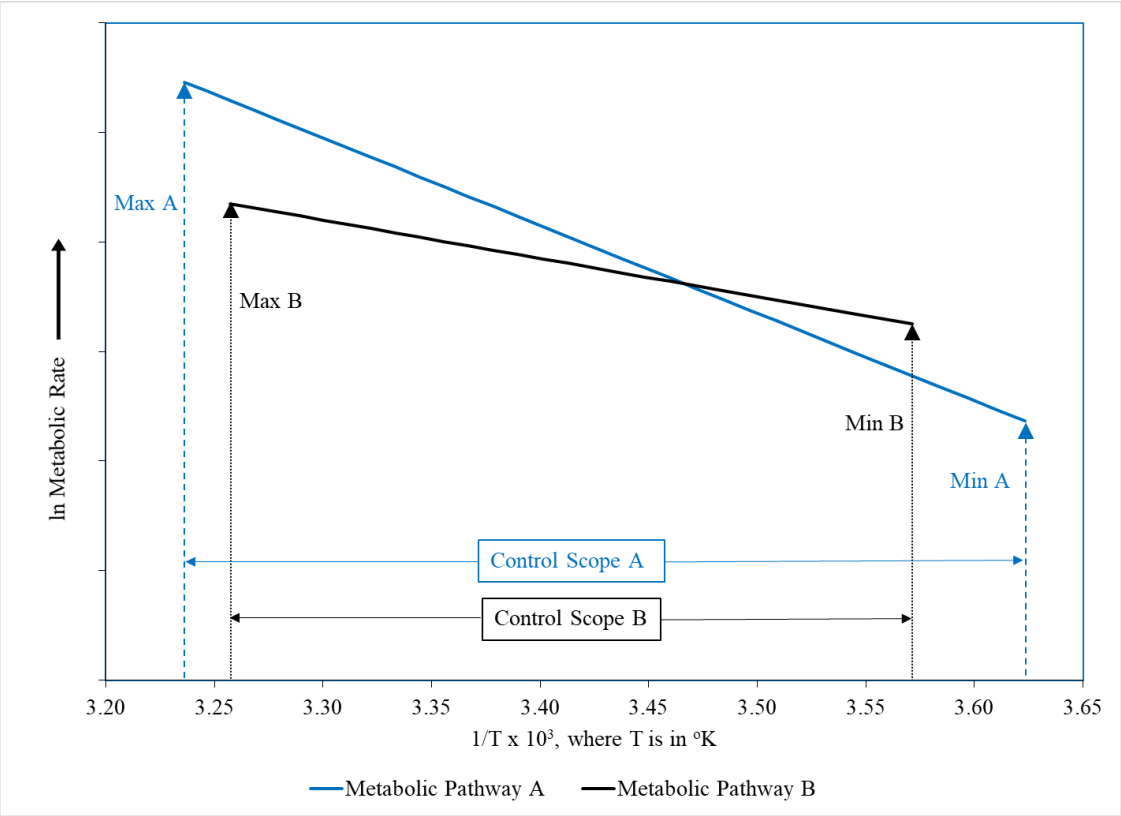

Figure 8. Representational Arrhenius plot.
Inverse temperature (Kelvin) effects on ln of metabolic rate indicators (e.g., O_2 consumption rate or growth rate). See text for description.

Controlling Factors in Plueronectiformes

The controlling effect of temperature on metabolic rate in SFL also can be shown using an Arrhenius plot. Using SFL SMR O_2 mass flow rate ($\dot{M}O_2$)[2], weight and

[2] When O_2 consumption, or flow, is measured as a change in mass per unit of time, e.g., milligrams O_2 per hour, the abbreviation $\dot{M}O_2$ is appropriate. When measured as a change in volume, e.g., milliliters O_2 per hour, the abbreviation $\dot{V}O_2$ is preferable. In practice, however, $\dot{V}O_2$ is often used interchangeably with $\dot{M}O_2$ (the reverse being less common, but still valid). $\dot{V}O_2$ and $\dot{M}O_2$ are used interchangeably herein for consistency with referenced work.

temperature data collected by Mr. Herschiel Tuley at the Texas Parks and Wildlife, CCA Marine Development Center (MDC), Flour Bluff, TX (unpublished data), an Arrhenius plot was produced (Figure 9) demonstrating the effects of temperature on metabolic rate in SFL ranging from 0.42 g to 70 g. Data in Figure 9 are mean values obtained from 45 SFL. Despite the variance in the measured $\dot{M}O_2$ and the relatively narrow temperature range of the available data (low 16.4°C, high 26.6°C, median 21.1°C) the trend in the data indicates the Arrhenius effect of temperature on routine metabolism of juvenile SFL.

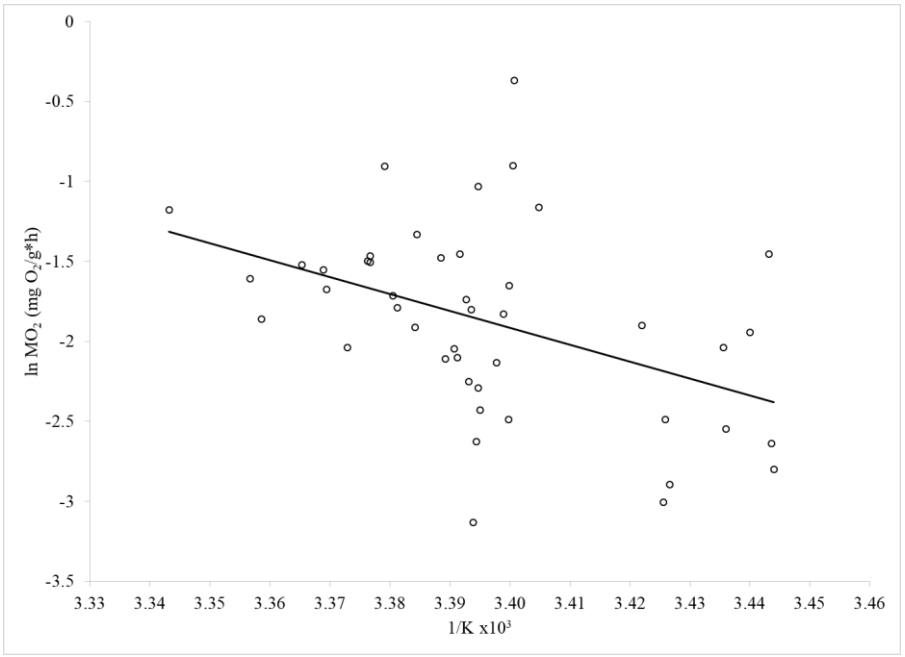

Figure 9. Arrhenius plot of mean $\dot{M}O_2$ for SFL.
Measured at the Texas Parks and Wildlife Department, Marine Development Center, Corpus Christi, TX. Data unpublished. Weight range 0.42 g to 70 g. See text for discussion.

The Arrhenius plot also clearly indicates variance in $\dot{M}O_2$ measurements at any given temperature. Such variance results from difference in SFL mass, routine activity, and measurement error (Figure 10). Measurement error may also be due to the comparatively small sample size, instrument noise, or higher routine-activity level in some of the SFL measured.

Smaller fish have a greater per gram $\dot{M}O_2$ than larger fish, following the ¾-power rule developed by Kleiber (1932), and subsequently attributed to differences in the turnover rate of chemical energy, which is inversely related to mass (Kleiber 1975, Schmidt-Nielsen 1984, McNab 2002). This greater $\dot{M}O_2$ per gram demand of tissue is hypothesized to be met in lower-mass SFL by the contribution of cutaneous-sourced O_2 which is a known contributor to overall $\dot{M}O_2$ in many aquatic and semi-aquatic species (Steffensen et al. 1981, Meredith et al. 1982, Feder and Burggren 1985 Nov 1, Rombough 1998, Glover et al. 2013) but which declines in flounder as they grow, due to decline in the surface-area to mass ratio, and their dermis thickens (Burton et al. 1984, Burton and Burton 1989, Zhu et al. 2005). Recent thinking (West et al. 2000) suggests that the ¾ rule relates to the evolution of energy efficient, three-dimensional fractal material transport networks; building on the concept of maximized energy efficiency as an evolutionary adaptation dating back to at least Lotka (1922). If so, then supplemental cutaneous $\dot{M}O_2$ in SFL and other fish may be an evolutionary adaptation to meet metabolic demand or O_2 distribution. The alternate argument that supplemental cutaneous $\dot{M}O_2$ may simply permit a higher resting metabolic rate cannot be fully discounted in SFL. However, metabolic rate does not appear to increase in other fish

exposed to hyperoxia (Dejours et al. 1977, Berschick et al. 1987), suggesting that once metabolic $\dot{M}O_2$ demands are met, additional O_2 supplementation has no effect.

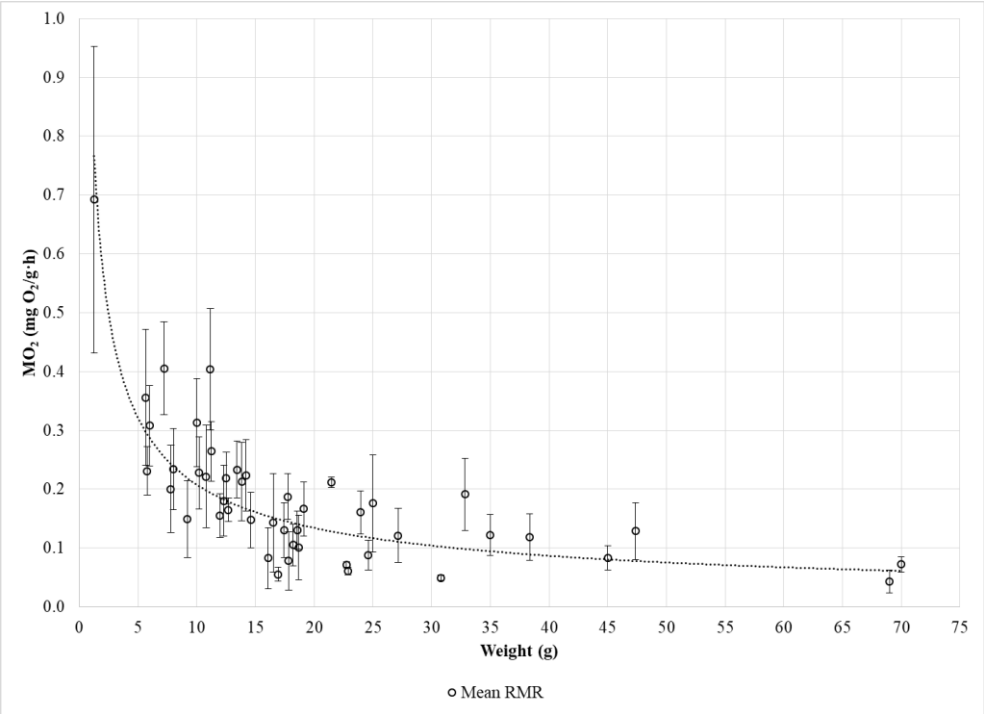

Figure 10. Southern Flounder mean $\dot{M}O_2$ (mg O_2/g fish·h) ± SD compared to weight (g).
Data unpublished, collected at the Marine Development Center, Flour Bluff, TX, by Mr. Herschiel Tuley. Averages are for SFL with ≥ 3 $\dot{M}O_2$ measures. Fit curve for $\dot{M}O_2 = 0.88 \cdot Wt^{-0.63}$, $R^2 = 0.58$.

Some general conclusions can be drawn from the MDC data regarding temperature effects on SFL metabolism, the primary example being the temperature quotient (Q_{10}) as defined in equation (2)

$$Q_{10} = (M_2/M_1)^{10/(T_2 - T_1)} \quad (2)$$

where M_1 and M_2 are the $\dot{M}O_2$ (mg O_2/g fish·h) values for reference temperatures T_1 and T_2 (°C or K).

The Q_{10} value for the MDC data set can be estimated using the trend-line formula, calculated using Excel, from the Figure 9 Arrhenius plot:

$$\ln \dot{M}O_2 = -10.556 \times \frac{1}{K} 10^3 + 33.974 \quad (3)$$

Using the maximum (T_2 = 26.6°C) and minimum (T_1 = 16.4°C) temperature values, and applying appropriate conversions, respective $\dot{M}O_2$ values of 0.29 mg O_2/g fish·h and 0.08 mg O_2/g fish·h were calculated. Applying these values to equation (2), the estimated Q_{10} for the MDC SFL may be produced:

$$Q_{10} = (0.29/0.08)^{10/(26.59 - 16.37)} = 3.5 \quad (4)$$

This value is substantially higher than independent SFL respirometry-based Q_{10} values reported by van Maaren et al. (2000), who listed Q_{10} values over several temperature ranges: 1.29 between 25°C and 29°C, 2.37 between 13°C and 17°C, 2.5 between 17°C and 21°C, and 2.68 between 21°C and 25°C. The discrepancies between van Maaren et al. (2000) and MDC SFL Q_{10} values may be due to differences in the mass of fish measured as the van Maaren et al. (2000) fish were more limited in size range at 5.5 g ± 1.9 g. Also, the van Maaren et al. (2000) respirometry measurements were conducted using ten fish to give a population mean mass-specific $\dot{M}O_2$; whereas, the MDC results are based on respirometry results from individual fish.

Limiting Factors

A limiting factor constrains metabolic reactions through the direct or indirect limitation of resources such as oxygen or substrates from feed. Another frequently

neglected aspect of maximum rate limitation is the rate at which metabolite removal occurs (Fry 1971). In Fry's view, the primary limiting factors are shortages of those materials essential for metabolism to occur—materials such as food for nutrients and nourishment, water, and O_2, as well as the removal of the end products of metabolism such as metabolites (e.g., nitrogenous wastes) and carbon dioxide (Fry 1971). While all are important, the most critical moment-to-moment limiting factor to which Fry drew primary attention is the acquisition and utilization of O_2 (Fry 1947, 1971, Neill et al. 1994, Claireaux and Chabot 2016).

Limiting Factors in Plueronectiformes

Availability of oxygen and energy-yielding substrates from food places limits on metabolic rate (Fry 1971, Yamashita et al. 2001) and within the literature the limiting effects of oxygen concentration, and its interaction with the controlling effects of temperature and fish size on flounder metabolism, are well established (Duthie 1982, van Maaren et al. 2000, Joaquim et al. 2004, Del Toro-Silva et al. 2008, Mendonca and Gamperl 2010, Capossela et al. 2012). When these factors co-vary, their interaction becomes complex, e.g., the joint influence of temperature and DO on flounder respiration rate, as measured by opercular movement (Watters and Smith 1973, Capossela et al. 2012). The effects of temperature and DO on respiration rate are, respectively, positive and negative. With increased body temperature, a corresponding increase in the organism's metabolism will increase O_2 demand until the maximum metabolic rate is reached (see Figure 3), which is the functional integral of the organism's combined chemical kinetic rates (Fry 1971). This will have a behavioral

influence as the fish's buccal-pumping rate rises to increase water flow over the gills ($\dot{V}_w$) to meet the higher metabolic demand. In addition, $\dot{V}_w$ exponentially increases with *decreased* DO, until physiological and/or physical capacity limits are reached, as the fish attempts to move oxygenated water more quickly through the gills, the combined effect of which is the reduction in overall efficiency of O_2 extraction from the water and increased metabolic work. When low DO is combined with increased temperature, the net effect is a greater increase in $\dot{V}_w$ than would be expected from low DO alone. Even when DO levels are at physiologically normal levels, the $\dot{V}_w$ at 30°C will be uniformly higher than at 22°C (Capossela et al. 2012).

The effects of temperature on heart rate (HR) and swimming speed in flounder are also well established, with HR increasing commensurate with temperature (Joaquim et al. 2004, Mendonca and Gamperl 2010). Interestingly, the cardiac stroke volume (i.e., the amount of blood pumped by the heart per beat) in flounder appears to be only marginally influenced by temperature (Joaquim et al. 2004, Mendonca and Gamperl 2010) and swimming speed (Joaquim et al. 2004). Thus, in flounder, $\dot{Q}$ appears primarily responsive to HR, which contrasts with the relation typical for other fish in which $\dot{Q}$ is mainly increased by an increase in stroke volume (Satchell 1991). The literature-based data on the effects of temperature and DO on $\dot{V}_w$, which impacts oxygen extraction efficiency (Capossela et al. 2012), and temperature on $\dot{Q}$ are critical components of metabolic rate and of the Southern Flounder respiratory model.

The limiting effects of DO are mostly realized upon reaching the limiting oxygen concentration (LOC) for routine metabolism (LOCr); i.e., the DO level at which RMR

becomes dependent on DO. The LOCr thus represents the DO level at which routine metabolic rate is no longer sustainable, causing the fish to curtail its activities (e.g., swimming, food processing) or seek better oxygenated or/and cooler waters (Neill et al. 1994). As DO declines further still, even SMR no longer can be sustained by aerobic means; the DO at which this occurs has been termed the critical oxygen concentration (or tension). At sustained DO values below that critical for standard metabolism, the organism must die or rely on anaerobic mechanisms.

For the low-DO-tolerant SFL, the LOCr should be correspondingly low. To evaluate this hypothesis, LOCr for SFL was estimated from data collected during previously-mentioned respirometry experiments. Analysis of the data set revealed a mean LOCr of 2.01 ± 0.74 mg O_2/L water. Deubler and Posner (1963) estimated the lethal DO limit was about 1.1 mg O_2/L water in the SFL, suggesting that once LOCr is reached, the lethal limit for minimal metabolism lies only about 1 mg O_2/L water lower.

Along with low DO, Fry (1971) also considered the limiting effects of high carbon dioxide (CO_2), which through enzymatically-facilitated reaction with water is converted into carbonic acid (H_2CO_3). Carbonic acid will further dissociate to bicarbonate ion (HCO_3^-) and hydrogen ion (H^+), affecting the acid-base balance in the tissues by lowering pH (Cameron 1989), which can affect swimming speed due to its impact on muscle physiology (Fry 1971). Furthermore, changes in pH, either up or down, can also limit or control hemoglobin O_2 affinity (Weber and de Wilde 1975).

While pH can act as a limiting factor (Fry 1971), the acid-base balance system is subject to temperature control (Cameron 1989). Furthermore, in fish the process of CO_2

re-formation, that is the catalysis of HCO_3^- and H^+ within erythrocytes by carbonic anhydrase to form water and CO_2 for elimination from the organism, may itself be limited by the availability of chloride ions (Cl^-) within the erythrocyte as this ion appears to be necessary for active transport of HCO_3^- across the erythrocyte membrane (Perry 1986), exemplifying how access to nutrients and metabolites necessary for osmoregulation can also affect metabolism.

The effect of pH on flounder does not appear to be notably different from that in other fishes. However, there is evidence that Starry Flounder *Platichthys stellatus* can separate and delay the impact of metabolic acidosis from respiratory acidosis by several hours following exhaustive exercise (Wood et al. 1977).

Masking Factors

Homeostatic maintenance of an organism's internal milieu requires acquisition and utilization of resources and expenditure of energy (Eddy and Handy 2012), with the amount, or channeling, of energy available to the organism having consequent effects on available metabolic scope. A masking factor is an additional environmental factor that modifies the expenditure of energy for a particular physiological operation (Fry 1971). This definition of a masking factor differs from Fry's original concept (Fry 1947), wherein masking factors were described as having an inhibitory effect on a "second identity" such that it would not operate normally if the masking factor were present. This is likely due to the realization by Fry that masking effects on energy exchange within a system can be either positive or negative, as demonstrated by the two examples provided in his 1971 paper.

In his first example, water salinity changes the metabolic energy required to maintain homeostatic ion levels within the tissues. Therefore, as water salinity increases so may the amount of energy expended for ion excretion, although the fish's internal environment with respect to ion concentrations will remain relatively constant; consequently, the animal's overall metabolic scope is reduced (Fry 1971).

In his second example, Fry discusses the anatomical *retia mirabilia* countercurrent heat exchanger in tuna and lamnid sharks. The *retia mirabilia* is a vascular structure within or associated with the red muscle that evolved to resist heat loss by allowing heat from the blood, leaving the muscles to warm the blood returning from the gills which are close to thermal equilibrium with the environment. This structure enables the muscle to be maintained at a higher than ambient temperature without much added metabolic cost. This may incur an indirect metabolic cost as the warmer muscle tissue will respond to the increase in temperature by maintaining a higher metabolic rate (Fry 1971).

Masking factors typically induce an obligatory load on metabolism necessary for maintaining physiological homeostasis (Neill et al. 1994), which includes ion-osmoregulation and thermal control (Fry 1971, Neill et al. 1994). However, masking effects may also include metabolic work done to resist pathological consequences of certain pollutants and parasites (Neill et al. 1994, Neill et al. 2004). While pollutants and parasites are important ecological considerations, discussion of masking factors within Pleuronectiformes will focus on the physiological masking involved in thermal control and ion-osmoregulation.

Masking Factors in Plueronectiformes

Any masking effect of thermoregulation in Pleuronectiformes are unlikely to significantly impact, given that flatfishes, like the majority of fish species, are ectothermic (Eddy and Handy 2012). Intriguingly, the overall average resting metabolic rate of flatfishes appears to be relatively low, as evidenced in a review of the average resting metabolic rates of six taxonomic fish orders (Gadiformes, Pleuronectiformes, Salmoniformes, Perciformes, Anguilliformes, and Cypriniformes). Clarke and Johnston (1999) reported that the Cypriniformes (Carps, Minnows) and Anguilliformes (Eels) had the lowest rates. However, the Pleuronectiformes did have greater metabolic-rate variability than the other taxonomic orders, although this is potentially due to better environmental adaptations rather than physiological variance (Clarke and Johnston 1999).

For euryhaline Pleuronectiformes species, ion-osmoregulation represents a continuous but variable metabolic load, depending upon the ion and osmotic gradients between the external and internal environment (Evans et al. 2005, Soengas et al. 2007, Tseng and Hwang 2008). For example, in the SFL, the metabolic impact of ion-osmoregulation is greatest when juvenile SFL make the transition from high-salinity seawater (SW) to low-salinity freshwater (FW), and vice-versa when sexually mature SFL travel to the open ocean to spawn. Tipsmark et al. (2008) performed an extensive investigation of juvenile SFL responses to salinity shifts. Their analysis found that SFL undergo a "crisis-then-regulation" response of up to 4 days following the shift from FW to SW and vice versa. During this transition, they found immunoreactive changes within

gill cells which "increased plasma cortisol and protein expression of Na^+, K^+-ATPase and Na^+, K^+, $2Cl^-$ cotransporter in the primary gill filament." Also reported were changes to insulin-like growth factors, claudin protein synthesis (responsible for forming tight junctions between gill epithelial cells), and messenger RNA changes. Changes in cell gene expression and protein synthesis cause an increase in cellular metabolism, impacting the resting metabolic rate. From this information, it may be inferred that SFL need adequate time (> 4 days) to acclimate to environmental salinity shifts. Once adaptation has taken place, however, the effects of different salinities appear to have impacts that are statistically significant, but with minimal practical impact on SFL temperature tolerance (van Maaren et al. 2000). Salinity has been shown to affect growth rate on SFL, with a salinity of approximately 5 ppt being optimal (Yamashita et al. 2001).

Directive Factors

Any perceived gradient factor which influences metabolic response, to include behavioral responses, were considered directive factors by Fry (1947). In later years, Fry would clarify sensory perception as a transductive response, i.e., any environmental condition which is either directly sensed via sensory organs (e.g., eyes and ears) or non-sensorial means, such as light effects on hormone levels, can direct the organism's physiology or behavior (Fry 1971). Other environmental factors that may be included as directive are temperature (Fry 1947, 1971), toxins (Fry 1971), and O_2 concentration (Neill et al. 1994).

With respect to fish, directive behavioral selection due to thermokinesis, i.e., movement of a fish to a preferred temperature within the habitat, is an important consideration in the study of fish metabolism as acclimation temperature can affect a fish's temperature preference (Fry 1971). In a test environment offering the fish a temperature gradient, selection for the preferred temperature likely will affect the measured metabolic rate (Fry 1958).

Directive Factor in Plueronectiformes

Transductive responses to shifts in environmental conditions are the hallmark of directive factors (Fry 1971). For demersal SFL living in coastal estuaries and streams, the ability to move in response to unfavorable environmental conditions may be more limited. This may explain why SFL and other flatfish have broader temperature and DO tolerances than other fishes. Deubler and Posner (1963) used DO and temperature as directive factors to assess tolerance limits by studying the withdrawal behavior of post-larval SFL acclimated to various temperatures in response to DO. Their study showed post-larval SFL acclimated to 6.1°C, 14.4°C, and 25.3°C were able to tolerate average DO levels ranging as low as 1.09, 0.68, and 1.03 mL O_2/L water, respectively; avoidance behavior was initiated in some SFL once DO fell below 3.7 mL O_2/L water. The primary difference between the three temperature-treatment groups was the respective average time-to-escape durations of 23 min, 13 min, and 7 min. As temperature directly influences metabolic rate, it is not surprising that hypoxia and thermal directive factors are tied to the fish's $\dot{V}O_2$ and environmental temperature, which is the conceptual basis behind the Q_{10} ratio shown in equation (2).

Other potential directive factors for SFL may include salinity and light levels (Yamashita et al. 2001) and toxic contaminants (Brown-Peterson et al. 2015).

Swimming for most flatfish is energetically expensive due to their negative buoyancy (Joaquim et al. 2004). Thus, many flatfish species, when faced with a directive-factor stressor, appear to engage in a "burst-avoid-recover" strategy by engaging in anaerobic fueled maximal swim effort followed by a period of rest to recover from lactic acid build-up (Wood et al. 1977, Duthie 1982). This strategy reduces acute demand on immediate aerobic MS by spreading the aerobic metabolic work of recovery over time. This allows the fish to place the lowest demand on MS at any given moment. Concerning avoidance behavior, this may drive two potential strategies. The first being a high tolerance to stressors such as low DO, and the second to avoid parts of the habitat where sudden environmental change may be likely. Support for the former idea can be gleaned from the aforementioned low-DO tolerance capacity of flatfish like the SFL (Deubler and Posner 1963), but there is also evidence that some flatfish species like the juvenile Summer Flounder have developed a more heightened avoidance response to low DO which may cause them to avoid habitats prone to diel hypoxia (Brady and Targett 2010).

Preferred temperatures in flatfish vary by species and geographic location (Casterlin and Reynolds 1982, Scott 1982) but appear quite broad. Within Winter Flounder, the preferred temperature range is 8 to 27°C, with a mean preference for waters at about 18.7°C (Casterlin and Reynolds 1982). No clear temperature preference appears to have been established in SFL, although Reagan and Wingo (1985) report SFL

have been collected in waters with temperatures ranging from 5 to 35°C. This range agrees with McDonald et al. (2016), who reported a lower temperature limit in juvenile and adult SFL down to 4°C. As reported by van Maaren et al. (2000), the upper lethal temperature limit ranged from 33 to 39°C for the 13 and 29°C-acclimated SFL groups, respectively.

Evolutionary Considerations

Metabolic scope and environmental factors logically had a role in Pleuronectiformes' evolutionary adaptation to a euryhaline existence. Current evidence suggests Pleuronectiformes began evolutionary adaption to the demersal niche of estuarine habitats during the Eocene epoch (Friedman 2008). These adaptations introduced new environmental-factor relationships with potential impacts upon MS. These include: 1) an increase in osmoregulatory metabolic load (a masking factor) from changes in salinity (Soengas et al. 2007, Tseng and Hwang 2008); 2) higher metabolic demand while swimming compared with non-demersal fish (Joaquim et al. 2004), parallel with adaption to a more sedentary, ambush-predator lifestyle (Wenner and Archambault 2005) and atrophy of the air bladder causing negative buoyancy (Hughes 1963); 3) physiological and morphological adaptations to the greater fluctuation in DO found in estuaries (Stevens et al. 2006, Mandic et al. 2009).

If, as Lotka (1922) postulates, environmental adaptation is the evolutionary consequence of selection for the most energy-efficient metabolic pathways, then the SMR of extant SFL is the lowest possible (or achievable) for survival in coastal habitats for this species. While Lotka's hypothesis is difficult to quantify without a means of

comparing the metabolic rates of extant to extinct Plueronectiformes, it does raise the possibility that the MS of extant Plueronectiformes provides the greatest energy potential for maintaining homeostasis in coastal environments when exposed to lethal, controlling, limiting, masking and directive factors. How Pleuronectiformes and SFL respond physiologically to these factors is of prime importance, given the need to model these physiological responses to predict the amount of available energy needed for growth.

Summary

In his work categorizing and qualifying the environmental factors that impact metabolism and metabolic scope within an organism, F.E.J. Fry established an ecological paradigm to assess the organism's interaction with its environment. The concept of metabolic scope allows an organism's autecology to be considered, then systematized relative to those factors that regulate (control), load (mask), restrict (limit), kill (lethally interdict) or guide (direct) the organism's metabolic responses as well as its distributional responses to heterogeneity of environment within its habitat (Fry 1947, 1971, Neill et al. 1994). Of the many factors with which any poikilotherm must contend, temperature and DO are exceptionally influential—temperature, because it influences metabolic rate through its thermodynamic effects on cellular reaction rates, and oxygen because it catalyzes the energy-yielding reactions necessary for powering metabolic work.

Fry's conceptual model can be transformed into a computer simulation model that permits quantitative representation and prediction of an organism's physiological and behavioral responses to environmental conditions, as represented in Figure 11.

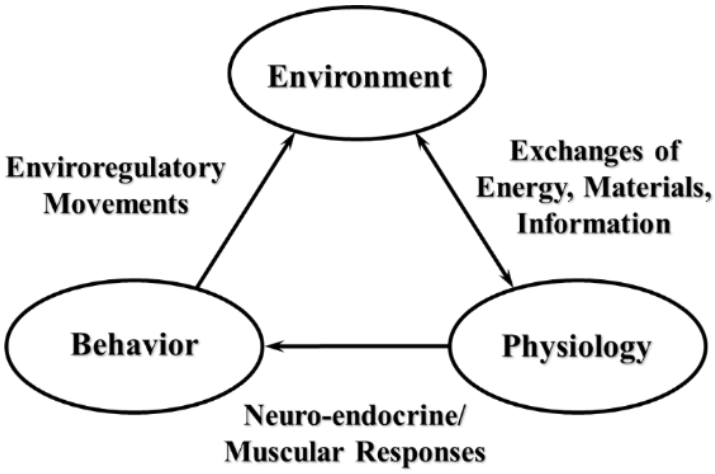

Figure 11. Interrelationship of environment, physiology, and behavior.
Reprinted with permission from Dr. William H. Neill.

CHAPTER IV

ECOPHYSIOLOGICAL MODELING

All models are wrong, but some are useful – Box (1979)

Introduction to Dynamic Systems Models

Mathematical modeling is characterized by Van den Berg (2011) as "…a description of an experimentally delineated phenomenon by means of mathematics, with the view to capturing the salient aspects of the phenomenon at hand." If done correctly, biological models can provide new insights, from biological systems to populations, unattainable through standard experimentation due to cost, size of the experiment, or ethical concerns. However, done improperly, the results can range from conspicuously wrong, to the potentially more damaging situation wherein output appears reasonable but is incorrect and misleading. Attempts to avoid such errors have led to the optimization of modeling procedures. Only by following best practices can we hope to achieve a model that best represents the system being modeled.

As the study of biology and ecology has progressed, so has the need become greater to model the interlocking components that make up complex systems. A system may, for this discussion, be broadly defined as a conceptualization of a component of a larger "organized whole" whether that be an organism or an ecosystem (Grant et al. 1997, Van den Berg 2011). Graphic representation of a simple system is shown in Figure 12, wherein input *X* impacts the state of the system *Y* with output *Z*. How these

components interrelate determines whether the system is a "static," "comparative static," or "dynamic" system (Hannon and Ruth 1997, Van den Berg 2011). If each variable is considered as a function of time, *t*, and *Y(t)* is set to a steady-state function, then *Z(t)* will be determined by the function *X(t)*, that is Z*(t)* is the output to *X(t)*. If *t* is set to a specific point in time (e.g., $t = 1$), the system would be considered static, but if *t* changes then the system will change over time and become comparative static (Hannon and Ruth 1997) such that *Z* will have a specific value relative to *X* at any given *t*. If *Y(t)* is not steady-state, then *X(t)* will influence but not directly determine *Z(t)*, thus making the system dynamic (Hannon and Ruth 1997, Van den Berg 2011). Unlike the static model, *Z* will not necessarily have the same value for *X* at any given *t* because *Y(t)* introduces a dynamic component into the system (Van den Berg 2011).

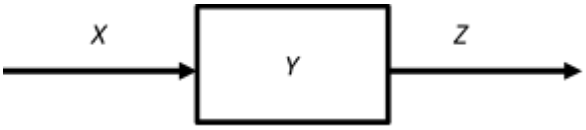

Figure 12. Simple dynamic system.
Based on Van den Berg (2011).

Alternatively, a model's design may be statistically or mechanistically based (Enberg et al. 2008). Statistically based models are generally, but not necessarily, characteristically static or static comparative, while mechanistically based models aim to simulate the multiple processes that influence an organism's anabolic and catabolic metabolism, and trend towards being dynamic models. Models described by Enberg et

al. (2008) as statistical are those of von Bertalannfy and Roff, with mechanistic examples given as the Fish Bioenergetics model developed at the University of Wisconsin-Madison, the dynamic energy budget (DEB) of Kooijman, and Ecophys.Fish.

Static and statistical modeling has provided useful information and insight into ecology and physiological ecology (PE), particularly for organismal growth and metabolic scaling predictions (von Bertalanffy 1950, McNab 2002, West and Brown 2005, Enberg et al. 2008, Kerkhoff 2012, McNab 2012). Dynamic and mechanistic models make the system more responsive to changes in conditions as would be encountered in nature, increase model fidelity, but introduce the need to manipulate and manage more variables and interactions. Before the introduction of computers, this was a daunting task; therefore, it is not surprising that application of systems modeling had to wait until after the development of the electronic computer for systems modeling to gain a footing in research (Grant et al. 1997).

Though computers in the 1960s permitted the processing of ever more complex ecological models (Grant et al. 1997), their scarcity limited the availability of systems modeling to only a few researchers. Perhaps one of the most significant technological contributions to the benchtop researcher has been the development of personal computers and dynamic systems modeling software. Non-dynamic systems modeling programs and options are currently available, such as direct programming using computer languages (C, JAVA, basic, etc.) or programs designed for general research such a Matlab® or Dynamo (Ford 1999) and statistical models like R (Bolker 2008). Moreover, software innovation has now provided researchers the ability to model the

dynamic system itself, using a graphic interface in which system processes and flows are represented using icons similar to those shown in Figure 12. The advantage of this design is that no prior programming experience is necessary, making modeling more accessible to those without programming experience, although the researcher must still provide the mathematical rules and relationships defining and relating model components. Several programs use this modeling methodology, including Stella®, Vensim®, Powersim® (Ford 1999), and MATLAB Simulink (Mangourova et al. 2011).

Regardless of the software used to model a dynamic system, it is important to lay the groundwork for the types of models and what constitutes a successful model. This will be accomplished by analyzing the components of modeling theory, which outline the models conceptual framework upon which the specific components are overlaid. The discussion will then lead to an introduction of static and dynamic metabolic growth models as the development of Respiratory Model, Dynamic (RMD) is ultimately intended to be integrated into such a model. The discussion of dynamic growth models will include an introduction to Ecophys.Fish (Neill et al. 2004), an isee Systems, Stella® dynamic systems modeling program originally developed for use with Red Drum but has also been adapted to use with two sole species *S. solea*[3] and *S. senegalensis* (Fonseca et al. 2010). In discussion of the Ecophys.Fish growth model, the Stella® modeling

[3] *Solea solea* has multiple common English names as reported by Tous et al. (2015): Black Sole, Common Sole, Dover Sole, Parkgate Sole, River Sole, Sea Partridge, Slip, Southport Sole, Tounge, and True Soul. The common name chosen for use in this dissertation is "Common Sole."

"system platform" also will be addressed as this is also the modeling system used to develop RMD. The discussion will then culminate in a review of static SFL growth prediction models from the literature.

From the growth model discussion, the emphasis shift to discussion of static and dynamic $\dot{V}O_2$ modeling in fisheries research and the need to develop such a model for the SFL.

Modeling Theory and Application

Concurrent with the rise in dynamic systems modeling as a technical enterprise was developing a modeling process, i.e., the steps necessary for developing and applying a successful model. Unfortunately, no consistent approach to modeling theory seems to have evolved; so, each text written on modeling methodology comes with a differing set of approaches (Grant et al. 1997, Hannon and Ruth 1997, Ford 1999, Caswell 2001, Bolker 2008, Van den Berg 2011). These methods are not necessarily detrimental as different model objectives might necessitate different approaches. In general, though, most modeling processes contain these basic principles:

1) Identify, decide, and define the problem (i.e., what needs to be modeled).
2) Decide on the type of model to use.
3) Identify the flow, variables, and other processes needed to emulate the problem.
4) Develop, build, and program the model.
5) Evaluate the model in relation to real-world data and conditions.

6) Once satisfied, the model provides a reasonable approximation of the processes it is designed to emulate, use the model to predict environmental or experimental outcomes based on known or hypothetical conditions.

These six steps will serve as the framework for discussing the modeling process used to develop and validate RMD for general utility and as an intended input component for a SFL-oriented version of the E.F growth model. Therefore, it is prudent to review the development of growth models, particularly for fish, and SFL in particular.

Fish Growth and Bioenergetics Models

Since the first scientific discourse on the limits of biological growth by Galileo (1638), the concept of growth, i.e., the relative change in mass of the individual organism over time, has garnered interest among naturalists and biologists. Indeed, the cursory consideration permitted here on the history of growth studies is predestined to present a narrow perspective and omit some rich history of this topic. Nonetheless, a few names do come forward within the literature with sufficient frequency to merit inclusion. While early work by Thompson (1942) had discussed growth using statistical models based on data gathered for humans, it was the theory of growth by Ludwig von Bertalanffy (von Bertalanffy 1934, 1938) that was to have the greatest influence on ecology (Enberg et al. 2008). Basing his work on the insights first put forward by Putter (1920), von Bertalanffy, publishing in German and English, was initially influenced by studies on the rate of chemical reactions. Eventually, von Bertalanffy concluded that growth resulted from a balance between the catabolism of body mass and anabolism of surface, through which an organism assimilates resources (von Bertalanffy 1950,

Kerkhoff 2012). Von Bertalanffy's work resulted in two general growth models designed to emulate the observed growth rate of organisms, one for estimating length and the other for mass. These have been used extensively by biologists and ecologists within fisheries. Both models implement logarithmic (negative exponential) growth. Von Bertalanffy presented the general length-model shown in equation (5).

$$l = L_\infty - (L_\infty - l_0)e^{-kt} \quad (5)$$

where L_∞ is the final length for time t tending to infinity (i.e., asymptotic mean length),[4] l_0, is the length at time (t) = 0, and e is the natural-log base.

The value of L_∞ may alternatively be thought of as the maximum possible length of the organism, and the transformation rate k as a declining growth rate constant (Enberg et al. 2008). Von Bertalanffy's consideration of the basic components that go into L_∞ and *k* distinguish his model because these two variables are rate limiters to growth. Although not explicitly stated, the amount of energy available not only is a consideration of material available for anabolism but also the energy used during catabolism, a concept explored in detail by Fry's concept of MS (Fry 1947, 1971) and Neill and Bryan's MS_{growth} (Neill and Bryan 1991).

If the initial length of the organism is considered to be zero, then the equation (5) can be re-written, per Enberg et al. (2008), as

[4] This is the net result kept simple for clarity. In his paper von Bertalanffy (1938) defines L_∞ = E/k, where E is the amount of introduced reacting material and k is the rate of transformation of substance *a* (e.g., food and nutrients) into *b* (e.g., body tissue).

$$l = L_{\infty}\left(1 - e^{-k(t-t_0)}\right) \quad (6)$$

where L_{∞} is again the asymptotic mean length of the fish if it grew forever, k is a curvature parameter, and t_0 is the "mathematical age" of the fish at which length (l) is theoretically zero.

Conversion of von Bertalanffy's equation to growth estimates by weight requires including an anabolism constant (a) and an age-length relation exponent (b) as mass increases the number of dimensions that must be considered. Equation (7) shows the von Bertalanffy formula for weight as described by Enberg et al. (2008)

$$W = aW_{\infty}\left(1 - e^{-k(t-t_0)}\right)^{b} \quad (7)$$

The von Bertalanffy model has proven useful for growth estimates, although the exponent values a and b originally used by von Bertalanffy have since been shown to be inappropriate (Enberg et al. 2008). Another criticism of the model is its assumption that all catabolism and anabolism are used for growth and maintenance (Enberg et al. 2008). This assessment has given rise to bioenergetic growth models such as that by Roff (1983) who split energy and resource expenditure between somatic and gonadal tissue, mathematically expressed in equation (8) (Roff et al. 2006). An important component of the Roff model is the "gonadosomatic index" (GSI) which is the gonad mass to somatic mass ratio. The GSI was an attempt to tie in the metabolic cost of reproduction to the overall MS, assuming that the remainder would be available for growth (Roff et al. 2006).

$$W_{t+1} = f(W_t) - g(GW_t) \quad (8)$$

where, W_{t+1} represents one reproductive cycle with the function $f(W_t)$ being the rate of growth between t and $t+1$. The function $g(GW_t)$ represents the amount of somatic biomass allocated to the gonads over the same period (Roff et al. 2006).

Though the Roff (1983) model, when expanded to address the growth functions, is more complicated than the von Bertalannfy model, it nonetheless remains a static model that makes several assumptions about somatic and gonadal growth rates and assumes some allometric relationships that may not be correct in all circumstances (Enberg et al. 2008).

As models became more complex, so did the basic metabolic theories with respect to energy allocation. An example is the Dynamic Energy Budget (DEB) developed by Kooijman (2010), which takes as a basic premise that all organisms consist of energy in the form of structural body mass and reserves, the latter of which is used for somatic work (e.g., digestion, maintaining homeostasis), building new structures (i.e., growth), reproduction, etc. (Kooijman 2010). While the DEB model can be applied using a wide array of software, of note is the effort by van der Veer et al. (2001) who applied the DEB theory using Stella® to model growth in four flatfish species, Plaice, European Flounder *Platichthys flesus*, Dab *Limanda limanda*, and Common Sole.

The shift from comparative static to dynamic systems like DEB has become more common, and dynamic modeling software like Stella® has greatly expanded the ability to better resolve bioenergetic demands for fish growth such as cost of ingestion, digestion, egestion, activity, reproduction, and growth (Enberg et al. 2008).

The E.F Stella® model by Neill et al. (2004) is another good example of a dynamic growth model that applies Fry's growth and metabolism theories. Recall that the E.F model was originally developed to model growth in Red Drum and, later adapted by its authors to model growth in the freshwater Bluegill. However, others have taken the basic model and adapted it to model growth in the two species of juvenile Sole, *S. solea* and *S. senegalensis* (Fonseca et al. 2010), Japanese Flounder *Paralichthys olivaceus* (Yamashita et al. 2017), the Pacific White Shrimp *Litopenaeus vannamei* (Walker 2009) and even the SFL (Del Toro-Silva 2008).

Southern Flounder Growth and Bioenergetics Models

Given the popularity of SFL as a commercial and sport fish, it is not surprising this species should be the subject of growth and bioenergetic models. The most common static models of SFL have been mass or length projections based on catch data categorized by US state from samples caught along the GoM or Atlantic coasts. These models will be discussed first, followed by von Bertalannfy length/weight temporal models, which have also been liberally applied to SFL growth, though with considerably more variance in final estimates.

Southern Flounder-specific bioenergetics models have received less attention, with only one static model apparent within the literature (Burke and Rice 2002). Nonetheless, this SFL bioenergetics model provides for an independent comparison, based on independently collected and fitted data that helps validate aspects of RMD.

Comparative Static Growth Models for Southern Flounder

By far, the majority of SFL growth models are comparative-static, often simply logarithmic or power functions fitted to measured length and weight, length and age, or weight and age data. Southern Flounder are widely distributed along North America's GoM and southern Atlantic coastline, so growth of this species has been estimated for every relevant US coastal state by researchers over several decades. These growth estimates are well synopsized by the Gulf States Marine Fisheries Commission (VanderKooy 2015). Length and weight growth estimates for juvenile SFL up to 160 mm from four GoM States (Texas, Louisiana, Georgia, and NW Florida) and South Carolina on the Atlantic coast are shown in Figure 13 along with additional growth estimates obtained from the literature for Mississippi (Corey et al. 2017) and South Carolina (Wenner and Archambault 2005) as well as growth data obtained from the TPWD-CF's, Marine Development Center over 8 years from 2009 to 2017. VanderKooy (2015) cited primary sources, and the derived formulae used from all sources, are provided in the caption. Although the majority of cited growth models are based on data for adult SFL, the graphic data are limited to SFL <160 mm TL and < 60 g to compare those estimates to the MDC data and to decide whether these adult models can be adequately scaled down to fit growth for juvenile SFL.

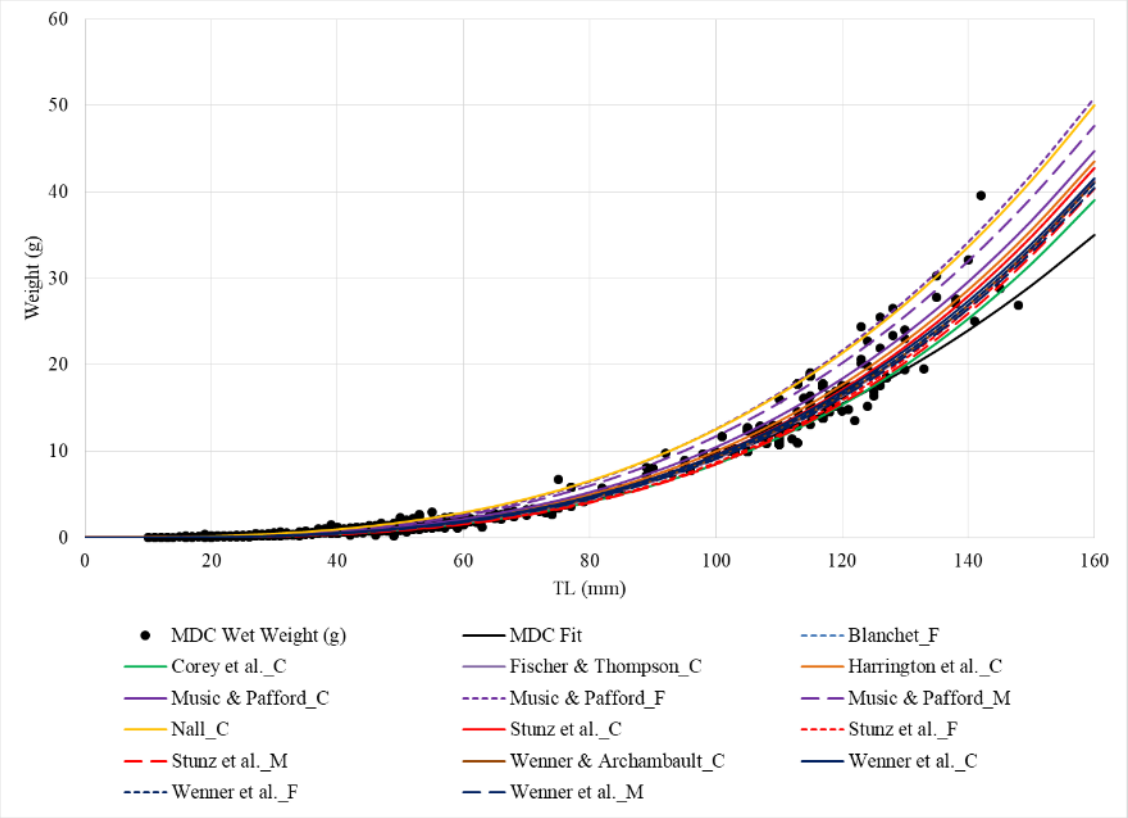

Figure 13. Comparison of SFL total length (mm) vs. weight (g) literature growth models to MDC data.

Legend notes: M = males (dashed line), F = females (dotted line), C = Combined (solid line). Static model original citation/source, state data collected, empirical formulae, r-squared and n value, if available: MDC Data Fit, Texas, C_Log_{10} Wt = 2.6745 x Log_{10} TL - 4.465, r^2 = 0.948, n = 693. Blanchet (2010), Louisiana, F_Log_{10} Wt = 3.18369 x Log_{10} TL – 5.386116. Corey et al. (2017), Mississippi, C_Wt = (2.82 x 10^{-6}) x $TL^{3.24}$, r^2 = N/A, n = 395. Fischer and Thompson (2004), Louisiana, C_Wt = (3.47 x 10^{-6}) x $TL^{3.21}$, r^2 = 0.98, n = 1236. Harrington et al. (1979), Texas, C_Log_{10} Wt = 3.13 x Log_{10} TL – 5.26, r^2 = 0.984, n = 2211. Music and Pafford (1984), Georgia, M_Log_{10} Wt = 2.98 x Log_{10} TL – 4.89, r^2 = 0.95, n = 12; F_Log_{10} Wt = 2.97 x Log_{10} TL – 4.84, r^2 = 0.98, n = 105; C_ Log_{10} Wt = 3.09 x Log_{10} TL – 5.16, r^2 = 0.98, n = 233. Nall (1979), Florida, C_ Log_{10} Wt = 3.1 x Log_{10} TL – 4.92, r^2 = N/A, n = 175. Stunz et al. (2000), Texas, M_Log_{10} Wt = 3.31 x Log_{10} TL – 5.69, r^2 = 0.975, n = 33; F_Log_{10} Wt = 3.3 x Log_{10} TL – 5.66, r^2 = 0.991, n = 206; C_ Log_{10} Wt = 3.27 x Log_{10} TL – 5.61, r^2 = 0.99, n = 239. Wenner and Archambault (2005), South Carolina, C_Wt = 0.0063 x (TL in cm/10)$^{3.1678}$, r^2 = N/A, n = N/A. Wenner et al. (1990), South Carolina, M_Log_{10} Wt = 3.17 x Log_{10} TL – 5.38, r^2 = 0.984, n = 675; F_Log_{10} Wt = 3.15 x Log_{10} TL – 5.33, r^2 = 0.995, n = 926; C_ Log_{10} Wt = 3.13 x Log_{10} TL – 5.28, r^2 = 0.994, n = 1753.

With few exceptions, the variance of the predictive SFL weights for a given length show little divergence until TL exceeds about 60 mm. However, even past 60

mm TL variation of only 4 to 5 g is seen at 120 mm for most of the models with notable exceptions being those by Harrington et al. (1979) and the male and female models by Music and Pafford (1984) which showed greater mass gain with increased length, even for SFL TL under 80 mm. Also notable is the fit line from the MDC data, which predicts less mass with increased size. The lower values of the MDC data are possibly due to fewer data points for juvenile SFL over 80 mm, and the data are being extrapolated for greater lengths and weights while most of the other models are based on adult SFL size and weight data which were extrapolated to lesser lengths and mass. Another possibility is the MDC SFL were simply underweight (for their TLs) compared to other sources due to differences in growth conditions. Nevertheless, the MDC growth curve appears to correlate well for SFL less than 80 mm TL. Some of the variability between models might be due to regional variation in length-weight relations for SFL. However, based on the overall consistency in the observed TL vs. weight for SFL living in coastal waters from Texas up to the Carolinas, it is likely most of the variance is due to a combination of varying sample size or possible sample-selection bias (i.e., sampling SFL only over a specific size).

Von Bertalannfy Growth Modeling for Southern Flounder

Since its introduction to the fisheries community, the von Bertalannfy temporal length-growth model—see equation (6)—has been widely applied. Data for the model can be obtained by measuring the fish and establishing a mean length (typically total length) and determining age (in years) by counting the otolith annuli (VanderKooy 2015). These data can then be plotted to obtain estimates of L_∞, k and t_0. In theory, this

formula allows determination of age by measuring the fish's length, a quick and convenient method useful for field estimates of age. However, in practice, von Bertalanffy estimates appear to have a greater degree of variance than length and weight relationships. This is not surprising as length and weight are geometrically related whereas length and age may be poorly correlated due to the myriad of environmental factors that can affect growth over time such as food and nutrient availability (i.e., energy to exploit MS_{growth}), mean temperature, mean DO, parasites, etc. As a result, von Bertalanffy estimates vary considerably within SFL population, as evidenced in Figure 14 which shows the predicted length versus age (in years) determinations from five different researchers across five states as compiled by VanderKooy (2015). As can be seen, there is considerable variability in the estimated L_∞ for the populations reported, although the results highlight the sexual dimorphism in size of sub-adult and adult SFL. It is also interesting to note that all but one of the von Bertalanffy models estimate a significant initial positive mean length (79 to 159 mm) at t_0. The one outlier from Blanchet (VanderKooy 2015) estimated a mean t_0 length of about negative 45 mm, an untenable starting condition.

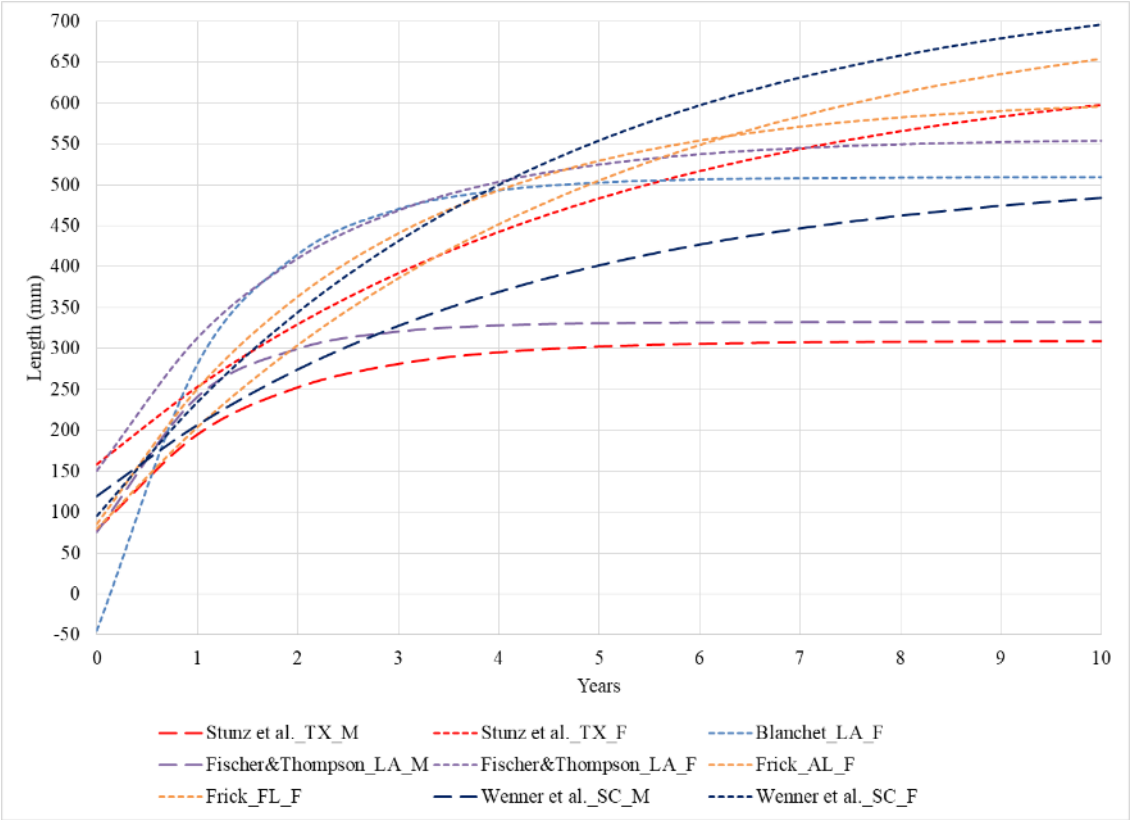

Figure 14. Von Bertalannfy rate predictions of SFL length vs. age.
Data: M = males (dashed line), F = females (dotted line). Legend: Source_State_Sex. F = female, M = male. From formulae compiled by VanderKooy (2015).

Due to the broad temporal scale (years) typically considered with this model, using the derived formula to determine growth over shorter time scales (e.g., weeks) is problematic as variance in the initial data has greater influence at smaller scales. For example, juvenile SFL growth data by age from the MDC is compared in Figure 15 to the sources shown in Figure 14 with the time scale converted to days. The mean MDC length is for days post-hatch. Due to the short time scale, the relationships appear linear.

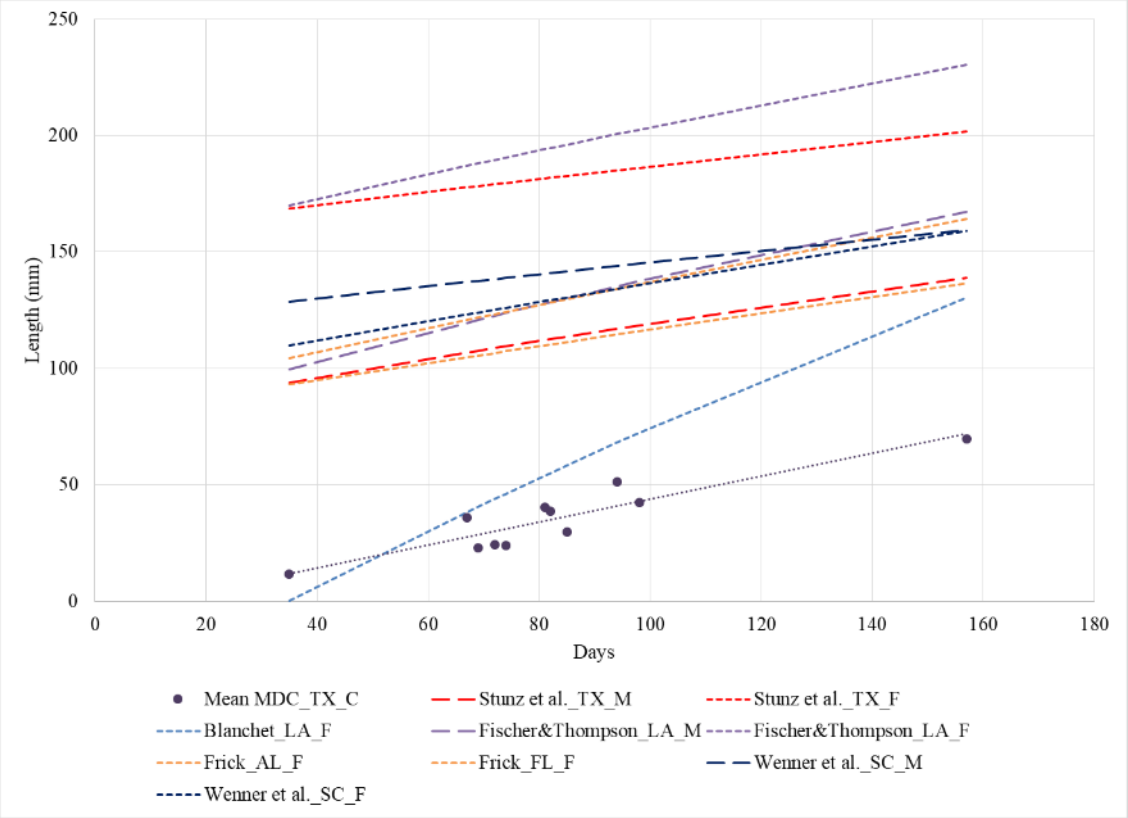

Figure 15. Mean MDC juvenile SFL length over time (days) with von Bertalannfy estimates from literature.
Data: C = combined (MDC data only), M = males (dashed line), F = females (dotted line). Legend: Original source_State_Sex. From formulae compiled by VanderKooy (2015). Mean MDC data shown with regression line, $r^2 = 0.84$. MDC SFL days post hatch shown (n): 35 (n = 20), 67 (n = 20), 69 (n = 50), 72 (n = 49), 74 (n = 10), 81 (n = 20), 82 (n = 80), 85 (n = 20), 94 (n = 205), 98 (n = 60), 157 (n = 32).

The intercept for the linear regression line for the MDC juvenile SFL is about negative 5 mm indicating that MDC SFL growth rates were lower than the majority of the literature data available. Of the literature sources listed by VanderKooy (2015), only the data from Blanchet (2010) are similar to the MDC data. Even here, the estimates for growth past about 50 days are much greater than that recorded in the MDC data. This may be due to the MDC flounder spawning later in the spawning cycle compared to wild

SFL. The von Bertalannfy model's comparison to recorded data shines a light on the necessity for a large enough n-value when developing von Bertalannfy models to ensure an applicable model across all age ranges. It would also suggest that many of the von Bertalannfy models reported in the literature are only broadly representative of age-length relationships for SFL.

Comparative Static Bioenergetics Models for Southern Flounder

Bioenergetics considers the energy available to, and its uses and changes within, a biological system or organism (Haynie 2001). Thus, energy from feed becomes a resource that can be measured and applied to the biological work of catabolism or anabolism.

The importance of energy as a biologic resource was perhaps first recognized by Boltzmann in an 1886 popular lecture on the second law of thermodynamics. Boltzmann observed that life was the "struggle for entropy" (Boltzmann 1886). Subsequent to Boltzmann's observation, energy as a resource has been considered as a selective force in evolution (Lotka 1922), mass scaling (Kleiber 1932), and of course bioenergetics (Jobling 1994).

Comparative static mass/length temporal growth prediction models, though quite useful, are somewhat limited in their utility as they consider growth (e.g., length and weight) but often do not account for the processes involved in growth. For example, von Bertalanffy's transformation rate *k*, which provides an accounting of the energy/mass consumed versus body mass acquired, simply combines (and therefore ignores) more complex bioenergetic processes into a simple variable. When these bioenergetic

processes are expanded for modeling consideration, the components most used are allocated into the three energy components associated with metabolism, wastes (nitrogenous and fecal), and growth (Winberg 1960), although other sources incorporate wastes into the metabolic cost of feeding (Jobling 1994). Bioenergetic models may also consider the energetic costs of environmental factors on these components (Fry 1947, 1971, Neill et al. 2004). Each component may be further broken down as warranted by the modeler. For example, the bioenergetic cost of waste may be considered the combined cost of energy lost as indigestible material from the digestive system and energy expended to remove nitrogenous waste. The concept of MS and MS_{growth} are other ways to represent these energy allocations.

Similar to growth models, comparative static bioenergetic models also have been much used over the years with a surge in application since the 1990s (Chipps and Wahl 2008, Hartman and Kitchell 2008). So prolific have these models become, each designed to measure a wide range of dependent variables such as individual or population growth, fecundity, predation, survival, etc. Considerable debate has arisen over the ability of these models to provide accurate predictions. This debate was begun by Ney (1993) but has remained unresolved as this was still an item of debate in the literature 15 years after Ney published his concerns (Chipps and Wahl 2008, Hartman and Kitchell 2008). Nonetheless, interest in the utility of bioenergetics models by researchers has resulted in a collaborative effort to provide an easily accessible computer model for individual and population predictions; in its most current configuration the model, known as Fish Bioenergetics 4.0 (Deslauriers et al. 2017), which uses the R

programming language (R Core Team 2017) to provide bioenergetics models for a wide range of fishes, including SFL. Unfortunately, this open-source program was non-functional upon attempted use with SFL by the author. It is also worth noting that the source for the SFL variant of this program is from a single source, a bioenergetics model developed by Burke and Rice (2002).

Based on data collected from SFL caught in North Carolina, the Burke and Rice (2002) static bioenergetics model fits the data to several equations based on a generic fish bioenergetics model developed for the antecedent Fish Bioenergetics 3.0 program, developed by Hanson et al. (1997). The primary equation is a general growth equation with secondary and tertiary equations used to calculate variables within the first equation (e.g., food consumptions and resting metabolism). Given the importance of this model as the principle source of SFL bioenergetics and growth within the literature, it is prudent to delve further into this model. The results are useful for comparison to RMD and the SFL variant of E.F.

The primary Burke and Rice (2002) formula, shown in equation 9, quantifies growth as shown.

$$G = C(1 - f - u - s) - (R \cdot ACT) \quad (9)$$

where G is defined as both "somatic and reproductive growth" with a presumed unit measure of mm growth per gram of tissue per day, C is food consumption per day (g food/g fish·day) with f, u and s being energy lost due to egestion (feces), excretion (urine), and specific dynamic action (SDA). Growth energy is further reduced by the product of energy lost to maintain resting (or standard) metabolism (R) and an activity

multiplier (ACT). Fixed variables within this equation are f, u, s, and ACT, set to 0.104, 0.079, 0.161, and 2.1, respectively for SFL (see Burke and Rice's paper for each variable's source). Variables C and R, calculated from secondary equations, are shown in equations 10 and 16.

The value for *G* is presumed to be mm/g fish·day. Based on the formula it would appear to be a value of grams fish per day. Later in their paper, growth rates are reported in a graph as mm/day, the values of which correspond to the *G* values calculated for a 1-gram fish. Calculations were based on the assumption that *G* is expressed in mm/g fish·day. Predictions of SFL growth using this assumption appear to provide representative results. However, the lack of clearly defined units for *G* make for uncertainty. Nevertheless, since this model is used as the representation of SFL growth for the Bioenergetics 4.0 and earlier models, further review is pertinent.

Calculation of *C* is based on the assumption that daily food consumption rate is maximized (C_{max}), such that,

$$C_{max} = a \cdot W^b \cdot f(T) \tag{10}$$

where *a* is the intercept of consumption in grams food/g fish·day, *W* is wet weight of the fish in grams, *b* a weight-dependent exponent of consumption, and *f(T)* a temperature-dependent function. Burke and Rice (2002) set variables *a* and *b* to 0.1993 and -0.31, respectively, for the SFL. The temperature function *f(T)* is derived from the earlier work by Hanson et al. (1997) and is itself a multilevel formula,

$$f(T) = V^X \cdot e^{(X(1-V))} \tag{11}$$

where:

$$V = \frac{(T_{max} - T_a)}{(T_{max} - T_{opt})} \tag{12}$$

$$X = \frac{Z^2 \cdot \left(1 + \left(1 + \frac{40}{Y}\right)^{0.5}\right)^2}{400} \tag{13}$$

$$Z = Ln(Q_{10}) \cdot (T_{max} - T_{opt}) \tag{14}$$

$$Y = Ln(Q_{10}) \cdot (T_{max} - T_{opt} + 2) \tag{15}$$

T_{max} is the maximum tolerable temperature (above which food consumption stops), T_{opt} is the fish's optimal temperature for growth, T_a the ambient temperature, and Q_{10} the temperature-dependent metabolic rate multiplier. For SFL, Burke and Rice set the T_{max} at 40°C, T_{opt} at 30°C and Q_{10} to 2.126. The value for T_a is variable, but in their paper Burke and Rice (2002) used 28°C.

The only remaining variable to calculate is the resting metabolic rate, *R*, in mg O_2/g fish·h,

$$R = c \cdot W^d \cdot e^{(m \cdot T_a)} \tag{16}$$

where *W* is weight of the fish, T_a the ambient temperature, *c* the intercept of respiration (set at 0.018 mg O_2/g fish·h for SFL), and *d,* and *m* are coefficients set at -0.1397 (no

unit) and 0.0811 (1/°C), respectively. These parameters were based on data from 16 SFL (mass ranged 25.9 to 183.6 g) acclimated at 25°C at a salinity of 33 ppt. The negative value for the weight-dependent respiratory exponent *d* was determined by Burke and Rice (2002) via closed respirometry experiments and data from Taylor and Miller (2001).

The exponential decline in resting metabolic rate Burke and Rice (2002) observed is in accordance with the expected allometric negative exponential decline with increased weight reported by Kleiber (1932). However, the Burke and Rice (2002) model does not address the respiratory source of $\dot{M}O_2$ needed to meet the energy requirement of resting metabolism.

Burke and Rice Model of SFL Growth

The Burke and Rice growth model, which predicts a daily growth rate, does not readily lend itself to comparison to the SFL growth models previously discussed as these other models predict growth rates on a yearly time scale. However, a comparison is possible by estimating daily growth rates for 365 days per year until equivalent yearly rates are achieved.

A multi-year analysis for use compared to other models first required that *G* be calculated for a range of SFL sizes. Starting with a 1-gram fish, *G* was calculated on a spreadsheet using equation (9) for weights up to 5000 grams in 1-gram increments. The resultant table was then used as a reference table for determining length-dependent daily growth (in mm). The table is graphically represented in Figure 16.

To calculate the estimated Burke and Rice daily growth rate, an initial length of 50 mm was chosen as the day 1 start length as this represents an approximately 1-gram fish, the exact weight of which was calculated using the mass/length growth model developed by Wenner and Archambault (2005), which also correlates well with MDC growth data (Figure 13). Because the calculated estimate for *G* declines as a negative exponential function of mass, as shown in Figure 16, growth estimates needed to be adjusted using the aforementioned reference table with each daily change in mass. Thus, the starting length estimate for each new day was the sum of the previous day's starting and additional growth rate estimate (e.g., the day 2 length (51.7 mm) is the sum of the day 1 length (50 mm) and the estimated day 1 growth rate of 1.7 mm for a 1-gram fish, while day 3 would be the 51.7 mm plus that day's growth estimate). The results of this effort, calculated over a theoretical 10 year period, are shown in Figure 17 along with the examples previously presented in Figure 13. If the assumptions made are correct, the predicted growth curve, starting with a SFL of 50 mm in length, is within the size and age ranges observed by other researchers (VanderKooy 2015).

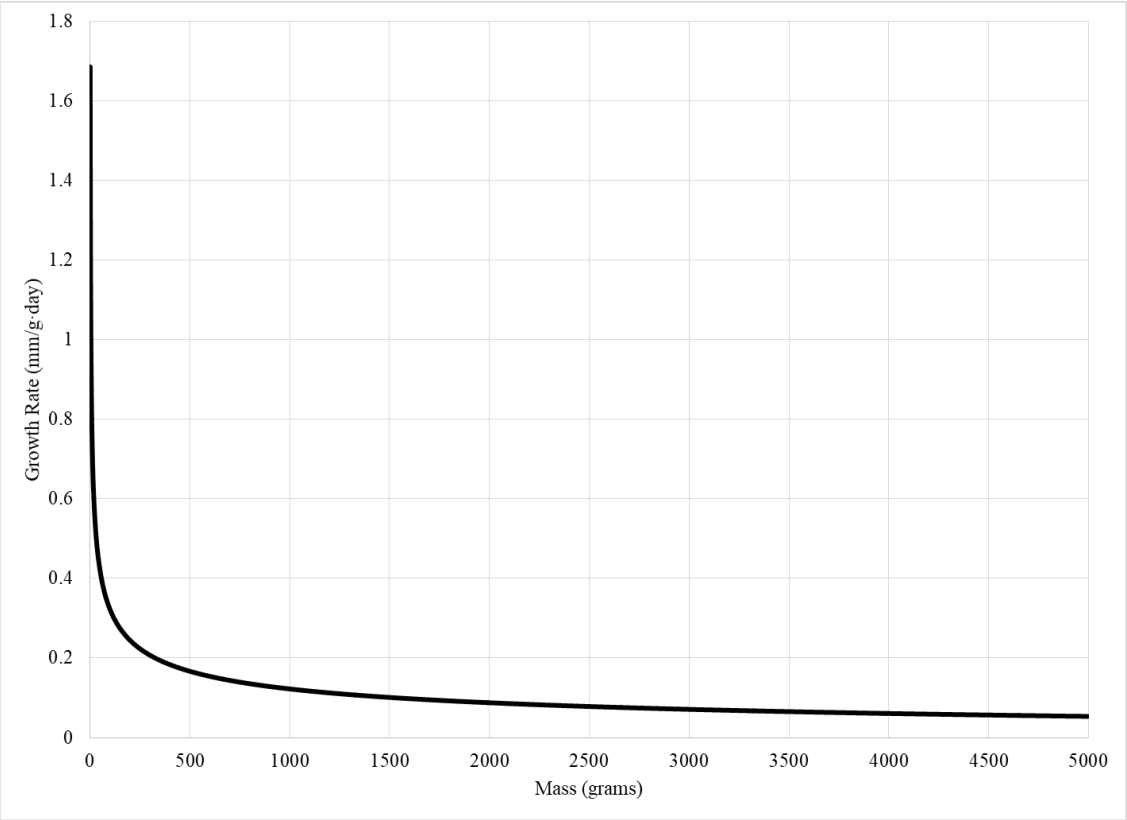

Figure 16. Estimated daily growth rate in length vs. mass for SFL adapted from Burke and Rice (2002).
See text for description and assumptions made.

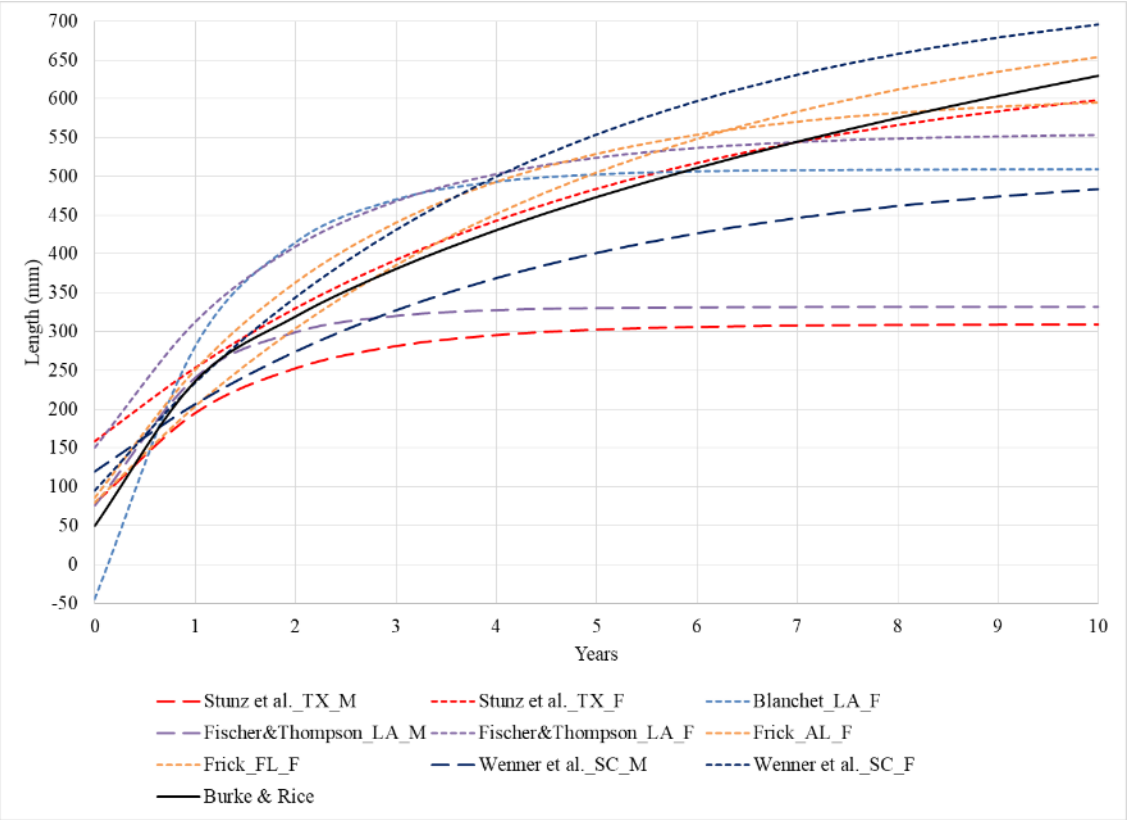

Figure 17. Comparison of Burke and Rice SFL growth model to other von Bertalannfy length-at-age predictions.
Burke and Rice growth prediction shown as solid line. See text for description and assumptions made. For description of von Bertalannfy models see caption for Figure 13.

Dynamic Growth and Bioenergetics Models for Southern Flounder

Unlike comparative static models (e.g., von Bertalannfy-based), which take a "top-down" approach to growth invoking fixed parameters, dynamic systems models can provide a more realistic "bottom-up" or "economic" approach by modeling the energy supply and expenditure of the organism to determine how much energy remains for growth. While more mechanistic, dynamic models involve more variables and their

interactions, making evaluation more complex. Nonetheless, results allow for greater synthesis through analysis of outcomes from the simulation with multiple inputs.

The Ecophys.Fish Dynamic Growth Model

The Stella® model Ecophys.Fish developed by Neill et al. (2004) explicitly incorporates Fry's concept of metabolic scope (MS) and responses to four of his five environmental- factor classes: controlling, limiting, loading, and lethal. (Directive factors, absent from E.F, were subsequently incorporated in EcoFish, an extension of E.F developed by Neill for teaching.[5]) The factors of all classes affect MS and MS_{growth}, as the model presumes that environment acts upon animal activity only via metabolism (Fry 1947, Neill et al. 2004).

The E.F model is comprised of two functional modules, or "sectors" – metabolism and bioenergetics, which work together to simulate energy acquisition and expenditure. The bioenergetics module (i.e., energy supply) derives the general energy density of the fish's biomass (GEfish) based upon the flux in caloric energy gained when "food" is consumed (in calories/g feed, termed "GEfeed"), versus that lost as wastes or expended in metabolism. As occurs in real organisms, the E.F model assumes that not all "food" consumed is converted to useful energy, as 10 to 25% is not digestible and ultimately is eliminated as feces, and another 5% is lost as nitrogenous excreta. About 15% of consumed energy is required to power the processes of digestion, assimilation

[5] See https://www.researchgate.net/publication/330845631_EcoFish_Introduction

and nutrient transformation (Neill et al. 2004). Ecophys.Fish treats the individual "fish" as an energy reservoir with a certain "energy density" which in times of food shortage or fasting (i.e., when feed energy is insufficient to meet activity and metabolic demands) declines, reflecting consumption of stored energy reserves; if sustained, the decline in energy density of the fish's biomass results in weight loss.

Conversely, in times of "feast," when intake of feed energy is modeled high, the fish grows in biomass energy density, then in biomass, per se. A unique feature of E.F is that feed consumption is also affected by MS_{growth}; should MS_{growth} decline due to, for example, low DO, feed consumption is restricted. Thus, the E.F model accounts for not only those factors that contribute to growth, but also those that mitigate it by removing energy from the system which, not surprisingly, are the metabolic costs associated with life and those factors, as outlined by Fry (1971), which constrain metabolism; the metabolic module of E.F addresses these.

The E.F approach to lethal factors focuses primarily on low DO, ignoring other lethal factors such as temperature (Neill et al. 2004). However, a potential limitation is that the omission of lethal temperature from the E.F model does not necessarily restrict growth estimates unless extreme environmental temperature ranges are considered. In the original E.F Red Drum model, the difference between ambient and acclimated DO levels (which can be set or variable values in Stella®) are considered to cause DO stress; if that DO stress level exceeds a programmed threshold, a fractional mortality "dose" due to low DO is accumulated over time (Neill et al. 2004). EcoFish adds to E.F's

repertoire of the lethal effects, including extreme temperature and toxic substances such as ammonia and copper.

Metabolic loading (or masking) within E.F is effected by adverse salinity (S), which necessitates computing the effect of non-optimal salinity levels causing elevation of standard metabolic rate. Considering the optimal salinity level (for Red Drum it is set to 10 ppt), a salinity variance (Svar) is calculated. This is used to establish a salinity limit value (SalL) that is based on a set upper and lower salinity level, and adjusted to compute the deviation in standard metabolic rate (Sgain), while taking into consideration ambient temperature relative to the fish's acclimation temperature (Neill et al. 2004).

As has been stated, DO presents the primary limiting factor for many aquatic species. Within the E.F model, the limiting effects of DO are modulated by the controlling effects of temperature and pH, affecting metabolic rate. More specifically, temperature effects on metabolic rate impact the lower DO limit (DOlim), the value below which metabolic rate becomes DO-dependent. This value, taken in conjunction with pH, is used to establish an adjusted DO level "A," calculated as the lesser of either ambient DO or the ratio of the DO limit and pH factor and multiplied by a weight corrective factor to establish the DO limit for a 1-gram fish. As with lethal factors, DO acclimation is considered as this will alter the simulated response. E.F's ability to model acclimation to environmental factors provides it capability for growth modeling not represented in non-dynamic models.

As DO is controlled by pH and temperature, it is not surprising that E.F uses these two variables as controlling factors. The powerful controlling effects of

temperature on poikilotherm standard metabolism is modeled in E.F as the Arrhenius effect. In contrast, active metabolism is subject to limitation by the DO level, DO acclimation state, a Bohr effect of pH, and finally, by an environmental-quality residual labeled as the intercept of the marginal metabolic scope (termed MMSO). Marginal metabolic scope (MMS), is a derivation based on Fry's MS and was introduced by Neill and Bryan (1991). Explicitly, MMS is the RMR $\dot{M}O_2$ value divided by the DO value at the point where $\dot{M}O_2$ intercepts LOCr and metabolism becomes oxygen dependent. A graphical representation of these relationships is shown in Figure 18. The MMS slope is multiplied by 1 mg O_2/L to keep the MMS units the same as $\dot{M}O_2$ and provide a useful measure of capacity for metabolic performance (Neill et al. 2004). In general, the larger the value of MMS, the greater the fish's capability for ecophysiological performance.

Neill et al. (2004) interpreted MMS as a measure of residual fitness between fish and total environment, with accommodation for the fish's environmental history. The "residual" part of this idea reflects the difference between environmental effects incorporated in the E.F model and those of total environment, much of which must remain unknown, perhaps even unknowable, to the modeler.

The E.F MMSO parameter is used with other metabolic impacting processes such as the pH factor, and ambient, limiting and acclimation DO, along with a "Winberg" factor to calculate an active metabolic rate. The Winberg factor is consistent with the concept of Winberg (1960), who reported that routine metabolism of typical fishes under natural conditions is approximately twice that of standard metabolism, i.e., SMR times 2.

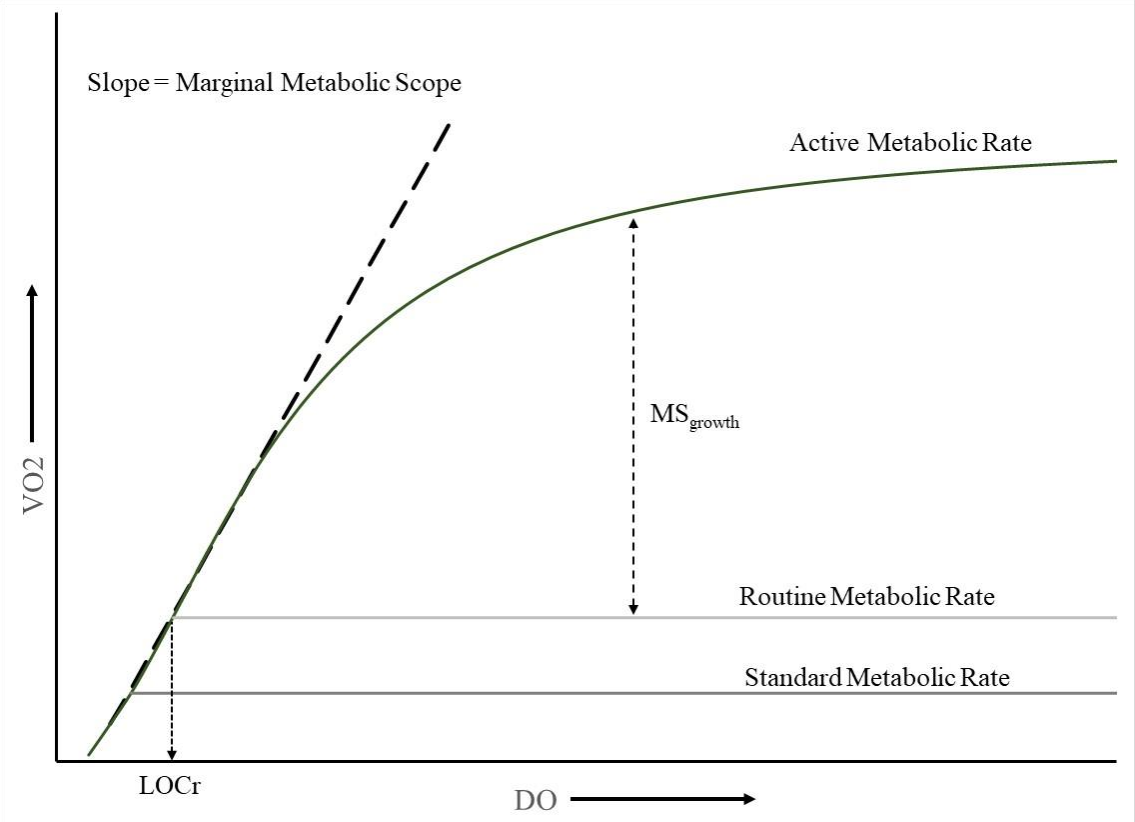

Figure 18. Relationship of marginal metabolic scope to metabolic rate, vs. DO.

For E.F to be an effective model, it must properly merge the metabolic and bioenergetic modules. The key to this conjoining is a mechanistic measure of metabolic capacity, namely the maximum amount of oxygen available to the organism, designated as $\dot{V}O_{2max}$. From Figure 18, it can be seen that the $\dot{V}O_{2max}$ is the $\dot{V}O_2$ at the point where any given DO level intercepts the AMR line. This maximum rate of oxygen use "corresponds with maximum rates of routine and feed-processing metabolism" (Neill et al. 2004). Feed processing, or specific dynamic action (SDA), has already been discussed as the approximately 15% of the feed consumed to meet the metabolic cost of

digestion and associated processes (designated "Msda" in the model) and is calculated by E.F as the product of SDA and the quotient of the feeding rate (Ac), a measure of energy acquired per fish mass per unit of time, and "oxycal," the caloric equivalent of one milligram of oxygen (3.4 cal/mg O_2) (Neill et al. 2004). The maximal amount of energy available for processing feed (Acmax) is the product of "oxycal" and the quotient of MS_{growth} and SDA (Neill et al. 2004). Thus, E.F is a mathematical representation of the organism being modeled as an energy flow system that the fish uses to "maintain and extend its being" (Fry 1971).

A significant difference between E.F and other models is the lowering of Acmax, as MS_{growth} declines. As MS_{growth} is tied to the active metabolic rate (Mact), which in turn is tied to DO, a reduction in DO leads to a reduction in MS_{growth}. Thus, as Acmax falls, metabolic energy availability to the "gut" of the fish becomes insufficient for feed processing, which subsequently limits energy and material availability for growth. While previously discussed models consider energy availability and consumption costs, they generally do not account for oxygen availability, limiting the utility of those models to only static normoxic environments.

Ecophys.Fish and an Introduction to Stella®

Adapting E.F to model a particular species requires changing E.F model parameters and even processes, and then comparing modeled growth to actual growth data from that species. Sometimes the requisite parameter changes can be estimated from available observations and data; other times, the process is simply one of trial and error to get the model to correctly simulate growth. This process is often easier for

researchers if the model is presented as a "stock and flow" process which categorizes and separates model components into useful visual flow components. As the dynamic systems modeling software Stella® uses this "stock and flow" method, and as E.F and RMD are Stella® based models, it is a prudent and timely opportunity to introduce the Stella® modeling process.

Stella® uses four primary "building blocks" as shown in Figure 19. Converters, represented by the small circles, can be used as place holders for needed inputs, be they constants, algebraic formulae or graphical functions. Action Connectors, represented by red arrows, not only show the relationship of model components to one another but programmatically indicate information inputs to other Converter or Flow processes. Flows are schematically represented as thick arrows with a circle in the middle. Atop the circles are representations of circular valve wheels viewed from the side. This arrangement is meant to evoke the image of a pipe with a control valve for that is the mathematical function of Flows, to control the "fill" or "drain" rate, depending on their relationship to the affiliated Stocks. Flow "rates" are determined either by algebraic formulas or fixed values. Stocks, represented by rectangles, indicate the net accumulation of materials via Flow input and/or output. Flows into and out of Stocks occur each time Step.

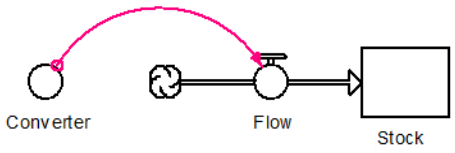

Figure 19. Stella® components.
Action Connector arrow in red.

Not shown in Figure 19 are Decision Process Diamonds, represented by diamonds (in Stella® 7 and subsequent versions), which are place holders for, and contain, sub-models. This graphic simply permits de-cluttering of the graphical model workspace and are used by E.F for this purpose.

Ecophys.Fish is a highly complex model, the major metabolic and bioenergetic Stella® components shown in Figure 20.

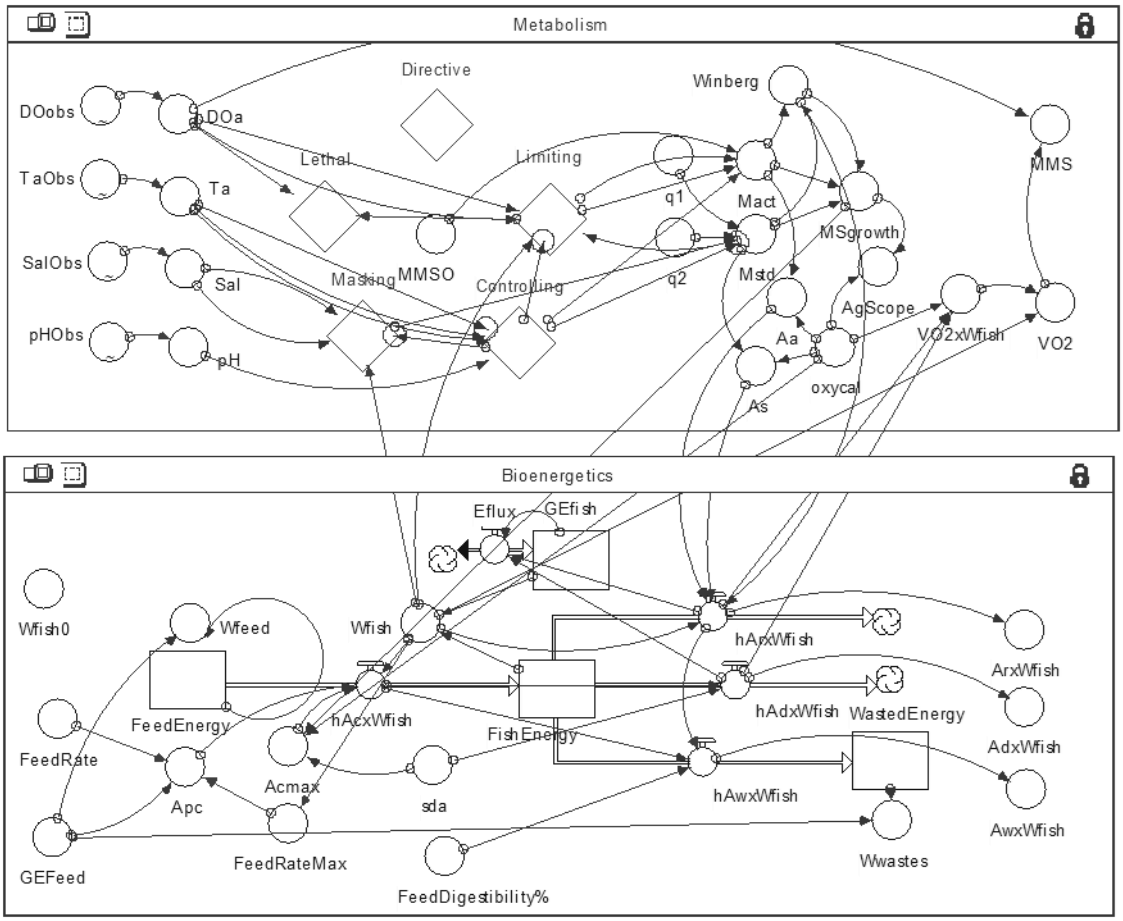

Figure 20. Ecophys.Fish Stella® model showing metabolism and bioenergetics sectors.

As can be seen, several of the components of the model previously discussed are present in the graphical module displays but with additional components added.

An example of the complex interaction between the primary Stella® model components can be seen in the feed energy flow in the Bioenergetics sector in Figure 20. Starting at the Stock component labeled “FeedEnergy,” which is used to “store” a set numerical value representing a fixed reservoir of feed energy available for the modeled

fish's consumption, the one Flow component attached to "FeedEnergy" is outward per the arrow indication. This Flow component "hAcxWfish" controls the caloric rate (per hour and per unit fish biomass) at which "FeedEnergy" is removed from the "FeedEnergy" Stock and transferred to "fill" the "FishEnergy" Stock in accordance with an algebraic equation which uses the input variables, as shown by the arrows, from Converters "Wfish," "Acmax" and "Apc." From a modeling perspective, the value of "hAcxWfish" acts as a flow resistor, the Step-by-Step rate determined by the Converter inputs. Although the "FeedEnergy" Stock is depleted during the model's run, the "FishEnergy" Stock represents a more dynamic relationship. While the inward flow from "hAcxWfish" fills the "fish Energy" stock, it is depleted by the three outward Flows of "hArxWfish," the loss of energy due to routine metabolism; "hAdxWfish," the metabolic cost of processing feed; and, "hAwxWfish," the loss via waste elimination. Algebraic equations determine these rates with dependent variable inputs from other model components inputs. It should be noted that Flow and Converter inputs can be not only from the Converters but also from Flows and Stocks.

SFL Growth and Bioenergetic Modeling Using Ecophys.Fish

The first alteration of the Neill et al. (2004) E.F model to model SFL growth was achieved by Del Toro-Silva (2008). However, the original Neill et al. E.F model was significantly altered from the original as 25 new processes were introduced to fit the model to the SFL. Thus, the Del Toro-Silva SFL model is more of a hybrid model, using the E.F model as the chassis upon which the new model was constructed.

Oxygen Transport Models in Fish

Use of $\dot{V}O_2$ or $\dot{M}O_2$ as a measure of an organism's metabolism (and MS) arises from the observation that ATP (energy) production in metazoans is primarily related to oxygen uptake, although anaerobic energy production may occur in special circumstances. For example, during exercise, up to 15% of a flatfish's energy may come from anaerobic metabolism (Duthie 1982), but because this O_2 debt eventually must be paid, it is generally valid that O_2 consumption is a measure of total metabolic activity on a sustained basis. The alternative method, involving direct estimates of thermodynamics via bomb calorimetry, requires placing the organism in a very restricted environment and would require very sensitive temperature sensors given the relatively low metabolic rate of poikilotherms. Despite its limitations, the utility of using oxygen flux as a determinant of energy-processing rates within an organism has driven the development of models for the transport and distribution of oxygen from the environment to the cellular mitochondria.

Computer Models of Oxygen Transport in Fish

As with the growth and bioenergetics models, without the aid of computers early fish cardiorespiratory models were by necessity static in nature. It is rather interesting to note that one of the earliest dynamic computer-based fisheries simulations was, in fact, an oxygen transport model. Developed in the late 1960s, Taylor et al. (1968) took advantage of the computing power afforded by a dated IBM 7040 digital computer, to develop a salmonid dynamic cardiovascular and respiratory model. In their detailed computer model, Taylor et al. (1968) used estimates of buccal volume, gill perfusion,

and feedback loops to emulate physiological regulation which allowed for modeling of hypoxia and exercise effects; they reported good correlation with actual measured data. Their model did not consider mass or temperature effects as both were fixed at 1 kg and 5°C, respectively.

The use of the IBM 7040 computer by Taylor et al. (1968) for physiological modeling of fish respiration appears to have stimulated interest in others. Shortly afterward, the same system was used by Scheid and Piiper (1971) for the modeling of the optimal theoretical lamellar morphology for use in other models. However, using computer models for modeling fish performance based on the cardiorespiratory dynamics appears to have taken a backseat to other approaches, particularly bioenergetics models. Other than Ecophys.Fish, no other Stella®-based model seems to have gained sufficient momentum beyond the laboratory for publication. This is undoubtedly true for flatfish. The development of RMD was implemented in-part as a means to address this discrepancy.

CHAPTER V

PHYSIOLOGY AND PHYSICS OF OXYGEN FLOW: FOUNDATIONS OF THE FLOUNDER RESPIRATORY MODEL

As in the model of Taylor et al. (1968) for salmonids, the Respiratory Model, Dynamic (RMD) was developed for SFL to model oxygen flow from the aquatic environment to the tissues. This modeling effort was facilitated using the Stella® dynamic systems modeling software to simulate the flow of oxygen from the aquatic environment through the fish's gills and skin and into the internal milieu via the circulatory system and finally to the tissues. Thus, RMD was designed to emulate, as practical, the corresponding anatomical and physiological components of what Taylor et al. (1968) so eloquently termed the "teleostean cardiovascular-respiratory complex." To achieve this goal, RMD uses a modular approach consisting of a core cardiorespiratory module with six sub-modules to calculate processes needed by components of the core module and two modules for inputting environmental and fish weight processes.

This chapter will cover the general scientific principles used to build RMD followed in the next chapter by discussing the RMD Stella® model itself, including specific calculations used, data interactions, data sources, assumptions, and concessions.

The *raison d'être* of RMD is to model the flow of O_2 from the aquatic environment to the tissues of the SFL. Within the model, $\dot{V}O_2$ (mL O_2/h), i.e., volume flow of O_2, is used during the model calculation process for ease of calculations but is converted to O_2 mass flow, $\dot{M}O_2$ (mg O_2/g fish·h), as a final output to bring dimensions

in line with most literature sources. This estimate becomes a measure of the metabolic rate within the SFL, which can help establish the energy available to the SFL for growth (i.e., MS_{growth}) in an SFL version of Ecophys.Fish, which will be discussed later.

Oxygen flow can be modeled using four physiological processes described by Jensen et al. (1993), based on original work by Dejours (1981). Each mathematical model is the product of O_2 flow, or conductance, and O_2 tension differences (often expressed as pressure differentials) between two different media (Dejours 1981, Jensen et al. 1993). Disregarding cutaneous respiration for the present, these processes are, 1) ventilation – the movement of oxygenated water through the buccal cavity of the fish and it's removal by the gills; 2) diffusion of O_2 across the gill epithelial and capillary endothelial tissue membranes, then into the red blood cells where it is chemically bound to hemoglobin (Hb); 3) transport of the oxygenated Hb (HbO_2) to the tissues via the bloodstream; and, 4) diffusion of O_2 from the blood to the tissues where it is used to produce ATP for cellular work. These processes are presented by Jensen et al. (1993) as oxygen mass (mg O_2) flow ($\dot{M}O_2$) formulae, as shown in equations (17) to (20), which are variants of Fick's law of diffusion (Fick 1995).

Ventilation:

$$\dot{M}O_2 = \dot{V}w \cdot \beta_w O_2 \cdot (PIO_2 - PEO_2) \tag{17}$$

Gill diffusion:

$$\dot{M}O_2 = \left(K_g \frac{A_g}{l_g}\right) \cdot (P_w O_2 - P_v O_2) \tag{18}$$

Blood oxygen transport:

$$\dot{M}O_2 = \dot{Q} \cdot \beta_b O_2 \cdot (P_a O_2 - P_v O_2) \quad (19)$$

Diffusion in tissue:

$$\dot{M}O_2 = \left(K_t \cdot \frac{A_t}{l_t}\right) \cdot (P_a O_2 - P_t O_2) \quad (20)$$

where $\dot{V}w$ is water flow (mL water) across the gills per unit time, PO_2 is O_2 pressure[6], A is diffusion area, l is diffusion distance, K is Krogh's diffusion constant, $\dot{Q}$ is cardiac output, and βO_2 is the O_2 capacitance coefficient ($\beta O_2 = dCO_2/dPO_2$, i.e., the change in O_2 concentration (mL O_2/mL blood·mmHg) with respect to change in O_2 pressure (mmHg). The sub-scripted indices refer to the following: w (water), I (inspired), E (expired), g (gill tissue), v (venous blood), a (arterial blood), b (blood, general), and t (tissue).

Equations (17) and (18) are used "as is" in RMD; these calculations provided $\dot{V}O_2$ results which were converted to $\dot{M}O_2$ by multiplying the $\dot{V}O_2$ value by the conversion factor of 1.42857 mg O_2/mL O_2 at standard temperature and pressure.

Equation (19) was modified for use in RMD as shown in equation (21).

$$\dot{V}O_2 = \dot{Q} \cdot C_a O_2 \quad (21)$$

[6] Gases dissolved in liquid do not exert pressure, the correct term being *tension* (Schmidt-Nielsen 1997); but, pressure is often used by convention.

In this variation, the estimate of arterial blood oxygen concentration (C_aO_2), in mL O_2/mL blood, is substituted for the value obtained from $\beta_aO_2 \cdot (P_aO_2 - P_vO_2)$. The rationale for this is presented in the Blood Oxygen Transport section.

The tissue diffusion equation (20) is not used in the model; the assumption being that generalized $\dot{M}O_2$ applies equally to all tissues. This is a concession to the very daunting challenge of trying to model O_2 diffusion across the myriad of variable capillary surface areas and diffusion distances of the different tissues found in the organs of all complex organisms. However, the estimated $\dot{M}O_2$ can be used in a growth model such as E.F to determine the maximum available oxygen supply per gram of tissue for metabolism.

The four-step approach described by Jensen et al. (1993) is by no means definitive. It does, however, establish a sequential approach, with each step dependent up the step before it. In other words, each step is rate-limiting for each subsequent step. As the first step, Ventilation then becomes the primary rate limiter. Each subsequent step cannot exceed the amount of O_2 obtained from Ventilation unless a supplemental means of O_2 is available, which for many fish (particularly flatfish) is possible through cutaneous respiration (Kirsch and Nonnotte 1977, Steffensen et al. 1981, Feder and Burggren 1985 Nov 1, Rombough and Moroz 1997, Rombough 1998, Glover et al. 2013).

This observation creates the necessity of adding a cutaneous respiration model to RMD to accurately represent the total $\dot{M}O_2$ available to the SFL. Subsequently, RMD again becomes a four-component model, with equations (17), (18), and (21) comprising

the core cardiorespiratory components of RMD along with the introduction of a supplemental cutaneous diffusion which adds a non-ventilation-limited component. This modification is schematically represented in Figure 21 where O_2 flow from the environment to the tissues is defined by the model's three cardiorespiratory components (Ventilation, Gill Diffusion, and Blood O_2 Transport) and the Cutaneous Diffusion component.

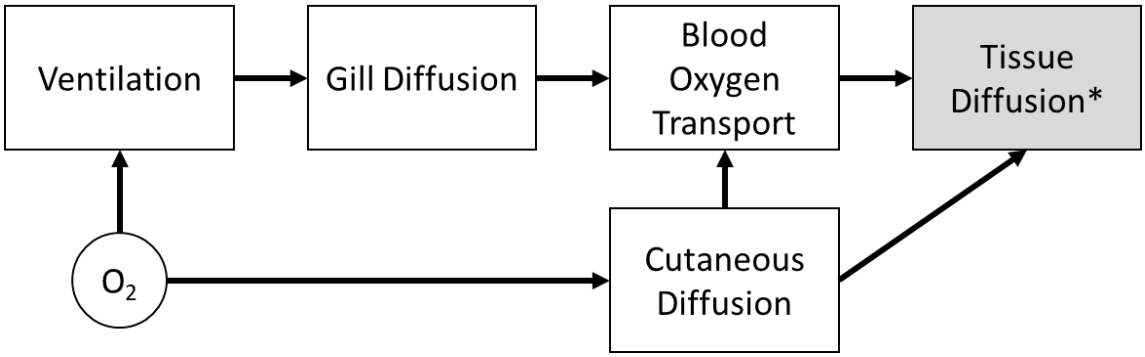

Figure 21. Schematic of cardiorespiratory module with gill and cutaneous respiration.
*Tissue Diffusion is not a component of RMD but is shown for clarity. See main text for details.

Ventilation

The ventilation model (equation 17) contains four variables—ventilation volume per unit time ($\dot{V}w$), the capacitance coefficient for O_2 in water (β_wO_2), the O_2 tension of water entering the gill exchanger of the fish (PIO_2), and the O_2 tension of water exiting the operculum (PEO_2). The PIO_2 and PEO_2 differential represents the O_2 extraction efficiency (Steffensen et al. 1982, Capossela et al. 2012) and will thus be discussed in

this context. The derivation of $\dot{V}w$ is via the product of ventilation volume, a function of the buccal cavity volume and ventilation rate.

Ventilation Volume

Movement of water past the gills in flounder is similar to that in most fish involving water drawn into the buccal cavity, pushed over the gills and into the opercular cavity where it is expelled back out into the environment, with the exception that in resting flatfish water is expelled solely from the upper operculum (Yazdani and Alexander 1967). The maximum volume of water drawn into the buccal cavity is determined by the maximum volume of the buccal cavity itself; however, resting ventilation volume tends to be less than the maximal volume as indicated by the ability of flatfish to increase ventilation volume under hypoxic conditions (Watters and Smith 1973, Kerstens et al. 1979, Steffensen et al. 1982, Tallqvist et al. 1999).

Reports of mean normoxic resting flatfish ventilation stroke volumes range from a low of 0.00265 mL water/g fish·stroke in Starry Flounder (Wood et al. 1979a) kept between 7.5 to 10°C, up to an average of 0.004 mL water/g fish·stroke in European Flounder at 10°C (Kerstens et al. 1979, Steffensen et al. 1982). When European Flounder were exposed to acute hypoxic water with a PO_2 of 30 mmHg (Kerstens et al. 1979) and 40 mmHg (Steffensen et al. 1982), the ventilation volume doubled. European Flounder acclimated to hypoxia and exposed to a PO_2 of 30 mmHg had breathing volumes almost three times that of normoxic flounder at rest (Kerstens et al. 1979).

Temperature effects on ventilation volume have been reported in flatfish by Watters and Smith (1973). However, the authors do not distinguish between volume

increases due to increased stroke volume versus increased ventilation rate which, as will be discussed, does change with temperature. Effects of temperature on ventilation stroke volume have been studied in Common Carp *Cyprinus carpio* (Klyszejko et al. 2003). In the carp study, ventilation stroke volume was assessed from 10 to 25°C. Ventilation stroke volume increased from 10 to 20°C but there was no difference in volumes at 20 and 25°C, suggesting an upper-temperature limit of ventilatory stroke volume.

Ventilation Rate

The ventilation rate in fish also responds to water PO_2 and temperature (Steffensen et al. 1982, Tallqvist et al. 1999, Maxime et al. 2000, Capossela et al. 2012). The most common method mentioned in the literature for determining ventilation rates in fish is to count the number of opercular movements per minute. For temperature acclimated flounder in normoxic water, ventilation rates can be quite variable. In the study by Wood et al. (1979b), the reported mean ventilation rate was 41.7 ± 1.6 beats per minute (bpm) in Starry Founder acclimated to between 7.5 to 10.5°C and salinity of 26 – 29 ppt. In the study by Steffensen et al. (1982), the average respiration rates in European Flounder and Plaice raised at 10°C, salinity 20 ppt, was 30 bpm and 25.5 bpm. Contrast this with the findings of Tallqvist et al. (1999) who, for juvenile European Flounder (mean TL = 40 mm) acclimated at 13°C and salinity 5.0 ppt, reported normoxic ventilation rates of 79 ± 11 bpm in their control group and 87 ± 10 bpm in their experimental group. The most obvious difference among these three studies was that Tallqvist et al. (1999) evaluated juvenile fish, while the other researchers evaluated adult fish. This suggests that flounder respiration rate may have an inverse relation to fish

weight, with ventilation rate declining as total buccal volume increases with increased body weight. Literature support for this hypothesis within flatfish was not available. Still, weight-related negative-exponential declines in respiratory rate have been observed in Stoplight Parrotfish *Sparisoma viride* (Van Rooij and Videler 1996) and Nile Tilapia *Oreochromis niloticus* (Yamamoto 1992, Barreto and Volpato 2006). In contrast, ventilation rates in the Common Carp are not affected by weight (Yamamoto 1991, Luo et al. 2020).

Ventilation-rate response to PO_2 changes within flounder is well substantiated (Kerstens et al. 1979, Steffensen et al. 1982, Tallqvist et al. 1999, Capossela et al. 2012). The reported ventilatory response within flounders is for ventilation rate to increase as PO_2 declines (Steffensen et al. 1982, Capossela et al. 2012), or remain relatively stable until reaching an upper hypoxic threshold at which point ventilation rates increase then plateau before declining (Tallqvist et al. 1999). Eventually, however, once a minimal hypoxic threshold is reached, ventilation rate starts to decline (Steffensen et al. 1982, Tallqvist et al. 1999, Capossela et al. 2012). The exact PO_2 at which this occurs has some variability, with reported values ranging from 60 mmHg (Steffensen et al. 1982) to 32 mmHg (Tallqvist et al. 1999), although it is possible for this threshold is even lower as some data ends at about 30 mmHg without indication of decline (Capossela et al. 2012).

Ventilation Flow

Temperature and PO_2 significantly impact $\dot{V}w$ in fish, although there is variation across species (Dejours et al. 1977, Steffensen et al. 1982, Capossela et al. 2012).

Unlike land vertebrates, which use PCO_2 as the primary physiological driver of respiration, fish respiration is PO_2-dependent. So much so that while hyperoxia (i.e., PO_2 greater than normal) has little effect on land vertebrate respiration, it suppresses fish respiration (Dejours et al. 1977).

The effect of lowered temperature and PO_2 is to increase $\dot{V}w$ and, with more pumped water over the gills to maintain the PO_2 to meet metabolic demand. In a study conducted by Capossela et al. (2012), the $\dot{V}w$ for two groups of Summer Flounder *Paralichthys dentatus* was measured at various PO_2 levels after the two groups were acclimated to 22°C and 30°C, respectively. Within the 22°C-acclimated group, $\dot{V}w$ increased five-fold, from approximately 10 mL water/g fish·h at a PO_2 of 140 mmHg to 50 mL water/g fish·h when PO_2 was 30 mmHg, following a pattern of increasing $\dot{V}w$ with falling PO_2. For the 30°C acclimated group, the response trend was similar: The effect of increased temperature was to increase the initial ventilation rate so that at a PO_2 of 140 mmHg the resting $\dot{V}w$ was about 20 mL water/g fish·h, rising to about 60 mL water/g fish·h when PO_2 fell to 46 mmHg (the lowest PO_2 for this group). The trend of increased $\dot{V}w$ with decreased PO_2 is supported by the studies of Steffensen et al. (1982) and Watters and Smith (1973). Steffensen et al. (1982) observed similar responses in 10°C-acclimated European Flounder and Plaice, although the $\dot{V}w$ maxima and minima were less than the corresponding rates reported by Capossela et al. (2012), ostensibly due to the lower temperature. However, there does appear to be some nuance in the relationship between temperature and oxygen level. In a study using anesthetized Starry Flounder by Watters and Smith (1973), the flounder were acclimated to temperatures

ranging from 9°C to 20°C, then evaluated at oxygen pressures ranging from 155 mmHg to 58 mmHg. As with the other studies cited, the general trend was a higher $\dot{V}w$ with increased temperature when the PO_2 was maintained above 120 mmHg. For hypoxic PO_2 values, the effect of temperature on $\dot{V}w$ was greater than that seen under normoxic conditions, although temperature still had an effect. For example, at 9°C, the hypoxic $\dot{V}w$ value was greater than for the normoxic condition at the same temperature. At higher temperatures, however, $\dot{V}w$ was suppressed under hypoxic conditions.

Oxygen Capacitance

The O_2 capacitance coefficient (βO_2), is the ratio of DO (mg O_2/L water) to PO_2 (mmHg) in water (equation 22). It is an expression of Henry's Law of solubility (Welch 1985).

$$\beta_w O_2 = \frac{DO}{PO_2} \tag{22}$$

where $\beta_w O_2$ is expressed in mg O_2/L water·mmHg, which can be converted to mL O_2/L water·mmHg by multiplying the result by 0.7 mL O_2/mg O_2.

Calculating $\beta_w O_2$ is a simple matter once DO and PO_2 are known. Oxygen pressure can be easily calculated as the product of the oxygen fraction (FO_2) in the atmosphere (currently at 0.209) and the total barometric pressure (760 mmHg at sea level and 15°C) (Welch 1985), although other factors like water vapor pressure can influence the total PO_2 over the water (Schmidt-Nielsen 1997). Oxygen tension in the water can be influenced by oxidative chemical reactions, consumption by microorganisms, and production of O_2 by photosynthetic microorganisms (Willmer et al. 2005).

Dissolved Oxygen Estimation

Calculating DO is complex, with "best-fit" polynomial formulae often used to account for the interactions of PO_2, temperature and salinity (Green and Carritt 1967, Benson and Krause 1984, Sherwood et al. 1991). Although the choice of a particular "best fit" DO formulation may be subject to differences of opinion, a selection must nonetheless be made. RMD uses the algorithm developed by Green and Carritt (1967), which accounts for temperature, salinity, and atmospheric pressure. The DO range for various temperatures and salinities at standard sea level atmospheric pressure of 760 mmHg is shown in Figure 22. The figure shows that increased water temperature has a significant negative impact on steady-state DO, averaging a decrease of slightly more than 1 mg O_2/L water for every 5°C increase in water temperature over the temperature range usually encountered by SFL. Increasing salinity decreases DO as a function of temperature. The decline in DO between a liter of freshwater (salinity 0 ppt) and seawater (salinity 35 ppt) at 5°C is a delta of about 3 mg O_2/L water while at 25°C the delta is approximately 1 mg O_2/L water. Reduced barometric pressure has the effect of lowering the overall estimated DO values, although the difference in DO between a barometric pressure of 760 and 750 mmHg is only about 0.1 mg O_2/L water (barometric effects are not shown in Figure 21).

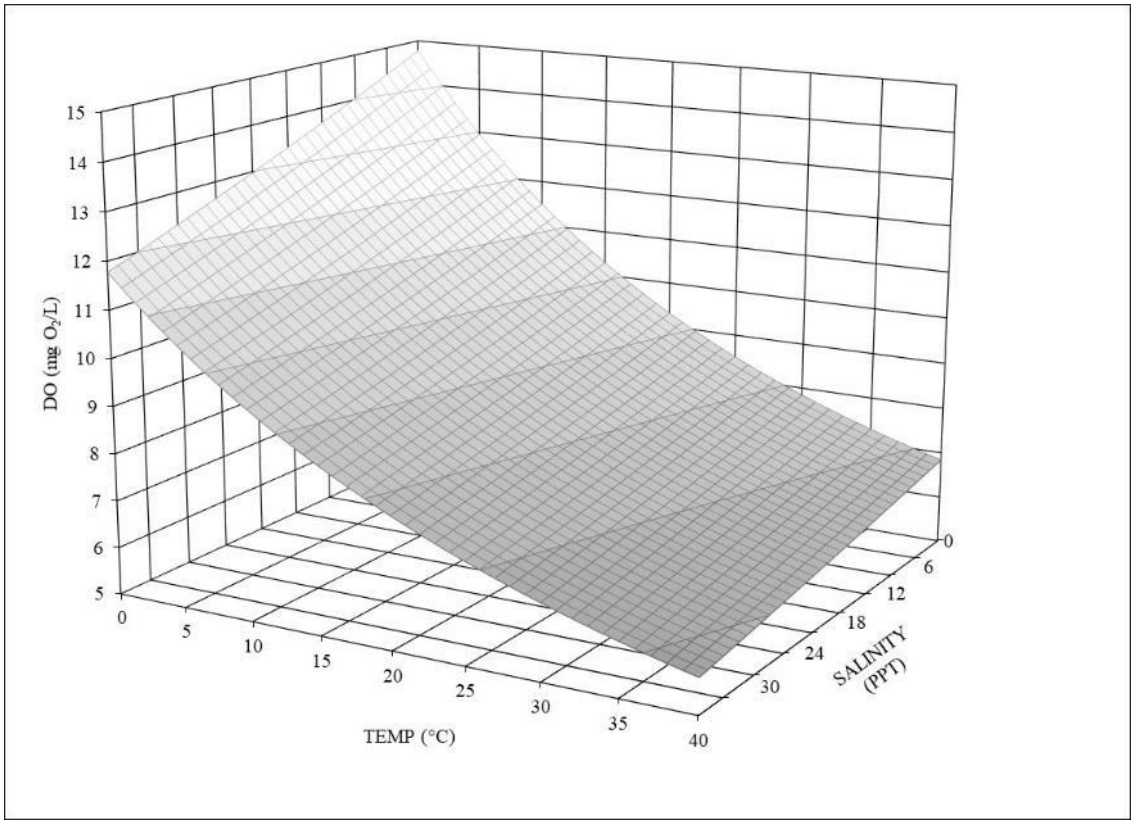

Figure 22. Effect of temperature and salinity on DO.
Based on the Green and Carritt (1967) algorithm at a barometric pressure of 760 mmHg.

Extraction Efficiency

Flatfish ventilation is affected by their benthic-adapted morphology. Water drawn in through the mouth does flow over both sets of gills, as in all fish. Water flow over the lower gills is normally routed and expelled through the upper opercular opening, although water can still be expelled through the lower operculum, especially during times of high respiratory demand (Yazdani and Alexander 1967). This arrangement does not appear to limit flounder oxygen uptake. As Watters and Smith

(1973) report, the extraction efficiency of oxygen, calculated as the difference between the PIO_2 and PEO_2, in the Starry Flounder was markedly better than the extraction efficiency of Rainbow Trout *Oncrhynchus mykiss*. For the trout exposed to a PIO_2 of 150 mmHg, the PEO_2 was approximately 90 mmHg, giving a 40% extraction efficiency; whereas, the flounder had a PEO_2 of about 40 mmHg, for a 73% extraction efficiency. In both species, Watters and Smith (1973) report that O_2 extraction efficiency decreases somewhat as PIO_2 begins to decline, suggesting no compensatory respiratory response occurs during the initial onset of hypoxia and suggesting that in both species an inherent initial tolerance to hypoxia may exist. However, once past each species' specific threshold, extraction efficiency appears to improve (though not to normoxic levels) as physiological equilibration occurs. Curiously, this brief decline in extraction efficiency is not reported by Steffensen et al. (1982) in the European Flounder or Plaice. Their data suggest a steady decline in extraction efficiency consistent with the decline in PIO_2. However, in fairness to Watters and Smith (1973), Steffensen et al. (1982) did not measure PIO_2 values in the 120 to 130 mmHg range within which Watters and Smith detected this anomaly. The Steffensen et al. (1982) study skipped PO_2 measurements for the interval from 140 mmHg down to just under 100 mmHg.

Diffusion Across Gills

The gill diffusion equation (18) is an applied version of Fick's Law of Diffusion which models $\dot{M}O_2$ across a membrane. The membranes in question for gill respiration are the gill epithelial and capillary endothelial cells that separate the oxygenated water from the blood (Dejours 1981, Shelton 1992). Membrane conductance processes and

variables for the equation affecting O_2 movement are Krogh's constant (K_g), gill area (A_g), and diffusion distance (l_g). The O_2 tension differential is determined by the difference between the water's oxygen pressure (P_wO_2) and the pressure of O_2 in the venous blood (P_vO_2).

Diffusion of O_2 across the gill is facilitated by the use of countercurrent exchange wherein water flow over the gills is in opposition to blood flow through the lamella capillaries (Jones et al. 1970, Hughes and Morgan 1973, Evans et al. 2005), a method of O_2 extraction that is exceptionally efficient (Kamiya and Yamamoto 2019). Modeling of gill countercurrent O_2 exchange, though an extensive and vibrant area of research (Piiper 1982, Malte and Weber 1985, Malte 1992, Kamiya and Yamamoto 2019), is not included in RMD for the simple reason that while countercurrent exchange modeling approximates $\dot{V}O_2$ across the gills, this process occurs in seconds, while RMD estimates $\dot{V}O_2$ across the gill on an hourly basis. Gill diffusion in RMD is thus an estimate of hourly gill $\dot{V}O_2$ *capacity*, rather than a direct estimate of $\dot{V}O_2$.

Krogh's Constant

Krogh's constant, named after Danish physiologist August Krogh, is the product of the aforementioned O_2 capacitance (or solubility) coefficient (βO_2) through a substance (i) and the O_2 diffusion coefficient (DO_2), which is a measure of the average amount of O_2 moving through a given area (typically cm^2) of the substance per unit time (Cameron 1989) as described in equation (23).

$$K_iO_2 = \beta_iO_2 \cdot D_iO_2 \quad (23)$$

When calculating KO_2, the obvious assumption is that βO_2 and DO_2 would pertain to the same substance. In a simple model, such as the diffusion of a gas through a single medium like a cell membrane or gel barrier, this would be the case. However, when modeling the flow of a gas molecule through organic tissue, the situation is more complicated as gas solubility and diffusivity differ between the two substances constituting the primary solvents in animal tissue: water and lipids. Water constitutes the bulk of the extracellular and intracellular medium with lipids making up the bulk of cellular membranes (Cameron 1989).

Oxygen is less soluble in water than in lipids (Battino et al. 1968, Windrem and Plachy 1980) with the measured βO_2 in olive oil and water at 25°C recorded at 0.116 and 0.0263 mL O_2/mL water·mmHg, respectively (Battino et al. 1968). Phospholipid membranes do not of themselves present a significant resistance to O_2 diffusion; instead, it is the presence of other molecules, particularly cholesterol, which can create barriers to O_2 diffusion (Subczynski et al. 1989, Subczynski et al. 1992, Subczynski and Wisniewska 2000). When non-miscible solvents such as water and a lipid membrane are in contact, and at equilibrium, the ratio of the O_2 dissolved in the lipid to the amount dissolved in water (i.e., $\beta_l O_2 / \beta_w O_2$) is known as the "partition coefficient" or the "distribution coefficient" (Kwon 2007). The partition coefficient for the Battino et al. (1968) data, 0.116/0.0263, produces a value of 0.44. The significance of the partition coefficient is its utility as a corrective factor for the estimation of DO_2.

Unlike $\beta_w O_2$, which can be calculated, $D_t O_2$ can be determined only through experimentation. Another important factor to consider is that DO_2 is temperature

dependent; so, in theory, experimental values would need to be determined across a range of temperatures, making estimation of D_tO_2 a potentially complicated process. Due to the complexity of determining molecular flux across micron-thick membranes using different membrane types, there is often much variability in reported diffusion rates, sometimes as many as four orders of magnitude (MacDougall and McCabe 1967).

Sidell (1998) reported that for the aerobic skeletal muscle in two groups of Striped Bass *Morone saxatilis* acclimated to 5 and 25°C, the measured average DO_2 values obtained by were 2.57 X 10^{-6} cm^2/s and 2.5 X 10^{-6} cm^2/s, respectively. These values are remarkably similar despite there being a 20°C difference in temperature. Early use of these values in the RMD proved insufficient to account for known temperature effects on membrane diffusion. Although some tissues like muscle may have evolved the capacity to alter membrane properties as an acclimation response to varying temperature, the reported values are not in agreement with other sources such as Fischkoff and Vanderkooi (1975) who report a more than two-fold increase in measured diffusion rates in erythrocyte plasma membranes at 25°C (2.2 X 10^{-5} cm^2/s) and 45°C (4.9 X 10^{-5} cm^2/s). The diffusion rates reported by Fischkoff and Vanderkooi (1975) are about ten times higher than the diffusion rates reported by Sidell (1998). These values are also much greater than the diffusion rates reported by Krogh (1941), who gave the respective diffusion rates of O_2 at 20°C through muscle and connective tissue to be 2.3 X 10^{-7} cm^2/s

and 1.83 X 10^{-7} cm^2/s.[7] Krogh's slower rates of diffusion could be due to his method of sample preparation in which the sample tissue may have been damaged as there is some speculation that in healthy tissue mitochondrial oxygen consumption creates a "pumping action which promotes microturbulence of the cell protoplasm" (MacDougall and McCabe 1967). Extensive human biomedical research regarding O_2 diffusion rates at 37°C produces rates of 1.0 X 10^{-5} cm^2/s for connective tissue (Weibel 1984), 7.0 X 10^{-6} to 2.0 X 10^{-5} cm^2/s for small-intestine submucosa, and 1.9 X 10^{-5} to 3.1 X 10^{-5} cm^2/s for the acellular tissue matrix Alloderm® (Androjna et al. 2008). The nearly threefold difference in diffusion rates at a fixed temperature from small intestine-submucosa data published by Androjna et al. (2008) demonstrates the variability and difficulty in establishing representative diffusion rates for any given tissue.

For modeling purposes, the study by Fischkoff and Vanderkooi (1975) of DO_2 across erythrocyte membranes at 25, 28, 37, and 45°C provided the most comprehensive data for use in the RMD. Because the equilibrium O_2 concentration would be greater within the cell membrane than in the more aqueous cell interior, it would impact the overall DO_2 through the cell membrane; therefore, Fischkoff and Vanderkooi (1975) divided their initial results by the Battino et al. (1968) partition coefficient of 4.4, with the understanding that due to limited data it is not known if this coefficient holds across all temperatures and membrane types. The partition coefficient values are supported by

[7] Values were converted from Krogh's 1941 text values for diffusion which are in cm^2 per minute rather than per second.

Windrem and Plachy (1980) who measured diffusion through phosphatidylcholine bilayers from 20 to 80°C. Diffusion rates at 20°C were determined to be between 1.0 X 10^{-6} cm^2/s and about 1.6 X 10^{-6} cm^2/s with long-chain phospholipids having higher rates of diffusion (Windrem and Plachy 1980).

As the actual [O_2] in the cell membrane and the interior of the cell are not in equilibrium, use of the partition coefficient DO_2 values in the RMD might not be exact. Still, without more definitive data from other sources, these data were accepted and used to calculate DO_2 in RMD. Using the Fischkoff and Vanderkooi (1975) data, values were plotted and fit to an exponential curve as shown in Figure 23. An exponential curve was determined to be the best fit and is consistent with other data for O_2 diffusion in water (Dejours 1979) and phosphatidylcholine bilayers (Windrem and Plachy 1980).

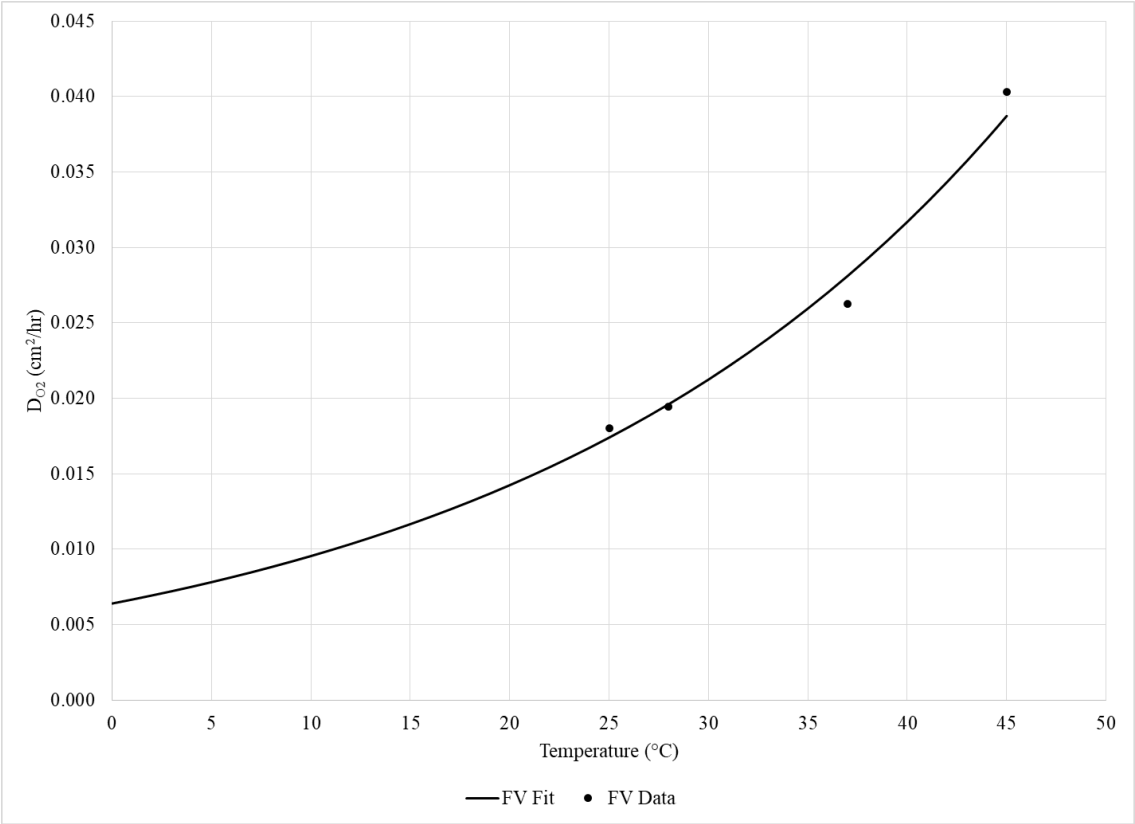

Figure 23. Plot based on erythrocyte plasma membrane diffusion rates and temperature as reported by Fischkoff and Vanderkooi (1975).
Data fit with exponential empirical curve ($DO_2 = 0.0064e^{0.04 \cdot T}$) by temperature. Oxygen diffusion rate converted to (cm^2/h).

Having established a representative value for β_iO_2 and D_iO_2, along with their caveats, the Krogh constant could be obtained. Within RMD, the units used are mL O_2/cm·hr·mmHg.

Gill Surface Area Estimation

Measuring gill surface area involves the tedious process of dissecting out the gill arches of a fish, counting the number and average length of gill filaments, obtaining the average number of lamellae per filament then obtaining the average lamellar surface

area using a microscope and *camera lucida* (Gray 1954). Through a commendable effort, Gray (1954) obtained reasonable allometric estimates of gill surface areas per gram of body weight for 31 species of fish, including three flatfish species: Sand Flounder *Lophopsetta maculata*, Winter Flounder *Pseudopleuronectes americanus*, and Summer Flounder. Given that SFL are within the same genus as the Summer Flounder, values for Summer Flounder were used for the development of RMD under the assumption that SFL gill surface-area relationships would be comparable. Gray's estimates for the Summer Flounder were based on an analysis of five fish with an average weight of 766 grams. Results were an average gill area/g fish of 242 square millimeters (mm^2), with maximal and minimal ranges of 328 mm^2 and 206 mm^2. The 242 mm^2 was used in RMD as the average gill surface area but converted to 2.42 cm^2/g fish for ease of calculation with other model components.

The question as to whether the gill surface area to body weight scaling relationship remains constant over the lifecycle of the flounder is difficult to answer due to limited specific data. A review of allometric scaling in fish and other species' respiratory surface areas by Schmidt-Nielsen (1984) suggests a linear relationship when weight is scaled logarithmically. The problem with logarithmic scaling is that differences at smaller scales are difficult to see as they get smoothed out in relation to the overall grand scale of such analyses. For example, a study by Oikawa and Itazawa (1985) evaluating the Common Carp *Cyprinus carpio* showed that the gill and body surface area in relation to body mass had a "triphasic allometry" difference between pre-larval (0.0016 to 0.003 g), post-larval (0.003 to 0.2 g) and juvenile and larger (> 0.2 g)

stages with allometric growth slopes of 7.066, 1.22 and 0.794 for each stage, respectively. The pre-juvenile growth slopes indicate that gill area growth is very rapid early in Carp development; however, a greater gill growth rate does not necessarily mean an increase in gill O_2 diffusion capacity as gill capillary development (i.e., perfusion) may not be complete. Although there are no conclusive data that differences in allometric growth occur in SFL, these observations give a reason to carefully consider the accuracy of gill area estimates, and hence diffusion capacity, for SFL below 1 g. However, as SFL below 1g appear to obtain a large percentage of their O_2 through cutaneous diffusion, as do many fish in the larval stages of development (Oikawa and Itazawa 1985), differences in O_2 contribution by the gills at this development stage may not significantly impact overall $\dot{V}O_2$.

Gill Diffusion Distance

The gill diffusion length, $l_{g,}$ is the membrane distance separating the oxygenated water from the red blood cells within the lamellar capillaries. The distance varies, with hypoxia intolerant species having short diffusion distances, e.g., 5 μm, while hypoxia tolerant species have longer distances, e.g., 10 μm (Perry and Gilmour 2010). This contrasts with Randall (1970), who reported gill epithelial thickness as typically between 1 to 5 μm. Since oxygen must pass through both gill and capillary cell membranes, and assuming capillary endothelial thickness is comparable to that of gill epithelium, the combined diffusion distance will be at least 2 to 10 μm and within the range reported by Perry and Gilmour (2010). Since the actual l_g for SFL is unknown, a value of 5 μm was chosen for RMD.

Cutaneous Diffusion

The role of cutaneous diffusion as an auxiliary mechanism for increasing $\dot{M}O_2$ independent of the respiratory system has been well established for flatfish (Kirsch and Nonnotte 1977, Nonnotte and Kirsch 1978, Dejours 1979, Steffensen et al. 1981). The process by which O_2 traverses the skin of the fish to the internal environment follows the pattern outlined in the gill diffusion equation (18); the only change required is to alter the sub-scripted indices from gill (*g*) to cutaneous (*c*):

$$\dot{M}O_2 = \left(K_c \frac{A_c}{l_c}\right) \cdot (P_w O_2 - P_v O_2) \tag{24}$$

As in the gill, K is Krogh's diffusion constant for cellular membranes, the value of which is assumed to be the same as for gill. The values for P_wO_2 and P_vO_2 in equation (24) also carry over from the gill equation as O_2 diffused through the skin is assumed to ultimately be integrated into the bloodstream, making P_vO_2 the lowest representative O_2 pressure for determining the pressure differential. It is recognized that this concession is not an accurate accounting because some of the O_2 diffused into the skin is consumed by the cutaneous tissue itself. In some fish species, the cutaneous-sourced $\dot{M}O_2$ is reported to be exclusively consumed by the skin while in other species, including flounder, there is a reported net inward flux of O_2 (Nonnotte and Kirsch 1978) beyond the skin, though some cutaneous O_2 very likely is consumed by skin tissues as well. Nevertheless, any influx of O_2 contributes to the whole organism's metabolic scope.

Where cutaneous values differ, and quite significantly, relative to those of the gills, are the cutaneous surface area (A_c) and diffusion distance (l_c). As a respiratory organ, the gill has undergone selective evolutionary pressures that have induced

morphological changes in the lamellae conducive to increasing surface area and reducing diffusion distance, with variances reflective of each species' environment (Hughes 1972, Hughes and Morgan 1973). Such adaptions result in rather delicate tissues protected by the opercula. On the other hand, skin and scales provide protection from the external environment.

The use of the skin as a site for respiration is strongly dependent on the thickness of the integument, which greatly affects the level of gas permeability and perfusion rate. Within vertebrates, cutaneous respiration is particularly significant in amphibians that have evolved highly vascularized and thin skin that in some species provides up to 100% of O_2 supply (Krogh 1904, Feder and Burggren 1985 Nov 1). Fishes, on the other hand, vary considerably in their use of skin respiration. Fish that have been shown to use cutaneous O_2 supplementation include Shanny *Lipophrys pholis*, Five-bearded Rockling *Ciliata mustela*, Butterfish *Pholis gunnellus*, Atlantic Cod *Gadus morhu*, Mudskipper *Periophthalmus modestus*, European Flounder, Common Sole, and the air-breathing swamp eels of the order Synbranchiformes. Even in these groups, cutaneous respiration primarily serves to supplement O_2 supply to the tissue and not as the primary O_2 source (Nonnotte and Kirsch 1978, Feder and Burggren 1985 Feb, 1985 Nov 1, Graham et al. 1987). A possible exception are scale-less eels whose skin appears to better facilitate cutaneous respiration (Nonnotte and Kirsch 1978). In many scaled fish species with cutaneous respiration, high skin capillary density is common and serves to offset the reduced diffusion capacity caused by the scales (Feder and Burggren 1985 Feb). Whether or not increased cutaneous capillarity is present in SFL is as yet undetermined.

Within flatfish, O_2 flux through the skin always appears to be less than that obtained through the gill. For example, in Plaice weighing 230 to 500 g, Steffensen et al. (1981) reported that under normoxic conditions (P_{O2} = 153 mmHg), cutaneous respiration accounts for approximately 27% of total $\dot{V}O_2$.[8] This lower $\dot{V}O_2$ compared to that for the gills is because diffusion distance across the skin (l_c) is considerably greater and diffusion area (A_c) considerably less than for the gill. Another factor not readily apparent is that while the skin surface area of flatfish increases with body size, a net benefit to diffusion, so does skin thickness (Burton et al. 1984), limiting diffusion. This dynamic has been observed in the Marbled Swamp Eel *Synbranchus marmoratus* and leads to a decline in cutaneous $\dot{M}O_2$ as the fish grows (Graham et al. 1987).

Flounder offer the added complication of differing skin thickness between the upper (eye side) and lower (blindside) surfaces, with the lower surface having thicker skin than the upper. For example, for a 250-g Winter Flounder, the upper surface skin thickness is between 40 to 50 μm while the lower surface thickness is around 55 μm (more than ten times the thickness of lamellae). For a 1000-g flounder, the values rise to about 55 μm for upper and 85 μm for lower surfaces (Burton et al. 1984). Thus, as Winter Flounder grow, cutaneous diffusion becomes more rate limited.

The impact of growth on skin surface area available for diffusion is generally positive; however, the overall diffusion efficiency declines with growth, primarily

[8] Interestingly, their data suggests that cutaneous $\dot{V}O_2$ is relatively greater under hypoxic conditions, with the skin contributing about 37% of total $\dot{V}O_2$ at an ambient P_{O2} of 40 mmHg.

because body surface area increases only by 2/3 that of increasing body mass (M_b) following the Surface Law shown in equation (25). Consequently, as overall tissue mass increases, which requires proportionally more oxygen, the rate of cutaneous O_2 diffusion across the skin cannot keep pace.

$$A_c = kM_b^{2/3} \tag{25}$$

This formula, first described by Meeh (1879), uses the coefficient *k* (sometimes called the Meeh coefficient) to account for differences in animal shape and density (Calder 1984, Schmidt-Nielsen 1984). For most animals, the value of *k* is estimated to range between 8 and 12; these values reflect that the majority of animals are essentially "round." Schmidt-Nielsen (1984) reports that the Meeh coefficient for typical fish is about 10. The Meeh coefficient for flatfish does not appear to have been of sufficient interest ever to have been estimated (nor at least published). More "flat" animals such as the bat and sugar glider are reported to have *k* values of 57.5 and 25.7, respectively, due to their flying membranes' large surface area. This idea encourages conjecture that flatfish morphology would itself support the case for an increased *k* value. Nevertheless, based on methods used to calculate a flounder's surface area (see below), the predicted *k* value for flatfish is also about 10.

The impact of the Surface Law can be represented by substituting A_c in equation (24) with equation (25).

$$\dot{M}O_2 = \left(K_c \cdot \frac{kM_b^{2/3}}{l_c}\right) \cdot (P_wO_2 - P_vO_2) \tag{26}$$

As can be ascertained from equation (26), the declining surface area with increased body mass is further degraded as skin thickness increases with increased body mass. The relationships of M_b to upper and lower epidermal thickness are described by Burton et al. (1984) as linear relationships with positive slopes as shown in equations (27) and (28).

Estimates from Burton et al. (1984) are, for mean upper surface epidermis (in μm)

$$l_{upper} = 0.0198M_b + 35.7 \tag{27}$$

; and, for mean lower surface epidermis (in μm)

$$l_{lower} = 0.04886M_b + 43.1 \tag{28}$$

These can be expressed symbolically, substituting the numerical values with the standard symbols for slopes as m and intercepts as initial skin thickness, l_0:

$$l_c = mM_b + l_0 \tag{29}$$

Substituting equation (29) into equation (26), $\dot{M}O_2$ from cutaneous diffusion can be expressed as a function of Krogh's coefficient, mass, and PO_2 differential:

$$\dot{M}O_2 = \left(K_c \cdot \frac{kM_b^{2/3}}{(mM_b + l_0)}\right) \cdot (P_wO_2 - P_vO_2) \tag{30}$$

The relevance of equation (30) is that it demonstrates that cutaneous $\dot{M}O_2$ efficiency can be expressed as being reliant upon body-mass-dependent surface area. Consequently, as a flounder's skin thickens with growth, cutaneous O_2 diffusion becomes less efficient. Cutaneous respiration in flounder may represent a spectrum, similar to the "triphasic allometry" in Common Carp gill surface area and mass reported

by Oikawa and Itazawa (1985). In that case, cutaneous $\dot{M}O_2$ in larvae and juvenile flounder augments total $\dot{M}O_2$ as the fish grows, eventually reaching an optimal l_c and A_c ratio beyond which surface area growth is incapable of keeping pace with increased skin thickness, leading to a net decline in cutaneous supplementation to total $\dot{M}O_2$. This proposition is supported by Graham et al. (1987) with the Marbled Swamp Eel, and by Rombough and Moroz (1997) with the larval Walleye *Stizostedion vitreum* , who report that cutaneous diffusion, "typically becomes limiting at a body mass of approximately 100 mg." Given that Walleye appear to not rely on cutaneous diffusion beyond the larval stage, but flounder do, the threshold of optimal l_c and A_c may be higher for flounder. RMD may facilitate the resolution of this issue and help guide further study.

Estimating Flounder Surface Area

A fundamental problem with using the Surface Law to calculate the surface area for SFL is not knowing the value for Meeh's constant (*k*), which, as mentioned, has not been experimentally determined. Another concern with this methodology is that not all organisms' surface area relationships necessarily follow the 2/3 power rule. Lacking experimental data, the surface area for RMD was calculated using geometric estimations.

The flounder body is essentially an ellipse with a tail, as shown in Figure 24. The surface area of SFL can be estimated by calculating the ellipse area corresponding to the fish's body length and width.

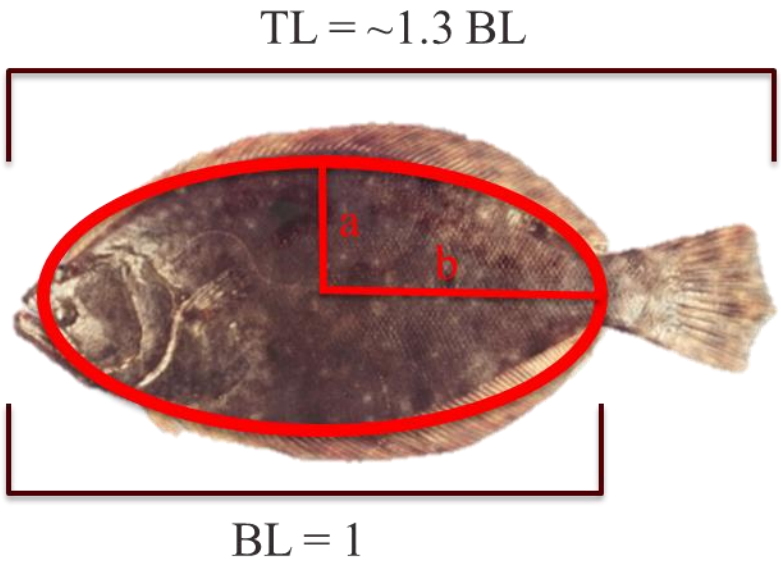

Figure 24. Estimation of flounder surface area using the ellipse.
Source: NOAA Photo Library.

The area for an ellipse is the product of pi (π) and the radii of the width (a) and length (b) of the ellipse.

$$A_E = \pi ab \tag{31}$$

Like most fish, size data for SFL is most often reported as the total length (TL) from snout to end of the caudal fin. To calculate the body surface area of an "elliptical fish" without the tail, a method was devised to convert TL measurements to body length (BL), or the length of the body minus the tail fin and caudal vertebrae (not to be confused with standard length which ends at the last tail vertebrae). If BL, and hence long diameter of the ellipse (i.e., b^2), is assumed to have an arbitrary value of 1, then the fin and caudal vertebrae length can be compared to BL. From photographs of SFL, it was estimated that tail lengths average approximately 1/3 body length. Therefore, the

total length of the SFL is roughly 1.3·BL. The ratio of BL to TL = 1/1.3 = 0.77. Body length of SFL can be roughly estimated from TL using the conversion equation (32).

$$BL = 0.77 \cdot TL \tag{32}$$

Once BL is determined, the radii width (a) and length (b) can be determined. The radius of the length is half the BL (½BL). For a true ellipse, the radius of the width is half that of the length radius, making the width radius a quarter of BL (¼BL). Thus, armed with only TL, a rough estimate of surface area for the SFL can be calculated by substituting equation (32) and appropriate ratio denominators into equation (31) to produce equation (33) for calculating the total surface area.

$$A_{SFL} = 2\left(\pi \cdot \left[\frac{0.77 \cdot TL}{2}\right] \cdot \left[\frac{0.77 \cdot TL}{4}\right]\right) \tag{33}$$

The calculated area of equation (33) must be doubled because SFL have two surfaces, upper and lower.

To be sure, the total amount of estimated surface area for diffusion will be somewhat larger than calculated because the formula ignores the surface area of the tail altogether and also fin tissue. This method also ignores the slightly increased surface area due to the body's curvature, treating each side as a flat surface. The measure, therefore, is a rough and conservative estimate of total surface area at best.

Using equation (33), the estimated total surface areas based on TL for 777 SFL measurements at the MDC were calculated. Total length estimates were then compared to the Surface Law estimates using the corresponding weight data from the MDC SFL data with a Meeh coefficient of 10 based on the value given for round fish by Schmidt-Nielsen (1984). The results are shown in Figure 25. The power estimate of 0.69 from

the MDC data is close to the 2/3 (0.67) power estimate of Meeh (1879),while the Meeh coefficient of 9.88 for the MDC data indicates that SFL surface area coefficient aligns closely with the Meeh coefficient given by Schmidt-Nielsen (1984) for fish.

The relation of weight to TL for appropriately nourished SFL is comparable to other flounder species as shown in Figure 13. Therefore, this geometric estimation of surface area may be useful for calculating surface areas for other flounder species, should such need arise, providing they too have an ellipsoid morphology.

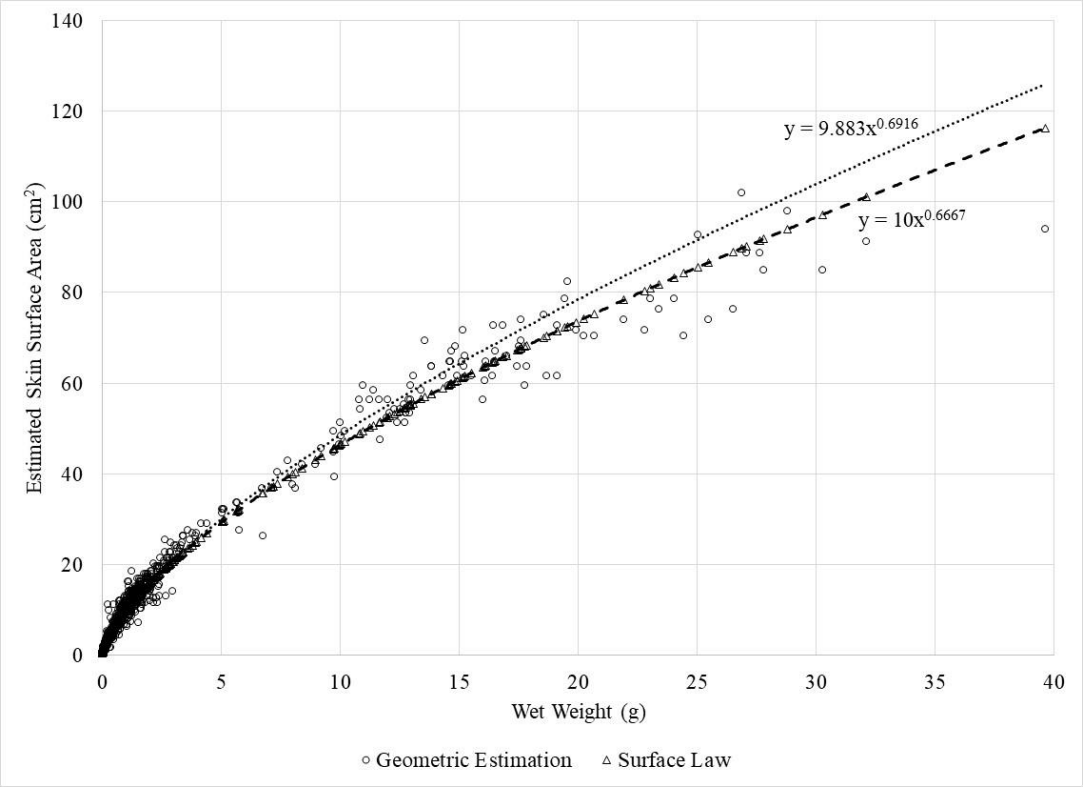

Figure 25. Comparison of surface law to geometric surface area estimates.
SFL total length and weight data used for calculations based on 777 measurements collected from 2009 to 2017 at the MDC, Corpus Christi, TX. Surface Law Meeh coefficient of 10 based on fish estimates from Schmidt-Nielsen (1984).

Blood Oxygen Transport

The blood oxygen transport formula shown in equation (21) models the flow of O_2 as carried through the circulatory system via the blood after crossing the gill membranes. While the gill formula describes the transitional movement of O_2 from the external to the internal environment, the blood oxygen transport formula describes, at least in theory, the distribution of this O_2 throughout the volume of the internal milieu. The conductance processes of this formula are $\dot{Q}$ and arterial blood O_2 concentration (C_aO_2).

Cardiac Output ($\dot{Q}$)

The determination of metabolic oxygen consumption in flatfish is predicated on estimating oxygen diffusion and blood perfusion in the gills. Perfusion is dependent upon cardiac output ($\dot{Q}$, mL/min·kg), which is a function of heart rate (HR) and ventricular stroke volume (SV, mL/kg). Determining $\dot{Q}$ in fish often requires direct measurement of heart rate and blood flow out of the heart using a surgically implanted transonic blood-flow probe placed directly around the ventral aorta (Joaquim et al. 2004, Mendonca and Gamperl 2010), a delicate and difficult task.

Allometric Estimation of Stroke Volume in Flatfish

To estimate $\dot{Q}$ for RMD, estimation of SV versus body size for SFL is required. As no method for SV estimation could be found in the literature and given the lack of access to specialists with the required skill set, and equipment, it was necessary to develop an indirect method to achieve this objective.

Schmidt-Nielsen (1984), citing data on heart size from 34 species of teleost fish, obtained the following equation for estimating heart mass (kg) where M_b is body mass in kg:

$$M_h = 0.0022 M_b^{1.026} \tag{34}$$

Thus, according to Schmidt-Nielsen, heart mass is about 0.22% of body mass, independent of body mass variation.

The next step was to calculate ventricle mass (M_v) and from that, because ventricular volume determines stroke volume, to estimate the relationship between M_v and SV. This task was achieved by using morphometric data from Joaquim et al. (2004) for two groups of Winter Flounder (one group raised at 4°C and the other at 10°C) to estimate the mean values of M_b, Ventricle mass (M_v), $\dot{Q}$, HR, SV, and stroke volume per gram of ventricular mass (SV_{vm}).

Heart mass can be estimated from equation (34) using mean body weights obtained from the two sample groups reported by Joaquim et al. (2004) at 4°C (n = 7, mean weight = 567 g or 0.567 kg), designated M_{h4}, and 10°C (n = 8, mean weight = 675 g or 0.675 kg), designated M_{h10}. Using the provided masses (in kg) gives the following estimates:

$$M_{h4} = 0.0022 \cdot 0.567^{1.026} = 0.00123\ kg = 1.23\ g \tag{35}$$

$$M_{h10} = 0.0022 \cdot 0.675^{1.026} = 0.00147\ kg = 1.47\ g \tag{36}$$

The next step was to estimate the percentage of M_h that is ventricular mass. This step was achieved using equation (37):

$$\% M_v = \frac{Mean\ Ventricle\ mass}{Estimated\ M_h} \cdot 100\% \quad (37)$$

Joaquim et al. (2004) estimated that mean M_v values for the 4 and 10°C groups were 0.28g and 0.34 g, respectively. Using these values, the percent ventricular mass can be estimated:

$$\% M_{v4} = \frac{0.28}{1.23} \cdot 100 = 22.8\% = \sim 23\% \quad (38)$$

$$\% M_{v10} = \frac{0.34}{1.47} \cdot 100 = 23.1\% = \sim 23\% \quad (39)$$

These particular estimates show that the relationship of ventricular mass to heart mass is about 23% for both temperature groups independent of weight. If this relationship is assumed to be valid across all weights, then M_v can be estimated as approximately 23% of total M_h for flounder as shown in equation (40).

$$M_v = 0.23 M_h \quad (40)$$

Using this estimate of ventricular mass, the next step was to determine the relationship between ventricular mass and ventricular stroke volume (S_{Vm}). This value also could be estimated from S_{Vm} data obtained from Joaquim et al. (2004), who give the S_{Vm} mean values for the 4 and 10°C groups as 1.05 (±0.12) and 0.95 (±0.11) mL/g ventricle, respectively, or an average of about 1 mL/g ventricle. Assuming a 1 mL/g ventricle output across all weights (and species), S_{Vm} can be converted from mL/g to

mL/kg by multiplying by 1000 g/kg. Thus, the per-kg SV relative to M_v and S_{Vm} becomes:

$$SV \cong M_v(1000 \cdot S_{Vm}) \tag{41}$$

Simplified, SV (in mL/kg) becomes:

$$SV \cong 1000M_v \tag{42}$$

Estimating stroke volume for a fish of specific body mass (SV_b) is calculated by dividing (42) by the total body mass of the fish:

$$SV_b \cong \frac{1000M_v}{M_b} \tag{43}$$

Substituting the results from equation (40) for M_v and simplifying, SV_b becomes:

$$SV_b \cong \frac{230M_h}{M_b} \tag{44}$$

Substituting equation (34) for M_h in equation (44) and simplifying, SV_b becomes a function of M_b (kg) as shown in equation (45). Thus SV may be calculated based solely on the mathematical ratio of the fraction of body mass that is M_v and total body mass:

$$SV_b \cong \frac{0.506M_b^{1.026}}{M_b} \tag{45}$$

Using the formula as a rough estimate and plotting stroke volume (mL/kg) against log10 weight (kg), a linear estimation of SV for flatfish in general vs. log weight can be generated (Figure 26).

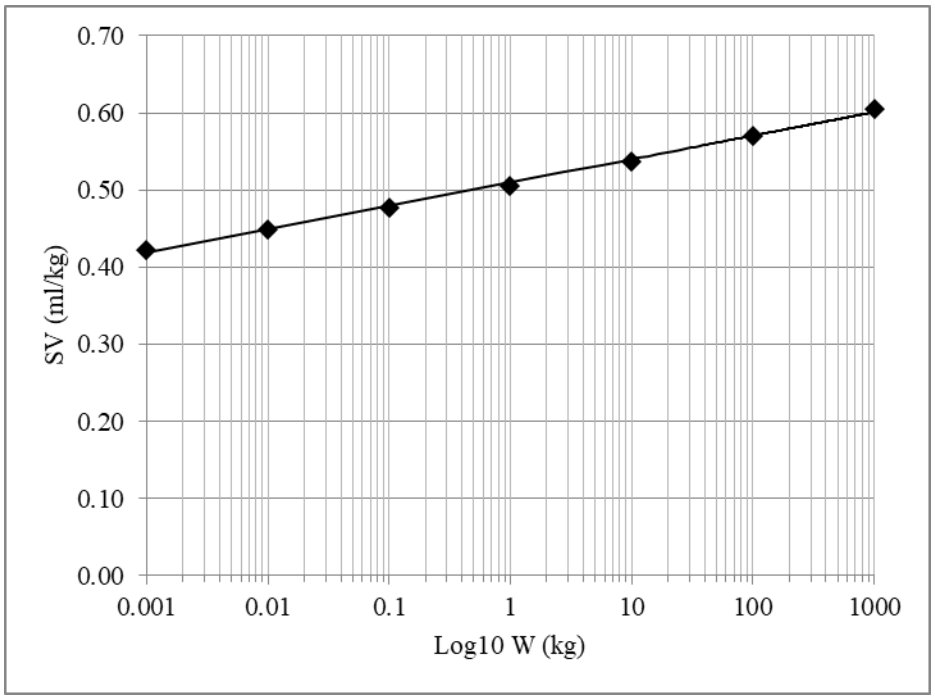

Figure 26. Estimation of flatfish stroke volume (mL/kg) vs. $\log_{10}$ weight (kg).
Based on equation (45).

Comparison of Allometric SV Estimation to Literature Values

Santer et al. (1983), directly measuring the body, heart and ventricle mass for 27 European Plaice reported the percent heart to body mass ratio to be 0.06% (± 0.023%), almost four times less than the value obtained here based on the Schmidt-Nielsen (1984) estimate. However, the Santer et al. (1983) estimate of the ventricle to heart mass ratio was 58.57% (± 11.5%), over twice the estimate obtained using the above calculations. More importantly, Santer et al. (1983) calculated the percent ventricle to body mass ratio to be about 0.035% (± 0.012%) producing an estimated SV of 0.35 mL for a 1 kg fish.

Other literature sources are somewhat more favorable to the allometric estimate. In the study by Mendonca and Gamperl (2010), two experimental groups of Winter Flounder were exposed to either 1) graded hypoxia (100% to 20% of air saturation) in sub-groups of 8°C and 15°C acclimated fish, or 2) acute temperature increase in 8°C acclimated fish with the temperature increased at 2°C per hour to a maximum of about 26°C. Blood flow was measured via cannulation of the caudal artery, and fish allowed to recover for 24 hours post-operation. Resting SV in the graded hypoxia, 8°C group, was 0.51 mL/kg until DO fell to about 30% air saturation at which SV rose to an average of 0.74 mL/kg. The graded hypoxia 15°C-acclimated fish were estimated to have a resting average SV of about 0.3 mL/kg which remained relatively unchanged even at 20% air saturation. The discrepancy between the allometric estimate and the literature value may, speculatively, be due to decreased cardiac demand in the 15°C acclimated group. For the acute temperature increase group (n=8, mean mass 0.54 ± 0.05 kg), SV ranged between 0.3 to 0.35 mL/kg below 18°C. Above 18°C, SV increased to 0.4 mL/kg, with a maximum of 0.45 mL/kg at 26°C. Mendonca et al. (2007), in a comparison of Winter Flounder cardiac performance to that of other species, indicated that fish acclimated at 8–10°C had an estimated resting SV of 0.21 (±0.09) mL/kg, and a maximum estimated SV of 1.1 (±0.14) mL/kg. However, in that study, resting SV was obtained in anesthetized fish and maximum SV determined by artificially increasing the pressure of returning blood to the heart. A more realistic appraisal of the resting versus active swimming SV of Winter Flounder is provided by Joaquim et al. (2004), who directly measured SV via transonic blood flow meters implanted in Winter Flounder

acclimated at 4 and 10°C and allowed to recover from surgery before experimentation began. Their results show that for resting flounder, SV averages 0.5 (±0.08) and 0.47 (±0.05) mL/kg in 4 and 10°C acclimated fish, respectively. During active swimming, Joaquim et al. (2004) report SV increased to 0.8 (±0.07) and 0.74 (±0.1) mL/kg in 4 and 10°C acclimated fish, respectively.

The SV estimation using the allometric method is close to the resting values for 4 and 10°C-acclimated fish reported by Joaquim et al. (2004). Results are also within the SV range for the graded-hypoxia 8°C-group of the Mendonca and Gamperl (2010) study but greater than their 15°C-graded hypoxia and acute-temperature-increase groups. Allometric SV estimates are much greater than those reported by Mendonca et al. (2007), but as they used sedated fish, this may have reduced SV output below that of non-anesthetized fish as suggested by the results of the other two studies. Therefore, it may be prudent and conservative to consider SV's allometric estimation as not representative of a truly resting SFL, a provision commensurate with RMD's assumption that SFL will be primarily resting but will have brief periods of activity over the one-hour interval simulated by the model.

Activity, Temperature and Hypoxia Effects on $\dot{Q}$

Activity increases metabolic demand and $\dot{Q}$, each of which rises appropriately as swimming speed increases (Duthie 1982, Joaquim et al. 2004, Ohlberger et al. 2005). Interestingly, Satchell (1991) asserts that, with increasing $\dot{Q}$ in fish, "Most of this increase is in stroke volume, little or none in heart rate." According to Satchell (1991), this is contradictory to what is seen in "higher" vertebrates. While this may be true for

most fishes, flatfish may be an exception to this rule. In the study by Joaquim et al. (2004), the 4°C- and 10°C-acclimated groups, when subjected to increased speeds by forced swimming showed an increase in $\dot{Q}$, but this increase was due almost exclusively to an increase in HR. Not surprisingly, the HR increase for the 10°C group was about 1.6 times that of the 4°C group, highlighting the significance of temperature on $\dot{Q}$ in particular and metabolic rate in general. The difference in SV between the two temperature groups was not significant, although Mendonca and Gamperl (2010) suggest some temperature effect on SV may occur.

RMD takes a neutral approach to activity effects on $\dot{Q}$. Given that flounder spend the majority of their time resting, and because RMD is designed to assess metabolic rate on an hour-to-hour basis, any short-term increase in an activity does not greatly affect the average resting metabolic rate.

The same is not valid for temperature and hypoxia effects on $\dot{Q}$. RMD accounts for temperature and hypoxia which are known to affect HR and, to a lesser extent, SV (Joaquim et al. 2004, Mendonca and Gamperl 2010, Capossela et al. 2012). The process by which this is accomplished in the model is tied to a series of non-physiological model components that are reserved for later discussion.

Oxygen concentration, like temperature, has an impact on $\dot{Q}$, again with HR being more affected than SV (Mendonca and Gamperl 2010, Capossela et al. 2012). The literature is clear that temperature has a significantly greater impact on $\dot{Q}$ than does low PO_2. Still, the relation of $\dot{Q}$ to hypoxia tolerance cannot be ignored as the two are intertwined. The ability of flatfish to accommodate hypoxia appears not to be due to the

gills' intrinsic efficiency, but to the cardiovascular system's ability to meet metabolic demand. Wood et al. (1979a) indicate that oxygen-transport efficiency across the gills is less than for highly active fishes such as Salmon. Flatfish respond to hypoxia by increasing gill perfusion through an increase in $\dot{Q}$, resulting in a lower ventilation-perfusion ratio ($\dot{V}_w/\dot{Q}$) compared to more active fishes. Other potential adaptations are effected within the blood by increased hemoglobin O_2 affinity (Weber and de Wilde 1975).

Blood O_2 Capacitance and Arterial-Venous Difference

Recalling that β_bO_2 is the ratio of the change in blood O_2 concentration (CO_2) to the change in arterial-venous PO_2, the product of β_bO_2 and $(P_aO_2 - P_vO_2)$ is C_aO_2 as shown in equation (21). RMD derives this value directly, calculating the arterial CO_2 (C_aO_2) by summing the amount of O_2 bound to hemoglobin (HbO_2, mL O_2/mL blood) and the amount of O_2 carried within the blood plasma (mL O_2/mL plasma). The amount of O_2 dissolved in plasma is relatively minimal and varies with temperature. Without any definitive data for O_2 solubility in SFL blood plasma, the SFL uses the solubility of O_2 in water. This value could be eliminated from the model without significant consequence but was included for model fidelity to observation. The primary component of C_aO_2 thus falls to the HbO_2 component. This variable is itself a function of the amount of Hb present in 1 mL of blood. For a healthy SFL, this is 0.15 g Hb/mL blood (Watters and Smith 1973, Park et al. 2012). The amount of oxygen carried by a gram of Hb in the Starry Flounder is about 1.12 mL O_2/g Hb (Milligan and Wood 1987), assuming the Hb saturation fraction determined by the Hill equation.

Hemoglobin Saturation and the Hill Equation

Except in a few rare instances, organisms reliant on blood O_2 transport do so by binding O_2 to one of four known proteins: hemoglobin, hemocyanin, chlorocruorin, or hemerythrin. Depending on the organism, these proteins can be carried in solution (all four proteins) or within blood cells (Hb and hemerythrin). In the majority of vertebrates, O_2 is transported in the blood exclusively by hemoglobin contained within cells (Willmer et al. 2005); the exception being the Antarctic Icefish *Chaenocephalus aceratus*, which lacks Hb and relies solely on O_2 dissolved in the blood plasma (Perry and Gilmour 2010).

The Hb protein structure is tetrameric, consisting of two pairs of α-chain and β-chain protein subunits. Within each subunit is a single porphyrin ring containing an iron atom in ferrous (Fe^{2+}) form, collectively called a "heme group" (Cameron 1989, Willmer et al. 2005). Each heme group can reversibly bind a single O_2 molecule, meaning that each Hb molecule can bind and transport up to four O_2 molecules. An important characteristic of the Hb molecule is its allosteric properties, whereby deoxygenated Hb maintains a "tense" state which has a low O_2 affinity. Binding of O_2 to the heme group of a single sub-unit induces conformational changes in the other sub-units causing the other sub-units to become "relaxed," increasing their affinity to O_2. This transition from tense to relaxed state progresses until all sub-units are bound with O_2 and is the main contributor to the familiar sigmoidal shape of the oxy-hemoglobin saturation curve (Stryer 1981). However, this sigmoidal shape may be altered by environmental and physiological conditions.

The binding of molecular ligands to receptors was famously modeled in the early 20th century by Hill (1913) and Barcroft (1913), commonly referred to as the Hill equation. Though not a physical descriptor of actual ligand-receptor physics (Weiss 1997), the Hill equation is adequately descriptive of O_2Hb saturation, often represented as Y in keeping with Hill's chosen designation, though in this iteration, the equation can be modified from a more generic form to that shown in equation (46):

$$Y = \frac{{PO_2}^n}{{P_{50}}^n + {PO_2}^n} \tag{46}$$

where PO_2 is oxygen pressure, P_{50} is the oxygen pressure at 50% Hb saturation, and n is the Hill coefficient.

Presumptively, the value of *n* represents the number of O_2 binding cites on Hb molecule, but even Hill (1913) understood this was not a valid representation. More accurately, the Hill coefficient represents an "interaction coefficient," signifying the "cooperativity" of O_2 with Hb (Monod et al. 1965). In this context, the Hill coefficient provides only an estimate of the minimal number of Hb binding sites involved (Weiss 1997). Nor is the Hill coefficient a fixed value as it, and the value for P_{50}, can vary with serum pH, although the variance in P_{50} is considerably greater than that seen for *n* (Weber and de Wilde 1975, Wood et al. 1975).

Environmental Adaptation and Variation in Flounder Hb Saturation

Given the extremes of environmental DO that fish encounter (the spectrum of which can run from hyperoxic down to anoxic), especially compared to the more favorable oxygen environment of land vertebrates, it is not surprising that selection

pressure has resulted in greater genetic variation in fish Hb compared to that of land vertebrates (Weber 2000). Across fish species, Hb adaptation reflects environmental history, with flatfish certainly being no exception, exhibiting variation in both pH effects on P_{50} and, to a lesser extent, on the value of *n* (Weber and de Wilde 1975, Wood et al. 1975).

Regarding the Hill coefficient in RMD, analysis of Hb characteristics in flounder by Weber and de Wilde (1975) was used to calculate *n*. Based on their data, the Hill coefficient for flounder lies within the range of 1.6 at pH 8.2 and 1.7 at pH 7.1. Compare to Plaice for which the reported Hill coefficient varied from 1.7 to about 1.9 at pH 8.2 and 7.1, respectively (Weber and de Wilde 1975). Increasing *n* results in a steeper rise in the Hb saturation curve centered on P_{50}.

Shifts in Hb saturation are impacted more by changes in P_{50} (PO_2 certainly also has an impact but is a property of the environment, not fish per se). Higher P_{50} values shift the Hb saturation curve to the right, shown in Figure 27, which compares the effects of different P_{50} values and Hill coefficients between the Starry Flounder and Rainbow Trout. The impact of pH, ATP, and temperature are not shown. Fish that are more aerobically active and less hypoxia tolerant like trout have higher P_{50} values correlating to a lower Hb affinity to O_2. This facilitates O_2 desaturation of Hb at the tissues but slows Hb saturation at the gills. Conversely, less active but more hypoxia tolerant species like flounder tend to have P_{50} values that are relatively low, corresponding to a greater Hb affinity to O_2. This affinity facilitates O_2 saturation of Hb at the gills but reduces the ease of O_2 "unloading" in the tissues (Perry and Gilmour 2010).

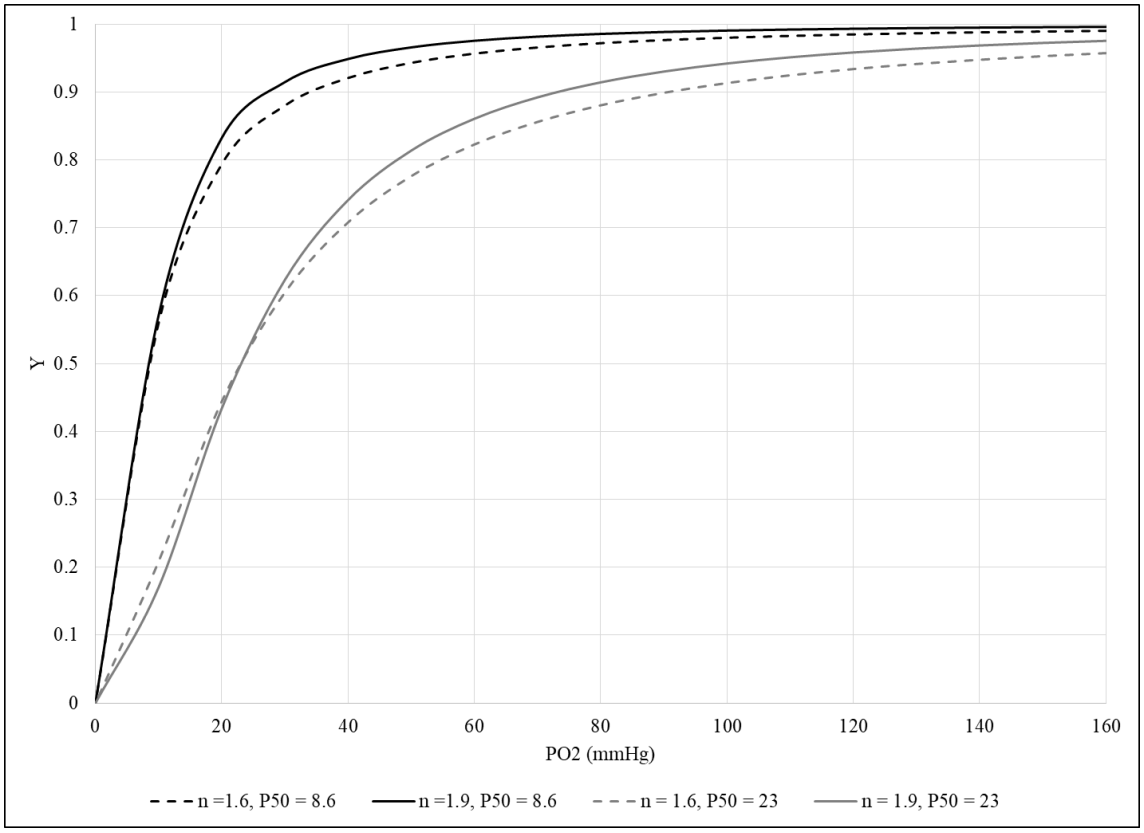

Figure 27. Hill coefficient and P_{50} effects on oxyhemoglobin saturation.
Black lines represent Starry Flounder, gray lines represent Rainbow Trout. Hill coefficient values adapted from Weber and de Wilde (1975), P_{50} values adapted from Perry and Gilmour (2010).

Multiple factors contribute to the shifting of P_{50}. Figure 27 highlights the impact of genetic adaptation differences between Starry Flounder and Rainbow Trout Hb genes resulting in amino acid sequence changes within α or β protein sub-units that alter the "tense" and "relaxed" characteristics, and hence O_2 affinity, of Hb (Weber 2000). More acute physiological shifts in P_{50} are the results of biochemical influence. The primary effector is pH, which profoundly impacts Hb affinity by lowering P_{50} as pH rises and increasing P_{50} as pH decreases. This is known as the Bohr effect, named after Christian

Bohr (Bohr et al. 1904) to whom is attributed discovery of this phenomenon. Other effectors shown to impact the O_2 carrying capacitance of blood in fish, and flatfish in particular, include temperature, chloride level, and organic phosphates such as adenosine triphosphate (ATP) and guanosine triphosphate (GTP) (Weber and de Wilde 1975, Weber 2000). Figure 28 presents a comparison of the effects of pH and temperature on P_{50} for three flatfish species.

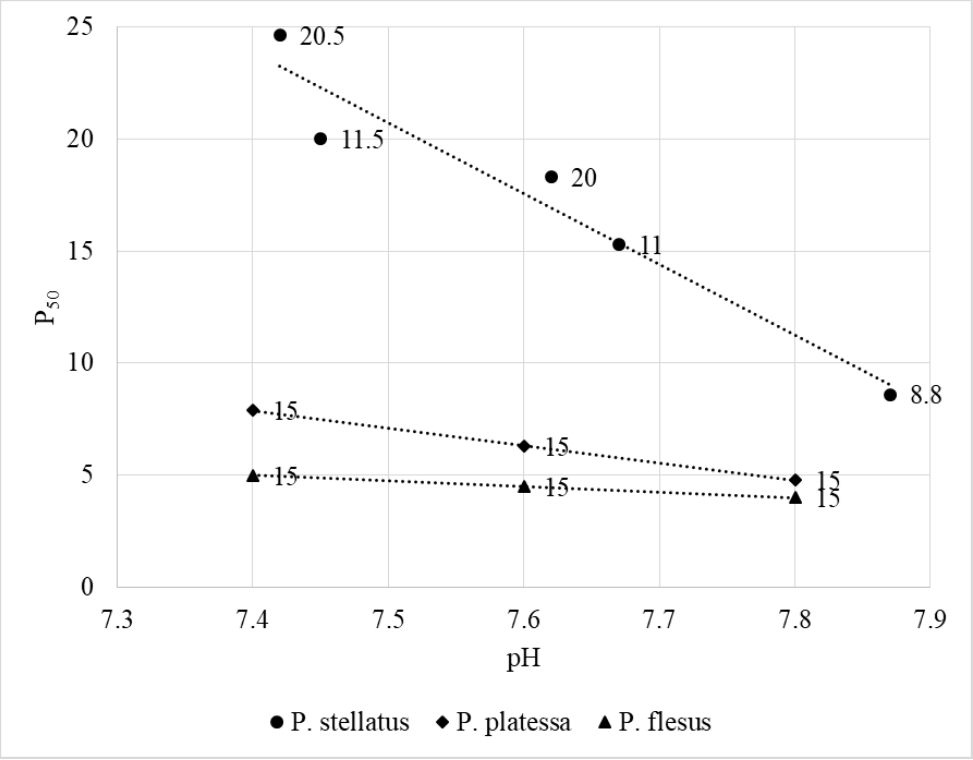

Figure 28. Genetic, pH and temperature effects on P_{50}.
Data points are coded by temperature in °C. Data for *P. stellatus* adapted from Watters and Smith (1973); *P. platessa* and *P. flesus* data adapted from Weber and de Wilde (1976).

The SFL respiratory model does not account for the effects of ATP, GTP, or chlorides on Hb affinity but does account for the effects of pH on *n* and P_{50}. The temperature effect is dealt with indirectly through its influence on pH, with pH decreasing linearly with increased temperature at a slope of -0.019/°C based on data presented in Cameron (1989), with a pH intercept set to 8.0 at T = 0°C.

Root Effect

A unique characteristic of fish Hb is the Root effect wherein certain conditions can lead to a reduction in the O_2 carrying capacity of Hb (i.e., inability to reach 100% nominal saturation). The primary effectors of the Root effect are low pH (high [CO_2]) (Root 1931) and high [ATP] in flatfish (Weber and de Wilde 1975). The Root effect's impact is somewhat controversial as pH must often fall below, and ATP concentrations rise above, normal physiological range for the effect to be seen (Weber and de Wilde 1975, Cameron 1989). Nevertheless, some fish like Plaice do appear to exhibit some degree of Root effect. However, with respect to flounder, the Root effect does not appear to be present at normal physiological pH and ATP concentrations (Weber and de Wilde 1975). Consequently, the Root effect is not factored into RMD.

Summary and the Oxygen Cascade

RMD attempts to model the flow of O_2 from the environment to the tissues using an elaboration of Fick's Law. This flow involves conductance and tension differentials (Jensen et al. 1993). Both affect the movement of O_2 which requires that work to be performed and thus metabolic energy to be expended. This work capacity comes from three energy sources – heat, chemical energy (in the primary form of ATP), and O_2

tension differentials. Interestingly, of these three, only tension differentials are directly addressed in Fick's formula, while effects of heat and chemical energy are implied.

In the case of tension differentials, the work capacity is the byproduct of O_2 consumption for ATP production via attachment of a phosphate group to ADP within the mitochondria, a process with maintains a low [O_2] relative to the external environment. This capacity provides the necessary work to move O_2 across membranes of the conductance components. Of course, the ATP produced is the primary energy source used by the muscles of the respiratory and cardiovascular systems to move O_2 across the gills ($\dot{V}w$) and distribute it throughout the organism ($\dot{Q}$), respectively. The minimum amount of ATP produced necessary to provide sufficient energy to just maintain $\dot{V}w$ and $\dot{Q}$, and other metabolic functions is the definition of SMR. Although ATP production is not exclusively dependent upon $\dot{V}O_2$ (Duthie 1982), the predominance of O_2 in total energy production has become a primary determinant of metabolic scope for eukaryotic organisms.

Understanding the physical and physiological processes involved in following $\dot{V}O_2$ from water to a cell is just the beginning of the journey. Application of these processes in an effective and efficient manner is necessary to accurately simulate $\dot{V}O_2$ within the SFL for use in metabolic processes such as growth across the animal's lifecycle under variable thermal, saline, and oxygen environments is the goal of RMD.

CHAPTER VI

THE FLOUNDER RESPIRATORY MODEL

The primary objectives of this investigation were to: 1) develop Respiratory Model, Dynamic (RMD), a mechanistic model of the dynamics of maximal oxygen uptake in Southern Flounder (SFL); and, 2) integrate RMD into the Stella® bioenergetic simulation model Ecophys.Fish (Neill et al. 2004), the latter first having been parameterized for SFL.

Although RMD was intended to simulate the cardiorespiratory and cutaneous O_2 uptake systems of SFL, the consequent model by necessity did incorporate data from other flatfish species. When possible, SFL data were used; but, if species-specific data were not available data preference was given to species within the same genus or closest taxon.

Model Overview

The functional and quantitative relationships described in the previous chapter were applied to help develop the stand-alone RMD. A good model is the integration of data and principles from multiple sources intended to enable adequate simulation of the modeled systems' dynamics. Just as the basic model schematic shown in Figure 21 acted as a springboard for discussing the physiological mechanisms and processes pertinent to RMD, the schematic shown in Figure 29 expands the view of these processes to highlight specifics used in the development of the Stella®-based RMD.

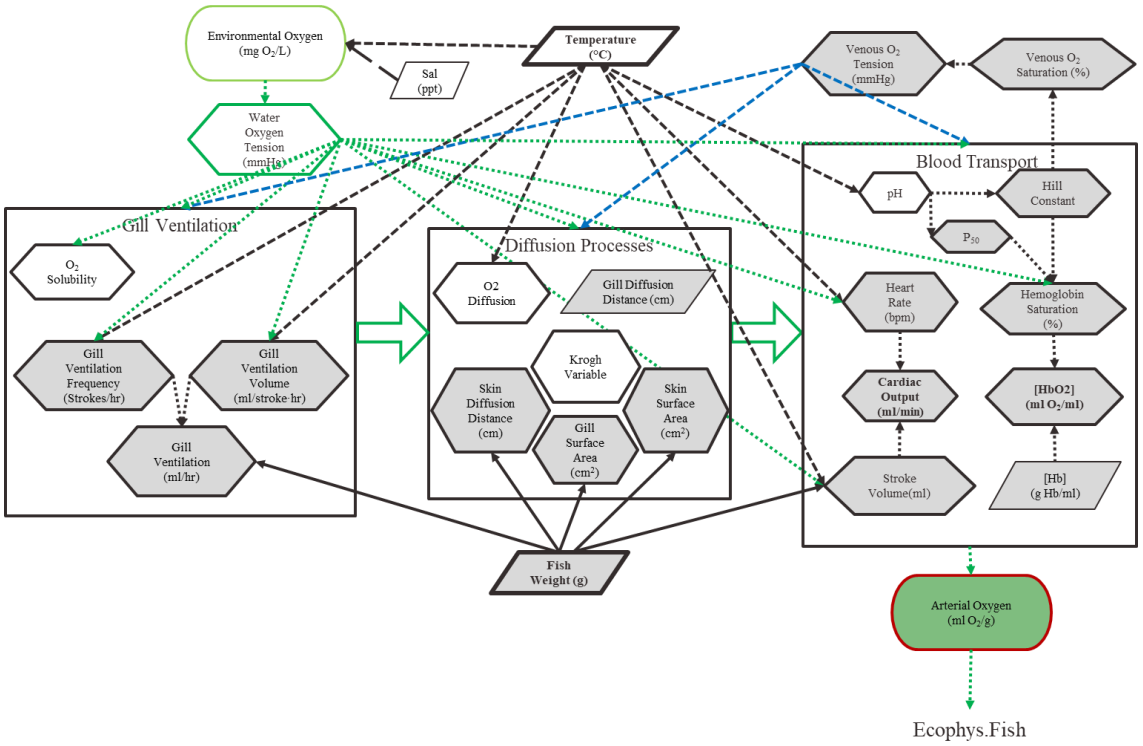

Figure 29. Flounder respiratory model (RMD) schematic.
Shaded components indicate physiological processes. Un-shaded components indicate physical or environmental inputs. Solid black arrows indicate fish weight (mass) input. Short dashed black arrows indicate temperature input while short dashed blue arrows indicated venous blood PO_2 input. Long dashed black arrows indicate salinity input. Large and dashed green arrows indicate oxygen flow and input, respectively. Oxygen is input on the upper left and flows to the right from gill respiration, diffusion via gill and skin, and blood transport in turn with the final output being $\dot{V}O_2$ for use in a bioenergetic growth model, e.g., Ecophys.Fish.

Model inputs can be either static (fixed) or variable using an equation or Stella® graphical function that allows the variables to change with each "step" of the model through time (DT). RMD's input variables include fish weight, temperature, O_2 pressure or fraction or DO (depending on the model variant), and salinity. Gill diffusion distance and blood hemoglobin concentration may be changed to simulate disease, anemia/blood loss, etc. However, these are held constant within a given "run" of the model.

While several factors influence physical components (e.g., salinity) and biotic states (e.g., animal weight), few have the impact of temperature, especially on poikilotherms such as SFL (Schmidt-Nielsen 1997). Temperature plays a pivotal role in the model, affecting physical variables such as PO_2 (a significant input in itself for all three major model processes), the Krogh coefficient via temperature effect on O_2 solubility, and pH. Physiological processes are also highly influenced by changes in temperature.

Other variables such as fish weight, and water and venous blood O_2 concentration, are also extensively used by the model. Weight plays an important role in the allometric estimation of the gill ventilation rate (based on buccal volume), cutaneous and gill surface area, cutaneous thickness, and heart size for estimating SV. Physical aspects of O_2 tension are used to determine O_2 solubility and diffusion (as driven by pressure differentials) through water and across tissue membranes. To account for physiological responses to hypoxia, the model uses O_2 tension input for the calculation of $\dot{V}O_2$ from the gills (via changes to respiration frequency and buccal stroke, or beat, volume) and cardiac function via hypoxia effects on HR, SV, and Hb saturation.

Calculations of O_2 output of the three main model components were handled as hourly $\dot{V}O_2$ calculations (in mL O_2/g fish·h) because volumetric O_2 flow is the most common unit used in the literature. Because some growth models such as E.F use mass flow, the RMD $\dot{V}O_2$ output is also converted to $\dot{M}O_2$ in mg O_2/g fish·h (not shown in the schematic).

The objective for each of the Ventilation, Diffusion (gill and cutaneous), and Blood Transport processes was to estimate the amount of oxygen each process provides given the available environmental O_2. Any potential intrinsic limitations within each $\dot{V}O_2$ model component (e.g., diffusion limitations due to temperature) limits the $\dot{V}O_2$ available for subsequent $\dot{V}O_2$ processes.

Model Formulas and Functions

Dynamic models such as RMD and E.F are mathematical chimeras, combining established theoretical equations like the Hill and Fick equations with empirical equations. Empirical equations are generated by taking available data and applying "best-fit" lines to provide estimates of data trends. However, empirical equations inevitably discount or ignore the variance seen in real-world systems.

Unless otherwise noted, every effort was made to have empirical equations in RMD closely approximate the physical and physiological data reported in the literature. In instances with limited literature data, fit lines were extrapolated. For example, this occurred when temperature data available from the literature did not extend to the model's full range. In some instances, relationships based on literature data were smoothed or adjusted if model outputs exceeded or fell short of known values. In these circumstances, outcomes were quite often achieved through trial and error and validated to the degree possible against data from experimental or literature sources.

RMD Input Processes Classification

To aid in understanding RMD input equations, as each is discussed, it will be given one or more of the following categorization descriptors:

- Empirical – an equation based on observed data, literature, or best-fit estimates (Riggs 1963).
- Theoretical – an equation/formula established in the literature which uses fixed and/or variable inputs to model a physical or physiological process (Riggs 1963). Examples are the Hill and Fick equations.
- Conversion – equation changes an input value unit to another unit for use in further calculations. For example, converting mL O_2/g fish·h to mg O_2/g fish·h.
- Decision – equation includes the use of logical (e.g., IF, THEN, AND, OR, ELSE) or selection (e.g., MAX, MIN) functions to direct the process path toward output. These types of functional relationships may include several equations and/or fixed values.

In addition to equations, model converters that provide inputs into processes will be described as follows:

- Fixed – input value is constant. Constants remain the same during a model run but may be manually changed between runs.
- Variable – input value may change during the model run. Method of change may be based on a formula or data set (e.g., a Stella® graphical input).

Model Components (Sectors)

RMD consists of eight preparatory sub-models (designated by sector frames in the model) that feed into the primary model which then calculates maximum-available

$\dot{V}O_2$. The arrangement of model stocks, flows, converters, and action connectors for all sectors is shown in Figure 30. An important aspect of the model is that while most physiological processes typically are measured in seconds to minutes, RMD uses a time interval (DT) of hours; so, all model values are converted to “per hour” outputs. This consideration was in tacit acknowledgment of RMD's intended integration into Ecophys.Fish which calculates growth on a per-hour basis.

The presentation of each model sector follows. Each narrative description is accompanied by a schematic of the sector that is being discussed. Action connectors within sectors are shown. Refer to Figure 30 to see action connectors between sectors. Sectors are arranged in the model to shorten flow connectors and make processes easier to follow, visually. Discussion of sectors, however, will be in a manner meant to facilitate understanding of the data flow process.

A concise listing of the RMD sector processes more amenable for conversion to other modeling systems or programming languages may also be found in Appendix B.

.

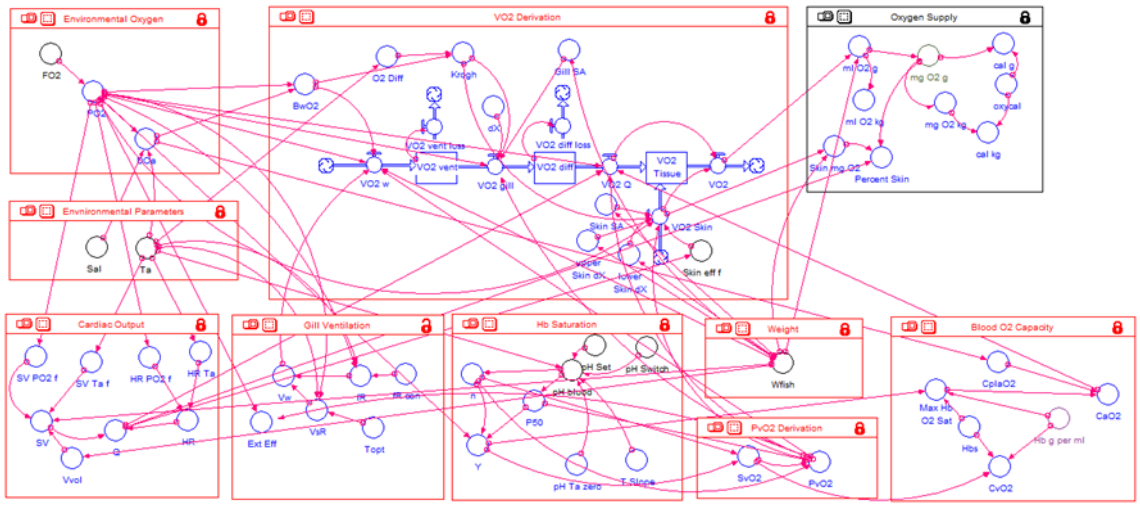

Figure 30. Flounder respiratory model (RMD) sectors.

Environmental Processes

Environmental processes shown in Figure 31 are direct inputs into the model. These inputs can be fixed or variable, depending on need. Salinity, "Sal," values are in parts per thousand (ppt) mass, with input ranging from 0 to 35 ppt. Ambient temperature, "Ta," is in degrees Celsius (°C) and ranges between 5 and 30°C for SFL. Any temperature can be input but temperature limitations within the model's Cardiac Output sector result in "death" of the SFL if the temperature falls below 4°C or exceeds 43°C. Inputs for all converters can be constants or variable using the Stella® graphical function or a time-dependent equation. These inputs represent the model's core starting processes as they establish the "environment" under which the model will operate.

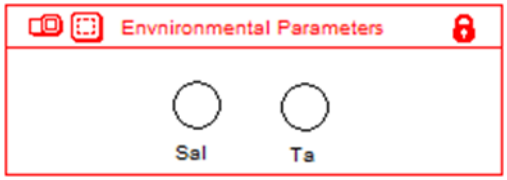

Figure 31. RMD environmental processes sector.

Environmental Oxygen

This sub-model, shown in Figure 32, is used to calculate the O_2 tension (as partial pressure, PO_2) from "FO_2," the oxygen fraction, and ambient dissolved oxygen ("DOa"), in mg O_2/L water.

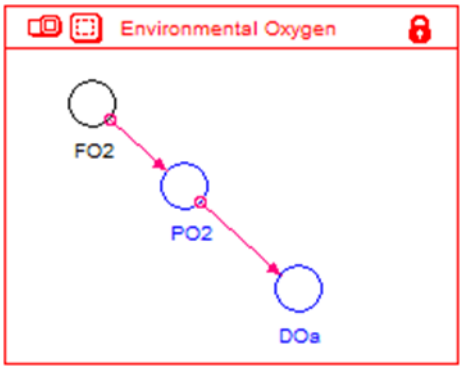

Figure 32. Environmental oxygen sector.

FO2 [Input: Fixed or Variable]

"FO2" sets the oxygen fraction used to calculate the partial pressure of O_2 in the water "PO2." The standard value used is 0.209 which represents the O_2 mass fraction in

the atmosphere. This value can be adjusted to produce lesser or greater "PO2" and "DOa" outputs.

PO2 [Equation: Theoretical]

Oxygen partial pressure, "PO2," or tension, is determined by Henry's Law of Solubility which assumes that the O_2 concentration in water is in equilibrium with the atmosphere. The value of "PO2" is the product "FO2" multiplied by 760 mmHg, the standard atmospheric pressure at sea level:

PO2 = 760*FO2

The use of standard atmospheric pressure of 760 mmHg must remain fixed because this value is used by the Green and Carritt (1967) equation to calculate "DOa." The use of a different barometric pressure will introduce error into the calculations. Adjustments to "PO2" can be made by changing the "FO2" value.

DOa [Equation: Empirical]

"DOa" uses an empirical equation developed by Green and Carritt (1967), with inputs of "Ta," "PO2," and "Sal," as follows:

DOa = (EXP((-7.424+(4417/(Ta+273.16))+(-2.927 * LOGN(Ta+273.16))
+ (0.04238*(Ta+273.16))) - ((Sal - 0.03)/1.805) * ((-0.1288 +
(53.44/(273.16 + Ta)) + (-0.0444 * LOGN(273.16 + Ta)) +
(0.00071 * (273.16+Ta)))))/22.414 * 32/760 * PO2)

Because three input processes determine the value of "DOa," the output value depends on initial conditions. If a specific "DOa" value is desired, the most efficacious

method is to adjust “FO2” to change the “PO2” output. While “Ta” and “Sal” may in theory be adjusted to produce a desired “DOa,” their influences on other model components would likely produce erroneous results. When running the model using laboratory or field data, the values of “Ta” and “Sal” can be changed to match observed conditions using a graphical function to produce results that are more representative of the conditions observed.

Gill Ventilation

This sector is used to calculate the flow of oxygenated water (mL water/g fish·h) across the gills, from which O_2 is extracted. Because the Gill Ventilation Sector (Figure 33) estimates the amount of O_2 in the water available for RMD input, it sets the maximal possible per hour $\dot{V}O_2$ value at any given DT.

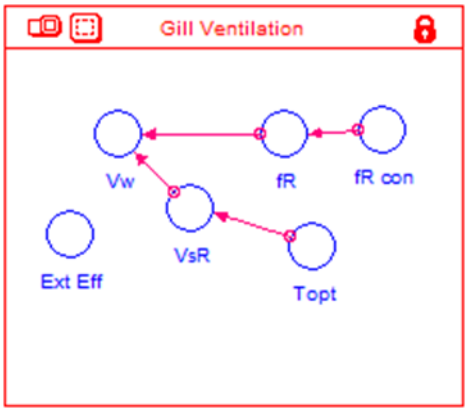

Figure 33. Gill ventilation sector.

fR con [Input: Fixed]

A fixed input constant to the breathing frequency calculation, "fR con" is used as a multiplier to adjust the respiratory frequency.

fR [Equation: Decision, Empirical]

Ventilation frequency, "fR," is affected by temperature and PO_2 (Kerstens et al. 1979, Steffensen et al. 1982, Tallqvist et al. 1999). Multiple methods were explored to derive ventilation frequency rates able to accommodate the effects of PO_2 and temperature across various ranges for each and still provide outputs that remain grounded in physiological reality. The result is an estimation of "fR" that relies upon establishing maximum and minimum decision processes to achieve outputs corresponding to the literature:

fR = (((-0.08*Ta^2+6*Ta)*fR_con)* 160/PO2) * MIN(1, PO2/30) *
MIN(1, PO2/20)

The output of "fR" is dependent upon inputs of "Ta" and "PO2" as well as a corrective constant "fR_con." The ventilation frequency equation "fR" has utility but cannot account for all potentially unknown variables. The solution to this problem was the adoption "fR_con" which can be used to adjust the output of "fR" to permit "Vw" values that allow for the production of $\dot{V}O_2$ outputs from RMD that are necessary to predict growth and model respirometry when integrated into E.F.

The temperature-dependent parabola -0.08*Ta^2+6*Ta provides for the non-linear temperature response baseline "fR" value shown in Figure 34. Modifications to account for changes in PO_2 are provided by taking the ratio $160/PO_2$ (160 mmHg is

assumed to be the max, but this can be set to a higher value if working with hyperoxic waters). This allows the ventilation rate to automatically increase as PO_2 declines so that the respiration rate doubles when PO_2 is 80 mmHg and quadruples when PO_2 is 40 mmHg.

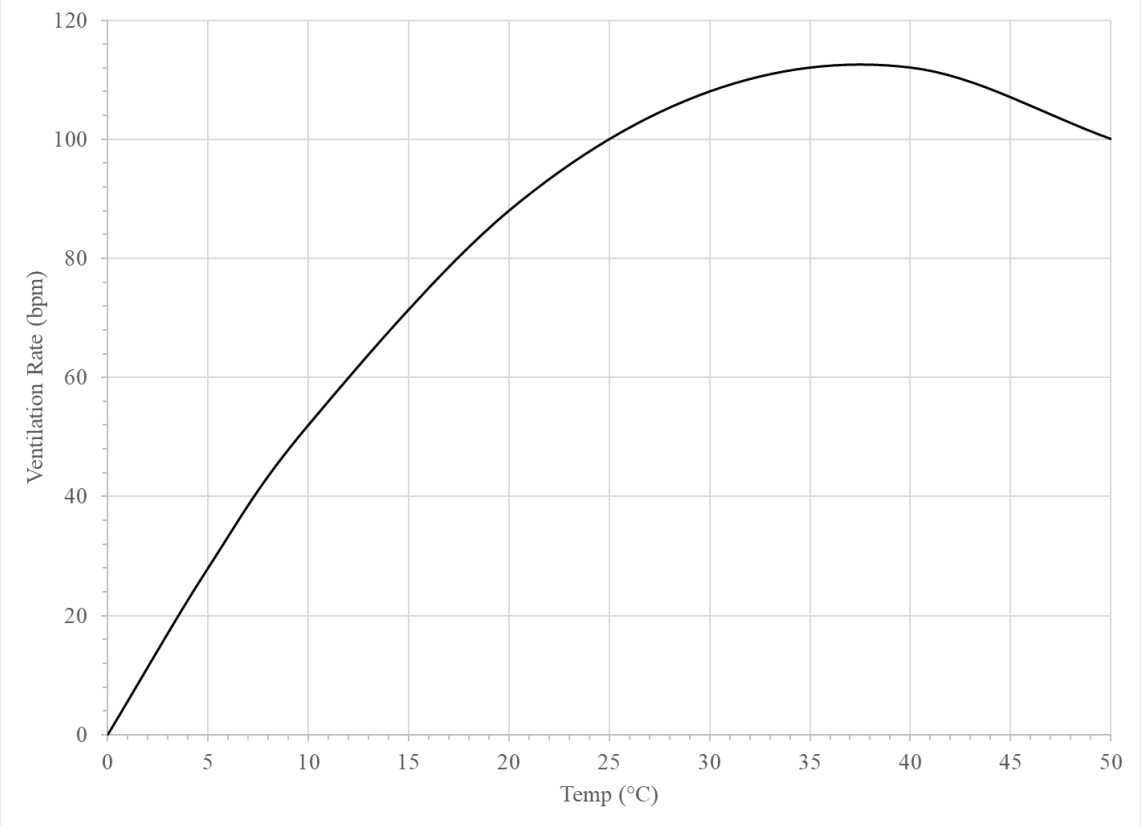

Figure 34. Baseline fR ventilation frequency.
Ventilation rate (beats/min) = -0.08*Ta^2+6*Ta. Values are multiplied by 60 within RMD to give beats/hr.

When PO_2 reaches 30 mmHg, ventilation rates level off and then decline or starts to decline immediately (Steffensen et al. 1982, Tallqvist et al. 1999). The method

chosen for RMD was to limit the peak "fR" at 30 mmHg with 20 mmHg PO_2 set as the point upon which "fR" starts to fall. This is achieved using the minimum functions MIN (1, PO2/30) and MIN(1, PO2/20). The output range of "fR" for various temperatures and PO_2 values is shown in Figure 35. In this graph "fR_con" was set to 25. Peak ventilation rates at 30 mmHg for temperatures above 20°C exceed 250 bpm, a very high value. Whether or not flounder species can accomplish this and higher rates has not been established, although exercising trout and salmon are reported to have ventilation rates as high as 1000 bpm (Eddy and Handy 2012). If such high rates are not consistent with SFL capabilities, then RMD "fR" estimates may not be reasonable under extreme hypoxic conditions. Given that PO_2 values just touch upon such low values during standard respirometry experiments, "fR" estimation as implemented here appears adequate for normoxic to mildly hypoxic environments. Even with exceptionally high "fR" values at extremely low environmental PO_2 values, $\dot{V}O_2$ output is significantly inhibited.

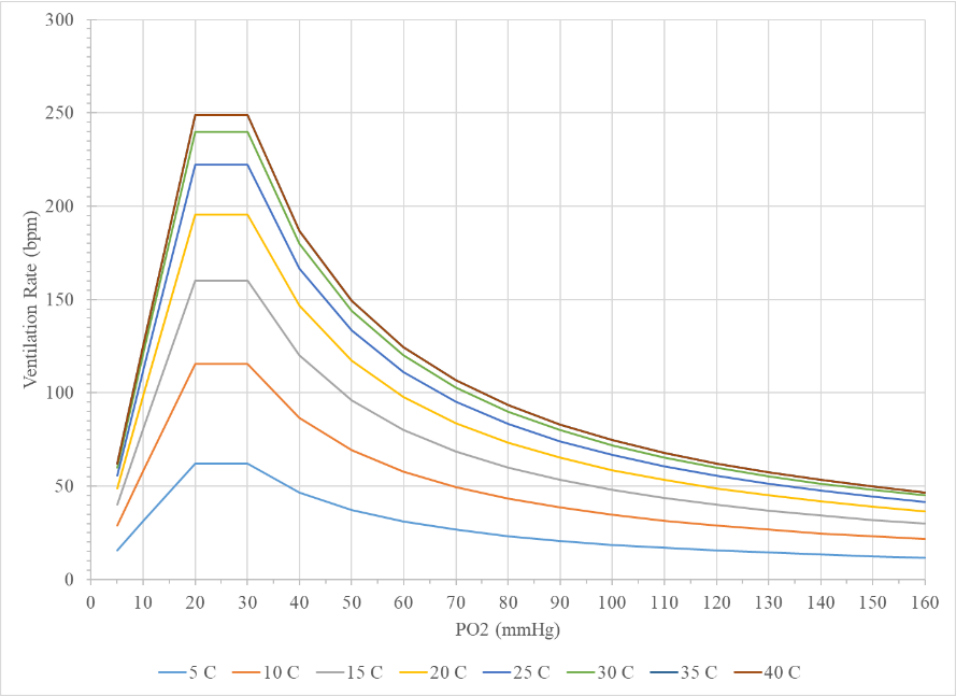

Figure 35. RMD "fR" output by temperature and PO_2.
"fR_con" = 25. Note that temperature change effects are not linear.

VsR [Equation: Decision, Empirical]

The volume per respiratory stroke, "VsR," (mL water/g fish·stroke) estimates the volume of water per gram-fish that may be pushed over the gills with each opercular beat. In a resting SFL, the full buccal volume may not be used, allowing for a "buccal reserve" to be called upon. As previously discussed, PO_2 strongly influences water volume per stroke (Kerstens et al. 1979). Less well established is the temperature impact on "VsR" volume in SFL. Given that buccal volume adjustment does occur in other species, the decision was made to include temperature effects. The programmed "VsR" volume increases linearly with temperature to a maximum of 0.014 mL water/g

fish·stroke, the upper limit reported by Kerstens et al. (1979) for hypoxia-acclimated European Flounder.

Using 0.008 mL water/g fish as the baseline value, the effect of PO_2 on buccal volume is adjusted up and down by multiplying this value by the ratio of 20 mmHg to the current PO_2. This increases "VsR" as PO_2 falls until reaching 20 mmHg, after which "VsR" declines. Buccal volume is limited to 0.014 mL water/g fish by the use of a MIN function. The result from this calculation is compared to the product of the baseline volume, 0.008 mL water/g fish, and the ratio of the ambient temperature, "Ta" to the fish's optimum temperature, "Topt," and the maximum volume used as final "VsR" value.

VsR = MAX(0.008 *Ta/Topt, MIN(0.008*20/PO2,0.014))

The "Topt" for SFL is 25°C, per van Maaren et al. (2000).

The output range for "VsR" by temperature and PO_2 is shown in Figure 36. As configured, the buccal volume is proportionally related to temperature, increasing or decreasing with a corresponding rise or fall in temperature. Oxygen pressure effects on "VsR" do not occur until PO_2 falls below a threshold level. Below the "Topt" of 25°C, "VsR" starts to increase at PO_2 levels greater than 20 mmHg. For example, at 10°C "VsR" begins to increase at 50 mmHg. At and above 25°C, the PO_2 threshold remains fixed at 20 mmHg. This method of estimating buccal volume creates a PO_2-dependent "VsR" minimum which follows the curve that each temperature-dependent "VsR" line intercepts at the left of the graph.

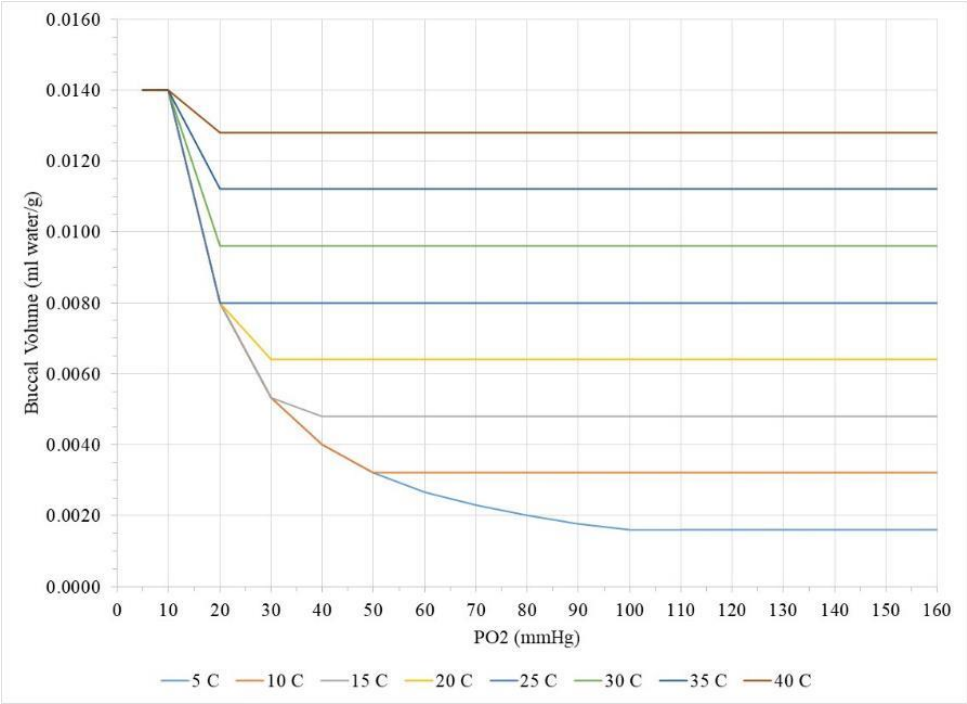

Figure 36. RMD "VsR" response to temperature and PO_2.

Vw [Equation: Empirical]

The amount of O_2 available for metabolic work depends on the amount of oxygenated water that can be moved across the gills.[9] "Vw" is the amount of water (in mL/g fish) that flows over the gills per hour and is the product of the respiratory frequency "fR" and buccal stroke volume "VsR."

$$Vw = fR * VsR$$

[9] Cutaneous respiration is a secondary source of O_2 supply, but water is not actively moved across the skin making it less efficient in O_2 extraction than the gills.

When combined as "Vw," temperature and PO_2 effects on "fR" (Figure 35) and "VsR" (Figure 36) produces the responses shown in Figure 37. The resultant ventilation curve is consistent with the temperature and PO_2 responses on gill ventilation as reported in the literature (Tallqvist et al. 1999, Capossela et al. 2012).

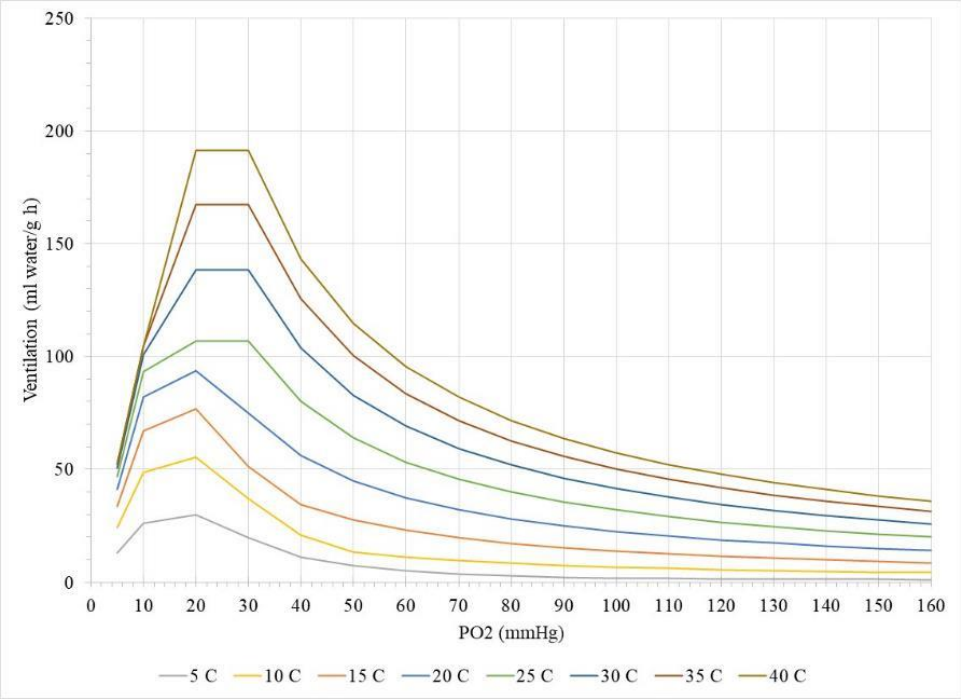

Figure 37. RMD "Vw" response by temperature and PO2.
"fR_con" = 25.

Hemoglobin Saturation

To better explain the calculation of Hb saturation, designated as "Y" in keeping with usage by Hill (1910), the discussion will start with sub-model output "Y" and work backwards (Figure 38).

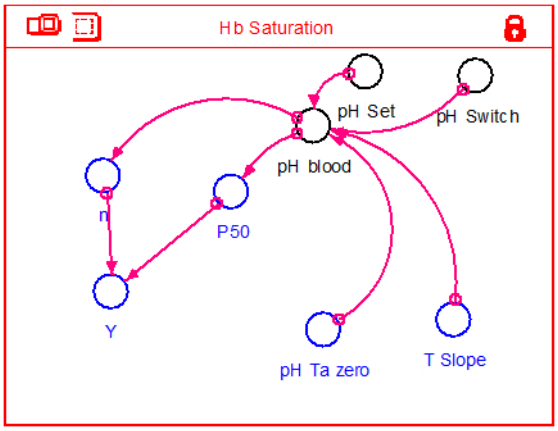

Figure 38. RMD Hb saturation calculation sector.

Y [Equation: Theoretical]

The value of "Y" is calculated using the Hill equation, shown in equation 46 of the previous chapter. Per the Hill equation, only two inputs to "Y" are required: the Hill coefficient "n" and "P50," both of which are dependent on the pH of the blood which is represented in the model as the converter "pH_blood."

n [Equation: Empirical]

The value of "n" is calculated via an empirical equation based on European Flounder data obtained from Weber and de Wilde (1975).

$$n = -0.264*pH\_blood+3.7$$

This formula produces an "n" value typically found over normal physiological pH ranges, the values of which start at just below 1.6 at a pH of 8.0 and increases to about 1.8 at pH 7.2 (Weber and de Wilde 1975).

P50 [Equation: Decision, Empirical]

The "P50" value is calculated based on data from Weber and de Wilde (1975) for red blood cells in suspension at 15°C. The calculation places "P50" just below 20 mmHg at a pH of 7.2, decreasing to about 7 mmHg at a pH of 7.8. To prevent negative values, which will occur at pH ranges greater than 8.28, a MAX function is used to keep the value ≥ 0.1 mmHg.

P50 = MAX (0.1, -16.786*pH_blood+140)

The linear inter-relationship of the calculated *n* and P_{50} values in relation to pH is shown in Figure 39. Differences in the rounding of output values create a slightly more negative slope for the "P50" estimates. Biochemical factors such as ATP and GTP, which can alter *n* and P_{50} at a specific pH in living flounder (Weber and de Wilde 1976, Weber 2000), are not currently represented in RMD.

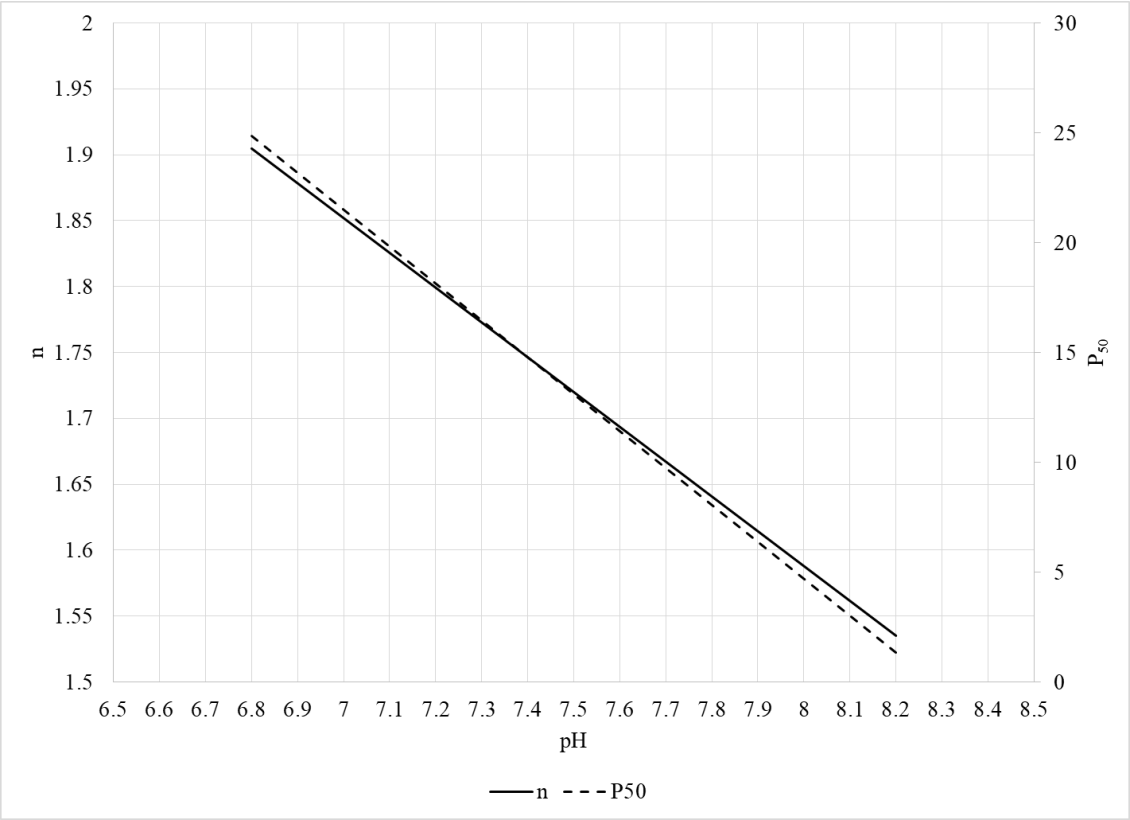

Figure 39. Relationship of Hill coefficient "n" and "P50" to pH, used in RMD.

pH Blood [Equation: Decision, Theoretical]

Computation of "pH blood" within the "Hb Saturation" sub-model is influenced by the external source input "Ta," and by sub-model inputs, "pH Ta zero" and "T Slope." The model also allows "pH blood" to be manually set rather than be estimated based on the above inputs. This is achieved through the use of input converters "pH Set" and "pH Switch."

pH blood = IF pH_Switch = 1 THEN (T_Slope*Ta+pH_Ta_zero) ELSE pH_Set

The inputs to “pH blood” are as follows:

pH Switch [Input: Fixed]

As with “DO Switch,” this converter is a simple mechanism to allow direct blood pH input. Setting “pH Switch” to 1 satisfies the logical requirement in “pH blood” to use the pH formula. A value other than 1 will use the value of “pH Set.”

pH Set [Input: Fixed or Variable]

This converter is used to set blood pH to a user-specified value rather than RMD’s calculated value. This feature is useful when integrating RMD with other models, such as E.F, to set pH which is generally only slightly higher than the surrounding water (Evans et al. 2005).

pH Ta Zero [Input: Fixed]

This converter sets the pH to 8 at 0°C. This converter could be integrated into the “pH blood” formula for simplicity but is kept separate to facilitate user change in the intercept point of “pH blood.”

T Slope [Input: Fixed]

Blood pH is negatively correlated with increasing ambient temperature in poikilotherms with the slope of the relationship differing among species (Cameron 1989). For poikilotherms as a group, a normal range is -0.008 to -0.021 pH/°C with an average slope of around -0.016 to -0.019 pH/°C (Cameron 1989). Because the relationship of blood pH to temperature for flounder has not been established, a conservative approach was taken and the value for “T_Slope,” was set to -0.019. This

baseline relationship of pH to temperature is shown below in Figure 40 with “pH Ta Zero” set to 8.

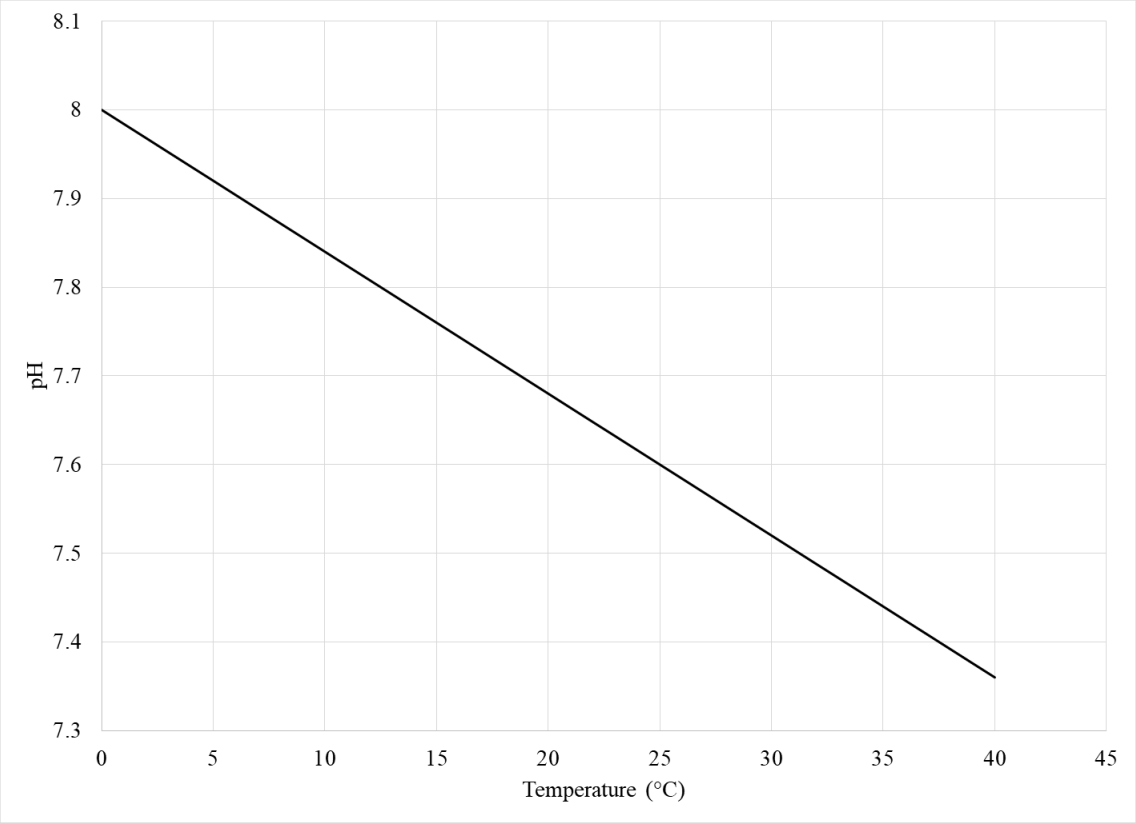

Figure 40. Baseline RMD blood pH response to temperature.
pH intercept, “pH Ta zero” = 8.

Blood Oxygen Carrying Capacity

The amount of O_2 which can be carried within the blood is managed by the “Blood O2 Capacity” sector shown in Figure 41.

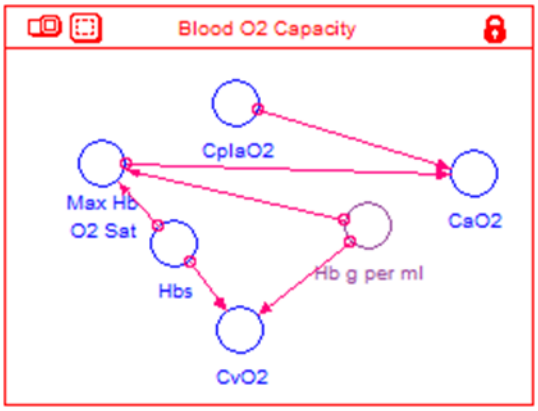

Figure 41. RMD blood oxygen carrying capacity sector.

CplaO2 [Equation: Conversion]

The figure includes the plasma O_2 carrying capacity "CplaO2," assumed to be equivalent to "DOa" in water but with units in mL O_2/mL plasma.

CplaO2 = DOa*0.0007

Hb g per mL [Input: Fixed]

The O_2 carrying capacity of blood is primarily dependent upon O_2 bound to Hb. The amount of Hb in the blood in g Hb/mL blood must be known to determine this value. Hemoglobin concentration differs among species and can be affected by blood loss from injury or disease (e.g., anemia). RMD uses the converter "Hb g per mL," with the value chosen as 0.15 g Hb/mL blood based on data from Olive Flounder *Paralichthys olivaceus* presented by Park et al. (2012) and Starry Flounder by Watters and Smith (1973).

Hbs [Input: Fixed]

The O_2 to Hb concentration value ($[O_2]/[Hb]$) is represented by "Hbs" in mL O_2/g Hb. Extensive data for humans sets this value at about 1.31 mL O_2/g·Hb (McLellan and Walsh 2004). However, within fish, the amount of O_2 bound to Hb varies across species (Weber 2000). Fortunately, Milligan and Wood (1987) analyzed Starry Flounder blood and reported a resting $[O_2]/[Hb]$ value of 0.05 mmol O_2/g Hb. This value corresponds to a value of 1.12 mL O_2/g Hb and is the value used in RMD.

Max Hb O2 Sat [Equation: Theoretical]

The converter "Max Hb O2 Sat" calculates the maximum potential amount of O_2 (in mL) that may be carried by 1 mL of blood at any given moment. It does so by multiplying the inputs from "Hbs," "Hb g per mL," and the blood O_2 saturation fraction "Y" from the "Hb Saturation" sector.

Max Hb O2 Sat = Hb g per mL*Hbs*Y

CaO2 [Equation: Theoretical]

Establishing the total O_2 carrying capacity of the blood in mL O_2/mL blood is achieved by summing the results of "Max Hb O2 Sat" and "CplaO2."

CaO2 = Max Hb O2 Sat+CplaO2

The "CaO2" value is used, along with "Q" to determine the $\dot{V}O_2$ capacity of the circulatory system which will be discussed below.

CvO2 [Equation: Theoretical]

Though not incorporated in the model, this equation is used to provide information on the estimated O_2 concentration remaining in the venous blood in mL O2/mL blood using three inputs, "Hb g per mL," "Hbs," and "SvO2," from the "PvO2 Derivation" sector.

CvO2 = Hb_g_per_mL*Hbs*SvO2

Venous Blood Oxygen Pressure (P_vO_2) Derivation

Calculation of the venous blood O_2 pressure, "PvO2," needed to generate the tension differences between water O_2 pressure for the gill diffusion equation (18) and arterial blood O_2 pressure for the blood oxygen transport equation (19) is accomplished within the 'PvO2 Derivation" sector shown in Figure 42.

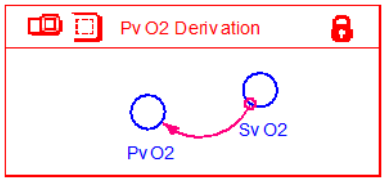

Figure 42. RMD PvO2 derivation sector.

A valid criticism of RMD is its reliance on modeling physiological processes, which can vary within seconds to minutes, and assuming those values can be applied across the model's hourly time scale. With respect to P_vO_2, the process is further complicating because P_vO_2 is an estimated value of $[O_2]$ in the venous blood, i.e., O_2 not

consumed by tissues after passing through the capillaries. However, RMD is intended to account only for the maximal rate of O_2 supply, not O_2 consumed. Predicting the average P_vO_2 over an hour to obtain the ΔPO_2 estimates for use in the Fick equation could be dealt with by setting the P_vO_2 value to a value or values found in the literature. An approach using fixed values might be sufficient in many situations, but a dynamic response is required to accommodate at least some of the effects of pH and temperature on Hb affinity (Soldatov 2003).

"PvO2" relies an estimate of the average O_2 venous blood saturation or "SvO2," the value of which is derived from inputs "n" and "Y" from the "Hb Saturation" sector. The value of "PvO2" is then calculated using "SvO2," and "n" and "P50" also from the "Hb Saturation" sector. As pH and temperature affect the value of "n," this variable is used to adjust the output value of "PvO2." Thus, the derived P_vO_2 in RMD is not an accurate physiologically-based calculation but is presumed to be a reasonable estimate.

SvO2 [Equation: Empirical]

The venous blood O_2 saturation fraction in the Starry Flounder stays remarkably high, ranging from 52.6% under hypoxic conditions to about 72% under normoxic conditions at a pH of about 7.5 (Watters and Smith 1973). Data provided by Wood et al. (1979a) on the same species placed the S_vO_2 at about 66% under normoxic conditions with a blood pH of about 7.9.

Because pH and temperature affect S_vO_2, an attempt was made to account for their influence when calculating "PvO2" while also retaining some connection to physiological processes. The process chosen derives an estimate based on a general

assumption of the Hill coefficient, namely that *n* can be thought of as representing the *minimum* estimate of the number of binding sites within a Hb molecule (Weiss 1997). During passage through the capillaries, most O_2 molecules dissociate from Hb but some O_2 remains bound. It is reasonable to assume that the average number of heme groups still bound to O_2 in venous blood will be closer to this minimal estimate than in arterial blood. Thus, within a given volume of venous blood, *n* may be thought of as a rough representation of the average (perhaps maximum average) amount of oxygen carried in a given volume of venous blood.

There are four O_2 binding sites available on a single Hb molecule. Each of the four Hb chains (two α and two β) represents a saturation fraction capacity of 0.25. Thus, if *n* were equal to 1, then Hb in venous blood is more likely to have one Hb sub-unit remain bound with O_2 after passing through the capillaries, resulting in a venous blood saturation level of 25%. As not all Hb in a given volume of blood is likely to desaturate evenly (some Hb molecules may fully desaturate while others may retain one or two molecules of O_2), the average value of *n* can be a fractional number (Hill 1913). For example, the Hill coefficient for the European Flounder ranges between 1.6 and 1.8 depending on blood pH (Weber and de Wilde 1975). Thus, the average number of Hb chains in a given volume of European Flounder venous blood still bound to O_2 molecules after passing through the capillaries would be expected to fall within this 1.6 to 1.8 range.

Subtracting *n* from 4 (the maximum number of possible binding sites) yields the number of Hb chains in venous blood *not* bound to O_2. Starting with *n* and dividing by

the number of unbound Hb chains (4-*n*) in a volume of venous blood, an estimate of theoretical venous blood O_2 saturation may be derived. When this value is multiplied by "Y," the starting arterial blood saturation level, the result is an estimate for S_vO_2 as follows:

$$SvO2 = Y*(n/(4-n))$$

The effects of DO calculated against three pH settings (7.0, 7.4, and 7.8) and temperatures (10, 20, and 30°C) using the "SvO2" equation are shown in Figure 43. Under normoxic conditions, "SvO2" values for the pH modeled fall between 68% and 81% saturation, results which are slightly higher than the values reported by Watters and Smith (1973) and Wood et al. (1979a).

This approach appears sufficient to provide an adequate estimate of "SvO2" for generating equivalent PO_2 differentials for use in the Fick equation variants. However, room for improvement of this aspect of RMD remains.

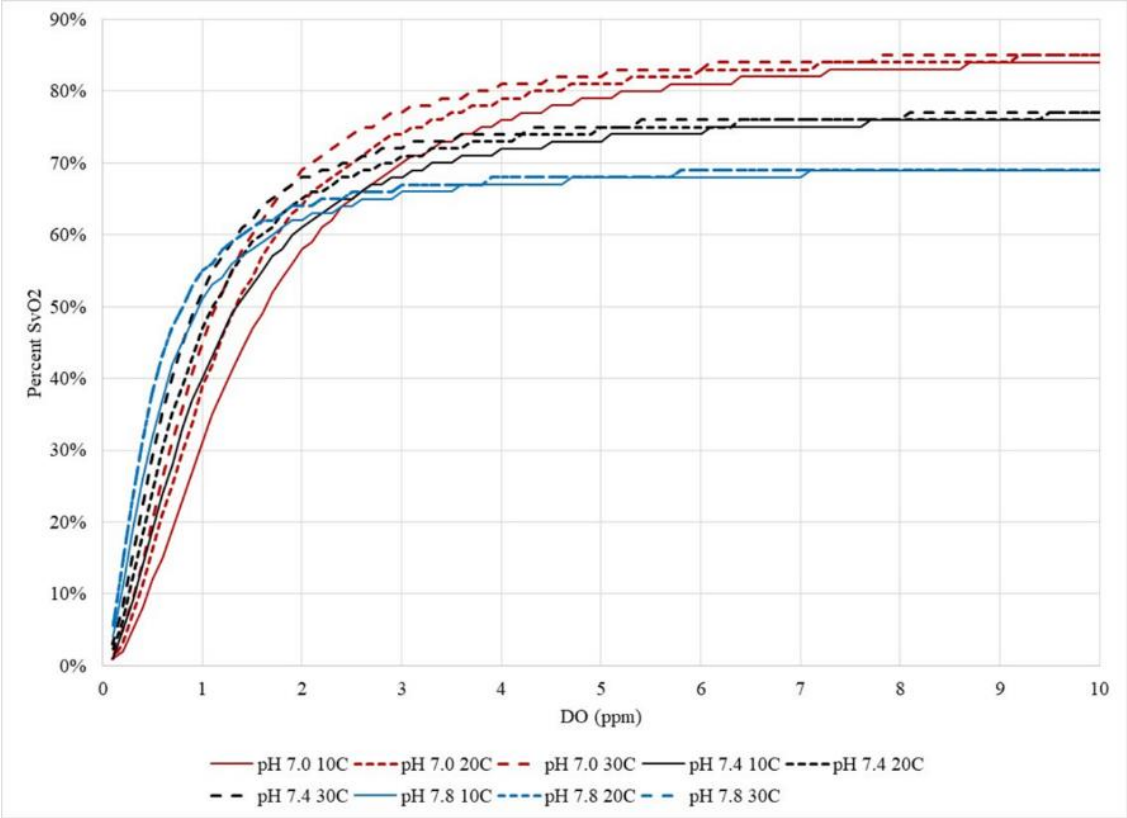

Figure 43. RMD SvO2 output by DO (ppm) by pH and temperature.
Color represents pH: red = pH 7.0, black = pH 7.4, blue = pH 7.8. Temperature represented by line style: solid = 10°C, short dash = 20°C, long dash = 30°C. Roughness of graphs due to step changes in RMD calculations.

PvO2 [Equation: Theoretical]

Venous blood O_2 pressure P_vO_2 can be estimated by re-arranging the Hill equation and substituting S_vO_2 for Y:

$$P_vO_2 = [(S_vO_2 \cdot {P_{50}}^n)/(1 - S_vO_2)]^{1/n} \quad (47)$$

The natural question that arises is does equation (47) produce representative values of flounder P_vO_2? Wood et al. (1979a) reported that for Starry Flounder in water with a mean PO_2 of 138.7 mmHg at temperatures between 7.5°C to 10.5°C and a pH of

7.87, the P_vO_2 was 13.4 mmHg. The RMD calculated "PvO2" value for a "PO2" of 138 mmHg at pH 7.87 and 10°C is 12.4 mmHg.

Watters and Smith (1973) in three separate tests of sedated Starry Flounder at 11.4, 11.7, and 19.4°C with the corresponding mean inspired PO_2 of 59.0, 126.3, and 148.5 mmHg and pH of 7.5 report mean P_vO_2 values of 23.4, 42.9, and 29.8 mmHg. The RMD calculated "PvO2" values using the Watters and Smith (1973) parameters were 22.9, 25.7, and 26 mmHg, respectively. Why Watters and Smith (1973) data had such disparity in the P_vO_2 values for PO_2 set at 126.3 mmHg and 148.5 mmHg is not evident but may be due to an increased $\dot{Q}$ response to the mild hypoxia environment which could decrease the time available to off-load O_2 in the capillaries. Although RMD output does not match the PO_2 of 126.3 mmHg P_vO_2 estimate, the other estimates are more encouraging.

When set to the parameters outlined by Cech et al. (1977) in Winter Flounder with a Ta of 10°C, pH of 7.8, and PO_2 = 90 mmHg, the RMD "PvO2" was 14.4 mmHg versus a reported P_vO_2 of 31 mmHg. This may result from a hypoxia response in the fish resulting in a lesser O_2 diffusion rate at the tissue level due to increased $\dot{Q}$ or other physiological responses such as in blood ATP concentration which causes a Bohr shift in the oxygen saturation curve (Wood et al. 1975).

The similarity of RMD results to those of the Wood et al. (1979a) study and two of the three Watters and Smith (1973) experiments is encouraging, although the larger difference relative to the third Watters and Smith (1973) experiment suggests there may be additional effects not modeled.

Cardiac Output

The Cardiac Output sector (Figure 44) is the last physiological sub-model necessary for $\dot{V}O_2$ calculations. The output of this sector is cardiac output, represented by "Q," which is the product of heart rate "HR" and stroke "SV." While a simple calculation, the components "HR" and "SV" are adjusted by temperature and PO_2 using converters "SV PO2 f," "SV Temp f," "HR PO2 f," and "HR Ta" where the "f" in the first three converters indicates the inclusion of correction "factors" which are small adjustments to SV or HR. The influence of "Ta" on "HR" and "SV" is greater than the influence of "PO2" which generally has little impact on "Q" except under hypoxic conditions. The remaining "SV" input variable "Vvol" calculates the ventricular volume of the SFL "heart" using the weight estimate described in Chapter V.

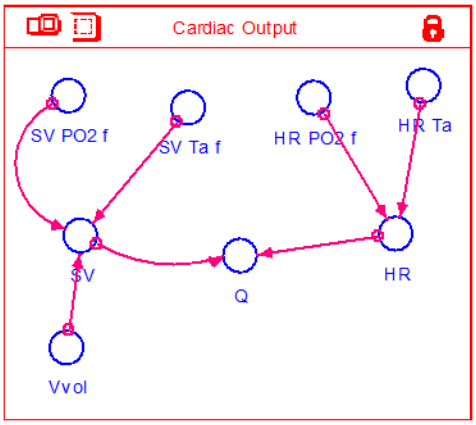

Figure 44. Cardiac output (Q) derivation sector.

HR Ta [Equation: Empirical]

Variable "HR Ta" provides a Ta-dependent heart rate in beats per hour (bph) using a calculated fit to HR data collected from Summer Flounder by Capossela et al. (2012). The equation uses a parabolic equation to generate a peak HR of about 4212 bph (70.2 beats per minute, bpm) at 23°C as shown in Figure 45. The parabola reaches zero at about 4°C and 41°C, the physiological equivalent to heart stoppage. Thus, the equation invokes minimum and maximum lethal temperature limits for SFL metabolism. The lower limit is 1°C lower than the 100% mortality temperature observed for SFL by Prentice (1989). The ultimate maximal lethal temperature for an acclimated SFL is less well established. A study by van Maaren et al. (2000) reported a lethal temperature of 39°C in a 29°C acclimated SFL. To provide a margin of error for a greater maximal lethal temperature, the parabola calculation used sets the maximal lethal temperature at 41°C. With these caveats established, the "HR Ta" decision and empirical formula used in RMD is as follows:

HR_Ta = MAX(0, ((-0.2*Ta^2+9*Ta-31) * 60))

The use of the MAX function limits the "HR Ta" value to positive values only.

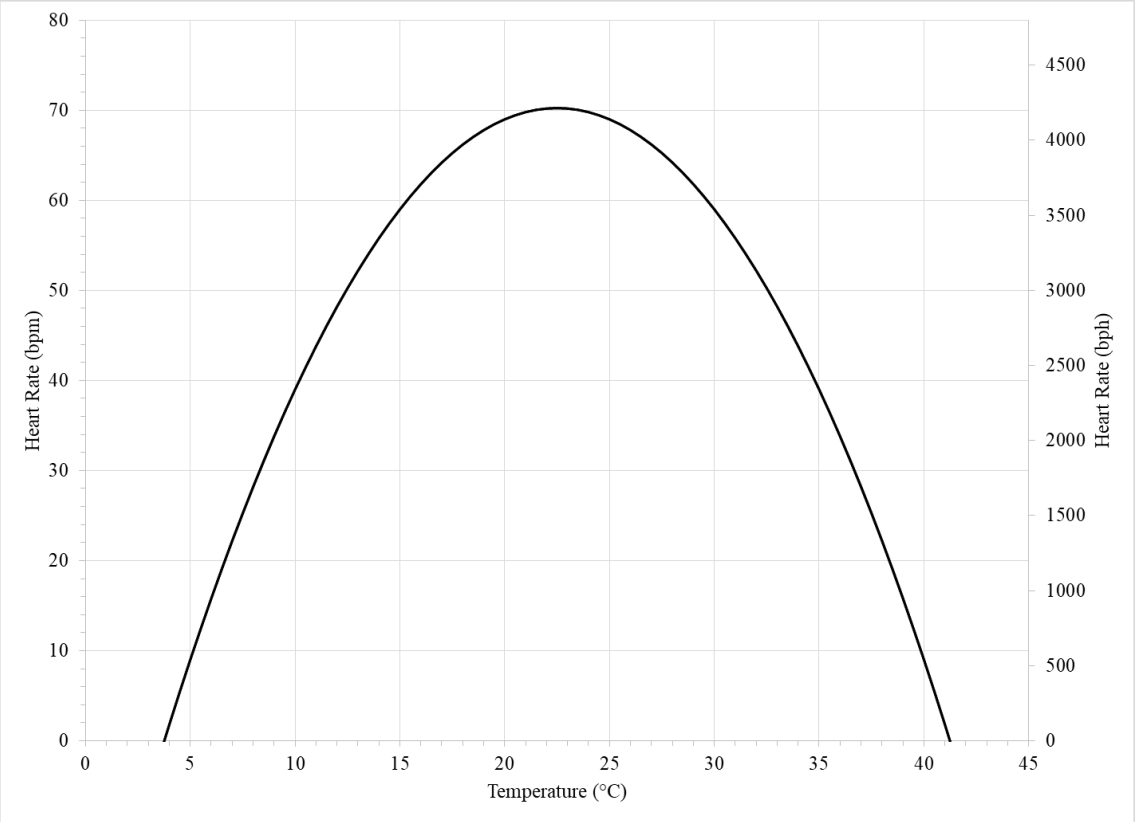

Figure 45. RMD temperature-dependent heart rate calculation.
Heart rate in beats per minute (bpm) and beats per hour (bph). Zero intercepts correspond to minimum and maximum lethal temperatures.

HR PO2 f [Equation: Decision, Empirical]

With baseline "HR" established by "HR Ta," the variable "HR PO2 f" serves as a correction factor which modifies the HR output based on PO_2. Because the "HR Ta" value can vary dramatically, the effect of "PO2" on "HR" must have an equal effect on "HR" across all "Ta" inputs. Data from Mendonca and Gamperl (2010) supports a decline in HR with decreasing PO_2 in Winter Flounder acclimated to 8°C. Interestingly, this decline was not evident for 15°C acclimated fish. However, in the study by

Capossela et al. (2012), the two groups of Summer Flounder acclimated at 22°C and 30°C each showed a decline in HR with decreasing PO_2. These data sets were used as the basis for estimating "HR PO2 f."

HR_PO2_f = MIN(1, (0.0054 * PO2 + 0.68))

This equation sets the limit at which hypoxia begins to decrease "HR," to a "PO2" of ≤ 60 mmHg. Above 60 mmHg "HR PO2 f" is set to 1 (equal to no HR correction) meaning that under mild hypoxia and normoxia "HR" is only affected by "Ta." Once "PO2" falls below 60 mmHg as shown in Figure 46, then "HR PO2 f" output begins to decline with a minimal "HR PO2 f" correction factor (intercept) of 0.68 when Ta = 0°C.

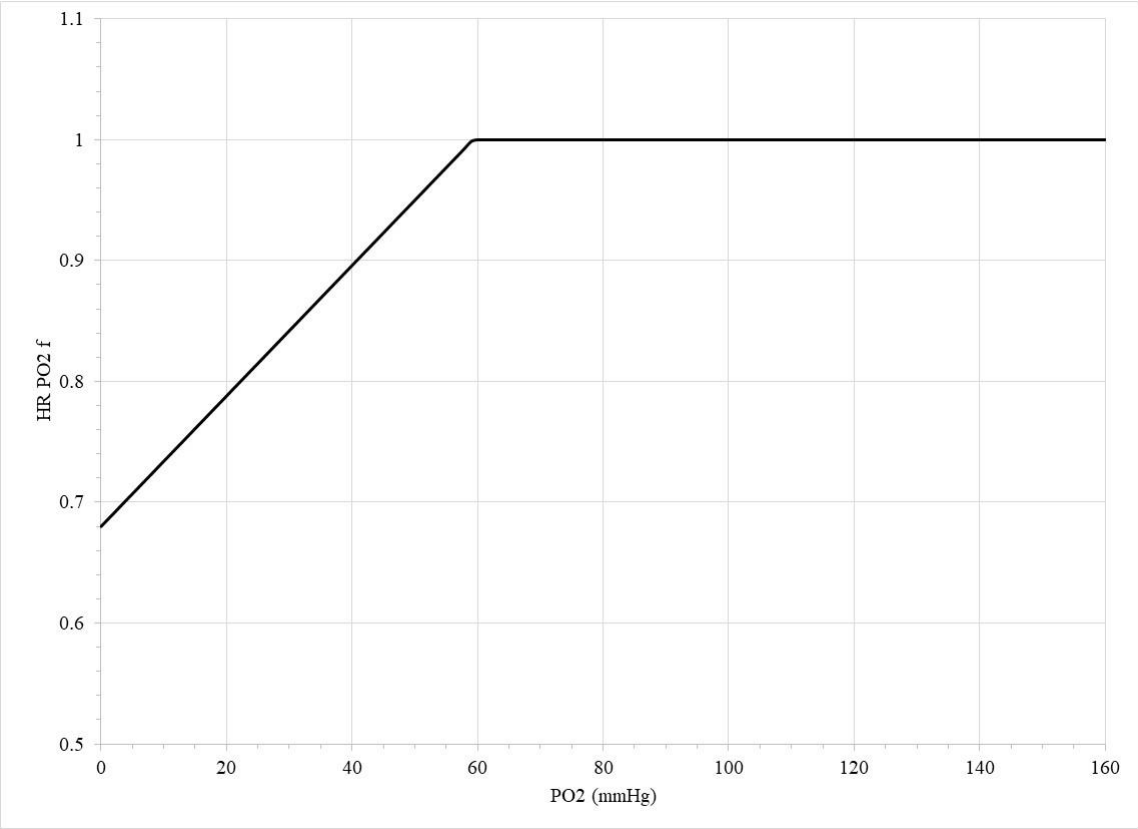

Figure 46. RMD "HR PO2 f" response to PO_2.

HR [Equation: Theoretical]

The final HR calculation is done in converter "HR" which is the product of "HR Ta" and "HR PO2 f."

HR = HR_PO2_f*HR_Ta

Vvol [Equation: Theoretical, Conversion]

Ventricular volume, "Vvol," uses equation (45) to estimate the SV for a fish of given weight in mL per kilogram. As fish weight "Wfish," is entered into the model in grams, it must be converted to kilograms for this equation, by dividing "Wfish" by 1000.

Vvol = (0.506*(Wfish/1000)^1.026)/(Wfish/1000)

SV PO2 f [Equation: Decision, Empirical]

Winter Flounder data from Mendonca and Gamperl (2010) are again used to derive this formula wherein SV increases when O_2 saturation falls below 30%. Assuming at 100% saturation that water PO_2 = 160 mmHg (based on a total atmospheric pressure of 760 mmHg), then 30% of 160 mmHg is 48 mmHg. However, for consistency with other hypoxia estimates, the hypoxia response threshold for "SV PO2 f" was set at 60 mmHg. When estimated PO_2 falls below this 60 mmHg threshold, "SV_PO2_f" applies a correction factor that increases "SV" up to a maximum value of 1.4, although this value is unlikely to be reached in normal applications of the model. When "SV PO2 f" values are above 60 mmHg, then the "SV PO2 f" output is fixed at 1 (see Figure 47).

SV PO2 f = MAX(1, (1+(0.4-0.4*(PO2/60))))

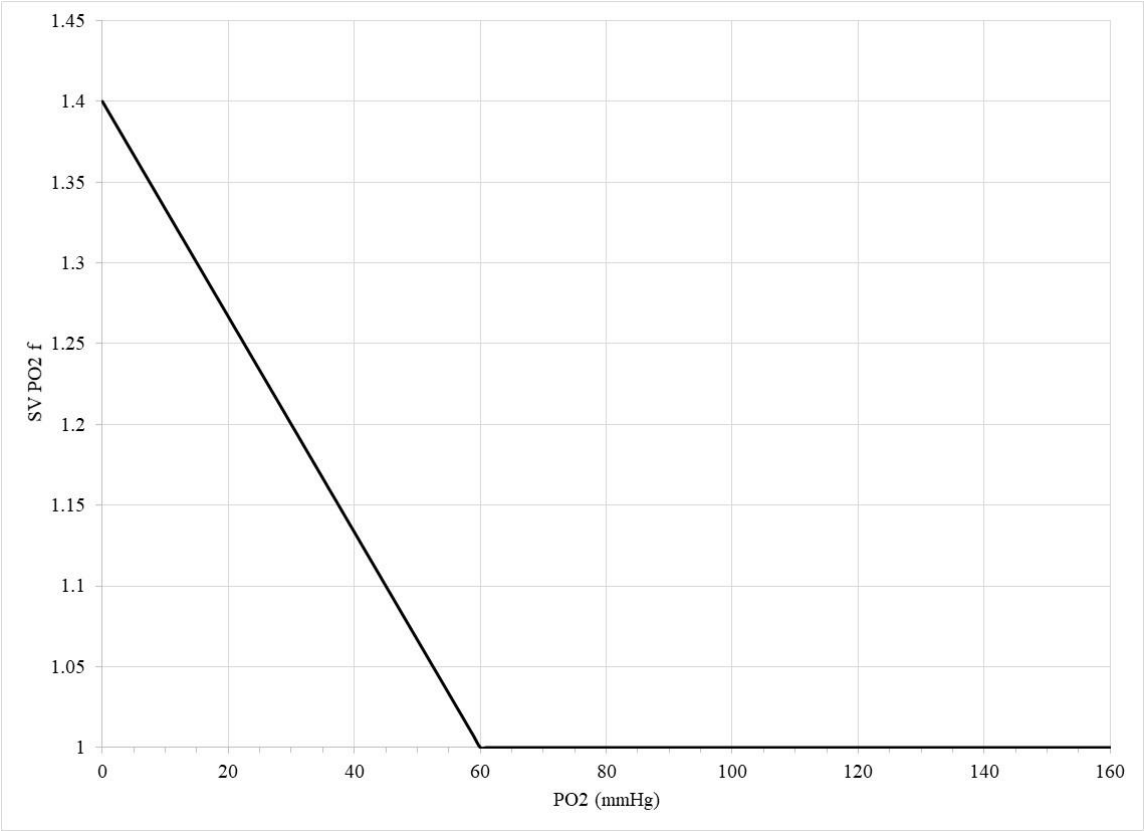

Figure 47. RMD "SV PO2 f" response to PO_2.

SV Ta f [Equation: Decision, Empirical]

The temperature-dependent correction factor "SV Ta f" adjusts "SV" based on "Ta" input. The formula used to calculate "SV Ta f" is based on Winter Flounder data from Mendonca and Gamperl (2010). As the SV fraction increases with Ta (see Figure 48), a minimum (MIN) function is used to limit the correction factor to no more than 1.4.

SV Ta f = MIN((EXP(0.0135*Ta)),1.4)

The value of "SV Ta f" reaches its maximum at about 25°C, the SFL optimal temperature per van Maaren et al. (2000), then levels out. As with "HR Ta," because no

data above 26°C is provided by Mendonca and Gamperl (2010), it is presumed that the value stays constant, although SV may decrease along with "HR" as thermal stress increases. Below 25°C the influence of Ta on "SV" decreases, with "SV Ta f" reaching 1 at Ta = 0°C. As currently modeled, RMD assumes that at all temperatures for which SFL survive, there is a > 1.0 correction factor influence on SV.

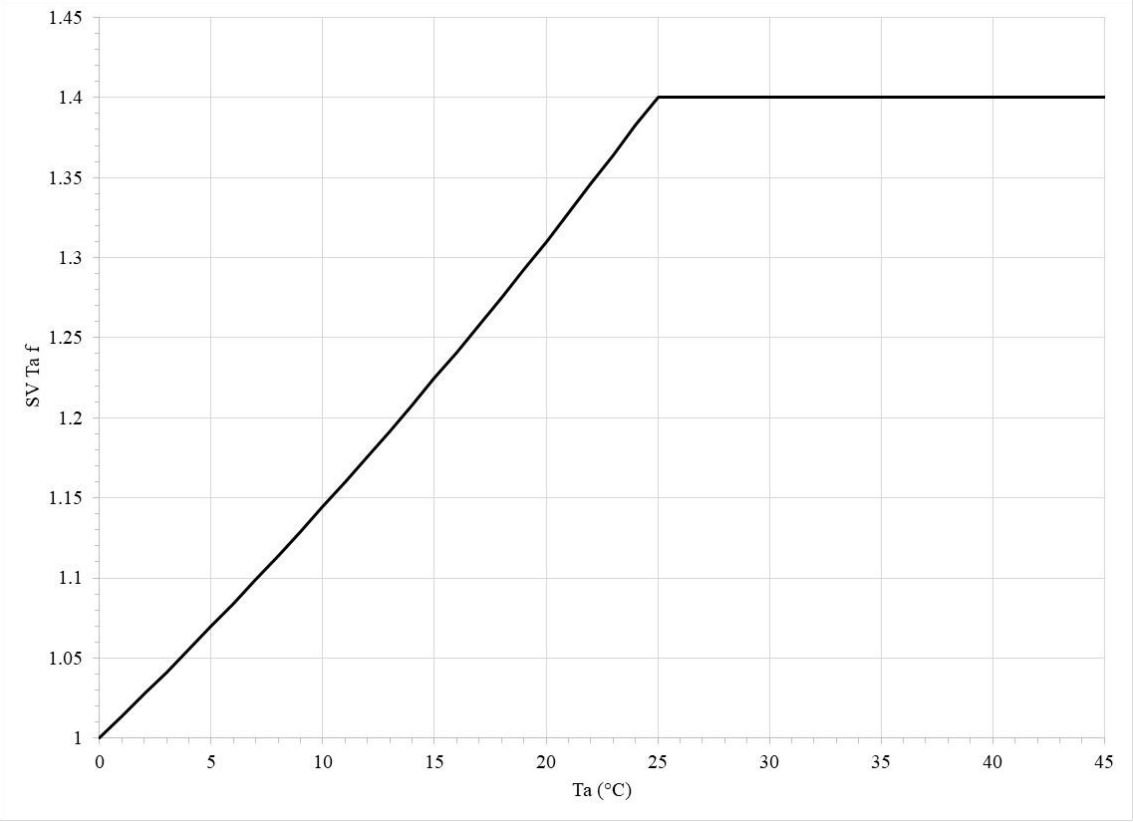

Figure 48. RMD "SV Ta f" response to Ta.
Peak SV response reached at "Topt" and assumed to remain level.

SV [Equation: Theoretical, Conversion]

Using “Vvol” to establish a “normal” ventricular volume, the result is modified by fractional inputs “SV PO2 f” and “SV Ta f” to produce an estimate of stroke volume, “SV.” Re-conversion of the allometric “Vvol” formula from kg to g is also accomplished in this calculation.

SV = (Vvol*Wfish/1000)*SV_Ta_f*SV_PO2_f

Q [Equation: Theoretical]

Having established “SV” and “HR,” the product of these two values will provide the cardiac output “Q.”

Q = HR*SV

The effects of “Ta” and “PO2” on “Q” output in RMD are shown in Figure 49. The graph shows that due to the compensatory mechanisms used in RMD, changes to PO_2 do not greatly impact “Q,” unlike thermal effects that exert a substantial influence.

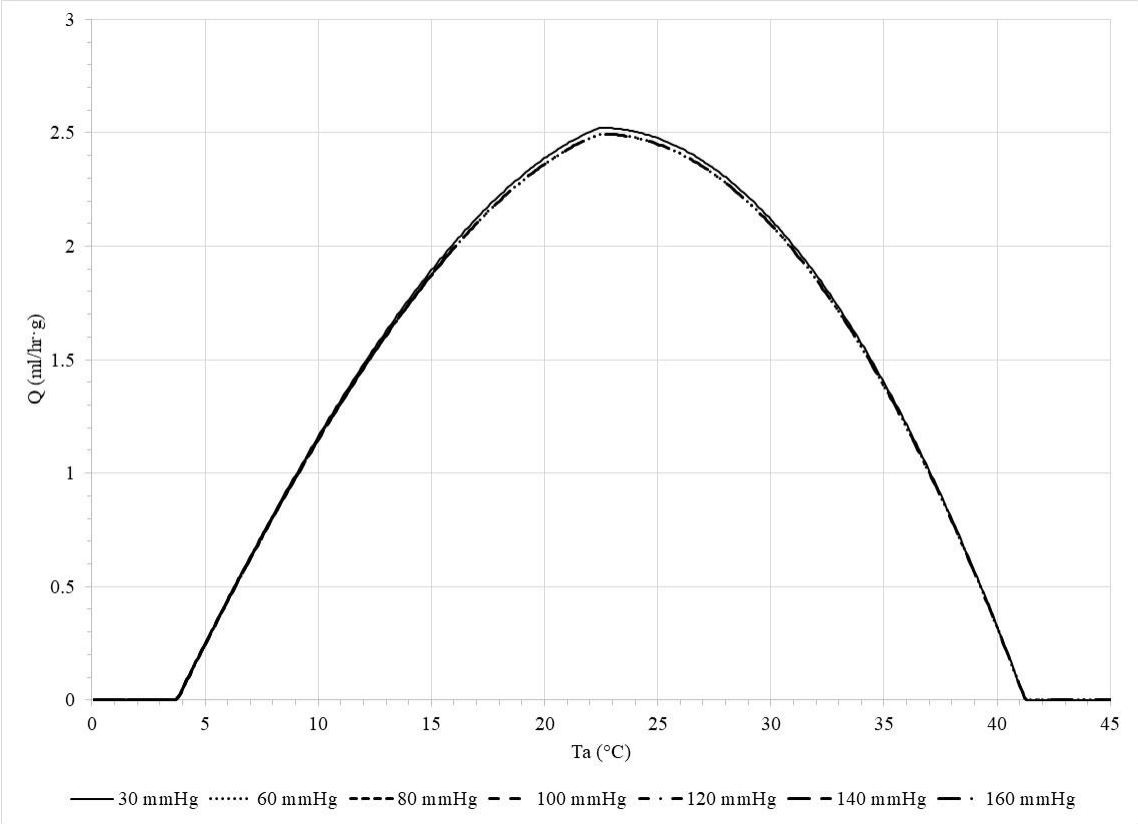

Figure 49. RMD "Q" output vs. Ta across PO_2 for 1 g SFL.

VO2 Derivation

All RMD components, or sub-models, discussed have been involved in the derivation of support data necessary for calculating $\dot{M}O_2$. Data from these sub-models are then fed into the "VO2 Derivation Sector" (Figure 50), which uses equation converters along with flow process and modeled stocks to compute an estimated maximal $\dot{V}O_2$ availability output. Starting on the left, O_2 supply models corresponding to ventilation, gill diffusion, blood transport, and cutaneous diffusion, as defined by equations (17) – (19) and (24), represent the first three flow processes, labeled "VO2 w,"

"VO2 gill," and "VO2 Q." However, each flow process is essentially an independent model for estimating $\dot{V}O_2$; thus, integrating them in series limits $\dot{V}O_2$ to the flow process with the lowest output value. That is, if the output value of "VO2 w" is less than the estimated capacity of "VO2 gill" and "VO2 Q" then this flow process becomes the overall $\dot{V}O_2$ rate limiter. Generally, "VO2 w" is the rate limiter for most simulations in which components are set for normal environmental conditions. It is possible, however, that circumstances can be created, particularly during simulated exposure to low PO_2 and low or high temperature, such that "VO2 gill" or "VO2 Q" may become the rate limiters. Artificial restrictions can also be modeled such as anemia or blood loss (via reduction of "Hb g per mL") or gill damage (via reductions of "Gill surface area"), as might occur from industrial oil spills (Brown-Peterson et al. 2015).

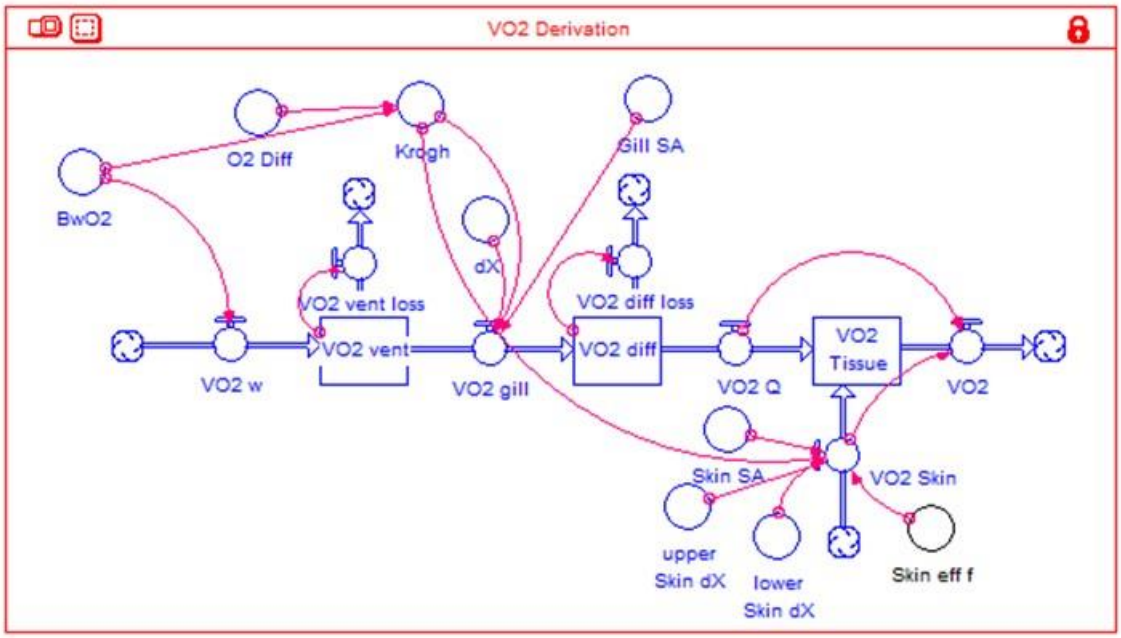

Figure 50. RMD VO2 derivation sector.

The cutaneous contribution to $\dot{V}O_2$, "VO2 Skin," is not limited by other respiratory processes as it constitutes a direct, additive input to the total $\dot{V}O_2$. However, all $\dot{V}O_2$ flow processes are impacted, either directly or indirectly, by "Ta" and "PO2."

Discussion of the "VO2 Derivation Sector" will follow the model's left-to-right flow starting with the acquisition of O_2 through ventilation.

Ventilation

The ventilation components of the "VO2 Derivation" model are shown in Figure 51. External sector inputs to "VO2 w" include "Vw," "PO2," "PvO2," and "Wfish." Within this sector, the solubility of O_2 in water is provided by "BwO2." Estimation of $\dot{V}O_2$ as affected by the ventilation process is performed in the flow component "VO2

w": that ventilation output is transferred to the stock component "VO2 vent" for use by "VO2 gill" (not shown). To prevent outputs of "VO2 w" (representing excess O_2 not consumed), from accumulating in the "VO2 vent" stock cache, the flow component "VO2 vent loss" is used to clear the stock after each calculation step. Though primarily a modeling-process requirement, the use of "VO2 vent loss" roughly reflects the fact that O_2 not consumed during respiration returns to the environment, or limits the uptake of "new" O_2.

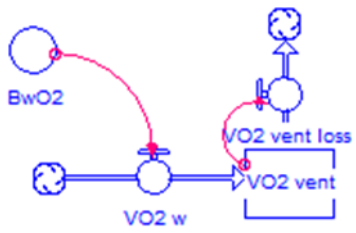

Figure 51. Ventilation component of VO2 derivation.

BwO2 [Equation: Theoretical, Conversion] [10]

The O_2 water capacitance coefficient, defined as $\Delta[O_2]/\Delta PO_2$ in units of mL O_2/L water·mmHg, is determined by the formula:

BwO2 = (DOa*0.7)/PO2

[10] Standard nomenclature for capacitance coefficients is the Greek capital beta, β, but as Stella does not support Greek letters, the Latin B is used.

As "DOa" is in mg O_2/L, it is converted to mL O_2/L by multiplying the DO value by the conversion factor 0.7 mL O_2/mg O_2.

VO2 w [Equation: Theoretical, Conversion]

Ventilation equation (17) inputs of "Vw" and "BwO2" are needed to calculate the conductance component of the diffusion equation (Jensen et al. 1993). Diffusion components of equation (17), inspired O_2 (PIO_2) and expired O_2 (PEO_2), correspond to the PO_2 in the water entering the buccal cavity and exiting the operculum, respectively. The value of PIO_2 is equivalent to the "PO_2" in inspired water, which is calculated in the Environment Processes sector. Expired PO_2 is the PO_2 remaining in water exiting the operculum following extraction of O_2 by the gills. The estimation of PEO_2 presents additional challenges for the experimenter and the modeler. For the experimenter, measuring PEO_2 requires care to prevent expired water mixing with the external medium. Oxygen in water exiting the gills can be measured by placing a cone over the operculum (Kerstens et al. 1979, Steffensen et al. 1982) or by inserting a sampling cannula into the operculum (Capossela et al. 2012). Measuring PEO_2 is not possible for the modeler, but an alternative solution exists.

The O_2 extraction efficiency of the water-perfusion counter-current gas exchange is efficient, so much so that in theory, PEO_2 is near that of venous PO_2 (Hughes and Morgan 1973). Thus, the substitution of PvO_2 for PEO_2 and PO_2 for PIO_2 in the ventilation equation allows estimation of the O_2 differential. The efficacy of this approach may be validated through a comparison of the estimated extraction efficiencies

when using PO_2 and PvO_2 against measured extraction efficiencies obtained by measuring PIO_2 and PEO_2.

Fish gill O_2 extraction efficiency is calculated with equation (48), which takes the ratio of the difference between inspired and expired PO_2 over the inspired PO_2 (Dejours 1981). Substituting PO_2 for PIO_2 and PvO_2 for PEO_2 extraction efficiency can be estimated.

$$Extraction\ efficiency = \frac{PIO_2 - PEO_2}{PIO_2} \cong \frac{PO_2 - PvO_2}{PO_2} \quad (48)$$

Extraction efficiency estimations using RMD calculated across PO_2 and PvO_2 ranges for a 500 g SFL at 10, 22, and 30°C are shown in Figure 52. RMD estimates appear comparable to extraction efficiencies reported for Summer Flounder, which is within the same genus as SFL, acclimated to 22°C and 30°C by Capossela et al. (2012). Compared to data for European Flounder acclimated to 10°C, RMD extraction efficiency calculations are higher than those presented by Steffensen et al. (1982), particularly at PO_2 levels > 60 mmHg.

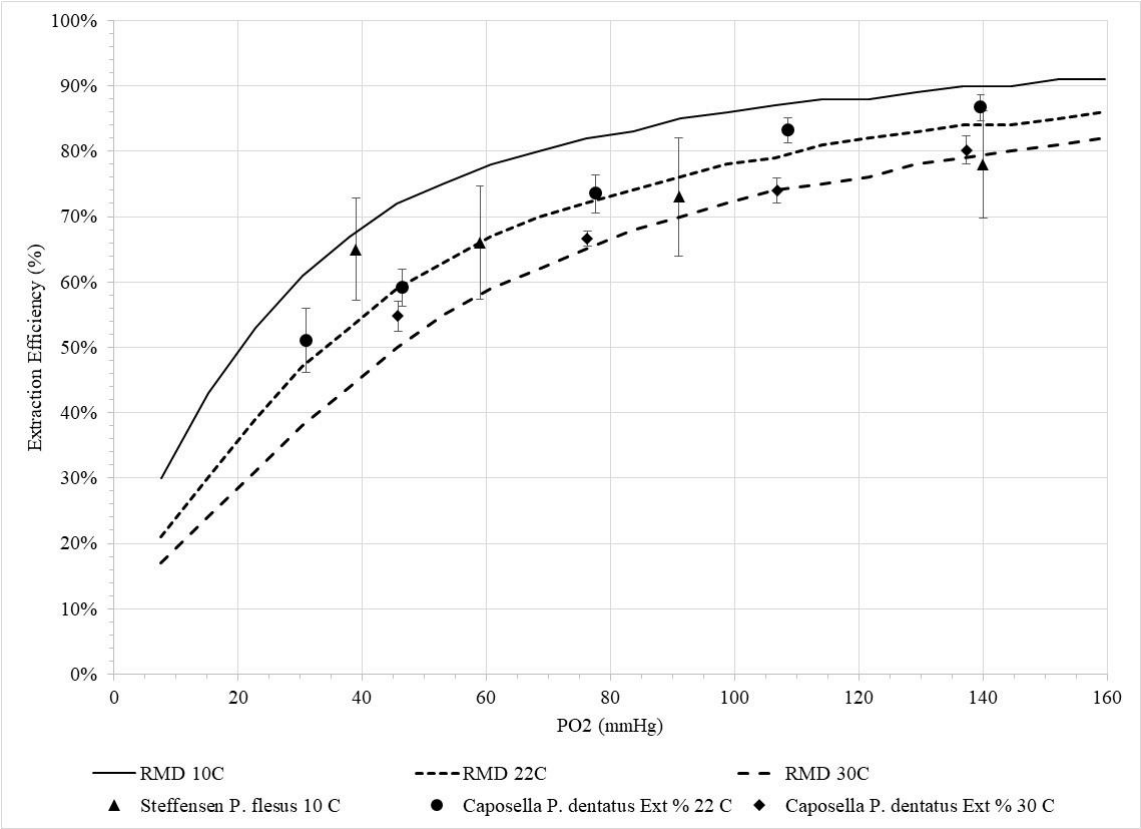

Figure 52. Comparison of RMD calculated O_2 extraction efficiency to literature. Extraction efficiency data for *P. flesus* at 10°C (triangle) from Steffensen et al. (1982), and for *P. dentatus* at 22°C (circle) and 30°C (diamond) from Capossela et al. (2012). RMD settings: salinity = 5 ppt, Weight = 500g. RMD estimated pH, P_{50}, *n* values: at 10°C, pH = 7.8, P_{50} = 8.9, n = 1.6; at 22°C, pH = 7.6, P_{50} = 13, n = 1.7; at 30°C, pH = 7.4, P_{50} = 15, n = 1.7.

Substituting PO_2 for PIO_2 and PvO_2 for PEO_2, "VO2 w" is re-formulated within RMD as follows:

$$VO2\ w = (Vw*Wfish)*(BwO2/1000)*(PO2-PvO2)$$

The product of "Vw" and "Wfish" estimates the oxygenated water flow over the gills in mL/hr. This value is multiplied by "BwO2" adjusted to give the O_2 capacitance in mL O_2/mL water·mmHg. When multiplied by the O_2 tension differential in mmHg,

the product is the estimated $\dot{V}O_2$ from gill ventilation in an SFL of given weight in mL O_2/hr.

The remaining components of the ventilation calculation, the Stella® stock "VO2 vent" and flow "VO2 vent loss," are used, respectively, to "store" or cache the data from "VO2 w," which is then input into the next component of "VO2 Derivation"; and, to "drain" the stock (i.e., clear the cache) should the value in the "VO2 vent" stock value exceed the capacity of the "VO2 gill" flow component. Under normal circumstances, once water flows through the buccal cavity of a fish, across its gills and out the operculum, any O_2 remaining in the expelled water is no longer available for consumption. The use of "VO2 vent loss" in the model provides the model equivalent, preventing the creation of an O_2 "reservoir" from any residual $\dot{V}O_2$ that might remain in the stock.

Gill Diffusion

The gill diffusion component of RMD shown in Figure 53 estimates the flow of O_2 that occurs across the gill and capillary network using equation (18). It is contained within the Stella® flow component "VO2 gill." External sector inputs into "VO2 gill" include "PO2" and "PvO2" which have been previously discussed. Additional inputs are provided by converters labeled "O2 Diff," "Krogh," "Gill dX," and "Gill surface area." These O_2 conductance components will be addressed first followed by a discussion of integrating all the input components into "VO2 gill."

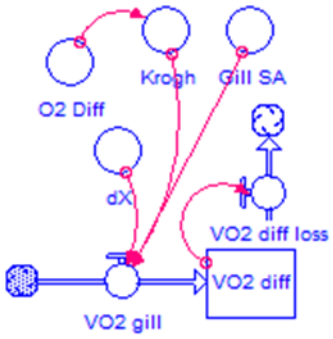

Figure 53. Gill diffusion component of VO2 derivation.

O2 Diff [Equation: Empirical, Decision]

Oxygen diffusion across a cell membrane in cm^2/h is estimated using the converter "O2 Diff." The empirical formula used was obtained from the data provided by Fischkoff and Vanderkooi (1975) as shown in Figure 23.

O2 Diff = 0.0064*EXP(0.04*Ta)

Krogh [Equation: Theoretical, Conversion]

The "Krogh" converter calculates the Krogh constant in mL O_2/cm·h·mmHg. The Krogh constant is the product of the O_2-water capacitance coefficient "BwO2" and O_2 diffusion "O2 Diff." As with the calculation of "VO2 w," the capacitance coefficient "BwO2" is divided by 1000 to obtain per mL units, or in this case, the equivalent per cubic centimeter (cm^3) of water.

Krogh = O2_Diff*(BwO2/1000)

Gill SA [Equation: Empirical, Decision]

Baseline gill surface area "Gill SA" is set to 2.42 cm^2/g fish based on average gill surface area from Summer Flounder (AKA Fluke) data as reported by Gray (1954).

Gill surface area = 2.42 *Wfish

Gill dX [Input: Fixed]

Gill diffusion distance "Gill dX" is nominally set to 0.0005 cm (5 μm) but this value can be reduced as desired. The use of cm is in keeping with other diffusion distances within the model.

VO2 gill [Equation: Theoretical]

"VO2 gill" uses a Stella® flow component to calculate the O_2 flow, using equation (18) with inputs from "Krogh," "Gill SA," and "Gill dX," and O_2 tension components "PO2" and "PvO2."

VO2 gill = Krogh*(Gill_SA/dX)*(PO2-PvO2)

The output of "VO2 gill" is sent to the stock component labeled "VO2 diff." This represents the $\dot{V}O_2$ amount that has diffused across the gill and capillary-cell membranes available for the next component in the $\dot{V}O_2$ cascade, "VO2 Q." As with "VO2 w," any O_2 that does not diffuse across the gills (i.e., remains dissolved water) is lost back to the environment. To prevent the accumulation of "VO2 gill" output within the "VO2 diff" stock, the contents of "VO2 diff" are removed with each model cycle (i.e., DT) by the flow component "VO2 diff loss."

Blood Oxygen Transport

Blood O_2 transport within the RMD "VO2 Derivation" model is represented only by the Stella® flow component "VO2 Q" shown in Figure 54. The output of "VO2 Q" flows into "VO2 Tissue" stock where it is combined with the output of "VO2 skin," discussed below.

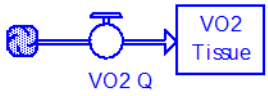

Figure 54. Blood O_2 transport component of VO2 derivation sector.

VO2 Q [Equation: Theoretical]

The calculation of "VO2 Q" in mL O_2/h is based on the Fick equation shown in equation (19) as the product of cardiac output "Q," in mL blood/h, and the arterial O_2 concentration "CaO2," in mL O_2/mL blood, which is converted to the carrying capacity of blood, in mL O_2/mL blood·mmHg, through the division of "CaO2" by "PO2." Arterial O_2 pressure is assumed equal to "PO2" so that the calculated O_2 tension becomes the difference between this value and the calculated venous PO_2, "PvO2."

VO2 Q = Q*(CaO2/PO2)*(PO2-PvO2)

The capacity of "VO2 Q" generally exceeds that of the "VO2 w" and "VO2 gill." However, the inclusion of "VO2 Q" allows the modeling of those circumstances wherein "Q" or "CaO2" outputs are sub-par such as might be encountered at extreme

temperatures for “Q” or if “Hg g per mL” were to be reduced to simulate anemia or blood loss in SFL.

Cutaneous O_2 Diffusion

Using equation (24), RMD calculates cutaneous O_2 diffusion, “VO2 Skin, with inputs from converters skin surface area, “Skin SA,” and skin thickness estimates for upper, “upper Skin dX,” and lower, “lower Skin dX,” surfaces of the SFL. The model also includes a converter to allow for manual adjustments of cutaneous diffusion efficiency as shown in Figure 55.

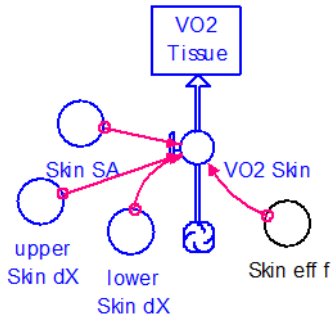

Figure 55. Cutaneous diffusion component of VO2 derivation sector.

Skin SA [Equation: Theoretical]

The equation used for “Skin SA” is based on the MDC SFL data fit-line shown in Figure 25 in which surface area was first estimated using TL data and equation (33). Recall that the empirical equation based on the MDC data gave an estimated Meeh constant close to the predicted value of 10 and a body weight power exponent was slightly greater than 0.69, versus the ideal Surface Law value of 0.67. However, the 0.69

value is within the range of the minimum exponent value of 0.53 in dairy cattle and the maximum exponent value of 0.74 in domestic fowl, as reported by Calder (1984).

The surface area calculation for SFL does not address the potential additional surface area for O_2 diffusion afforded by the SFL tail and fins. Nor the does the estimate take into account the possible additional surface area due to curvature of the SFL body, as the area formula assumes a flat surface. To account for these additional surface areas, the decision was made to use a weight exponent of 0.7.

Skin SA = 10*Wfish^0.7

Upper Skin dX & Lower Skin dX [Equation: Empirical, Conversion]

RMD uses equations for upper and lower skin distance adapted from Winter Flounder skin thickness empirical equations reported by Burton et al. (1984). The equations have been slightly altered, and results converted to cm from μm by dividing the results by 10,000.

Upper Skin dX = (0.0198*Wfish+36)/10000

Lower Skin dX = (0.04886*Wfish+45)/10000

Skin eff f [Input: Fixed]

The variable "Skin eff f" allows the skin diffusion efficiency to be manually adjusted should the RMD user desire to determine the effects of reduced cutaneous respiration on overall $\dot{V}O_2$. The default setting of "Skin eff f" is 1, indicating no change in cutaneous respiration produced by "VO2 Skin." If, for example, the effect of being buried in sediment, which impacts water flow over the skin, is to be simulated, then the

value may be reduced to any fraction less than 1. Setting "Skin eff f" to zero will eliminate altogether the contribution of cutaneous respiration to the $\dot{V}O_2$ output of RMD.

VO2 Skin [Equation: Theoretical]

Calculation of the $\dot{V}O_2$ via skin contribution to RMD is achieved using equation (24) as applied by the Stella® flow component "VO2 Skin" using inputs from "Skin SA," "Upper Skin dX," "Lower Skin dX," and "Skin eff f." Because "Skin SA" is estimated using equation (33) which calculates the surface area of the whole SFL (i.e., both upper and lower skin surfaces), the value of "Skin SA" is divided by 2 to give the mean SA for a single side of the SFL.

Additional inputs are provided by "Krogh," as it is assumed that diffusion capacity through cutaneous tissue membranes is the same as via gill tissue membranes. Oxygen tension difference is determined using "PO2" and "PvO2."

```
VO2 Skin = ((Krogh*((Skin_SA/2)/upper_Skin_dX)*(PO2-PvO2)) +
           (Krogh*((Skin_SA/2)/lower_Skin_dX)*(PO2-
           PvO2)))*Skin_eff_f
```

The output of "VO2 Skin" is sent to the stock component "VO2 Tissue" where this value is added to the value produced by "VO2 Q." Thus, "VO2 Tissue" is the integration point within RMD for respiratory and cutaneous-sourced $\dot{V}O_2$.

RMD $\dot{V}O_2$ Output

The cumulative values of "VO2 Q" and "VO2 Skin" are summed and stored in the Stella® stock "VO2 Tissue" which is "drained" by the final output component of the primary model "VO2" as shown in Figure 56.

Figure 56. $\dot{V}O_2$ output component of VO2 derivation sector.

VO2 [Equation: Theoretical]

The value of "VO2" is the sum of "VO2 Q" and "VO2 Skin" and "drains" the "VO2 Tissue" stock each step of RMD execution.

VO2 = VO2_Q+VO2_Skin

"VO2" is the prime output of RMD, representing the O_2 flow capacity in mL O_2/h based on SFL weight, input temperature, salinity, ambient pressure and, if desired, pH and DO. As the total $\dot{V}O_2$ available for a SFL of a given weight, it represents the gross volume of O_2 available per hour. While of interest, this value is not generally useful when evaluating metabolic rate as it does not provide a value per unit weight. To determine the mass value "VO2" output must undergo one more processing step which is accomplished in the last RMD sector to be discussed, "Oxygen Supply."

Oxygen Supply

The "Oxygen Supply" sector, shown in Figure 57, consists of a series of converters that translate the output of "VO2" into several useful formats with differing units for use in other models or comparison to literature data.

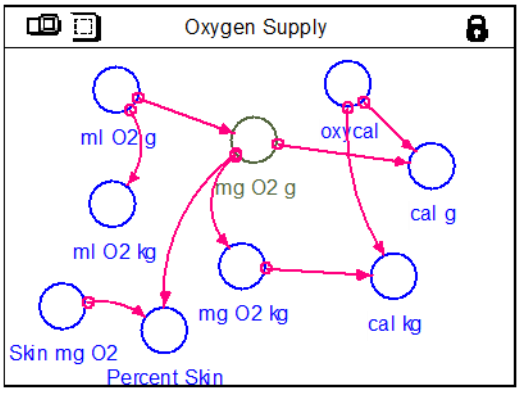

Figure 57. Oxygen supply derivation sector.

Because RMD relies on input data best expressed in mL O_2, the first step in unit conversion is to express "VO2" as a per-unit of mass (in this case, grams).

mL O2 g [Equation: Conversion]

Using inputs from "VO2" and "Wfish," "VO2" output is simply divided by "Wfish" to give a $\dot{V}O_2$ output labeled "mL O2 g" with units in mL O_2/g fish·h. Because the model uses hourly time intervals, the hour reference is left off of labels for simplicity.

mL O2 g = VO2/Wfish

The output of "mL O2 g" is then used by several other converters to obtain useful units.

mL O2 kg [Equation: Conversion]

In "mL O2 kg" the results of "mL O2 g" are converted to mL O_2/kg·h.

mL O2 kg = mL_O2_g*1000

mg O2 g [Equation: Conversion]

Here, "mL O2 g" is converted from a volume O_2 flow ($\dot{V}O_2$), in mL O_2/g fish·h, to a mass flow ($\dot{M}O_2$) value, in mg O_2/g fish·h, using the conversion value of 1.4286 mg O_2/mL O_2, which is the molecular weight (32 g/mole) divided by 22.4 liters/mole, the volume of 1 mole of O_2 at standard temperature and pressure, dry (Lide 2003).

mg O2 g = mL_O2_g*1.4286

The output of "mg O2 g" is significant because Ecophys.Fish uses this unit of measure. The integration of "mg O2 g" into E.F will be discussed in the next chapter.

mg O2 kg [Equation: Conversion]

"mg O2 kg" converts "mg O2 g" into mg O_2/kg·h.

mg O2 kg = mg_O2_g*1000

oxycal [Input: Fixed]

This converter sets the oxycaloric equivalent value of 1 mg O_2 at 3.4 calories/mg O_2 (Brett and Groves 1979).

cal g & cal kg [Equation: Conversion]

Using inputs from "mg O2 g" and "oxycal," "cal g" converts the output of RMD into a caloric value of cal/g fish·h. Substituting "mg O2 kg" for "mg O2 g," the converter "cal kg" provides an output estimate in cal/kg fish·h.

cal g = mg_O2_g*oxycal

cal kg = mg_O2_kg*oxycal

Skin mg O2 [Equation: Conversion]

The converter "Skin mg O2" was added to RMD to facilitate review of the cutaneous contribution to $\dot{M}O_2$, in mg O_2/g fish·h, using inputs from "VO2 Skin" and "Wfish."

Skin mg O2 = (VO2_Skin/Wfish)*1.4286

Percent Skin [Equation: Theoretical]

The converter "Percent Skin" was added to the model to assess the percentage of the cutaneous $\dot{M}O_2$ contribution to the overall $\dot{M}O_2$ output. The output values of "Percent Skin" can be compared to cutaneous respiration percentages reported in the literature to validate that the RMD cutaneous respiration settings produce comparable results.

Percent Skin = (Skin_mg_O2/mg_O2_g)*100

The "Krogh" coefficient in the "VO2 Skin" equation is the product of "BwO2" and "O2 Diff." Both of these inputs are products of "Ta," "Dosat," and "PO2," the interplay of which has a great influence on "Percent Skin." Figure 58 shows the effect of DO from 7 to 4 on skin diffusion efficiency at 25°C with "Skin eff f" = 1 for a SFL up to 500 g. When the temperature is dropped to 15°C with a DO of 4 mg O_2/L water, the effect increases the contribution of "VO2 Skin" to the total $\dot{V}O_2$ output. This is because PO_2 is less (although DO is the same and "O2 Diff" declines), resulting in a higher "BwO2" so that the percent contribution by the skin is comparable to the value seen at DO of 5 at 25°C.

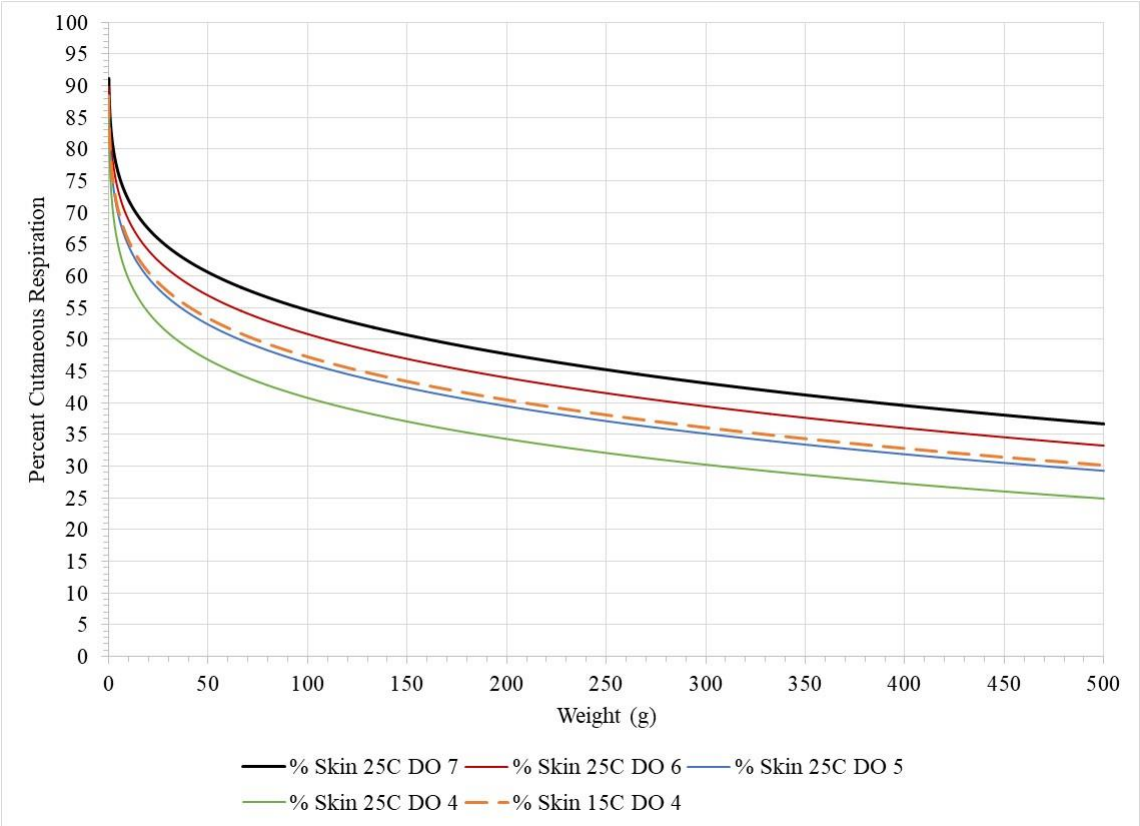

Figure 58. RMD percent contribution of cutaneous respiration to total $\dot{V}O_2$.
Effect of DO from 7 to 4 on percent contribution at 25℃ (solid lines). Effect of change in temperature shown for 15°C with DO = 4 (dashed line). See text for explanation.

CHAPTER VII

INTEGRATION OF THE FLOUNDER RESPIRATORY MODEL WITH ECOPHYS.FISH

The final output of Respiratory Model, Dynamic (RMD) estimates the hourly oxygen flow ($\dot{V}O_2$) available per gram of tissue. The model simulates the both O_2 uptake at the gills and the cutaneous contribution to $\dot{V}O_2$ as a function of SFL body size (and by default, age), with larva up to juvenile sizes benefiting more from cutaneous-sourced O_2 than adults.

The $\dot{V}O_2$ output of RMD was intended as input to the coupled bioenergetics growth model Ecophys.Fish (E.F) (Neill et al. 2004), introduced in Chapter IV, provides the growth model with a $\dot{V}O_2$ estimate-based mechanistic system of ecophysiological responses. This chapter will address the integration of RMD into E.F, and the methods used to optimize the E.F-RMD hybrid model for best fit of outputs to those observed in experiments.

Production of an E.F-RMD version benefitted from addition of several new components. These new E.F-RMD components will be discussed at the end of the chapter, including two new sub-models developed for simulation of starvation death and to display specific respirometry outputs useful for fitting E.F-RMD to data from the Cool-Warm experiment at MDC. For components left un-altered in the integration of RMD, the reader is referred to Neill et al. (2004) for an in-depth description of the E.F model.

Configuration of the E.F-RMD Model

The Stella® graphical representation of E.F-RMD configured to assess SFL growth data obtained from the MDC experiment is shown in Figure 59. In this representation, the primary E.F components have been grouped into two sectors, "Metabolic Rate and Control" which models the effects of environmental factors established by Fry (1971), to simulate MS_{growth}. The other sector, "E.F Growth," is the growth-simulating component of E.F. Above these are the RMD sectors described in the previous chapter.

Also shown are the new sectors that predict death due to starvation (black framed sector), control the simulated respirometry (small green framed sector), and the determination of RMR at the point of limiting oxygen concentration (LOCr). The ratio of RMR and LOCr is used to determine the marginal metabolic scope (MMS) (large green sector).

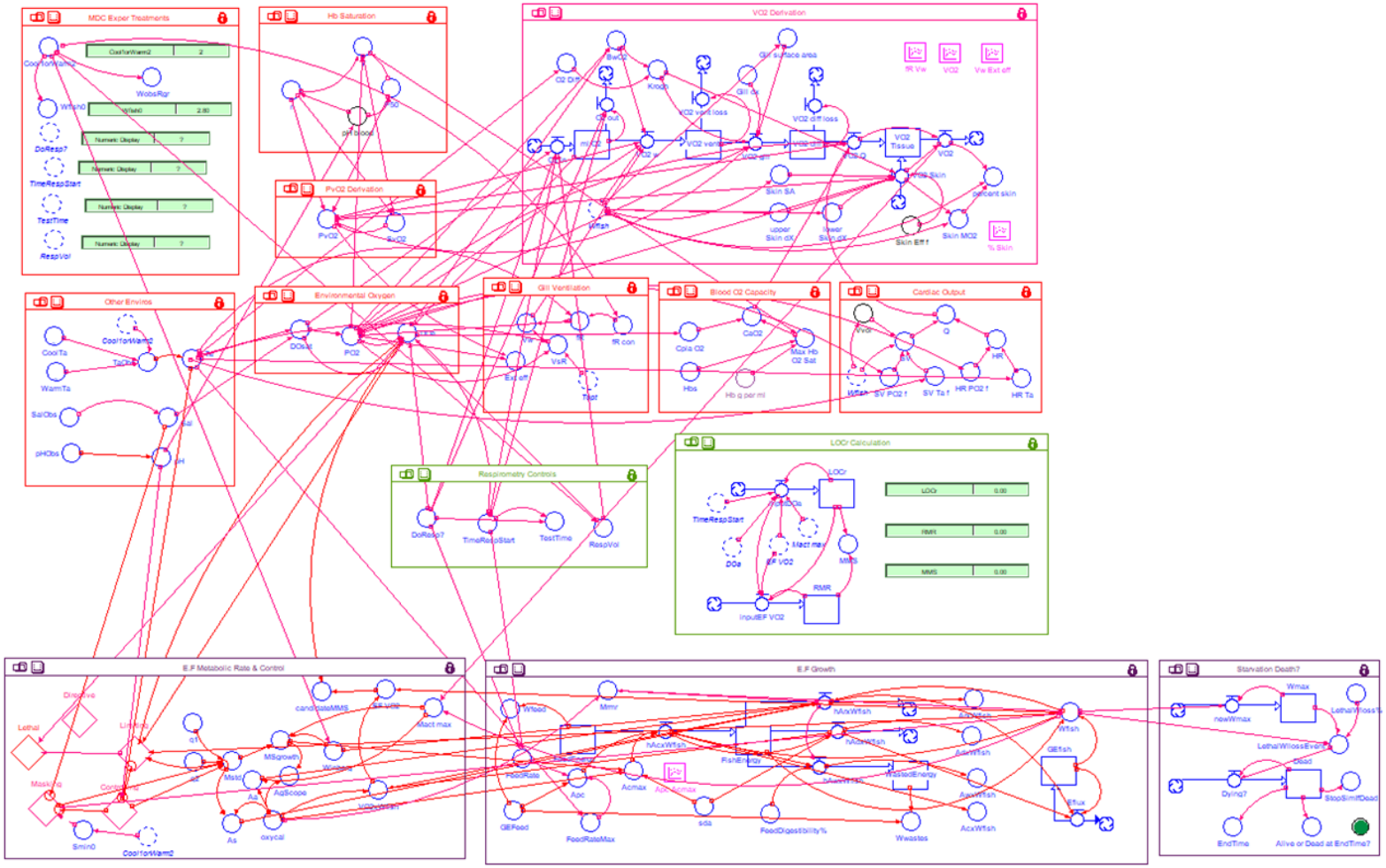

Figure 59. Ecophys.Fish-Respiratory Model, Dynamic: STELLA® model of Southern Flounder growth.
MDC Cool - Warm model.

Shared Inputs

Both RMD and E.F require environmental inputs to function. For E.F-RMD, the temperature, pH, and salinity inputs are grouped and shared. Oxygen-related components are grouped in a separate sector (either as PO2 or DO). Unlike the basic RMD model, which determines DO from PO2 based on the fraction of O2 in the environment, E.F-RMD uses two alternative DO inputs; either the Green and Carritt (1967) calculation to produce "DOsat," which assumes a fixed O2 fraction, or "DOa," which is based on the amount of O2 on a volumetric basis in the simulated respirometer modeled within RMD.

Integration of RMD into E.F

RMD provides source control of the maximal available $\dot{V}O_2$. The converter "VO2" combines respiratory and cutaneous sourced $\dot{V}O_2$ in ml O_2/h and is the primary RMD export to E.F, where it is converted to mg O_2/g fish·h and labeled "Mact max," the maximum active metabolic rate given current environmental conditions and physiological limitations. The substitution of RMD-derived $\dot{V}O_2$ within E.F removes any influence of the E.F-derived "Mact" by the "Limiting" decision diamond. The integration of E.F with RMD moves the role in calculating the limiting influence of $[O_2]$ on metabolic rate to the inherent and emergent O_2 control mechanisms within RMD.

Input from E.F into RMD

To serve as a respiratory sub-model of E.F, RMD requires feedback to account for changes in environmental conditions. Ecophys.fish's primary state-change output is, as befitting a growth model, the weight of the subject fish, "Wfish," which significantly impacts RMD's $\dot{V}O_2$ calculations.

Model Parameterization for Growth and Respirometry

Growth occurs only if a surplus of energy is available after meeting the organism's routine metabolic requirements (Fry 1971, Neill et al. 1994). Energy for growth is sourced from chemical combustion of food with O_2 (von Bertalanffy 1957, Neill et al. 2004, Stevens et al. 2006, Kerkhoff 2012). Growth can be limited or accelerated by adjusting the metabolic and the caloric energies allocated for growth and/or by adjustments to the metabolic costs such as the RMR and costs associated with digestion and waste removal. While multiple variables can be adjusted in either sector, only a few keystone variables need adjustment. If altered, a keystone variable substantially impacts the outcome without causing outcomes to exceed normal physiological ranges and/or inappropriate impacts on other processes.

The components of the metabolic sector which have the most influence on metabolic rate in the control of growth are all inputs to "MSgrowth": "Mact max," "Winberg," and "Smin." Within the growth sector, "GEFeed" and "FeedRateMax" affect energy availability while "sda" and "FeedDigestibility%" affect energy costs or loss. The process by which these components are adjusted is discussed in the next sections.

Growth Control: Metabolism

Not surprisingly, the parameter "MSgrowth" plays a key role in affecting simulated growth. It is calculated by subtracting the product of the "Winberg" value and the standard metabolic rate "Mstd" from "Mact max" as indicated:

MSgrowth = Mact_max-Winberg*Mstd

Essentially "MSgrowth" is an energy-balance model, with available energy for growth provided by "Mact max." Metabolic energy is removed via the maintenance "costs" represented by "Winberg" and "Mstd." Increasing "Mact max" and/or decreasing "Winberg" and/or "Mstd" increases MS_{growth} and vice versa.

Changing the flows affecting "MSgrowth" is a simple matter. This is certainly true for "Winberg," which is a fixed value, but as "Mact max" and "Mstd" are the end products of a multitude of other variables and calculations, the use of one or more keystone processes in proceeding calculations has proven more effective.

MSgrowth Control: Mact Max

Controlling the effect "Mact max" has on growth means controlling the $\dot{V}O_2$ output of RMD. There are, of course, multiple components of the model that could be altered to achieve this. However, the most effective means of adjusting $\dot{V}O_2$ was finding and using a variable that impacts all $\dot{V}O_2$ calculations while maintaining the model's fidelity within physiological limits.

Fortunately, the model's design is such that adjustments to gill ventilation, "Vw," the first O_2 supply source, impact all subsequent $\dot{V}O_2$ calculations except cutaneous $\dot{V}O_2$, which can be adjusted by changing the skin diffusion efficiency fraction found in

"Skin eff f." Because cutaneous diffusion efficiency declines at a fixed rate with growth and is a passive process dependent upon environmental conditions, "Skin eff f" is generally not changed.

Use of fR Con for Managing Growth and Respirometry

Variation of "fR con" proved effective for adjusting modeled water flow over the gills, and thus ventilation-sourced $\dot{V}O_2$ from "VO2 w" ("VO2 w" being the product of ventilation volume "VsR" and ventilation frequency "fR" – see previous chapter). Of the two variables, "fR" has the greatest capacity for adjustment and is why the adjustment constant "fR con" was included in the model. It is through "fR con" that the "VO2" and subsequently "Mact max" value can be most efficaciously adjusted.

When fitting E.F-RMD to a growth model, the value of "fR con" may be set to a value that best approximates the observed growth when the model is run. In this circumstance, a variance in the "fR con" value may be permissible. However, when fitting the model using simulated respirometry to observed data, the value of "fR con" may require a particular value to achieve accurate results.

Simulated respirometry was used for the determination of the limiting oxygen concentration for routine metabolism (LOCr), which is the DO level corresponding with the intercept of routine metabolic rate (RMR) with the active metabolic rate, construed as equivalent to "Mact max." As simulated respirometry proceeds, "Mact max" declines as "DO" in the simulated "respirator tank" becomes limiting.

When fitting E.F-RMD to respirometry data, the objective is for simulated RMR to intercept "Mact max" at the observed LOCr. Achieving this requires some precision.

The "Mact max" value at the start of simulated respirometry must be at a specific value, and $\dot{V}O_2$ (i.e., rate of O_2 is removed from the respirometer) must also be at a specific rate so that the slope of the decline for "Mact max" intercepts RMR at the correct DO level. Because of the importance of "fR con" in determining "Vw," its value must also be precisely set, if the model respirometry output is to be fit to the desired LOCr value.

MSgrowth Control: Winberg

The input variable "Winberg" is an application of "Winberg's rule," which nominally sets RMR as a multiple of SMR (Winberg 1960, Neill et al. 2004). The Winberg value is often assumed to be about 2, i.e., RMR is twice SMR, but this may not always be the case. Potentially the "Winberg" value may vary by species and/or across environmental conditions. From the modeler's perspective, the uncertainty of the "Winberg" value is advantageous as it allows adjustments within the model while still allowing for the maintenance of model fidelity. Still, there are limits to the allowable variance of "Winberg." A Winberg value of 1 simply means that RMR equals SMR, which is unlikely unless the fish is comatose. Too high a Winberg value and the RMR would be too metabolically costly for the fish to survive and grow. While no firm range has been established, when adjusting the model Winberg value, an attempt was made to keep it within the 2 ± 0.5 range.

MSgrowth Control: Mstd

Standard metabolic rate is a function of "Mstd," which in E.F is a function of the loading effect of salinity "S," thermal acclimation "Taccl," and thermal stress "Tstress" effects as shown.

Mstd = S*EXP(q1*Taccl)*EXP(q2*Tstress)

Adjustment to "Mstd" can be achieved through the thermal variables "q1," the acclimated thermal steady-state rate constant, and "q2," the thermal stress transient state rate constant (Neill et al. 2004). While either "q" variable may be adjusted to impact "Mstd," only "q1" was used for fitting E.F-RMD to data, to avoid any unforeseen interactions that might occur when changing more than one parameter within an exponential function.

An adjustment may also be made to "Mstd" by changing the salinity loading (or masking) factor "S" which in E.F is defined:

S = Smin+Sgain*Svar

Of the three variables that define "S," it is "Smin," the minimum of "S" at optimal salinity, that provides the most useful means of adjustment. Calculation of "Smin" is shown below as a function of fish weight and "Smin0," which is defined by Neill et al. (2004) as "the ultimate intercept of standard metabolic rate."

Smin = Smin0*Wfish^-0.2

When fitting E.F-RMD to other growth models, the preferred method for metabolic adjustment to "Mstd" was achieved by making adjustments to "Smin0" and using the thermal acclimation variable "q1."

In summary, growth control for fitting E.F-RMD output to measured growth data can be accomplished of "MSgrowth." The metabolic scope for growth variables deemed best for fitting E.F-RMD output to data are "fR con," "Winberg," "Smin0," and "q1."

The resulting "MSgrowth" value is then exported to the "E.F Growth" sector where, because the energy unit of choice for E.F is the calorie (specifically calories per day), "MSgrowth" is converted to calories/time by multiplying any given metabolic rate by the oxycaloric conversion factor of 3.4 cal/mg O_2 (Neill et al. 2004).

Growth Control: Caloric Intake

Modulation of caloric content and consumption of "feed" to affect model growth is well established (von Bertalanffy 1938, 1957, Roff 1983, Neill et al. 2004, Stevens et al. 2006). The three variables within the "E.F Growth" sector that affect "feed" caloric content are "GEFeed," "FeedRate," and "FeedRateMax." Of these three variables, only "GEFeed" and "FeedRateMax" are useful for controlling available "calories" as "FeedRate" is a fixed value of 1. Caloric consumption, and hence calories not available for growth, may be modified through adjustment of the specific dynamic action constant "sda" (a percentage estimate of energy expended for digestion) and "FeedDigestibility%" a percent measure of how much food consumed is digestible, the remaining fraction being non-digestible waste. The metabolic cost of nitrogenous waste is not adjustable and fixed within E.F at 5% of available energy.

Caloric Control: GEFeed

The most direct method to control feed-energy intake within E.F-RMD is through the adjustment of "GEFeed," which establishes the caloric content of feed per gram as-fed (Neill et al. 2004). Caloric content of food has a significant effect on a flounder's growth rate (Seikai et al. 1997). For example, growth-maximizing feeds such as the Mysid Shrimp *Taphromysis bowmani Bacescu* have an energy content of over

4000 cal/g feed dry weight (Johnson and Hopkins 1978). Change in "GEFeed" is at the discretion of the modeler; however, a fixed value between 1000 to 4000 cal/g feed typically is mandated by known energy-density of the particular feed or forage. Changing "GEFeed" within a model run certainly is not prohibited, and even becomes appropriate under simulated conditions of temporal variation in feed composition or availability. However, as a general rule, using a fixed "GEFeed" for each model run eliminates the introduction of any possible confounders to calculating growth. All growth comparisons conducted for the validation of E.F-RMD were accomplished using fixed "GEFeed" values for each growth simulation conducted.

Caloric Control: FeedRateMax

Control of caloric intake can also be achieved by adjusting the rate at which feed is consumed. Within E.F this is controlled by the function "FeedRateMax." The standard "FeedRateMax" value used within E.F is a negative-power function of weight, as shown in equation 49.

$$FeedRateMax = T_f \cdot {W_{fish}}^{b} \tag{49}$$

The output of function "FeedRateMax" represents the maximal daily rate of feeding and physiological processing (Neill et al. 2004), with exponent *b* being a negative value that sets the rate of decline in feed rate per-unit body weight, with further adjustments to the maximum feed rate possible through the use of a temperature-dependent quadratic equation represented by T_f.

This "FeedRateMax" model is consistent with growth studies of Japanese Flounder, by Iwata et al. (1994) and Seikai et al. (1997), who found daily feed rate is

influenced by both weight *and* temperature. Iwata et al. (1994) demonstrated that as weight increased, feed rate declined. In contrast, temperature effects were more nuanced, with growth rate peaking at an optimal temperature range and stabilizing or, in some cases, slightly declining when the ambient temperature was below and above an optimal temperature.

The effects of increasing body weight on feed rate decline may have been independently identified by Neill et al. (2004) when modeling the "FeedRateMax" for Red Drum *Sciaenops ocellatus*. The initial use of a simple power function proved insufficient, necessitating the introduction of a natural negative log function for the *b* exponent in equation (49) to fit the observed data. However, other variants of E.F have used a fixed *b* value of -0.3 which has also worked well for E.F-RMD.

Although temperature effects were not factored into the "FeedRateMax" calculation of the Red Drum E.F model, the success of Neill et al. (2004) in factoring weight effects on feed rate validates the utility of controlling feed energy within the model using "FeedRateMax." Thus, weight effects, via exponent *b*, and temperature effects, via variable T_f, in the basic equation were pursued to further refine caloric growth control within E.F-RMD.

Using the observations of Iwata et al. (1994) as a reference, temperature effects on feed rate were expressed using the parabolic formula shown in equation (50)

$$T_f = -xT^2 + yT \tag{50}$$

where *x* and *y* are constants and T is the temperature in °C.

The values for *x* and *y* may need to be independently determined by the modeler for each data set analyzed. For example, the following "FeedRateMax" formula was used to fit E.F-RMD growth output to a growth algorithm from pond-grown SFL for data collected by Sea Center Texas at Galveston ponds.

FeedRateMax = ((-0.000046*Ta^2+0.0046*Ta)* Wfish^-0.3)

Figure 60 graphically shows the T_f value across temperatures when T_f = -0.000046*Ta^2+0.0046*Ta.

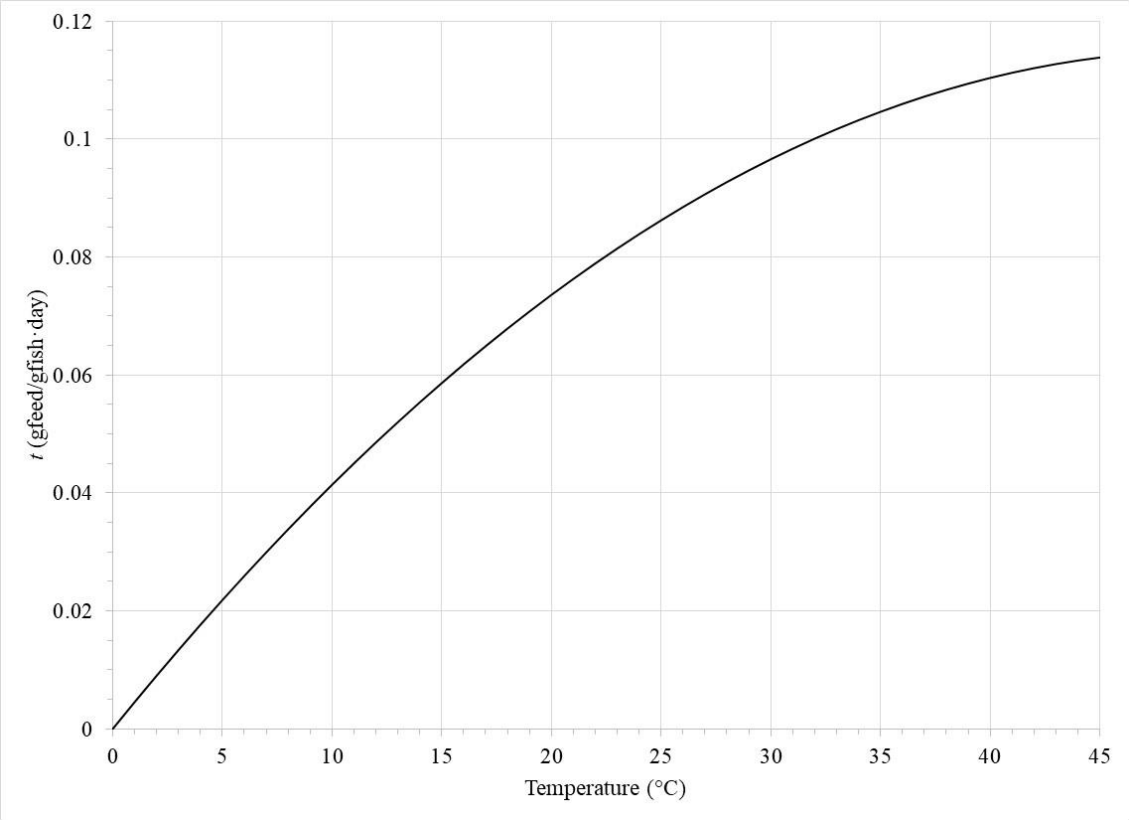

Figure 60. Example T_f output for FeedRateMax fit to SCT pond data.
Formula: T_f = -0.000046*Ta^2+0.0046*Ta.

Under certain conditions, when the weight range of the fish being modeled is limited, it may be possible to use a "FeedRateMax" function that accounts only for temperature effects. This exception was discovered when fitting the "FeedRateMax" to data for SFL raised at the MDC under Warm and Cool temperatures. Initially, two "FeedRateMax" equations were used to obtain a proper growth match for each temperature condition. However, when the "FeedRateMax" value for each group was graphed (see Figure 61), it became apparent that an overall temperature linear trend existed independent of weight. When calculated, "FeedRateMax" increased with temperature according to the following equation:

FeedRateMax = 0.0001*Ta^2

This calculation permitted the use of a single, linear equation that could be used to predict "FeedRateMax" under both temperatures regimes without the need for two independent equations.

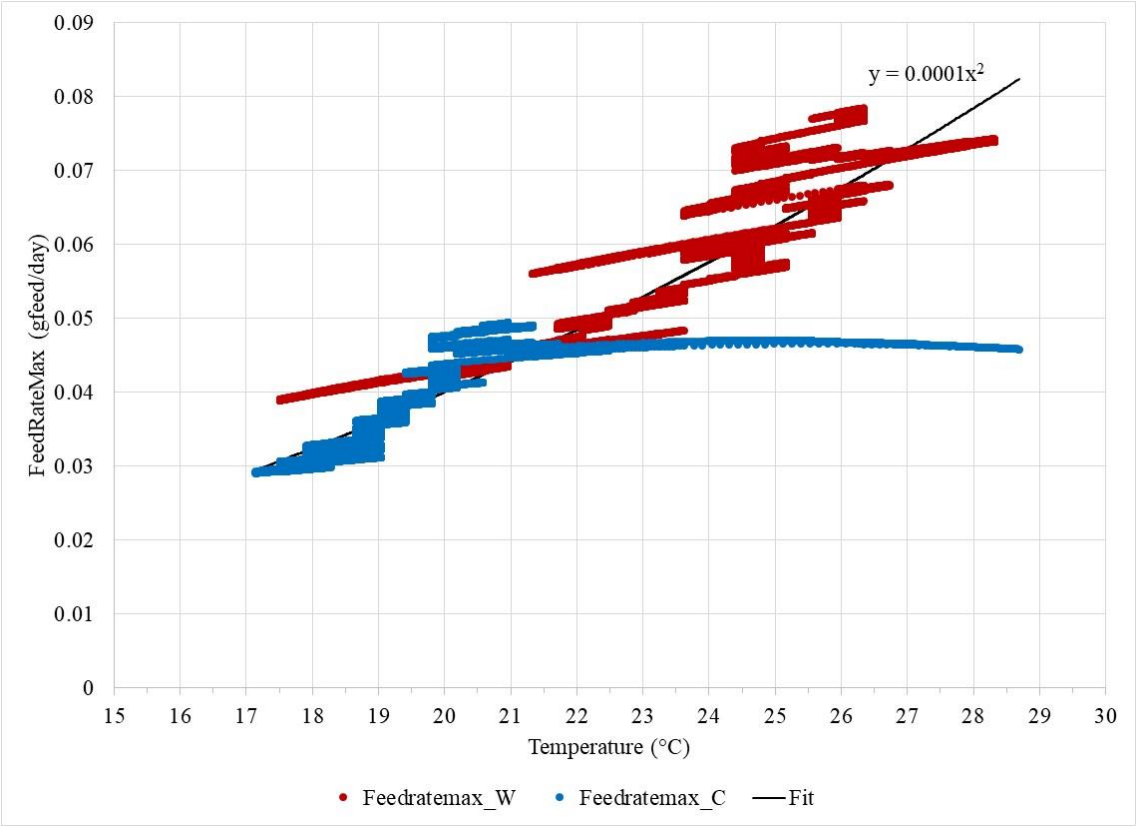

Figure 61. Calculated FeedRateMax fit to MDC Warm and Cool data.
FeedRateMax Warm (FeedRateMax_W – red) and Cool (FeedRateMax_C – blue) fit using thermal and weight effects calculation. Linear fit line and equation based on the trend-line calculated using Excel. The significant thermal excursions in Cool data were due to power failure during the study resulting in tank warming until power was restored.

As stated, the linear relationship (excursion aside) between these two data sets may be the exception, and care should be taken not to assume a linear thermal relationship independent of weight exists in all situations.

Caloric Control: Feed Costs and Inefficiency

Not all calories liberated from feed are available for metabolism and growth. Digestion of the food and subsequent nutrient-processing impart an energy cost, represented by "sda." Within E.F-RMD, the "sda" value is fixed but can be adjusted

before running the model. The current "sda" is set to 0.14, or a 14% cost for digestion and other feed-processing costs.

Another variable to consider is "FeedDigestibility%" which is a measure of the feed that is "digestible" and provides calories for metabolism and growth. The nominal setting for "FeedDigestibility%" is 0.9, or 90%, but this may be reduced as needed before running the model. For prepared feeds of inferior quality, it may be considerably lower.

E.F-RMD Alterations and Additions

The developer of Ecophys.Fish, Dr. William Neill, continued his work with E.F beyond the model reported in Neill et al. (2004), including the added capability for simulated respirometry. This feature has been incorporated into E.F-RMD with minor modifications.

To aid in the review and analysis of E.F-RMD during its development, two add-on models permitted the prediction of "starvation death" of an SFL should conditions be inadequate to support the maintenance of body energy and mass, and a sub-model for determining LOCr, the limiting oxygen concentration for routine metabolism, which represents the convergence of maximum (active) and routine metabolism. Neither of these two sub-models is necessary for E.F-RMD to function, but they provide significantly added awareness of the model's output performance, particularly when fitting model output to data; thus, they may be considered integral parts of E.F-RMD.

Respirometry Controls

Respirometry controls are found in the "Respirometry Controls" sector shown in Figure 62. The converters found in this sector are used to activate the respirometry function. They establish when this occurs during the growth simulation and set the "respirometer" volume.

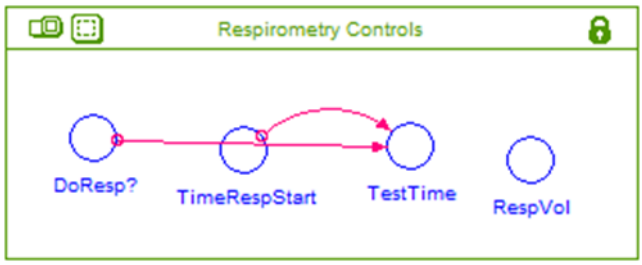

Figure 62. RMD respirometry controls sector.

DoResp? [Input: Fixed]

The converter "DoResp?" is the switch used to turn the respirometry function on or off. If the value is set to zero, then the respirometry function is deactivated according to the criteria found it "O2 in" and "O2 out." A value other than zero will activate the respirometry function (setting value to 1 is expected).

TimeRespStart [Equation: Decision]

The converter "TimeRespStart" sets the time for starting respirometry, which is 24-time steps (i.e., DTs) prior to the proscribed end run-time. Since the model time intervals are in hours, this corresponds to 24 hours before the model stop time.

TimeRespStart = STOPTIME-24

The “TimeRespStart” value is also used by the E.F “FeedRate” function to trigger fish “fasting” by setting the “FeedRate” value to zero, 24 hours before the start of respirometry, i.e., TimeRespStart - 24.

TestTime [Equation: Decision]

The converter “TestTime” allows the model run to be paused, if desired, when respirometry starts. The pause allows the user to inspect state of the model at the beginning of simulated respirometry. This feature can be deleted or disabled by changing “PAUSE” to “TIME” in the equation.

TestTime = IF DoResp? = 0 THEN TIME ELSE (IF TIME =
TimeRespStart + 1 THEN PAUSE ELSE TIME)

RespVol [Input: Fixed or Variable]

“RespVol” sets the respirator’s “water volume,” in liters. Volumes are generally set to between 1 to 4 L. The larger the volume, the greater the “volume” of O_2 available within the “ml O2” stock, and the longer before LOCr is reached. This allows adjustment of the rate of O_2 decline in the “ml O2” stock at any given $\dot{V}O_2$, with larger volumes providing slower rates of decline, and therefore more sensitivity when determining LOCr.

DOa [Decision, Theoretical]

One respirometry controller not within the “Respirometry Control” sector is “DOa” which is found in the “Environmental Oxygen” sector. This decision function

calculates DO decline when virtual respirometry is activated by converting the value of "ml O2" stock back to mg O_2/L. Otherwise, the value for this parameter is the same as the estimated DO from "DOsat."

DOa = IF DoResp? = 0 THEN DOsat ELSE (IF TIME < TimeRespStart THEN DOsat ELSE (ml_O2/0.7)/RespVol)

Respirometry

Respirometry was added to E.F-RMD by attaching flow and stock components to the "VO2 w" inlet flow in the "VO2 Derivation" sector of RMD. In its basic form, RMD assumes an unlimited "water" supply to the "VO2 w" flow (symbolized by a cloud on the end of the flow icon). By adding a flow and stock to the $\dot{V}O_2$ model, see Figure 63, O_2 "volume" available to "VO2 w" can be limited to simulate a closed respirometry system. Components of the model are "O2 in" which models O_2 volume (in mL) being supplied per hour, "ml O2" is the stock function which "collects" the available O_2 while "O2 out" clears the value in "ml O2" after each DT when in non-respirometry mode. When respirometry is started, "O2 in" and "O2 out" controls are set to zero so the amount of O_2 available to the model becomes fixed to the amount "trapped" in the "ml O2" stock.

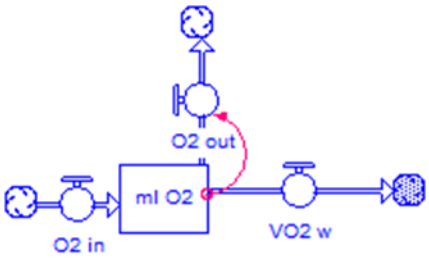

Figure 63. RMD respirometry component model.
"VO2 w" included to show how model integrates into $\dot{V}O_2$ derivation.

O2 in [Equation: Decision, Theoretical]

The "O2 in" flow function controls the amount of O_2 in mL available for use by the model using Boolean functions and four input processes: "DoResp?," "DOsat," "RespVol," and "TimeRespStart."

O2 in = IF DoResp? = 0 THEN (DOsat*0.7)*RespVol ELSE (IF TIME < TimeRespStart THEN (DOsat*0.7)*RespVol ELSE 0)

If "DoResp?" is set to 0 (i.e., off), then the volume of O_2 availability to the model is limitless. The amount of O_2 (in mL) at any given moment is determined by the theoretical function (DOsat*0.7)*RespVol. As DO is in mg O_2/L water, multiplying by 0.7 converts this value to mL O_2/L water. Multiplying by "RespVol" in L reduces the value to available O_2 volume. If "DoResp?" is set to any value but zero, then the respirometry function is enabled but will not activate until the model run time meets the criteria established by "TimeRespStart." Before starting the respirometry function, O_2 availability is determined by (DOsat*0.7)*RespVol. When respirometry start time is

reached the value of "O2 in" is set to zero, stopping any O_2 "flow" into the "ml O2" stock.

O2 out [Equation: Decision]

The flow function "O2 out" acts as a valve, allowing the value of the stock "ml O2" to "drain out" after each time interval, as the flow value equals that of the stock value if "DoResp?" = 0. If the respirometry function is activated, this "valve" is "shut" by setting the "O2 out" value to zero, thus fixing the "ml O2" stock value to that of the "O2 in" value at the DT just before the respirometry start time.

O2 out = IF DoResp? = 0 THEN ml_O2 ELSE (IF TIME <

TimeRespStart THEN ml_O2 ELSE 0)

Starvation and Death

The integrated E.F-RMD introduces several new sub-model components, the first of which is "Starvation Death?" (Figure 64), developed specifically for E.F-RMD to model fish death due to starvation.

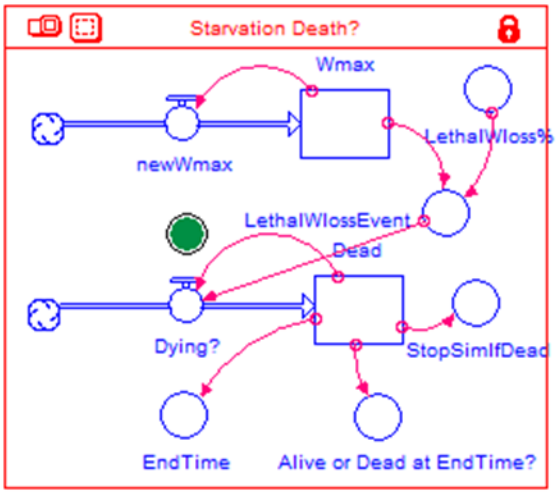

Figure 64. Starvation death sector.

The starvation sub-model consists of two flow and stock components which determine maximum fish weight at a given time and whether any weight decline results in death. Nominally, death occurs whenever Wfish has declined by 50 % of its previous maximum.

newWmax [Equation: Decision] and Wmax [Input: Variable]

This stock-flow arrangement uses Boolean statements to maintain a tally of "Wfish," retaining the positive value of the difference if "Wfish" is larger than the stock value of "Wmax," the maximum of previous DT fish-weight values within the current model run (initial value is also "Wfish"). If "Wfish" is less than the previous calculation, the value of "newWmax" is set to zero. Because stocks accumulate, i.e., sum, all input flows, if the "newWmax" output is zero, then stock "Wmax" retains the greatest weight reached up to that point in the model run.

newWmax = IF Wfish > Wmax THEN Wfish - Wmax ELSE 0

LethalWloss% [Input: Fixed]

This converter sets the percentage of weight loss at which the "fish" will succumb to "starvation." The default setting is 50, representing a 50% loss of body weight.

LethalWlossEvent [Equation: Decision, Theoretical]

This equation produces a binary output if "Wfish" declines below the "LethalWloss%" value of "Wmax" to determine if the lethal weight loss threshold is reached. With "LethalWloss%" set to 50, then "LethalWlossEvent" will be 1 if "Wfish" falls below 50% of "Wmax," otherwise the output will be 0.

LethalWlossEvent = IF Wfish < (1-LethalWloss%/100)*Wmax THEN 1
ELSE 0

Dying? [Equation: Decision, Theoretical] and Dead [Input: Variable]

This stock-flow arrangement of "Dying?" and "Dead" creates a logic switch, the binary output of which determines whether the SFL meets the criterion for death.

Dying? = IF (Dead = 0) AND (LethalWlossEvent = 1) THEN 1 ELSE 0

If "LethalWlossEvent" is 0 (i.e., weight loss threshold has not been reached), and the value of the stock "Dead" is 0, then the output of "Dying?" is 0, and the stock value of "Dead" remains 0. If the "LethalWlossEvent" output is 1 (weight loss threshold reached) and the SFL is not already dead (i.e., "Dead" = 0), then the output of "Dying?" is 1 and the stock value of "Dead" becomes 1, signaling a death event.

StopSimIfDead [Equation: Decision, Theoretical]

If the value of stock "Dead" is 1, the converter "StopSimIfDead" creates a mathematical exception error within Stella® by dividing 1, the value of "Dead," by zero. Otherwise, the value of "StopSimIfDead" remains at zero.

StopSimIfDead = IF Dead = 1 THEN Dead/0 ELSE 0

When a mathematical error occurs, Stella® stops the simulation and displays a warning to the user, a built-in and intentional feature of the program.

EndTime [Equation: Decision]

This function allows the modeler to know the time of "death" for the model's "From" and "To" run time specifications. For example, if the Stella® run specifications are set as "From: 1" and "To: 100" and the "death" criterion is met at model run time sequence 62, then the "EndTime" value will be 62; otherwise, it will display the final "To" value of 100 (i.e., the "STOPTIME" value).

EndTime = IF Dead = 0 THEN STOPTIME ELSE TIME

Alive or Dead at EndTime? [Equation: Theoretical]

Though this converter is a mathematical function, the output of "Alive or Dead at EndTime?" is used as a decision switch by the Status Indicator, shown as a green dot in Figure 64. The Status Indicator is a Stella® feature that allows visual confirmation of model conditions. As configured in this model, the Status Indicator remains green as long as the value of "Alive or Dead at EndTime?" is 1 (i.e., "Dead" = 0). If "Dead" = 1,

the output value becomes zero, and the Status Indicator flashes red to alert the modeler that starvation-death has occurred.

Alive_or_Dead_at_EndTime? = 1-Dead

Indication of death triggers model termination. This is a useful tool which can be used to predict lethal factors that impact growth, such as temperature and DO.

LOCr Calculation

Adding respirometry capability to E.F-RMD was not undertaken without purpose. Being able to conduct virtual "respirometry" enables the model to be properly parameterized so that model metabolic output indices such as LOCr, RMR, and MMS fit can be measured or calculated. This is accomplished in the "LOCr Calculation" sector, the structure of which is shown in Figure 65. External inputs to this model are "TimeRespStart," which was discussed above, "Mact max," also previously discussed, "EF VO2," the E.F calculated $\dot{V}O_2$, and "DOa," a decision function that calculates DO decline when virtual respirometry is activated.

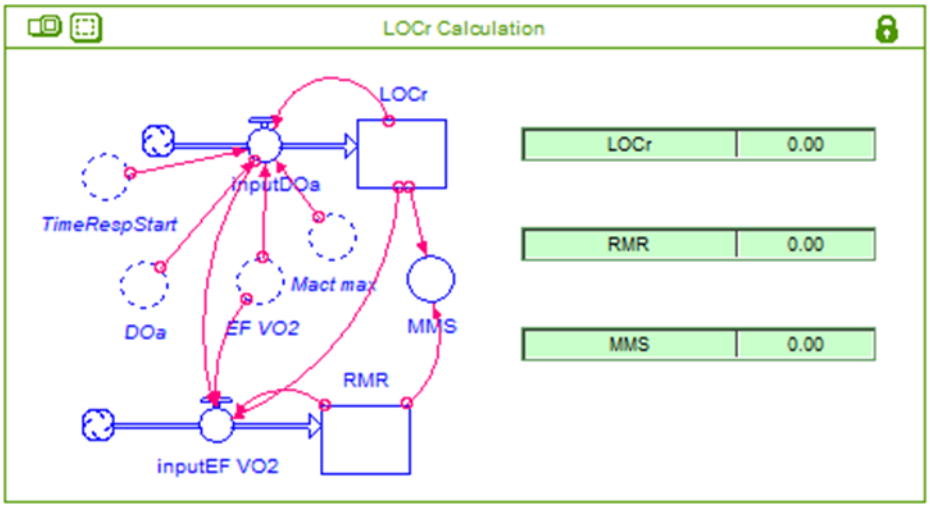

Figure 65. RMD LOCr calculation sector.

External inputs to this model are "TimeRespStart," which was discussed above, "Mact max," also previously discussed, "EF VO2," the E.F calculated $\dot{V}O_2$, and "DOa." Within the "LOCr calculation" sector are two flow and stock functions which calculate LOCr and RMR. Calculation of LOCr uses the flow component labeled "InputDOa" and the stock "LOCr." The calculation of RMR uses the flow component labeled "inputEF VO2" and stock "RMR."

InputDOa [Equation: Decision, Empirical]

The "InputDOa" equation uses Boolean functions to determine that if two conditions are met, that the time sequence is one greater than the respirometry start time and that the "EF VO2" values are greater than 95% the "Mact max" value. If these conditions are met, the output value is the difference between "DOa" and the value of

the stock "LOCr" per time-change interval. Because the two conditions are only met once during any given model run, the value that "fills" the stock is the LOCr value.

InputDOa = (IF (TIME > TimeRespStart + 1) AND (EF_VO2 > 0.95 * Mact_max) THEN DOa - LOCr ELSE 0)/DT

InputEF VO2 [Equation: Decision]

This flow-stock function inputs the E.F-calculated $\dot{V}O_2$ into the stock "RMR" at the moment when LOCr is reached. The default input value is 0 unless certain criteria are met: if either the value of flow "InputDOa" or stock "LOCr" exceed 0.001 mg O_2/L water (which will not happen unless the "InputDOa" criteria are met) *and* the value of stock "RMR" is 0, then "inputEF VO2" inputs the value of "EF VO2" into stock "RMR." Once the "RMR" equals the "EF VO2," the decision criterion that "RMR" equals zero is no longer met, and the default output of the flow returns to zero.

inputEF VO2 = (IF ((inputDOa > 0.001) OR (LOCr > 0.001)) AND (RMR = 0) THEN EF_VO2 ELSE 0)/DT

MMS [Equation: Theoretical, Decision]

The margin of metabolic scope "MMS" is the ratio of the values in stock "RMR" to "LOCr." "MMS" is calculated for each DT, but the value of "LOCr" is zero until "InputDOa" criteria are met. To prevent a mathematical fault error from occurring when the "LOCr" is zero, a MAX function is used to set the denominator no less than a value 0.001.

MMS = RMR/MAX(0.001,LOCr)

Summary

The integration of E.F-RMD goes beyond E.F's obvious fusion with RMD. Each model consists of sub-models developed as independent models in their own right before being integrated into each major model. The first and most basic step in the integration process is to identify common variables so that these can be shared to reduce overall model complexity. The most obvious examples with E.F-RMD are environmental input conditions such as temperature, salinity, DO, PO_2, and pH. Less obvious is fish weight which plays a significant role in cardiac and buccal volumes, gill and skin surface area within RMD and the determination of metabolic rates within E.F.

Beyond fish weight and environmental inputs, integration of the RMD $\dot{V}O_2$ output into E.F required proper union of the two models' functionalities. The parts of E.F that yielded an empirical measure of active metabolic rate (Mact) were successfully replaced by RMD, to provide for a system of more mechanistic relations faithful to known respiratory and circulatory physiology of fish. Moreover, RMD explicitly embraced cutaneous respiration that logically is so important to oxygen-uptake in Southern Flounder and other flatfishes at smaller sizes.

Finally, the integrated model was equipped with features that enhanced its utility and convenience. These included components for simulating respirometry with display of RMR, LOCr and MMS endpoints, and for simulating mortality due to starvation.

CHAPTER VIII

MODEL EVALUATION

No model is perfect, and all models are built on the assumption that the output provides information relevant to real-world observations. The inherent limitation of models similar to E.F-RMD is that they are efforts to use basic equations to capture dynamic events influenced by multitudes of physical, chemical, and biological interactions. If properly conceived, models provide useful and credible information. Therefore, how we assess that utility and credibility is an important component of the modeling process.

Determining the efficacy of a model may be facilitated by the adoption of an evaluation process. As mentioned in Chapter IV, approaches to modeling theory are varied but agree on the broader steps of conceptualizing and structuring, creating, evaluating, and applying the model (Grant et al. 1997, Hannon and Ruth 1997, Ford 1999, Caswell 2001, Bolker 2008, Van den Berg 2011).

Statistical Measurement of Model Consistency with Observed Data

The E.F-RMD model was evaluated by assessing "goodness-of-fit" (GoF) between observed (*Yobs*) and modeled (*Ymod*) output values via Pearson's coefficient of

determination (R^2)[11] (Quinn and Keough 2002) and "Consilience" (C) (Neill et al. 2018).[12] Unlike R^2, which measures the GoF to a least-squares regression line, C is a measure of the GoF to the "line of perfect agreement" between *Yobs* and *Ymod*, Perfect agreement between paired values of *Yobs* and *Ymod* for all pairs in a dataset yields C = 1. A value of C less than 1 indicates a less than perfect fit, with the value going negative for fits worse than a random scatter of points with the same mean and variance as the Yobs set. Unlike other GoF statistics designed to assess the accuracy of statistical models, C is "…intended to capture and portray mechanistic truth about the system being modeled" (Neill et al. 2018).

Consilience values are considered significant if $C > C'(\alpha)$, where C' is the critical value of C for a given α. For a given value of α, the value of C' is calculated relative to sample size using an "empirical reverse power-hyperbolic function" described by Neill et al. (2018). For all analyses reported, a C value was considered significant for a given data set if C was greater than C' at $\alpha = 0.05$, written as $C'(0.05)$.

The determination of C' allows for calculation of the probability distributions across sample sizes for different α values (Neill et al. 2018). Although $\alpha = 0.05$ is

---

[11] In keeping with the rationale given by Neill et al. (2018), R^2 is used instead of r^2 as RMD and E.F-RMD are complex dynamic models, and they are more similar to multiple rather than simple regression models.

[12] For a more detailed explanation of Consilience, please see "Consilience: A Holistic Measure of Goodness-of-Fit": https://www.researchgate.net/publication/328465276_Consilience_A_Holistic_Measure_of_Goodness-of-Fit_revised_21Oct2018

considered significant, the calculated probability of C having a greater value than C', written as Pr(C>C'), may be lesser or greater than the P<0.05 objective.

All GoF comparisons were performed using a Microsoft Excel spreadsheet developed by Neill et al. (2018) which may be found online at: http://people.tamu.edu/~w-neill/Consilience/HGoFtemplateM5-18Mar18.xlsx

The P-values given for C analysis of RMD and E.F-RMD outputs to observed data are the spreadsheet-calculated type-l error probability. All significant (P<0.05) Consilience estimates presented in tables will be indicated with an asterisk (*).

Example Models

To better differentiate between R^2 and C, two hypothetical models (A and B) are shown in Figure 66. If their R^2 values are equal, then models A and B produce values of Ymod with equally "good" fits to their respective linear-regression lines, but that does not indicate how well the outputs of models A or B agree with *Yobs*. In this example, model B has a greater C value than Model A, meaning that Model B's output values are in better agreement with the observed data than those of Model A, even though both models have the same R^2. The calculated $C'(0.05)$ value for both models is 0.628, given that both have the same Yobs values. For Model A, computed C = 0.321 and, as it falls below the $C'(0.05)$ value, is not significant. For Model B, computed C = 0.887, which is greater than the $C'(0.05)$ value and is thus significant.

Using R^2 results only, it would be difficult to declare which model best matches the observed data. Consilience analysis allows us to do just that.

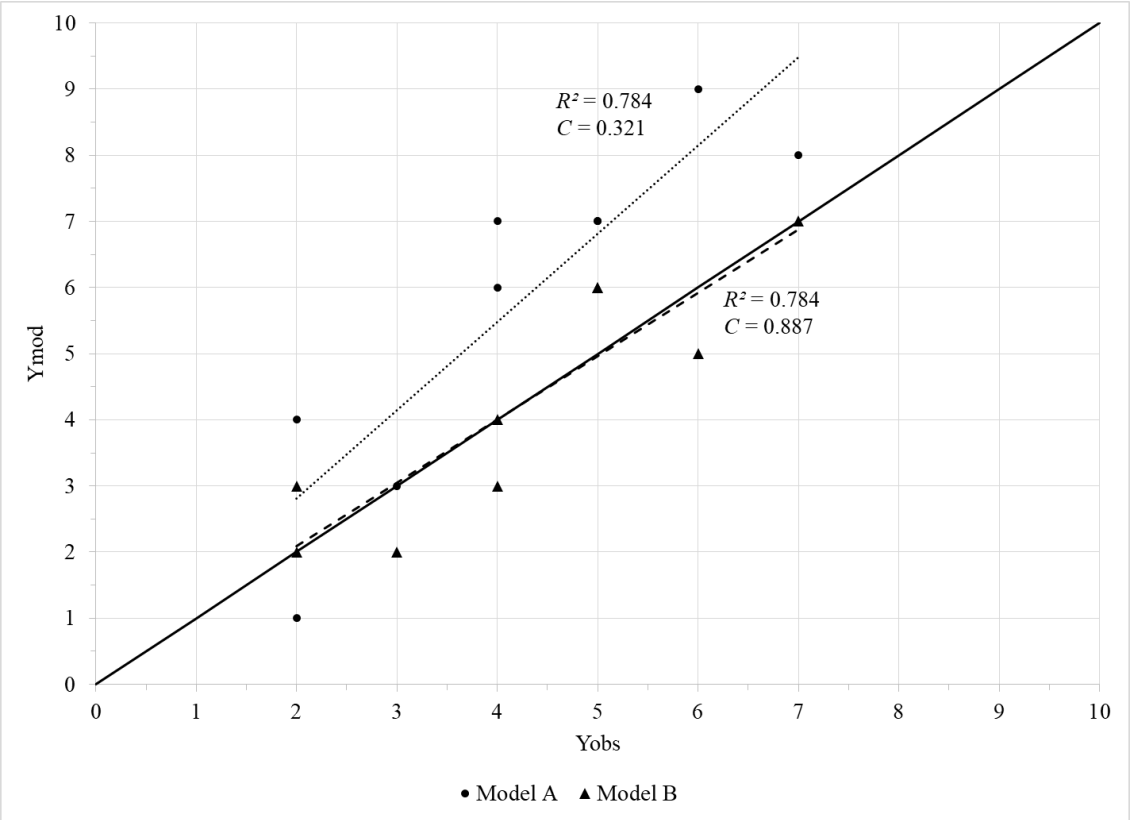

Figure 66. Example showing differences between the coefficient of determination and consilience measures.
Model A shown as solid circles with short-dash fit-line. Model B shown as solid triangles with long-dash fit-line. $C'(0.05) = 0.628$. Pr(C>C'): Model A, P>0.1, Model B, P<0.01.

Data Variation and Correlation Analysis

While there are many limitations to E.F-RMD and other deterministic models, the most conspicuous is the general lack of realistic output variation. Whereas observed data for a population of fish can vary considerably within a given time-period (e.g., fish weight in a population of the same age), a deterministic model will invariably produce the same output values given the same initial and experimental conditions. The absence of data variation in model output simplifies a complex system by masking the nuances of

un-modeled effects and error in measuring responses from biological systems. Such masking can have benefits as deterministic model results can give the modeler perspective on a variable's specific performance under specific conditions, which can be of benefit when trying to understand causes of observed system behavior. Should the modeler wish to understand the performance of a variable under different conditions, then the model input variables can be reconfigured and the model re-run.

In circumstances where GoF is imprecise due to large data variance, there is the option to fit a trend-line through the observed data to "smooth the data" to obtain an average value for a given dependent variable. While having utility, this process does change the nature of the analysis as the investigator is no longer comparing modeled output with actually observed data. Rather, GoF comparison would be between a simplistic model (i.e., a best-fit trend-line equation)[13] and a complex one (e.g., E.F-RMD). In this situation, statistical analysis is now between two estimated mean trend-lines with fewer degrees of freedom. Reduction of variance using a trend-line equation simplifies the process of fitting a dynamic model. The end-result is a dynamic model that can provide an estimated mean dependent variable value for a given independent variable and the dependent variable's trend across multiple independent variables (e.g., value and change in $\dot{V}O_2$ with respect to change in body weight). Thus, when modeling to observed data with high variance, one may find that a dynamic model has good

[13] Trend-line best fit being determined by the least-squares regression equation which produces the greater R^2.

Consilience with outputs from the trend-line model, despite both models having poor Consilience with the observed data.

In circumstances with less observed data variance, Consilience and R^2 analysis of observed data and trend-line will be more comparable. Since the modeler does not always get to choose the type and quality of available data – and may not even have access to the raw data – understanding model analysis options with their abilities and limitations is important. Accordingly, the results of the analysis can be appropriately represented, and more importantly, not misrepresented.

Data Sources and Analysis Methods

The data sets used for fitting and evaluating RMD and E.F-RMD are discussed below. These unpublished data were obtained from the Texas Parks and Wildlife, Coastal Fisheries Division, Marine Development Center (MDC), Corpus Christi, TX, and Sea Center Texas (SCT), Lake Jackson, TX. These are good examples of how the amount of information within a data set can vary. Even when working with constrained data, modeling can be accomplished, and analysis can be conducted, albeit with limitations.

MDC Cool – Warm Experiment

Mr. Herschiel Tuley graciously provided the data set from laboratory experiments conducted at the MDC. Juvenile SFL (n = 59) were divided into two groups: Cool (17 – 22°C, initial n = 32) and Warm (20 – 26°C, initial n = 27). These thermal regimes were imposed over 177 days. Subject fish were fed mysids twice daily to satiation; periodically, the fish were weighed and some subjected to routine

respirometry (Springer and Neill 1988, Walker et al. 2011) , to measure growth rate and to assess growth and weight effects on $\dot{M}O_2$.[14] Water salinity for Cool and Warm groups averaged 30.7 ppt (SD ± 2.7). Dissolved oxygen levels, measured prior to the start of each respirometry session, averaged 7.2 mg O_2/L water (SD ± 0.67). Over the course of the experiment, SFL were weighed five times, with average fish weights ranging from 2.24 g to 12.79 g. Table 1 shows the average weight for each temperature group recorded at the start of the experiment (2 Aug 2017, day 0) and weights on days 12, 47, 111, and 175, along with the number of fish measured, and average tank water temperature. Hours subsequent to the 2 Aug 2017 start date are also listed, because E.F-RMD simulations involve an hourly time-step (DT).

[14] Due to power failure caused by a hurricane, the Cool group was exposed to higher temperatures over 48 hours resulting in an overlap in temperature exposures.

Table 1. MDC Cool-Warm experiment, measured SFL weights and temperature.

Cool Tanks						
Date	Days after 2 Aug	Hours after 2 Aug	n	Avg. Wt (g)	Wt SD	Med. Ta (°C)
2-Aug-17	0	0	32	2.24	0.34	20.57
14-Aug-17	12	288	31	2.31	0.29	19.81
18-Sep-17	47	1128	31	3.05	0.39	20.95
21-Nov-17	111	2664	31	6.23	1.03	19.42
24-Jan-18	175	4200	28	10.06	1.36	18.66

Warm Tanks						
Date	Days after 2 Aug	Hours after 2 Aug	n	Avg. Wt (g)	Wt SD	Med. Ta (°C)
2-Aug-17	0	0	27	2.80	0.27	25.95
14-Aug-17	12	288	24	2.69	0.55	25.95
18-Sep-17	47	1128	23	3.82	0.79	24.79
21-Nov-17	111	2664	21	8.13	1.63	25.17
24-Jan-18	175	4200	17	12.79	1.73	22.09

The growth data from Table 1 were plotted (Figure 67) and fit with exponential growth curves, with the intercept forced to the average weight observed on day zero. Microsoft Excel® was used to determine the exponential equation trend-lines. These trend-lines were used by E.F-RMD to help fit the model output to the observed data. However, for analysis, E.F.-RMD results were only compared against the five observed growth values from Table 1 by taking the E.F-RMD estimated weight at the corresponding hour of model run-time.

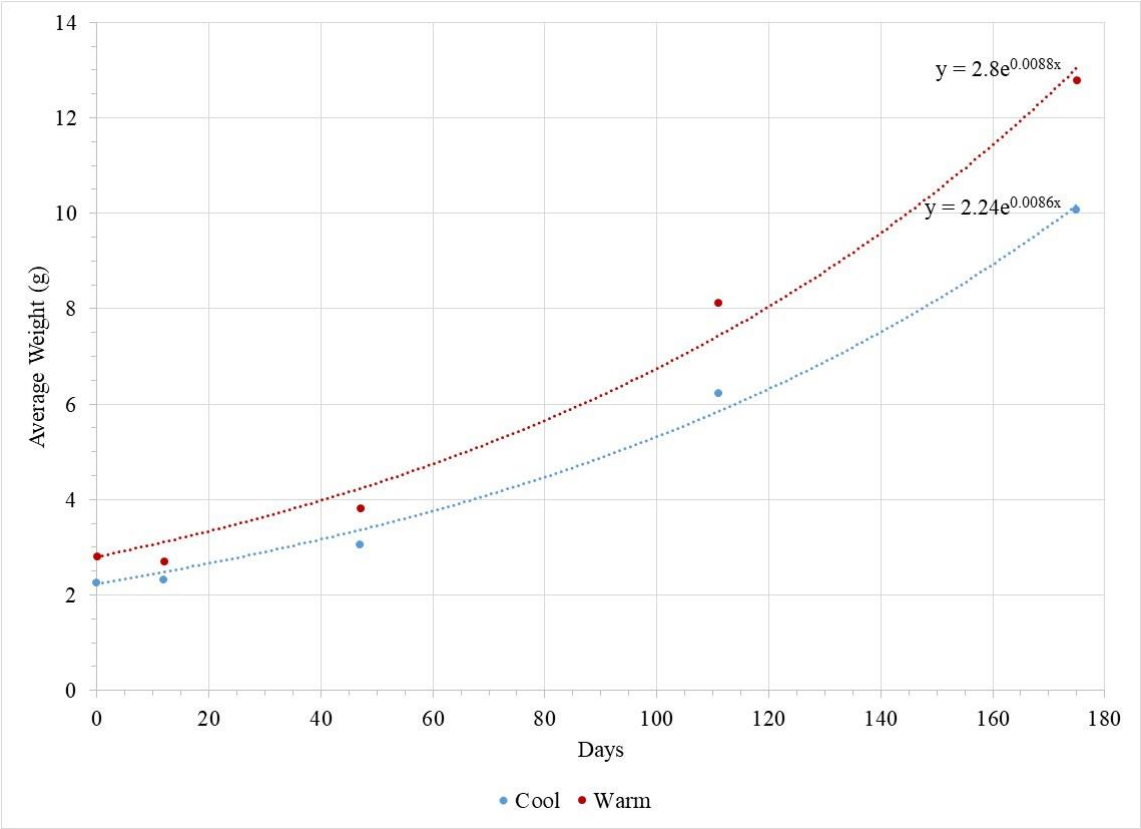

Figure 67. MDC Cool-Warm experiment, fish weight vs. days after beginning of experiment.
Observed mean weight (circles) for Cool (blue) and Warm (red) treatments, overlaid with trend-lines with their equations.

Respirometry evaluations were conducted at 1 to 2-week intervals during the experiment and prior to the experiment's termination.

Sea Center Texas, Pond Data

Weight and time (day) post-hatch data were obtained for SFL as measured by SCT staff from grow-out ponds located near Lake Jackson, TX during November, December, and January over three years (2009-2012). Fish were weighed at intervals over each of the 3 years, starting at 67 days post-hatch. Time post-hatch, weights,

number of fish measured, and average weights plus deviations are shown in Table 2. Hours post-hatch are also listed because E.F-RMD simulations have a one-hour DT.

Table 2. SCT Galveston pond data measured SFL weights.

Days post-hatch	Hours post-hatch	n	Avg. Wt (g)	Wt SD
67	1608	20	0.68	0.29
72	1728	49	0.17	0.07
81	1944	20	0.91	0.42
82	1968	80	0.67	0.37
85	2040	20	0.24	0.07
94	2256	5	1.17	0.37
98	2352	60	1.01	0.42
157	3768	32	3.05	0.82

As with the MDC data, fish-weight averages from Table 2 were plotted vs. time (Figure 68) and fit with a power curve. Because the size data first became available on day 67, the graph starts at day 60. Microsoft Excel® was used to calculate weight-at-time trend-lines. The trend-lines were used by E.F-RMD to help fit the model output to the observed data. However, for analysis (just as with the MDC data), E.F.-RMD outputs were only compared against the eight observed mean-weight values from Table 2 by taking the E.F-RMD estimated weight at the corresponding hour of model run-time.

Temperature data for the SCT pond study were not reported; so, modeling used average temperature data for Galveston Bay, obtained from the National Oceanic and

Atmospheric Administration (NOAA 2020). Average temperatures for Galveston Bay are 20°C in November, 15°C in December, and 13.3°C in January. Because temperature fluctuations over the time periods analyzed are not known, E.F-RMD growth was fit to the pond growth data using this linear temperature relationship: Ta = -0.0031*TIME + 24.988. Note that this equation yields 20°C and 13.3°C, respectively, at the start and end of simulation. Salinity was set to 30 ppt and pH at 8.3.

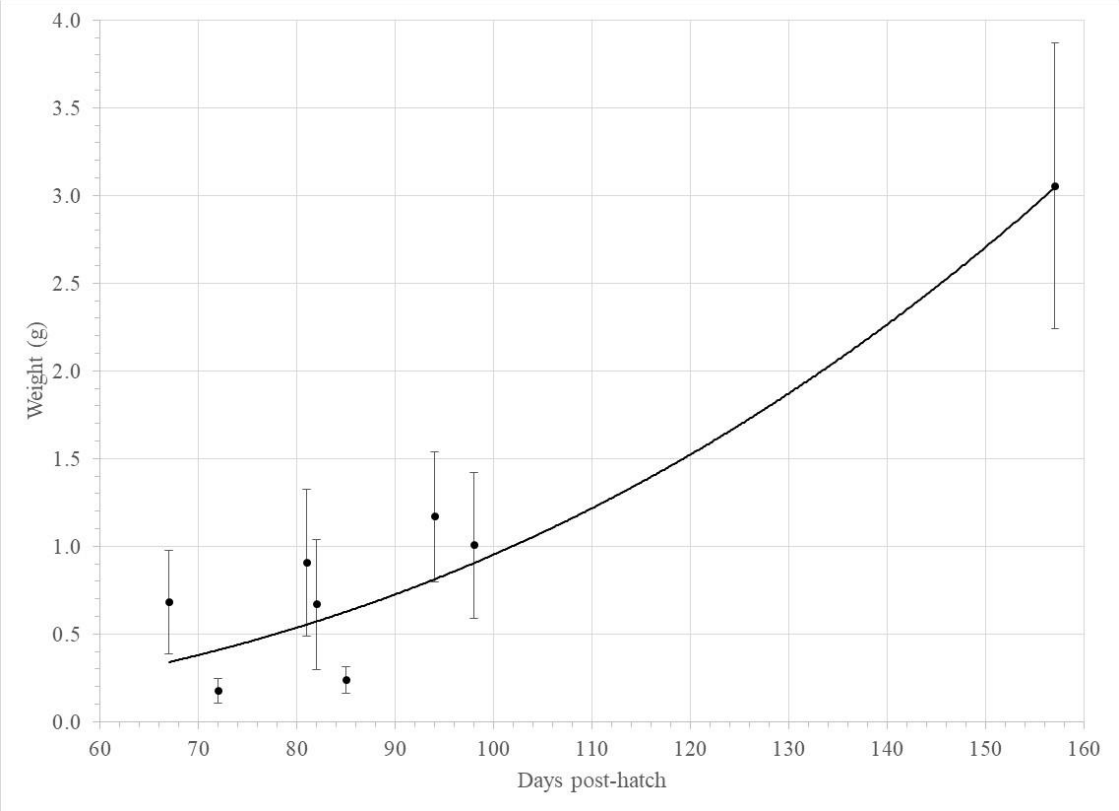

Figure 68. Galveston pond data for SFL weight (Mean ± SD) vs. time, with trend-line.
Trend-line, $R^2 = 0.552$.

Comparison of RMD to Cool - Warm Data

Automated routine respirometry (Springer and Neill 1988, Neill et al. 2004, Walker 2009) was performed with individual SFL, each fasted for one day before a test of several hours duration. Respirometry results for all the MDC Cool (Figure 69) and Warm (Figure 70) tests in relation to SFL weight are shown below. The $\dot{M}O_2$ values measured are assumed to be representative of routine metabolic rate. Power trend-lines were created for each temperature regime, and RMD configured for best-fit to each trend-line. Observed fish weight was correlated with the approximate RMD weight for comparison of observed averaged and estimated $\dot{M}O_2$. Model settings used to fit the data are shown in Table 3.

Table 3. RMD fit values.

	Cool	Warm
Temperature (°C)	18	23
Salinity (ppt)	32	32
DO (mg O_2/L)	7.9	7.1
PO2 (mmHg)	154	151
pH	7.7	7.6
fR con	5	18
Skin Eff f	0.84	1

Attentive readers may notice the maximum weight shown in the graphs are greater than the final weights from the growth analysis shown in Figure 67. This is due to additional weight data incorporated after data was collated for weight analysis.

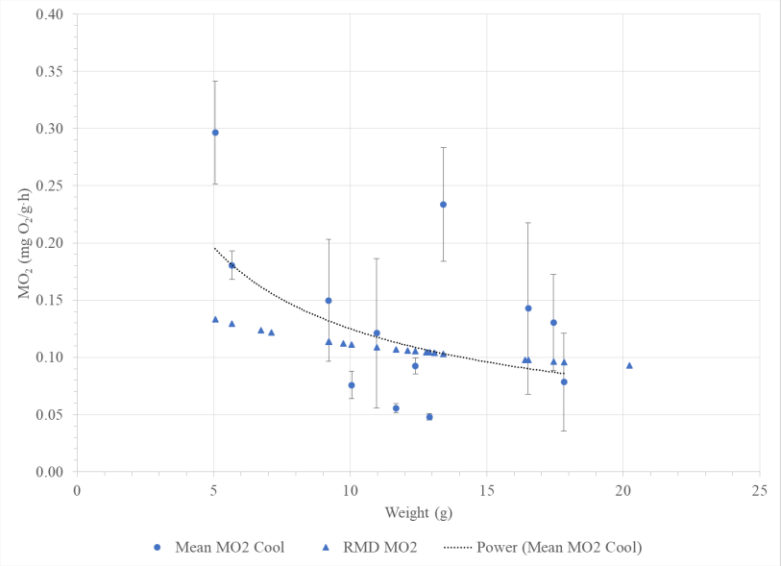

Figure 69. $\dot{M}O_2$ via routine respirometry for Cool treatment and RMD best-fit vs. SFL weight.
Mean $\dot{M}O_2$ values ± SD (blue circles with vertical error bars) from Cool treatment, together with power trend-line fit. RMD MO2 (triangles) indicates outputs of RMD fit.

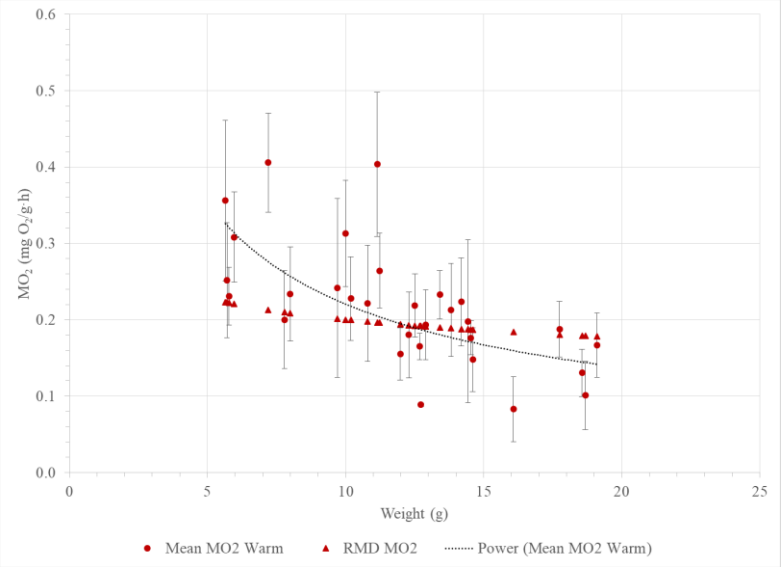

Figure 70. $\dot{M}O_2$ via routine respirometry for Warm treatment and RMD best-fit vs. SFL weight.
Mean $\dot{M}O_2$ values ± SD (red circles with vertical error bars) from Warm treatment, together with power trend-line fit. RMD MO2 (triangles) indicates outputs of RMD fit.

Analysis of Observed Data

Analysis of RMD best-fit output to the Cool and Warm mean observed data resulted in low R^2 values for both conditions (Table 4). Consilience between observed values and RMD outputs was low but still significant.

Table 4. Consilience and R^2 for observed data with RMD $\dot{M}O_2$ output.

	Cool	Warm
n	12	30
R^2	0.338	0.401
C (co-var-based)	0.559	0.572
$C'(0.05)$	0.554	0.361
Pr(C>C')	0.01<P<0.05*	P<0.01*

Consilience graphs comparing average Cool (Figure 71) and Warm (Figure 72) observed data with modeled data $\dot{M}O_2$ are shown below. Observed data values are presented with standard-deviation error bars to highlight the variability in the observed data.

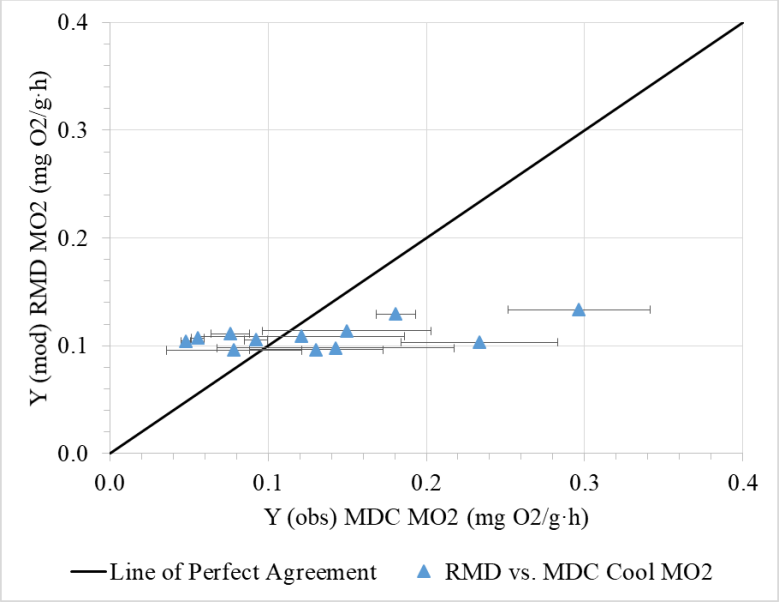

Figure 71. Observed average (±SD) Cool vs. RMD $\dot{M}O_2$ values, compared with the line of perfect agreement.
R^2 = 0.338, C = 0.559.

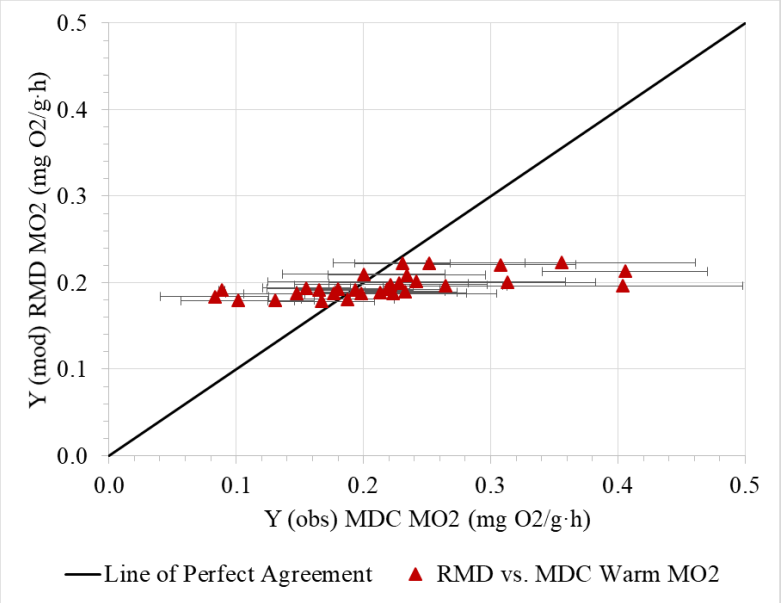

Figure 72. Observed average (±SD) Warm vs. RMD $\dot{M}O_2$ values, compared with the line of perfect agreement.
R^2 = 0.401, C = 0.572.

Trend-line Analysis

Trend-line analysis is a model-to-model comparison that may provide guidance for evaluating dynamic model response related to the mean response of two or more variables in the observed data. However, while trend-lines provide a more precise guide for fitting model output, it must be kept in mind that trend-lines are best-fit averages. The modeler can easily become overly-focused on modeling to the mean (i.e., trend-line) rather than modeling to the data.

For example, in the graphs comparing the Cool (Figure 69) and Warm (Figure 70) data from the MDC growth experiments, the trend-lines indicate that the per-gram $\dot{M}O_2$ decreases as fish weight increases. RMD $\dot{M}O_2$ data also shows this trend, although

it is apparent that RMD underestimates the $\dot{M}O_2$ in fish < 12 g for the Cool and Warm treatments. The higher $\dot{M}O_2$ in smaller fish within RMD reflects the cutaneous respiration input. I suggest that this is a contributor to the observed $\dot{M}O_2$ trend. This could be the result of failure of RMD to adequately account for changes in membrane permeability with temperature, overestimation of skin thickness, or inability to account for the existence of specialized skin circulation, all of which may affect cutaneous respiration (Burggren 1988).

Consilience analysis of model output to trend-lines can quantify model output for fitting the model. For example, consider the *C* and R^2 analysis of RMD results to the Cool and Warm data trend-lines is shown in Table 5. The analysis was accomplished by estimating $\dot{M}O_2$ using the Excel-derived power equation for the trend-line for each weight sample recorded and compared to RMD results. Results indicate significant results for both temperature treatments.

Table 5. Consilience and R^2 of trend-line data to RMD $\dot{M}O_2$ output.

	Cool	Warm
n	12	30
R^2	0.995	0.995
C (co-var-based)	0.746	0.694
C'(0.05)	0.554	0.361
Pr(C>C')	P<0.01*	P<0.01*

E.F-RMD Simulations of SFL Growth

E.F-RMD growth and percent-growth-per-day outputs were evaluated against MDC growth and respirometry data for Cool-Warm groups and SCT pond growth data from ponds located in Lake Jackson, TX (near Galveston, TX).

The starting weight for E.F-RMD was set to the lowest weight recorded and model start time adjusted to coincide with start date of the experiment (MDC data) or the number of days post-hatch (SCT data). The model end time was set to the time (in hours) when the final observed weight was recorded. Mean growth trend-lines were used to guide model settings, but the determination criteria for a successful growth match was how closely the final simulated weight compared to the final observed weight.

Starting weight-pair values for each data set were omitted from *C* and R^2 analysis, as model start weights were set equal to the first recorded data weights.

Percent Weight Change per Day Calculation

In addition to growth analysis by weight over time, *C* and R^2 analysis was also conducted for percent weight change per day (%Wtchg/day), with percent weight change based on the difference in a given weight (M_i) from the initial (i.e., starting) observed weight (M_0), per the calculation shown in equation (51).

$$\%Wtchg = \frac{M_i - M_0}{M_0} \times 100 \tag{51}$$

Then, the result was divided by the number of days between starting time and time of that particular evaluation, to compute %Wtchg/day.

MDC Cool – Warm Growth and Respirometry Comparison

The Cool – Warm growth and respirometry data were used as the primary data source for adapting and refining E.F-RMD into an effective growth model. To further ensure the E.F-RMD growth estimate's fidelity while maintaining the "metabolic physiology" integrity of the model, 24 hours before the model's run terminated, a simulated respirometry session was initiated. The model was then adjusted using the processes discussed earlier so that "Mact max" intercepted the estimated routine metabolic rate (RMR) at the observed lower oxygen concentration for routine metabolism (LOCr). This ensured that the model's estimated RMR was congruent with the average RMR seen during the final respirometry session conducted for the Cool and Warm groups prior to the termination of the experiment (see Table 6). Being able to shape the model to generally match its performance to observed metabolic scope for growth (MS_{growth}) and margin of metabolic scope (MMS) – while maintaining the model's fidelity to published information on SFL and other flatfishes – increased overall confidence in E.F-RMD.

Table 6. Observed values from MDC Cool and Warm experiment.

	Cool	Warm
Mean Ta (°C)	18.1	21.6
Mean end Wt (g)	9.0	5.7
RMR (mg O_2/g fish·h)	0.13	0.23
LOCr (mg O_2/L water)	2.82	2.74
MMS	0.046	0.084

Input Processes

The input settings used to configure E.F-RMD for Cool and Warm conditions are shown in Table 7. The measured temperature series used as input for simulating Cool and Warm treatments are shown in Figure 73. The prominent upward spiking in temperature at about 600-800 hours – especially conspicuous for the Cool treatment – was due to power failure caused by Hurricane Harvey.

Because DO varies inversely with temperature, the temperature fluctuations are shown in Figure 73 resulted in corresponding variation in estimated DO levels. The E.F-RMD calculated DO levels for each condition are shown in Figure 74.

Table 7. E.F-RMD fixed input for MDC Cool – Warm experiment.

	Cool	Warm
Starting Weight (g)	2.24	2.8
Salinity (ppt)	30	30
Mean PO2 (mmHg)	159	159
pH	8.3	8.3
“Respirometer” Volume (L)	2	4
fR con	24.55	50.3
Winberg	1.58	2.415
Skin Eff f	1	1
Smin0	0.043	0.043
q1	0.062	0.062
q2	0.09	0.09
GEFeed (cal/g)	1000	1000
sda	0.14	0.14
FeedDigestibility%	90	90

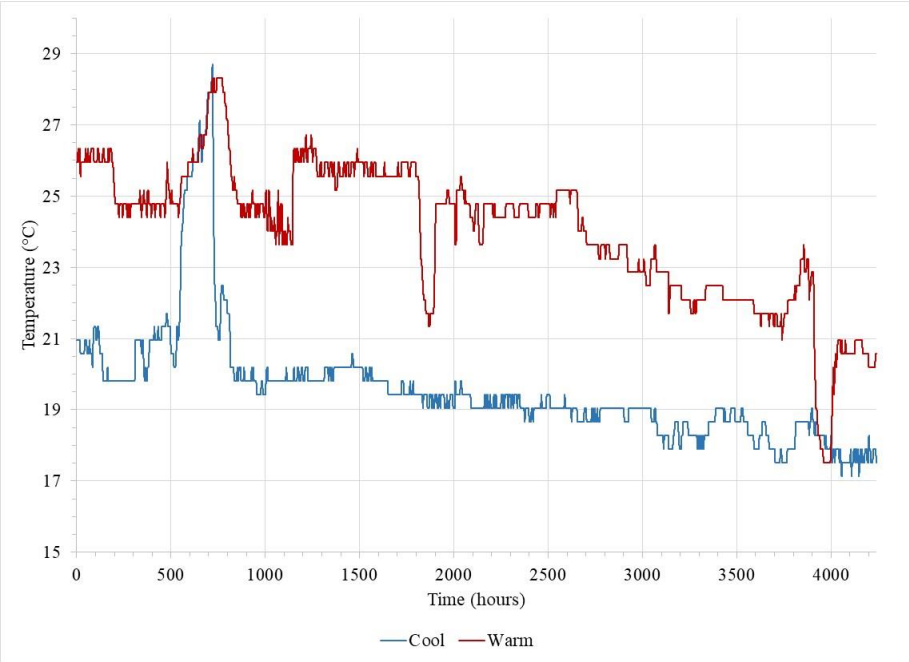

Figure 73. MDC Cool - Warm temperature regimes over the growth period.
Prominent temperature spike in Cool treatment at hours 600-800 due to equipment power failure.

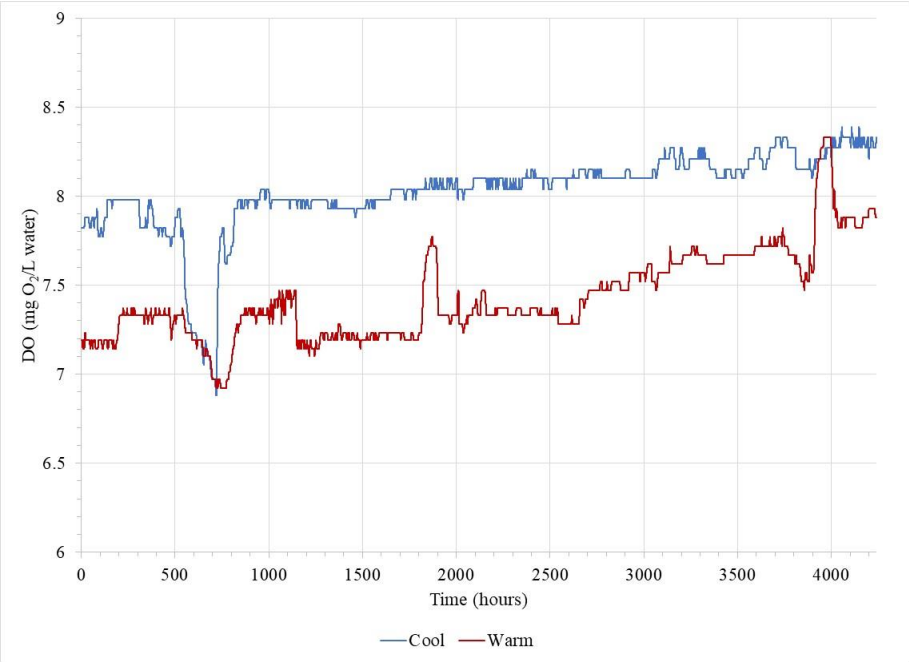

Figure 74. Estimated Cool - Warm DO regimes over the growth period.

Results and Analysis

As a dynamic model, E.F-RMD produces outputs that vary according to the input regime. For the MDC Cool – Warm experiment, temperature necessarily differed between Cool and Warm treatments and varied over the course of the experiment. The only environmental variable that remained stable was salinity, which was maintained near 30 ppt. In the E.F-RMD variant configured for the MDC Cool – Warm experiment, pH was fixed at 8.3 instead of being allowed to vary with temperature in keeping with the model's pH function. While simplifying the inputs, fixing pH resulted in a gill O_2 extraction efficiency near 99% during the non-respirometry phase of the model run, and low P_{50} and PvO_2 values (see Table 8 and Table 12). These values are below those

generated under conditions of variable pH. Thus, the "Mact max" output of the RMD portion of E.F-RMD is truly near the maximum possible active metabolic rate for both temperature conditions.

Cool Results – Growth and %Wtchg/day

Model input processes and values that remained fixed over the course of the growth phase of simulation are shown in Table 8.

Table 8. E.F-RMD respiratory variables with fixed input values – Cool treatment.

PO_2 (mmHg)	159
P_{50} (mmHg)	0.68
PvO_2 (mmHg)	0.9
O2 Extraction efficiency (%)	99

RMD estimated growth compared to the Cool trend-line growth is shown as a Stella® graph in Figure 75. The graph shows that E.F-RMD can be configured to match the trend-line model quite well, but it does not necessarily indicate how well the model weights compare to observed data.

The E.F-RMD simulated SFL weights were taken at model run times corresponding to the times of observed weight measurements from Table 1 for the Cool treatment, as shown in Table 9.

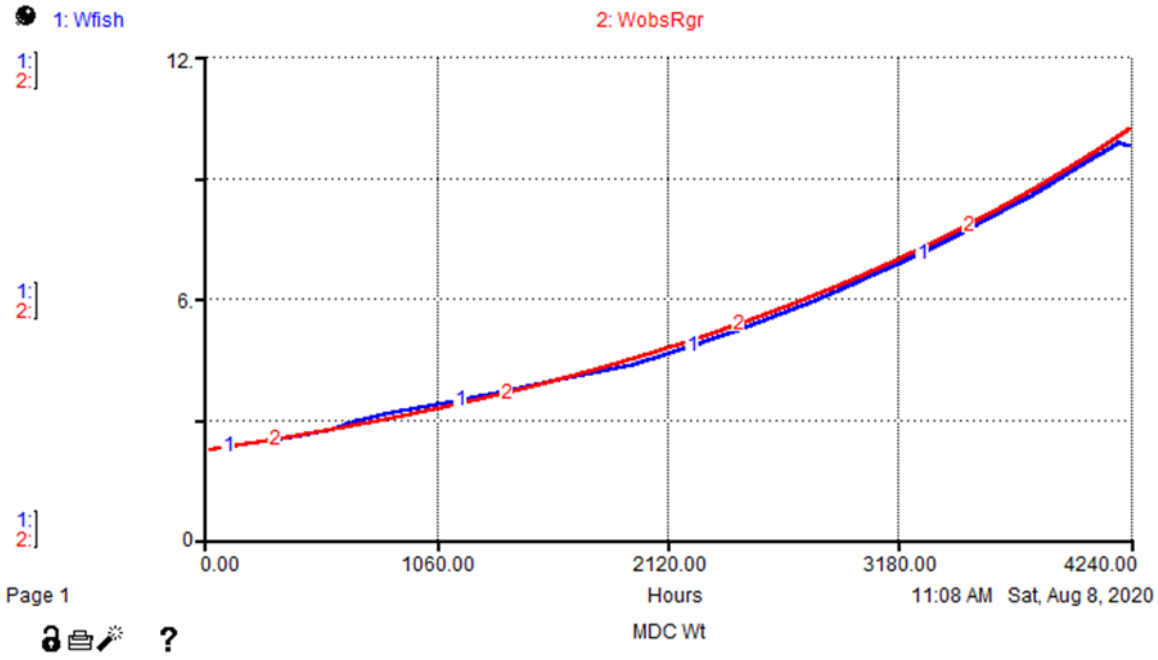

Figure 75. Stella® graph of E.F-RMD simulated vs. regression-"predicted" weight for the Cool treatment.
Model "Wfish" in blue (1); weight from regression of observed values on Hours "Wobsrgr" in red (2). The small dip in "Wfish" seen at the end of the growth period occurs at hour 4216 when DO begins to drop with the onset of simulated respirometry, when simulated fish were "fasted."

Table 9. Observed vs. E.F-RMD simulated weight and %Wtchg/day for Cool treatment.
Observed Avg. Wt from Table 1. %Wtchg/day calculated from Wt columns using equation (51).

	Cool Observed		Cool E.F-RMD	
Hours	Avg. Wt (g)	%Wtchg/day	Est. Avg. Wt (g)	%Wtchg/day
0	2.24	-	2.24	-
288	2.31	0.26	2.47	0.86
1128	3.05	0.77	3.44	1.14
2664	6.23	1.60	5.69	1.39
4200	10.06	1.99	9.92	1.96

Results from Consilience analysis are shown in Table 10 for Cool-configured E.F-RMD estimated growth by weight and %Wtchg/day. Goodness-of-fit graphs for weight (Figure 76) and %Wtchg/day (Figure 77) are shown below the table. Consilience between E.F-RMD output and Cool data for Weight and %Wtchg/day were significant.

Table 10. Holistic goodness-of-fit: E.F-RMD vs. MDC Cool for growth-related responses.

	Wt	%Wtchg/day
R^2	0.990	0.903
C (co-var-based)	0.995	0.891
C'(0.05)	0.842	0.842
Pr(C>C')	P<0.01*	0.01<P<0.05*

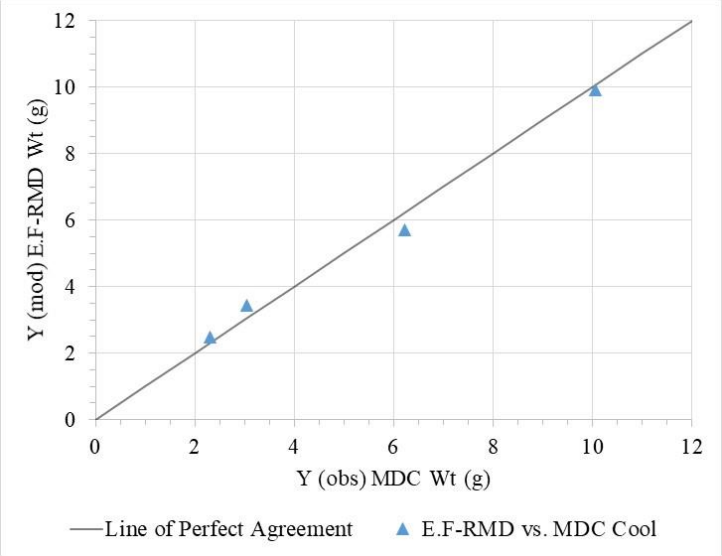

Figure 76. Observed MDC Cool means vs. E.F-RMD simulated weight relative to the line of perfect agreement.
R^2 = 0.990, *C* = 0.995.

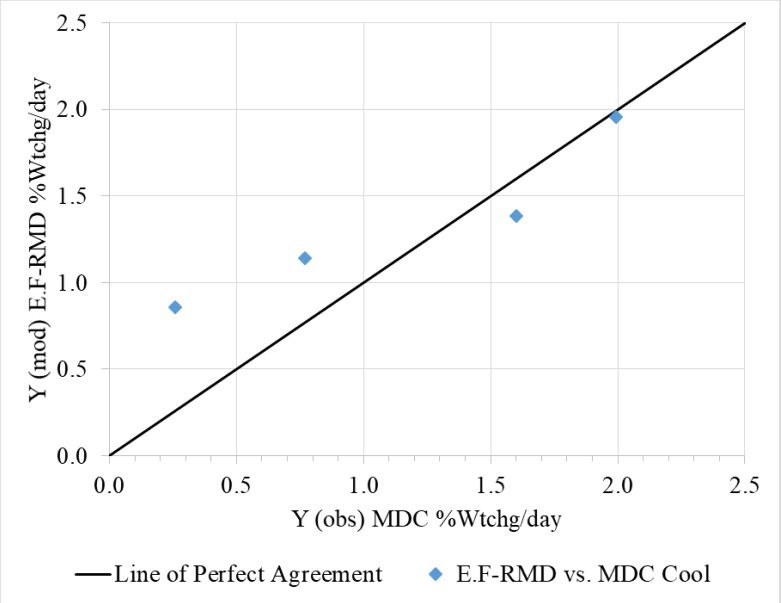

Figure 77. Observed MDC Cool means vs. E.F-RMD simulated %Wtchg/day relative to the line of perfect agreement.
R^2 = 0.903, C = 0.891.

Cool Results – Respirometry

The ability of E.F-RMD to accurately fit observed metabolic rates may be seen in Figure 78, which shows E.F-RMD outputs for "DOa," "Mact max," "EF VO2," "Mstd," and "Mrmr" for the terminal respirometry session. When simulated respirometry is initiated, as indicated by the drop in "DOa" and "Mact max," the point of intercept when "Mact max" equals "Mrmr," is the limiting oxygen concentration (i.e., DO level) for routine metabolic rate, that is, the LOCr.

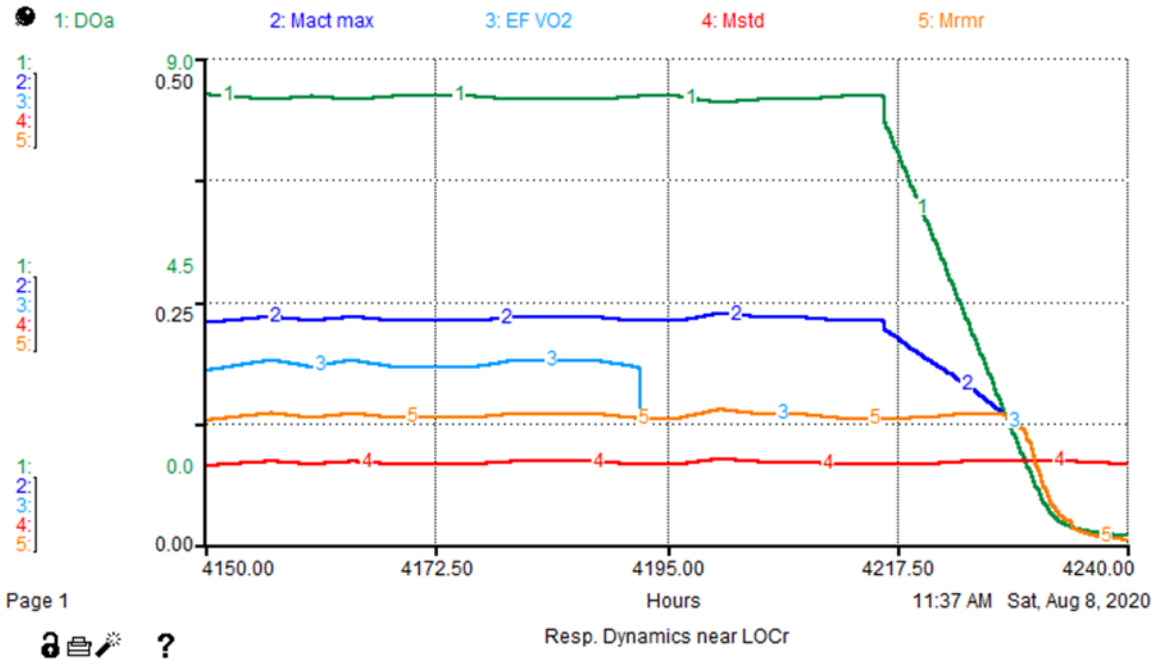

Figure 78. Stella® E.F-RMD respirometry responses for MDC Cool.

Table 11 shows that when configured for the Cool treatment, E.F-RMD accurately fit the Cool respirometry data. The model estimated SFL weight was 0.82 g higher than the observed data, and the mean Ta was 0.2°C lower. The similarity of weights simply means that the average weight of all the SFL chosen to undergo the final respirometry session was approximately the same as the model estimated weight when the simulated respirometry began.

Table 11. Comparison of MDC Cool respirometry endpoints with E.F-RMD outputs.

	Cool Observed	E.F-RMD Simulated
Mean Ta at LOCr (°C)	18.1	17.9
SFL Wt (g)	9.0	9.82
RMR (mg O_2/g fish·h)	0.13	0.13
LOCr (mg O_2/L water)	2.82	2.82
MMS	0.046	0.046

Warm Results – Growth and %Wtchg/day

Model output processes and values that stayed fixed over the course of the Warm treatment model run are shown in Table 12.

Table 12. E.F-RMD respiratory variables with fixed input values – Warm treatment.

PO_2 (mmHg)	159
P_{50} (mmHg)	0.68
PvO_2 (mmHg)	0.9
O2 Extraction efficiency (%)	99

Model growth compared to the mean growth trend-line for the Warm treatment is shown as a Stella® graph in Figure 79. E.F-RMD estimated weights, taken at model run

times corresponding to observed weight sample times, are shown in Table 13. Also shown are the %Wtchg/day values calculated from observed data and model output.

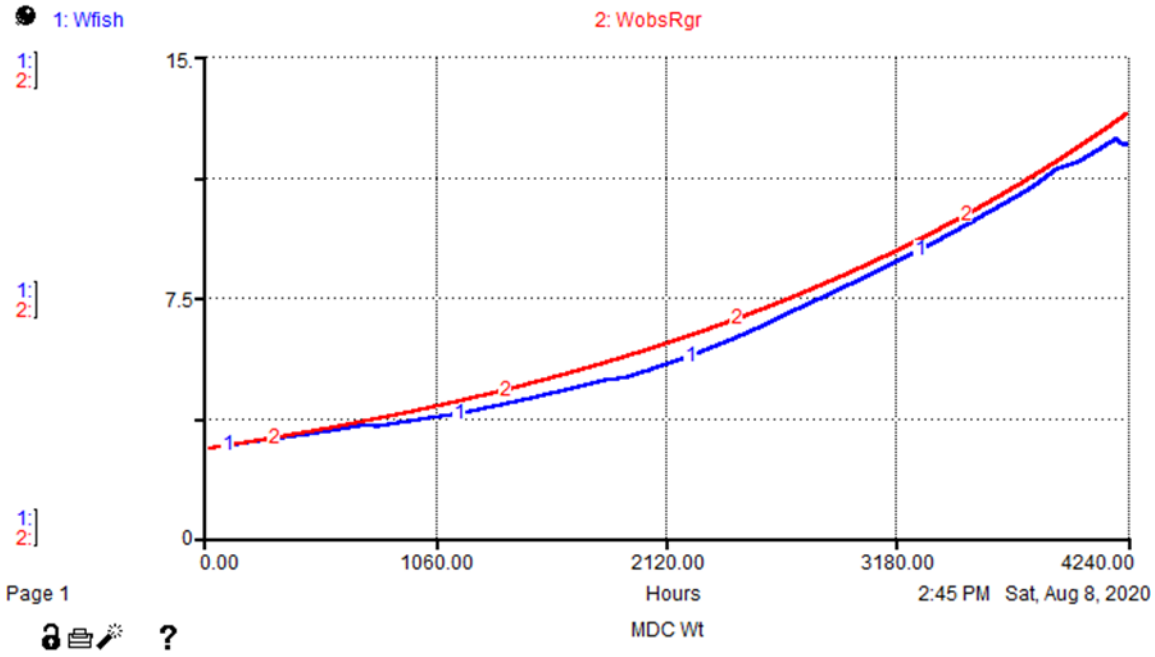

Figure 79. Stella® graph of E.F-RMD simulated vs. regression-"predicted" weight for the Warm treatment.
Model "Wfish" in blue (1); weight from regression of observed values on Hours "Wobsrgr" in red (2).

Table 13. Observed vs. E.F-RMD simulated weight and %Wtchg/day for Warm treatment.

Observed Avg. Wt from Table 1. %Wtchg/day calculated from Wt columns using equation (51).

	Warm Observed		Warm E.F-RMD	
Hours	Avg. Wt (g)	%Wtchg/day	Est. Wt (g)	%Wtchg/day
0	2.80	-	2.80	-
288	2.69	-0.31	3.08	0.83
1128	3.82	0.78	3.85	0.80
2664	8.13	1.72	6.98	1.34
4200	12.79	2.04	12.51	1.98

Visual inspection of Figure 79 suggests that Warm E.F-RMD, with the inputs shown in Table 7, was less consilient with the data than was its Cool-treatment counterpart (Figure 75). And, in fact, Consilience analysis (Table 14) indicated a reduction in *C* values (vs. those for presented for the Cool treatment, in Table 10), both for Wt and %Wtchg/day. That for %Wtchg/day declined to 0.84, which for a sample of size 5, is only marginally significant at alpha = 0.05. Figures 80 and 81 provide plots of modeled vs observed means for both Wt and %Wtchg/day, for the Warm treatment.

Table 14. Goodness-of fit: E.F-RMD to MDC Warm

	Wt	%Wtchg/day
R^2	0.983	0.708
C (co-var-based)	0.991	0.838
C'(0.05)	0.842	0.842
Pr(C>C')	P<0.01*	0.05<P<0.1

The apparent cause of lack-of-fit for the Warm treatment was negative growth observed for Warm treatment fish during the experiment's first 12 days. Cause of this aberrant response is unknown and naturally beyond the capabilities of E.F-RMD to simulate.

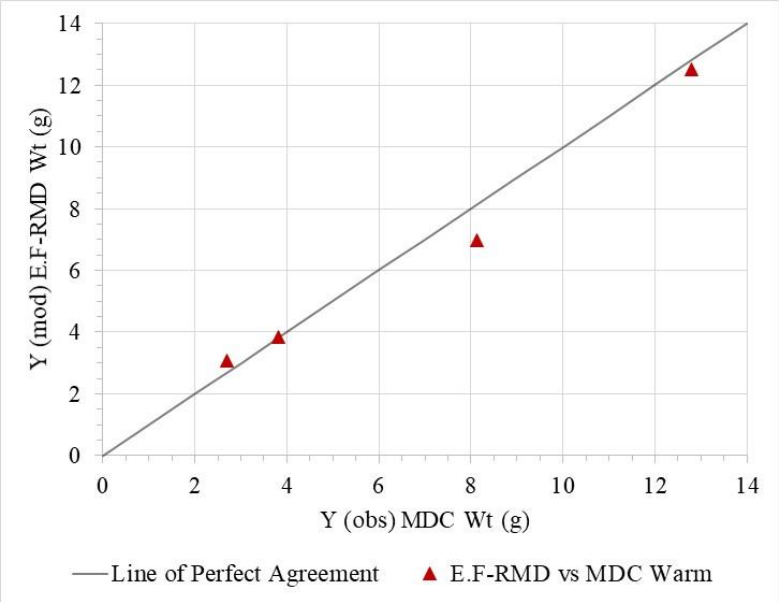

Figure 80. Observed MDC Warm means vs. E.F-RMD simulated weight relative to the line of perfect agreement.

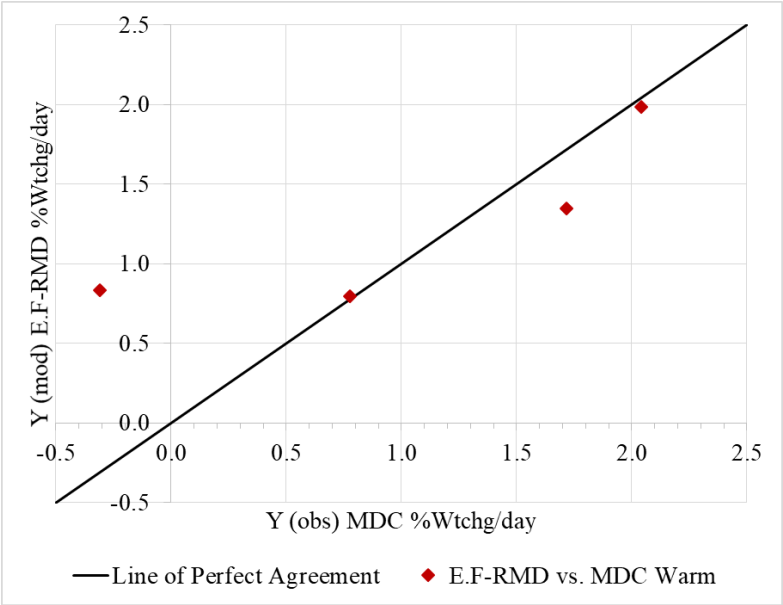

Figure 81. Observed MDC Warm means vs. E.F-RMD simulated %Wtchg/day relative to the line of perfect agreement.
R^2 = 0.708, C = 0.838.

Warm Results – Respirometry

The E.F-RMD outputs for simulates respirometry are shown in Figure 82, for Warm inputs (Table 12). The procedures and output variable names were the same as those for the Cool treatment.

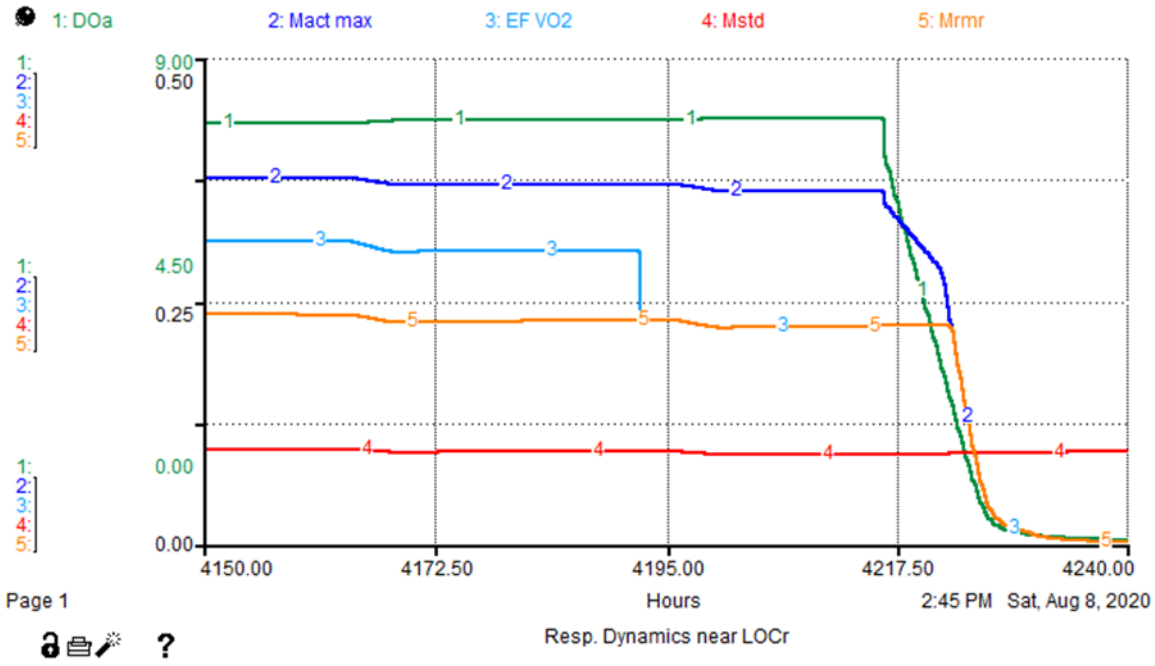

Figure 82. Stella® E.F-RMD respirometry responses for MDC Warm.

Table 15 shows the outputs of E.F-RMD compared to the Warm respirometry data. Again, as configured, the model output matches the RMR and LOCr values. The average weight of the actual fish chosen to undergo respirometry during the Warm experiment was 5.7 g while the model estimated weight at the time of respirometry was 12.3 g. This is not an indication that E.F-RMD is over-estimating SFL weight as it is the estimated average weight based on the fit to the growth curve. It just so happened the juvenile SFL randomly chosen for respirometry weighed less than the estimated mean weight based on the observed growth curve. However, the weight difference may have impacted E.F-RMD's estimated LOCr at "Mact max" and "Mrmr" interface values. The model attempted to fit these metabolic values based on a fish weighing 6.6 g more than

the fish actually placed in the respirometer. Model Ta at the time of respirometry was also 1.4°C lower than observed at final respirometry, but this should not have markedly affected the model's outcome.

Table 15. Comparison of MDC Warm respirometry endpoints with E.F-RMD outputs.

	Warm Observed	E.F-RMD Simulated
Mean Ta at LOCr (°C)	21.6	20.2
SFL Wt (g)	5.7	12.3
RMR (mg O_2/g fish·h)	0.23	0.23
LOCr (mg O_2/L water)	2.74	2.74
MMS	0.084	0.084

Integrated Cool-Warm Data Comparison

C and R^2 analysis for growth in weight and %Wtchg/day, given an appropriate metabolic sub-model, indicated that E.F-RMD was capable of accurately simulating juvenile SFL weight and the rate of weight change for the Cool treatment, but accuracy deteriorated somewhat for the Warm treatment. Considering that Warm-treatment SFL actually lost weight during the early phase of the experiment suggests the occurrence of events or processes beyond the scope of the model.

SCT Pond Growth Data

Without actual temperature data, and without any respirometry data for parameterizing RMD, several of the input processes used with the MDC Cool – Warm data were used to fit E.F-RMD to the SCT pond growth-data (Table 16). The most significant difference between the pond growth version of E.F-RMD and that for MDC Cool – Warm was the calculation used for "FeedRateMax" (described above) which involves both temperature and body weight. In addition, the "GEFeed" variable was increased to 2000 cal/g compared to the 1000 cal/g required for Cool-Warm. The increase was consistent with the presumed high protein salmon starter feed provided the SCT pond fish per Mr. Paul Cason of Texas Parks and Wildlife Department (personal communication, October 21, 2020).

Table 16. E.F-RMD fixed inputs and parameters for SCT Galveston pond study.

	Galveston pond
Starting Weight (g)	0.68
Salinity (ppt)	30
Mean PO2 (mmHg)	159
pH	8.3
fR con	26
Winberg	2.0
Skin Eff f	1
Smin0	0.043
q1	0.062
q2	0.09
GEFeed (cal/g)	2000
sda	0.14
FeedDigestibility%	90

E.F-RMD simulated weights and %Wtchg/day results corresponding to the post-hatch (hours) weight-sampling times are shown in Table 17. The observed %Wtchg/day values fluctuated conspicuously over time. Such fluctuation is likely the artifact of differing growing conditions between sampled ponds or even sampling error caused by variation in sampling methods, locations and times. For example, sample data for post-hatch day 81 was from a single pond, while day 82 weight data was from 4 ponds. Further, even though the ponds may have been co-located and subject to the same general environmental conditions, other factors might have differed such as salinity, feed quality and schedule, and the presence or absence of stressors such as toxins, parasites,

and predation. Despite the many potential sources of variation, the SCT pond data do show a growth trend. When E.F-RMD is configured to the settings in Table 16, the model estimated weights by day post-hatch appears to follow the trend-line curve but with values greater than the trend-line average. Visual comparison of the measured vs. modeled weights in Figure 83 shows that most of the model estimates fall within one standard deviation at days 81, 82, 94, and 98, but not on days 72 or 85 where much lower weights were measured. Recall that E.F-RMD starting weight was set to 0.68 g and output adjusted so that growth resulted in an end weight (3.05 g) that matched data, so it is not surprising these values correspond.

Table 17. Observed SCT pond vs. E.F-RMD estimated weights.

		Pond Observed		E.F-RMD Simulated	
Days post-hatch	Hours post-hatch	Avg. Wt (g)	%Wtchg/day	Est. Wt (g)	%Wtchg/day
67	1608	0.68	-	0.68	-
72	1728	0.17	-14.91	0.74	1.76
81	1944	0.91	2.37	0.87	2.00
82	1968	0.67	-0.13	0.89	2.06
85	2040	0.24	-3.62	0.94	2.12
94	2256	1.17	2.64	1.1	2.29
98	2352	1.01	1.53	1.18	2.37
157	3768	3.05	3.86	3.05	3.87

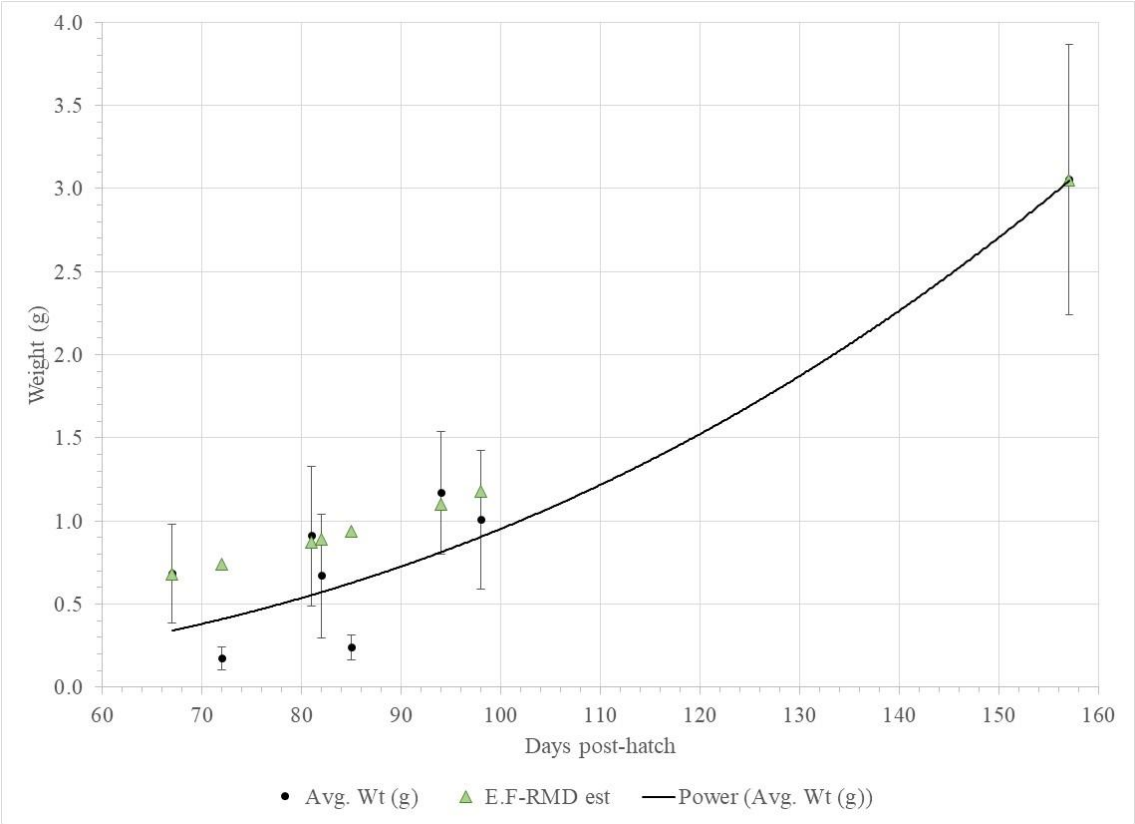

Figure 83. E.F-RMD simulated vs. SCT pond observed SFL weights and fit curve.

Consilience analysis of E.F-RMD to SCT pond data weights and %Wtchg/day is shown in Table 18. Significant Consilience (see Figure 84) was observed between the E.F-RMD-simulated and observed weights. Given that temperature was assumed to decline linearly over the course of the growth run for the SCT pond data, it would appear that E.F-RMD can be a useful tool for estimating SFL weights when not all environmental conditions are known.

However, when E.F-RMD %Wtchg/day results were compared to the estimated %Wtchg/day for the pond data, there was no *C* significance (see Figure 85). This result

is likely due to the aforementioned factors that may impact daily growth in ponds, together with normal sampling errors. While E.F-RMD can indeed exhibit negative growth in response to adverse environmental conditions and feed deficiency, there seemed no justification for programming such effects into the SCT pond variant of E.F-RMD.

Conclusion: Application of E.F-RMD to SCT Pond Study

All things considered, the performance of E.F-RMD relative to the SCT pond study seemed robust – despite the lack of significance in *C* for %Wtchg/day.

Table 18. Goodness-of fit: E.F-RMD to SCT pond data

	Wt	%Wtchg/day
R^2	0.917	0.282
C (co-var-based)	0.931	0.469
C′(0.05)	0.696	0.696
Pr(C>C')	P<0.01*	P>0.1

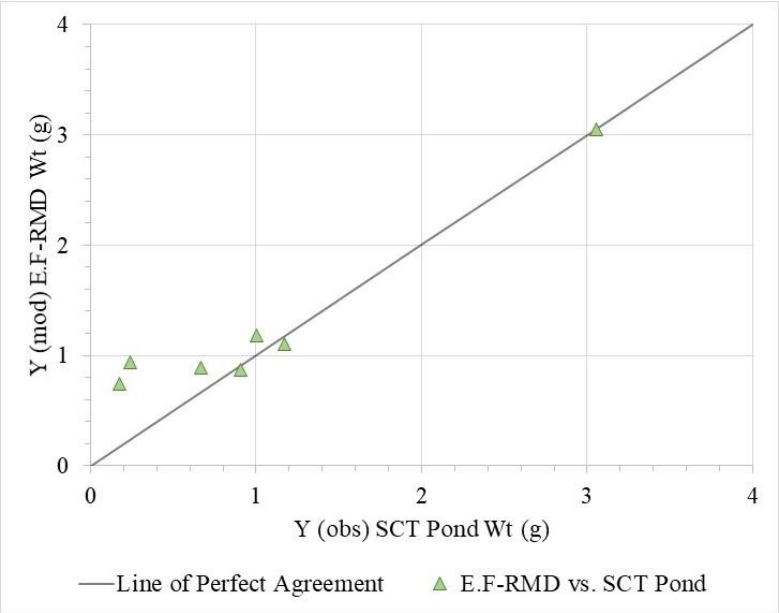

Figure 84. Observed SCT pond means vs. E.F-RMD simulated Wt relative to the line of perfect agreement.
R^2 = 0.917, C = 0.931.

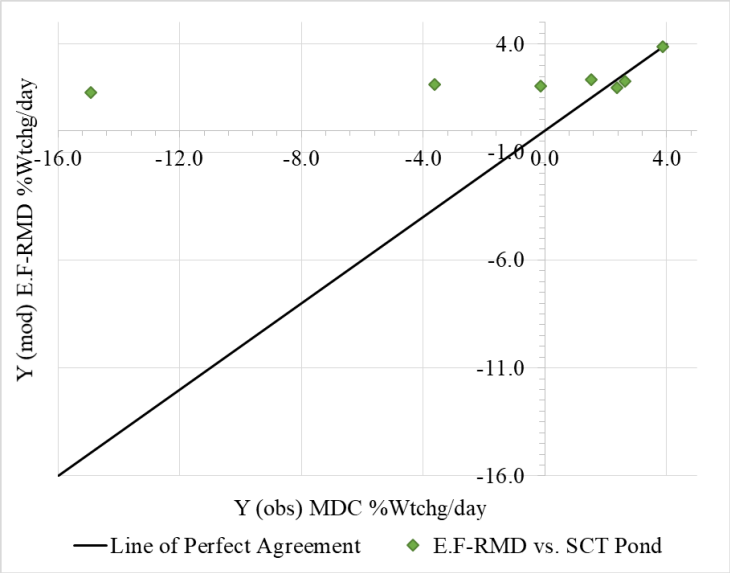

Figure 85. Observed SCT pond means vs. E.F-RMD simulated %Wtchg/day relative to the line of perfect agreement.
R^2 = 0.282, C = 0.469.

Evaluation of E.F-RMD Simulations Relative to Published Study of SFL Growth

Published research on SFL growth also was used to provide a check of model performance. Of particular value was growth data reported by Luckenbach et al. (2007), who as part of an investigation of insulin-like growth factor 1 in SFL, conducted two SFL growth trials, each at a pair of temperatures. In experiment 1, juvenile SFL with initial average weight about 1.9 g were raised at 23°C and 28°C over a 123 day period at a salinity of 5 ppt. In experiment 2, juvenile SFL with initial average weight of 0.28 g were raised at 23°C and 28°C over a 197 day period. Salinity in the second experiment started at 27 ppt, but was lowered over the course of the experiment to 4 ppt.

To model the declining salinity of Luckenbach et al.'s experiment 2, a stock and flow model was added to E.F-RMD as shown in Figure 86. The stock salinity reservoir, "Sal res," starts at 27 ppt, and is used as the salinity value for experiment 2 with "salt" being "removed" by "Sal out" at a fixed daily rate as defined by the ratio between the initial and end salinity (27 – 4 = 23) over the total time of the experiments (in hours). This results in a linear salinity decline over the duration of the experiment.

Sal out = 23/(STOPTIME-STARTTIME)

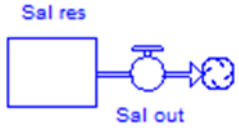

Figure 86. Salinity reduction model.
Used in E.F-RMD configured for analysis of Luckenbach et al. (2007) experiment 2.

The addition of declining salinity provided an opportunity to test E.F-RMD in an environment with a changing masking load. Unfortunately, Luckenbach et al. (2007) did not specify the DO or pH, so it was assumed that fish were normoxic throughout the experiment, and pH was set to 8.3 for consistency with the Cool-Warm data analysis. Air-saturated DO is inversely related to salinity, so the simulated DO for experiment 2 increased as salinity declined by approximately 1 mg O_2/L water over the course of the trial, for both temperature treatments. Experiment 1's simulated DO levels remained constant over the trial.

Luckenbach et al. (2007) measured growth four times over 120 days for Experiment 1, and 6 times over 200 days for Experiment 2 (Table 19).

Table 19. Experiments 1 and 2 weight data reprinted from Luckenbach et al. (2007).

Experiment 1			
		Avg. Wt (g)	
Day	Hour	23°C	28°C
1	24	1.86	1.91
30	720	5	6
60	1440	11	11
120	2880	53	36

Experiment 2			
		Avg. Wt (g)	
Day	Hour	23°C	28°C
1	24	0.28	0.28
60	1440	1	1
90	2160	6	6
130	3120	14	14
160	3840	32	21
200	4800	53	32

Growth data, by hours, for each experiment and temperature condition were plotted, and polynomial trend-line equations fitted (Figure 87).

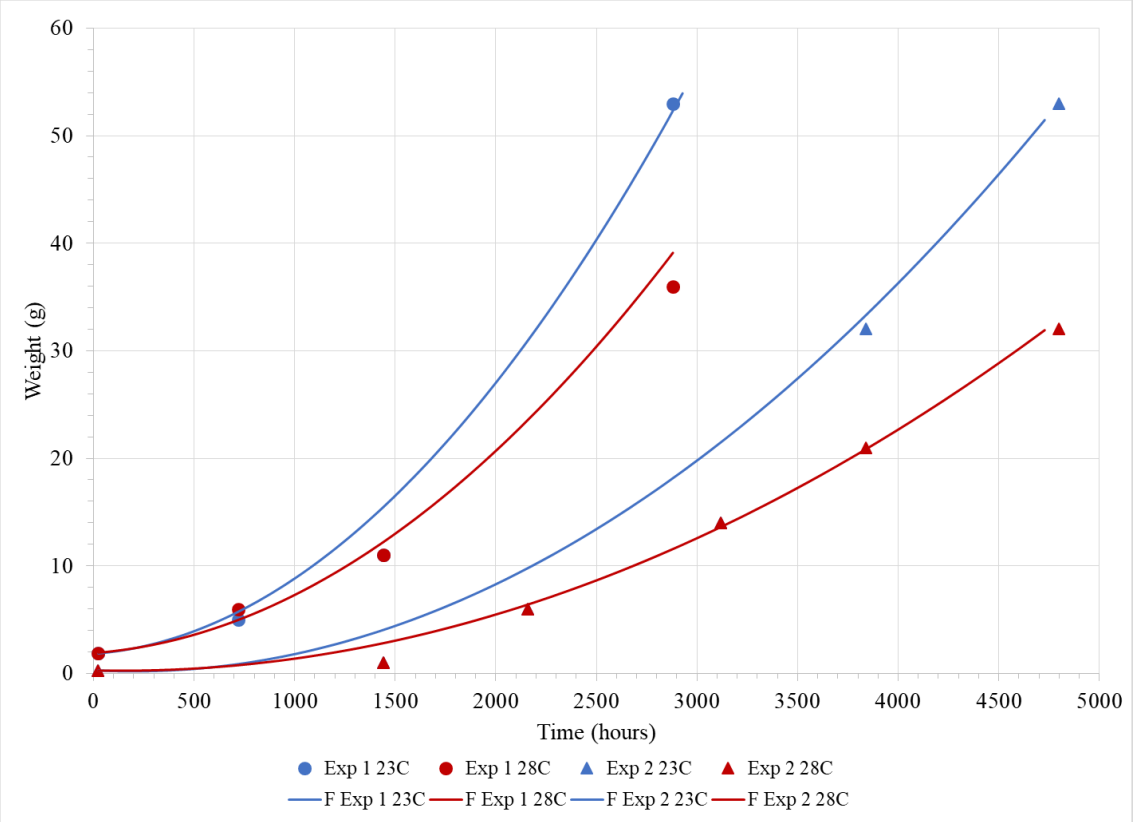

Figure 87. Luckenbach et al. (2007) experiment 1 and 2 average SFL weight-at-time with added trend-lines.
Experiment 1 (circles) was conducted over 123 days. Experiment 2 (triangles) was conducted over 197 days. Marker color: blue = 23°C, red = 28°C. Adapted from Luckenbach et al. (2007)

The fit equations used for growth comparison are presented in Table 20.

Variable TIME is in hours.

Table 20. Best-fit polynomial equations (2nd order) for Luckenbach et al. (2007) experiments.

Experiment	Temperature (°C)	Fit Equation
1	23	0.0000056*TIME^2+0.0014*TIME+1.83
	28	0.000004*TIME^2+0.0014*TIME+1.9
2	23	0.0000025*TIME^2-0.001*TIME+ 0.3
	28	0.0000015*TIME^2-0.0004*TIME+0.28

Initial conditions for E.F-RMD are shown in Table 21. Trial runs with the modified E.F-RMD model were initially conducted using the "FeedRateMax" temperature-only formulation to analyze the Cool – Warm data. This proved to be somewhat effective, but the "FeedRateMax" used in the SCT pond data, which also factors in fish weight, was used for the fits described below as it produced better results.

Table 21. E.F-RMD environmental inputs and parameters for Luckenbach et al. (2007) study.

	Exp. 1 23°C	Exp. 1 28°C	Exp. 2 23°C	Exp. 2 28°C
Starting Weight (g)	1.86	1.91	0.28	0.28
Salinity (ppt)	5	5	17 - 4	17 - 4
Mean PO2 (mmHg)	159	159	159	159
DO (mg O_2/L water)	8.58	7.89	7.6 – 8.6	7.0 – 7.9
pH	8.3	8.3	8.3	8.3
fR con	35	35	40	45
Winberg	1.8	1.9	2.07	2.05
Skin Eff f	1	1	1	1
Smin0	0.043	0.043	0.043	0.043
q1	0.062	0.062	0.062	0.062
q2	0.09	0.09	0.09	0.09
GEFeed (cal/g)	2000	2000	2000	2000
sda	0.14	0.14	0.14	0.14
FeedDigestibility%	90	90	90	90

E.F-RMD Simulation of Luckenbach et al. (2007) Study

E.F-RMD simulated weights for each experimental condition were obtained from the model run-time "hour" that correspond to the day weight measurements reported by Luckenbach et al. (2007) are shown in Table 22. Percent weight change per day for observed and modeled growth are presented in Table 23.

Table 22. Luckenbach et al. (2007) vs. E.F-RMD simulated weights.

Experiment 1					
		23°C		28°C	
Day	Hour	Obs Wt (g)	E.F-RMD Wt (g)	Obs Wt (g)	E.F-RMD Wt (g)
1	24	1.86	1.86	1.91	1.91
30	720	5	7.08	6	4.56
60	1440	11	16.68	11	10.77
120	2880	53	52.68	36	39.77

Experiment 2					
		23°C		28°C	
Day	Hour	Obs Wt (g)	E.F-RMD Wt (g)	Obs Wt (g)	E.F-RMD Wt (g)
1	24	0.28	0.28	0.28	0.28
60	1440	1	1.79	1	0.78
90	2160	6	4.42	6	1.59
130	3120	14	14.38	14	5.91
160	3840	32	27.61	21	14.31
200	4800	53	54.29	32	33.3

Table 23. Luckenbach et al. (2007) and E.F-RMD simulated %Wtchg/day.

Experiment 1					
		23°C		28°C	
Day	Hour	Obs %Wtchg/day	E.F-RMD %Wtchg/day	Obs %Wtchg/day	E.F-RMD %Wtchg/day
1	24	-	-	-	-
30	720	5.63	9.35	7.14	4.62
60	1440	8.19	13.28	7.93	7.73
120	2880	22.91	22.77	14.87	16.52

Experiment 2					
		23°C		28°C	
Day	Hour	Obs %Wtchg/day	E.F-RMD %Wtchg/day	Obs %Wtchg/day	E.F-RMD %Wtchg/day
1	24	-	-	-	-
60	1440	4.29	8.99	4.29	2.98
90	2160	22.70	16.43	22.70	5.20
130	3120	37.69	38.74	37.69	15.47
160	3840	70.80	61.00	46.25	31.32
200	4800	94.14	96.45	56.64	58.96

E.F-RMD simulations for the four experimental conditions are shown below as Stella® graphs. Each compares E.F-RMD simulated growth against the growth trend-lines from Table 20 . Each Stella® graph is followed by a goodness-of-fit table and Consilience graph for weight and %Wtchg/day.

Experiment 1, 23°C Growth

Simulated E.F-RMD growth compared to that observed in experiment 1 at 23°C is graphed in Figure 88.

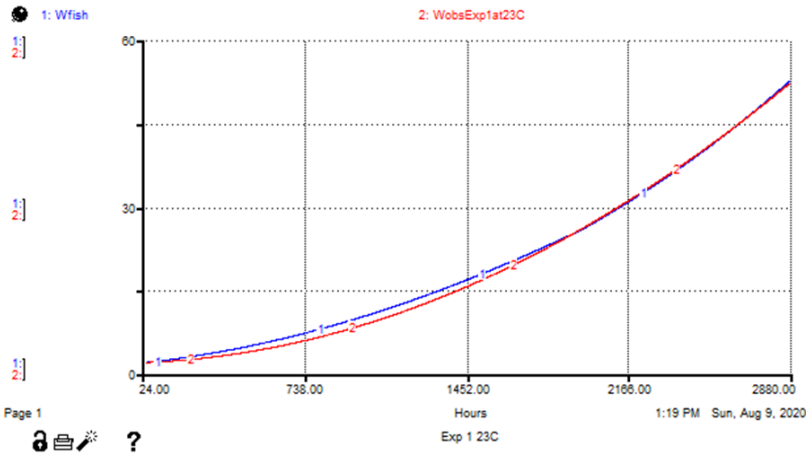

Figure 88. Stella® graph of E.F-RMD simulated SFL weight vs. Luckenbach et al. experiment 1, 23°C trend-line curve.

Weight and %Wtchg/day Consilience analysis for Luckenbach et al. (2007) experiment 1 at 23°C data and the corresponding E.F-RMD values taken at the same sampling hours are shown in Table 24. Results were significant both for weight and %Wtchg/day. Consilience graphs for weight (Figure 89) and %Wtchg/day (Figure 90) compare the E.F-RMD estimates to observed values at the same sample times relative to the line of perfect agreement.

Table 24. Goodness-of fit: E.F-RMD to Luckenbach et al. experiment 1, 23°C.

	Wt	%Wtchg/day
R^2	0.993	0.977
C (co-var-based)	0.991	0.924
C'(0.05)	0.905	0.905
Pr(C>C')	P<0.01*	0.01<P<0.05*

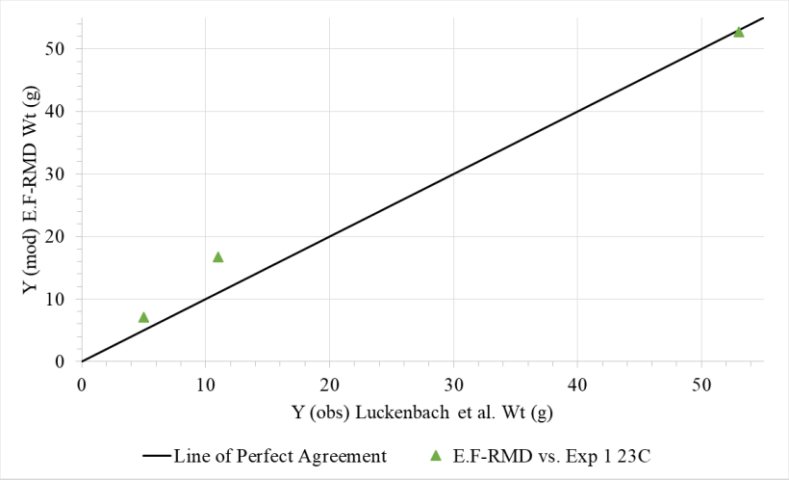

Figure 89. Observed vs. E.F-RMD modeled weight relative to the line of perfect agreement, for Luckenbach et al. experiment 1, 23°C.
R^2 = 0.993, *C* = 0.991.

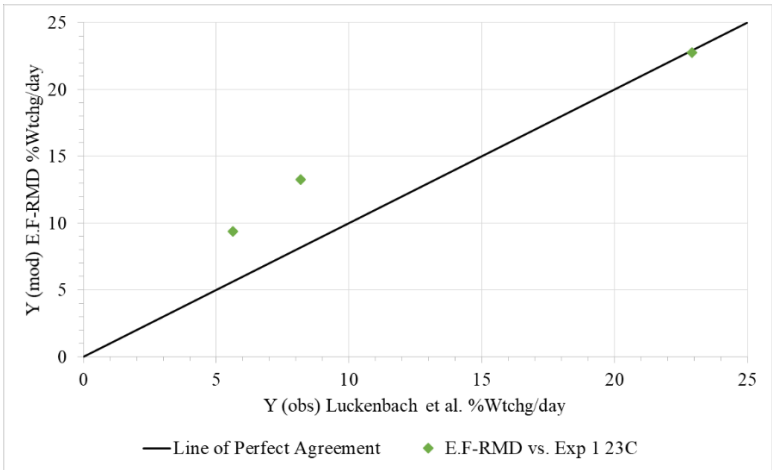

Figure 90. Observed vs. E.F-RMD modeled %Wtchg/day relative to the line of perfect agreement, for Luckenbach et al. experiment 1, 23°C.
R^2 = 0.977, C = 0.924.

Experiment 1, 28°C Growth

Simulated E.F-RMD growth compared to that observed in experiment 1 at 28°C is graphed in Figure 91.

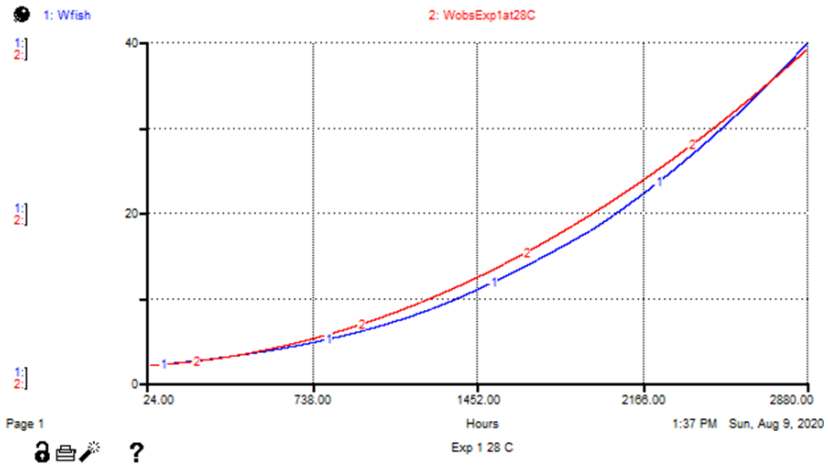

Figure 91. Stella® graph of E.F-RMD simulated SFL weight vs. Luckenbach et al. experiment 1, 28°C trend-line curve.

Results of the Consilience analysis between the observed and modeled weight and %Wtchg/day are shown in Table 25. As with the 23°C experiment, the 28°C experiment Weight and %Wtchg/day results were significant. Weight comparison of E.F-RMD to experiment 1, 28°C relative to the line of perfect agreement is shown in Figure 92, while the %Wtchg/day comparison is presented in Figure 93.

Table 25. Goodness-of fit: E.F-RMD to Luckenbach et al. experiment 1, 28°C.

	Wt	%Wtchg/day
R^2	1.000	0.974
C (co-var-based)	0.989	0.917
C'(0.05)	0.905	0.905
Pr(C>C')	P<0.01*	0.01<P<0.05*

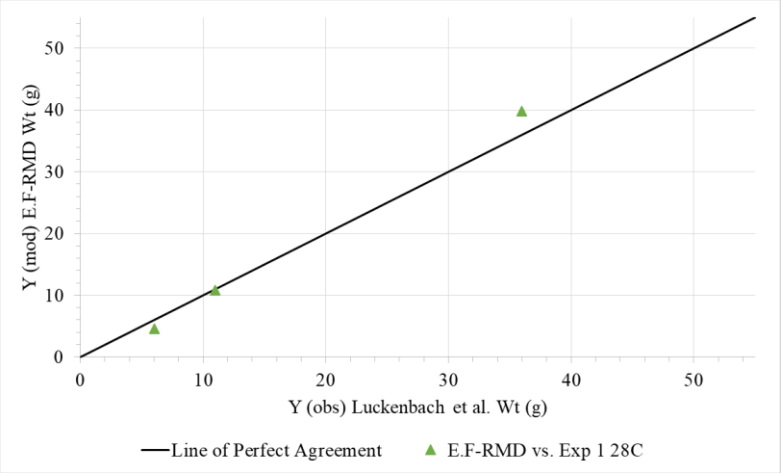

Figure 92. Observed vs. E.F-RMD modeled weight relative to the line of perfect agreement, for Luckenbach et al. experiment 1, 28°C.
R^2 = 1.000, *C* = 0.989.

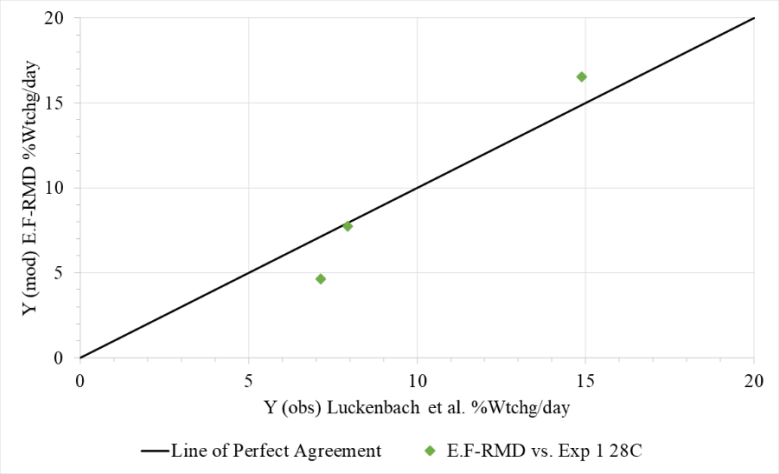

Figure 93. Observed vs. E.F-RMD modeled %Wtchg/day relative to the line of perfect agreement, for Luckenbach et al. experiment 1, 28°C.
R^2 = 0.974, C = 0.917.

Experiment 2, 23°C Growth

The estimated E.F-RMD growth compared to experiment 2, 23°C growth curve is graphed in Figure 94.

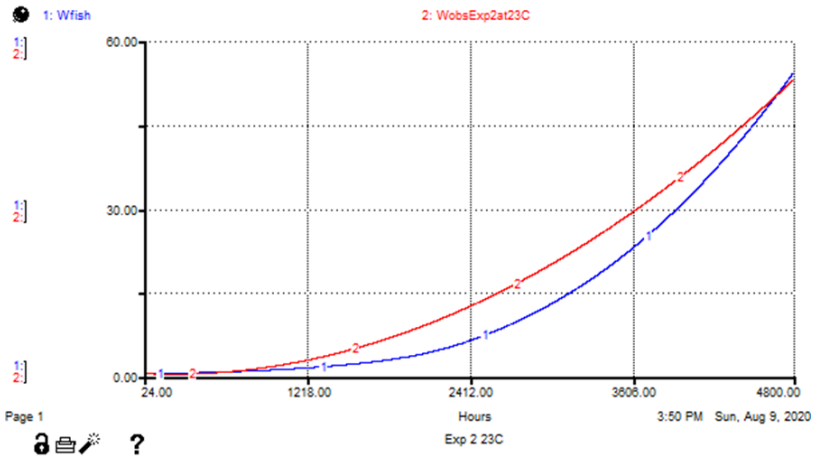

Figure 94. Stella® graph of E.F-RMD simulated SFL weight vs. Luckenbach et al. experiment 2, 23°C trend-line curve.

Results of the Consilience analysis of the Luckenbach et al. (2007) data growth trend-line for experiment 2, 23°C, to the E.F-RMD weight and %Wtchg/day simulation are shown in Table 26. Both weight and %Wtchg/day showed significance. Consilience graphs comparing weight are shown in Figure 95, while and %Wtchg/day comparison is shown in Figure 96.

Table 26. Goodness-of fit: E.F-RMD to Luckenbach et al. experiment 2, 23°C.

	Wt	%Wtchg/day
R^2	0.988	0.971
C (co-var-based)	0.995	0.988
$C'(0.05)$	0.786	0.786
Pr(C>C')	P<0.01*	P<0.01*

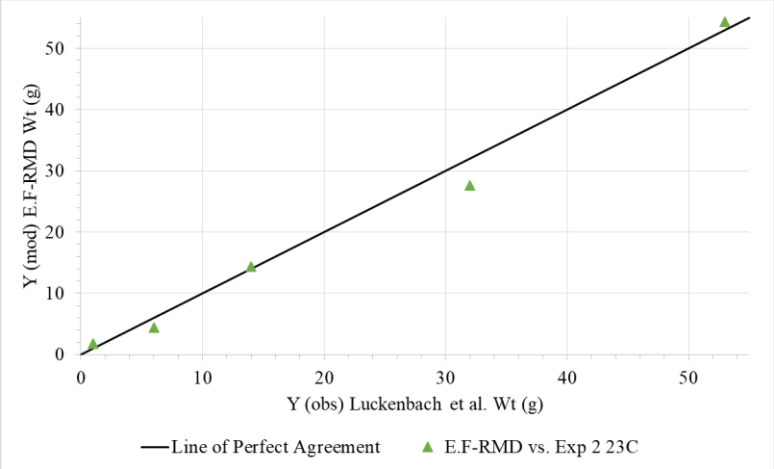

Figure 95. Observed vs. E.F-RMD modeled weight relative to the line of perfect agreement, for Luckenbach et al. experiment 2, 23°C.
R^2 = 0.988, C = 0.995.

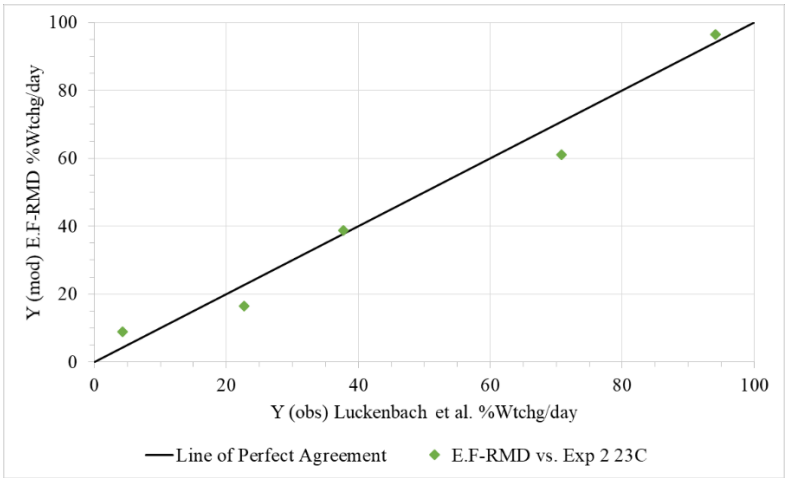

Figure 96. Observed vs. E.F-RMD modeled %Wtchg/day relative to the line of perfect agreement, for Luckenbach et al. experiment 2, 23°C.
R^2 = 0.971, C = 0.988.

Experiment 2, 28°C Growth

The simulated E.F-RMD growth compared to experiment 2, 28°C growth curve is graphed in Figure 97.

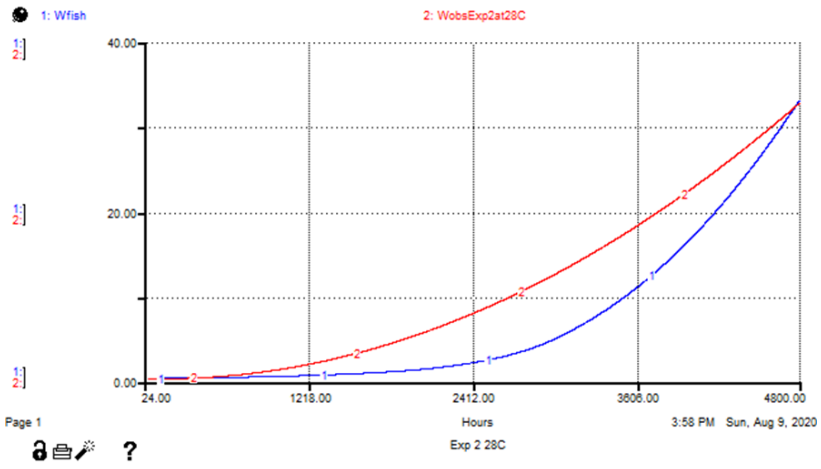

Figure 97. Stella® graph of E.F-RMD simulated SFL weight vs. Luckenbach et al. experiment 2, 28°C trend curve.

Results of the Consilience analysis of the Luckenbach et al. (2007), experiment 2, 28°C data growth trend-line to the E.F-RMD weight estimate are shown in Table 27. Weight correlation was significant between the data and E.F-RMD simulation while %Wtchg/day was not significant. The Weight Consilience graph is shown in Figure 98, with the %Wtchg/day graph shown in Figure 99.

The lower R2 and C values for experiment 2, especially at 28°C, may be indicative of weakness in E.F-RMD's ability to capture SFL growth effects of changing salinity, especially at elevated temperature. Also, there may have been

misrepresentation of weight effects on metabolic or bioenergetic processes in SFL of such small size as those used in the second experiment.

Table 27. Goodness-of fit: E.F-RMD to Luckenbach et al. experiment 2, 28°C.

	Wt	%Wtchg/day
R^2	0.911	0.787
C (co-var-based)	0.913	0.756
C'(0.05)	0.786	0.786
Pr(C>C')	P<0.01*	0.05<P<0.1

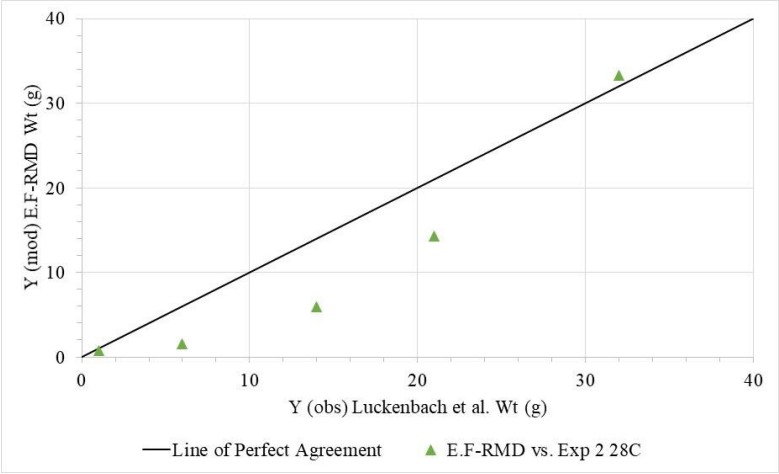

Figure 98. Observed vs. E.F-RMD modeled weight relative to the line of perfect agreement, for Luckenbach et al. experiment 2, 28°C.
R^2 = 0.911, *C* = 0.913.

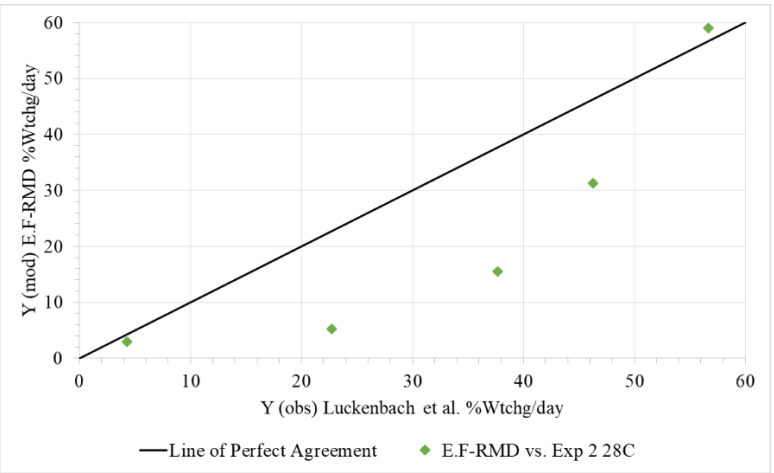

Figure 99. Observed vs. E.F-RMD modeled %Wtchg/day relative to the line of perfect agreement, for Luckenbach et al. experiment 2, 28°C.
R^2 = 0.787, *C* = 0.756.

Conclusion: Application of E.F-RMD to Luckenbach et al. (2007)

E.F-RMD results are significantly consilient under both temperature treatments for Luckenbach et al.'s (2007) experiment 1, both for weight-over-time and %Wtchg/day. *C* values also were significant for weight at both temperatures in experiment 2, but %Wtchg/day was significant only for the 23°C condition.

Changing salinity in experiment 2 may have exposed a potential limitation of E.F-RMD. While the E.F model does adjust to salinity, the RMD component does not.

Integrated Analysis of E.F-RMD Performance for the Three Studies

Objective assessment of E.F-RMD output relative to the observed growth data enables evaluation of the model's real utility, as an approach and as a tool for better understanding of SFL growth processes. The honest modeler must concede that significant goodness-of-fit between model and data can be taken as validation of the

model only for those given conditions. The real value of a growth model such as E.F-RMD lies in its ability to accurately simulate growth of the subject species in a variety of situations. Strengthening model validity is achievable by measuring model-data consilience across multiple studies. In the present instance, the available studies of SFL growth are three: MDC Cool - Warm, SCT pond, and Luckenbach et al. (2007).

An aggregate measure of Consilience (Neill et al. 2018) was applied, whereby Ymod-Yobs comparisons for the two emergent responses, Wt (over time) and %Wtchg/day, from the three studies were each treated as 3 independent samples (CaseMatch = No) for which joint Consilience (*jointC*) could be computed. This approach – treating 3 sets of same-Y response (e.g., Wt over time) as 3 sets of not-same Ymod responses, then computing their *jointC* – was not addressed by Neill et al. (2018), but senior-author Neill can find no particular fault in this approach.

Accordingly, *jointC* analysis of the three data sets was conducted for each variable, using the compact Consilience-calculator developed by Dr. Ray H. Kamps (Neill et al. 2018). Each data set was assigned a weighted value by the calculator of approximately 0.33. For *jointC* analysis, the data and simulated results from all subsets of the three studies were aggregated as a single Ymod-Yobs series.

The results of *jointC* analysis for the three data sets (Npairs1= 8, Npairs2 = 7, Npairs3 = 16; NpairsAll = 31) for weight and %Wtchg/day are shown in Table 28. Goodness-of-fit for E.F-RMD simulations to observed weights across all three data sets produced a *jointC* that was significant. Due to the poor growth fit for SCT pond, and to

a lesser extent, for Luckenbach et al. experiment 2, *jointC* for the %Wtchg/day was not as large, but still was significant.

Table 28. Goodness-of fit: *jointC* for weight and %Wtchg/day, all data sets.

	Wt	%Wtchg/day
JointC	0.968	0.757
C'(0.05)	0.356	0.356
Pr(C>C')	P<0.01*	P<0.01*

Goodness-of-fit graphs for weight (Figure 100) and %Wtchg/day (Figure 101) are shown below. As with the *jointC* analysis, Cool – Warm data are combined into one data set, as are the Luckenbach et al. experiments data.

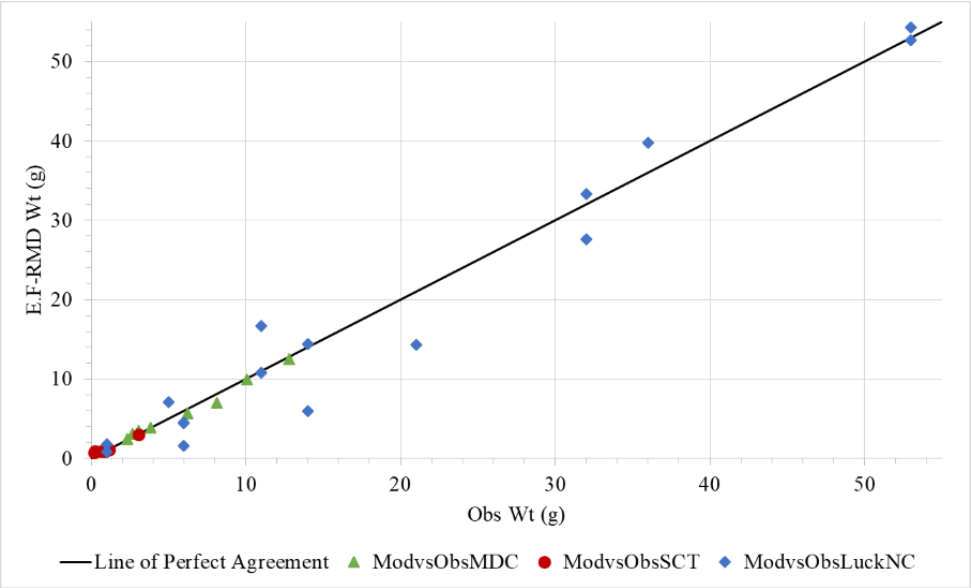

Figure 100. Observed vs. MDC, SCT, and Luckenbach et al. model weights relative to the line of perfect agreement.
JointC = 0.968.

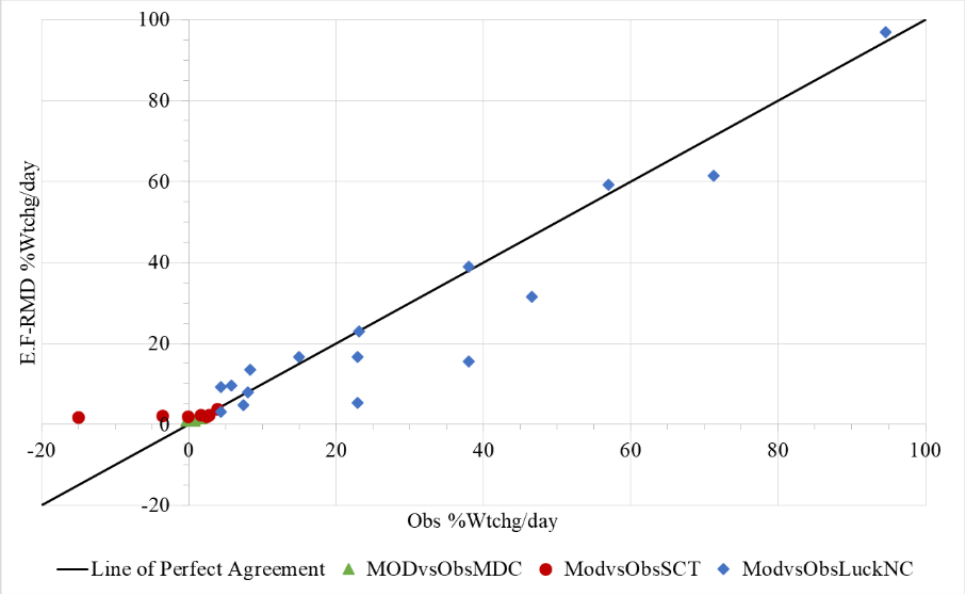

Figure 101. Observed vs. MDC, SCT, and Luckenbach et al. model %Wtchg/day relative to the line of perfect agreement.
JointC = 0.757.

Overall Conclusion: E.F-RMD as an Effective Growth Model

Observed vs. Model Consilience

Consilience of E.F-RMD outputs for weight-at-time with observation was significant ($P<0.05$) for all seven subsets of data; for %Wtchg/day, *C* was significant for four of the seven data sets. Non-significance was observed for %Wtchg/day for MDC Warm, SCT pond, and Luckenbach et al. experiment 2 at 28°C. A synopsis of significant versus non-significant results for weight-at-time and %Wtchg/day is shown in Table 29.

Table 29. Consilience significance for all studies.
Significant (+), not significant (-).

Data	Weight	%Wtchg/day
MDC Cool	+	+
MDC Warm	+	-
SCT Pond	+	-
Luckenbach et al., Exp 1 23°C	+	+
Luckenbach et al., Exp 1 28°C	+	+
Luckenbach et al., Exp 2 23°C	+	+
Luckenbach et al., Exp 2 28°C	+	-

Observed vs. Model Joint Consiliences

JointC between modeled and observed results for the three studies in aggregate was significant, both for weight-at-time and %Wtchg/day, with weight-at-time presenting higher consilience (*jointC* = 0.968, P<0.01). It is to be expected that weights for growing animals over time are less "noisy" than are what amounts to their time derivatives, %Wtchg/day. Thus, %Wtchg/day presents the more conservative measure of animal growth. And, to the extent that even *jointC* for %Wtchg/day was large and significant, E.F-RMD is declared a valid and useful model for simulating SFL growth and is thus potentially useful as a tool for use in Southern Flounder stock management.

CHAPTER IX

SUMMARY AND CONCLUSIONS

The Southern Flounder *Paralichthys lethostigma* (SFL) is an important commercial and sport fish occurring in coastal waters of the Gulf of Mexico and along the eastern seaboard of the USA, up to the Carolinas (Wenner and Archambault 2005). The life cycle of SFL exposes this euryhaline species to varying conditions of salinity, temperature, and oxygen (O_2). Movements between brackish estuaries and the open ocean challenge physiological homeostasis and impose metabolic loads, thus reducing metabolic scope for productive activities such as locomotion, growth and reproduction. Recently, SFL numbers have been in decline, owing perhaps to increased fishing pressure and to climate change (Munroe 2015, VanderKooy 2015)

Ecophysiological research and conceptualizations of fish metabolism and growth by Fry (1947, 1971) and by many other scientists have provided a logical foundation for modeling the respiratory and bioenergetic processes of SFL to better understand its growth and ecology.

Fry (1947, 1971) categorized the environment's components impacting fish physiology and consequently its growth. Fry drew particular attention to important interactions, such as that of the controlling factor temperature with the limiting factor oxygen, leading metabolic scope for growth.

The concepts of Fry (1947, 1971) and complementary bioenergetics modeling (e.g., Burke and Rice (2002) and predecessors) led to Ecophys.Fish (Neill et al. 2004),

which provided one foundation of the present work. E.F integrates bioenergetic and metabolic responses, and it accounts for the effects of multiple environmental factors and their interactions over time. Developed with isee systems' Stella® dynamic systems modeling software, E.F has proven utility as an adaptable model for simulating bioenergetics and growth of several fish species (Neill et al. 2004, Fonseca et al. 2010) and the Pacific White Shrimp *Litopenaeus vannamei* (Walker 2009).

Because of the Southern Flounder's fishery importance and concern about its declining stocks, the present study was undertaken, to develop and evaluate an E.F-based dynamic growth model for the Southern Flounder. The special ecophysiology of SFL–it being a flatfish and living mostly on or near the substrate–dictated that E.F be equipped with a more mechanistic representation of its respiratory physiology.

Thus, the responsibility of modeling O_2 flow, $\dot{V}O_2$, from the environment to the tissue in the SFL was also assumed, with the aim of providing the SFL-variant E.F model with this additional capability. This resulted in the development of what came to be called the Respiratory Model, Dynamic (RMD).

Computer modeling of fish respiration dates back to at least Taylor et al. (1968) and must account for multiple physical and physiological factors. For RMD, the approach was to model $\dot{V}O_2$ within the biological system based on the three components that control the flow of O_2 as it moves from the environment to the tissues; these three components are ventilation, gill diffusion, and blood transport.

The success of RMD as a fish respiratory model hinged upon establishing the range and response for each of the three model components, each configured on the basis

of current knowledge. RMD draws on multiple scientific disciplines; including, but no limited to, anatomy, physiology, and biochemistry. Such synergy of disciplines offered the prospect of finding emergent, even unanticipated results. Such was the case with the addition of cutaneous respiration as a contributor to RMD $\dot{V}O_2$ output.

Respiratory Model, Dynamic

Like all models, RMD started small but grew and became more complex as it evolved to meet practical simulation needs. Some choices made for inclusion in RMD were serendipitous, as the decision to include cutaneous respiration (discussed in detail below). Other components arose by obvious necessity, and while perhaps not as significant as cutaneous respiration, merit attention as potential contributors to our overall knowledge of SFL.

Allometric Cutaneous Respiration in SFL

Respirometry data (Figure 10) showed that fry and juvenile SFL have a higher per-gram $\dot{M}O_2$ rate than adult SFL. This decline in per-gram metabolic rate may be imposed by the metabolic power law (Kleiber 1932, Kleiber 1975, Schmidt-Nielsen 1984). RMD estimates of $\dot{M}O_2$ that incorporated cutaneous-sourced $\dot{M}O_2$ followed a similar negative-exponential trend-line that declined towards an apparent asymptote as the fish grew. This suggests that cutaneous-sourced $\dot{M}O_2$ may have evolved to meet the greater per-gram metabolic energy requirements of fry and juvenile SFL (Lotka 1922).

When configured optimally, RMD output suggested that within flounder, supplemental cutaneous respiration is an important contributor to $\dot{M}O_2$ in fry, juvenile, and young adult flatfish, becoming less so as the fish grows towards adulthood, due to

the increase in the mass-to-surface area ratio and skin thickness. Figure 102 shows estimated RMD $\dot{M}O_2$ (mg O_2/g·h) output for SFL weights between 1 and 1000 g with cutaneous diffusion set to 100% (maximum), 50%, 25%, and 0% efficiency using the RMD skin efficiency fraction, "Skin eff f," converter with DO = 7 mg O_2/L water, PO_2 = 129 mmHg, Ta = 15°C, and salinity = 30 ppt.

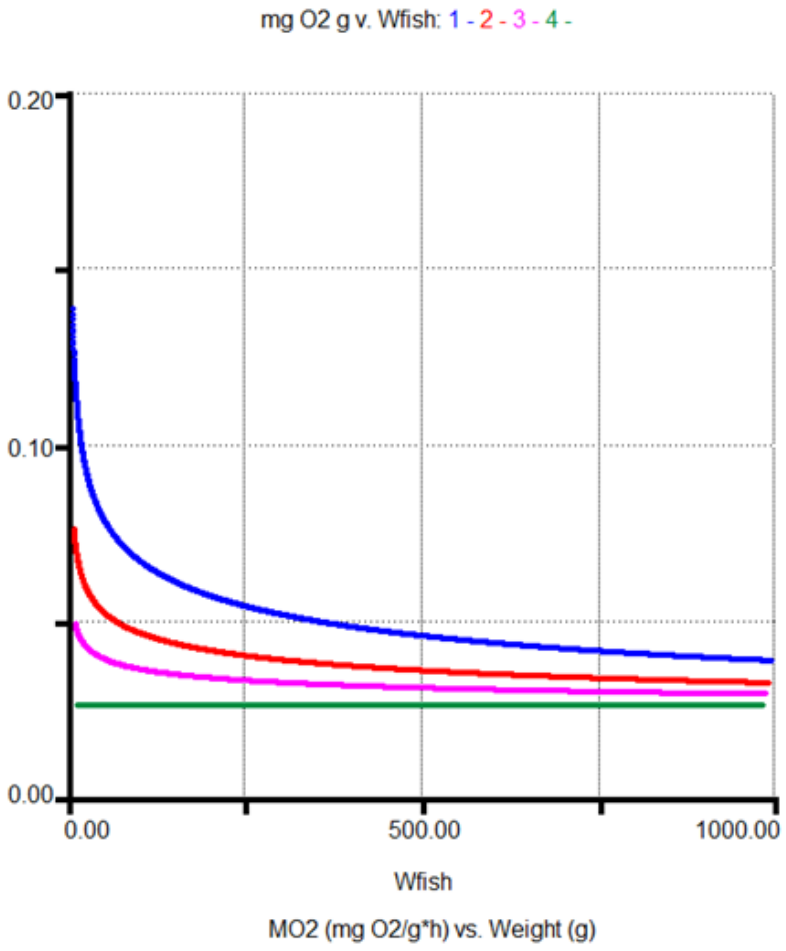

Figure 102. RMD Stella® plot – $\dot{M}O_2$ by weight, variable cutaneous efficiency.
Cutaneous efficiency: 100% (blue), 50% (red), 25% (magenta), and 0% (green). DO = 7 mg O_2/L water, PO_2 = 129 mmHg, Ta = 15°C, salinity = 30 ppt.

With the cutaneous fraction set to zero, per-gram $\dot{M}O_2$ remains flat (green line), and is the $\dot{M}O_2$ from RMD gill respiration only. Values vary with DO, Ta, salinity, and the amount of skin exposed to the water (i.e., how deep the SFL is buried in the substrate), but for any given environmental regime, it is the asymptotic minimum $\dot{M}O_2$ output. As the fish grows, RMD invokes increasing skin thickness with increasing body mass. The increase in skin thickness reduces O_2 diffusion which, when considered in the context of increasing body mass, results in a steady decline in the contribution of cutaneous O_2 to overall $\dot{M}O_2$.

RMD results suggest that cutaneous respiration in flounder depends on the mass of the fish, which may explain the variability observed in the literature on the relative contribution of cutaneous respiration in flatfish and other species. Rather than being a set percentage, the contribution of supplemental cutaneous respiration to overall $\dot{M}O_2$ changes with environmental conditions and over the life cycle of fish. When the conditions that produced the outputs shown in Figure 102 are graphed as percent cutaneous contribution, the results in Figure 103 show the relationship of mass-dependence of the cutaneous respiration contribution to the overall $\dot{M}O_2$.

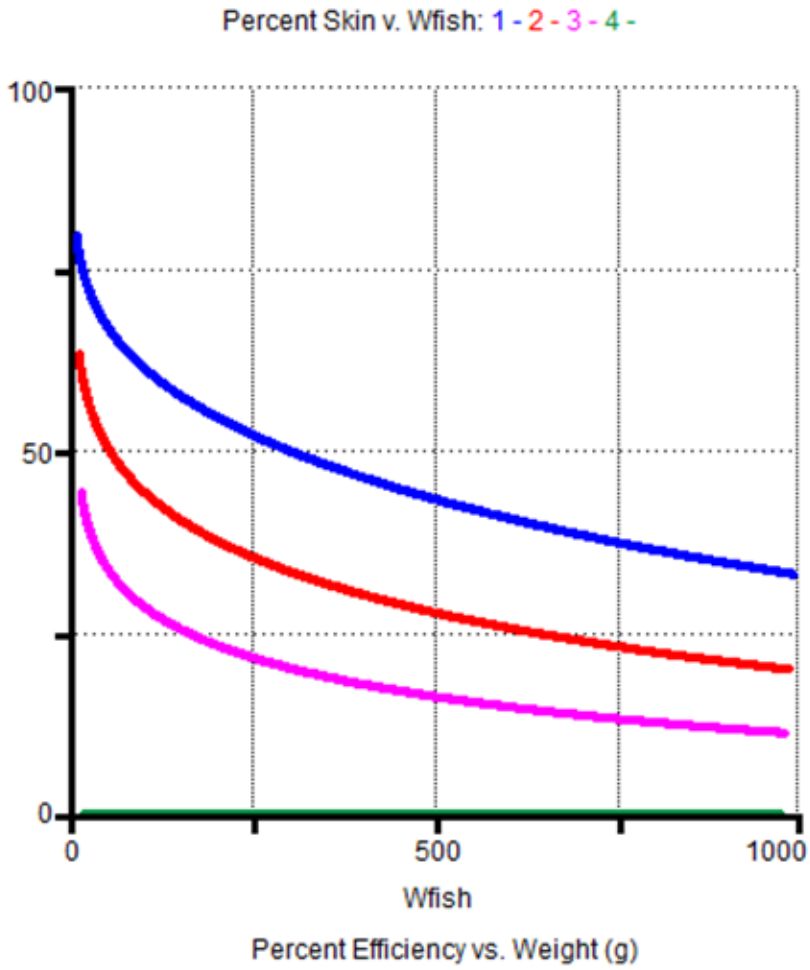

Figure 103. RMD Stella® plot – Percent cutaneous respiratory contribution.
Cutaneous efficiency: 100% (blue), 50% (red), 25% (magenta), and 0% (green). DO = 7 mg O_2/L water, PO_2 = 129 mmHg, Ta = 15°C, salinity = 30 ppt.

RMD uses fixed, linear slope values for calculating upper and lower epidermal thickness by weight. However, when compared to MDC Cool – Warm respirometry trend-line results, RMD underestimated the cutaneous $\dot{M}O_2$ contribution for SFL below 12 g. This is suggestive, but by no means conclusive, that SFL skin thickness growth may be non-linear, perhaps similar but opposite to the "triphasic allometry" observed in

Common Carp gill surface area, with slower epidermal tissue growth compared to the faster gill growth reported by Oikawa and Itazawa (1985).

Meeh Coefficient and Flatfish Surface Area

Using SFL growth data from the Texas Parks and Wildlife Department's Marine Development Center, the "Surface Law" coefficient *k,* also called the Meeh coefficient (see equation 25), for SFL was determined to be approximately 10. This value is in line with the value reported for typical fish (Schmidt-Nielsen 1984), indicating that, despite their morphology, flatfish surface area scales proportionately with those of "round" fish.

Although likely having utility to only a few researchers, a means of calculating surface area for ellipsoid-shaped fish based solely on total length (TL) was developed and presented in equation (33).

Flatfish Allometric Ventricular Volume

Starting with an allometric estimation for calculation of heart mass, see equation (34), and available literature data on ventricular mass compared to total heart mass, an allometric estimation of stroke volume for flounder was developed, see equation (45).

The E.F-RMD Growth Model

When properly configured, E.F-RMD appears to be an effective model for simulating SFL growth. The model can be fit to data in most circumstances by adjustment of only three shaping variables: "GEFeed," "Winberg," and "fR con," which respectively quantify gross energy of feed (cal/g), the ratio of routine metabolic rate to standard metabolic rate, and the ventilation-frequency constant by which ventilation

frequency is modified by adjusting the slope and magnitude of the temperature-dependent ventilatory rate response curve shown in Figure 34.

When considering modeled results relative to data, a model's sensitivity to changes in initial conditions is of concern (Grant et al. 1997). With complex and dynamic models such as E.F-RMD, some components are likely to have more substantial effects on the outcome. Within E.F-RMD, the processes with the greatest effects on growth outcome are "Winberg" and "fR con" as these impact output of "MSgrowth" and "Mact max," respectively. However, once E.F-RMD was shaped to fit a specific observational regime (i.e., MDC laboratory experiment, SCT pond trial, growth trials by Luckenbach et al. (2007)), it was able to adequately adjust for variation in initial fish weight, temperature and $[O_2]$ to provide growth outcomes comparable to those observed, as quantified via Consilience analysis of weight and percent weight change per day with respect to time.

Where the model does appear to falter is with respect to changes in salinity. E.F-RMD's inability to closely match growth observed in the second experiment by Luckenbach et al. (2007) indicates that E.F-RMD, like all models, is deficient. Only through further exploration of E.F-RMD via experimentation with a variety of environmental conditions, model assumptions and configurations can this and other limitations be addressed. It is also a reminder that models are never complete, but like the living organisms they attempt to simulate, constantly evolve.

Despite the admitted limitations of E.F-RMD, it represents an effective merger of a new and more mechanistic component for simulation of respiratory physiology of fish,

with an existing ecophysiological model of fish bioenergetics and growth. Moreover, RMD explicitly accommodates the contribution of cutaneous respiration to fish metabolism so important in flatfishes, especially smaller individuals. Finally, both components of E.F-RMD were successfully parameterized specifically for Southern Flounder.

REFERENCES

Anderson, J. D., W. J. Karel, and A. C. Mione. 2012. Population structure and evolutionary history of Southern Flounder in the Gulf of Mexico and western Atlantic Ocean. Transactions of the American Fisheries Society **141**:46-55.

Androjna, C., J. E. Gatica, J. M. Belovich, and K. Derwin. 2008. Oxygen diffusion through natural extracellular matrices: implications for estimating "critical thickness" values in tendon tissue engineering. Tissue Engineering Part A **14**:559-569.

Aquamaps. Accessed March 25, 2016. Computer generated distribution maps for *Paralichthys lethostigma* (Southern flounder). www.aquamaps.org.

Barcroft, J. 1913. The combinations of haemoglobin with oxygen and with carbon monoxide. II. Biochemical Journal **7**:481.

Barreto, R. E., and G. L. Volpato. 2006. Ventilatory frequency of Nile Tilapia subjected to different stressors. Journal of Experimental Animal Science **43**:189-196.

Battino, R., F. D. Evans, and W. Danforth. 1968. The solubilities of seven gases in olive oil with references to theories of transport through the cell membrane. Journal of the American Oil Chemists' Society **45**:830-833.

Bayha, K. M., N. Ortell, C. N. Ryan, K. J. Griffitt, M. Krasnec, J. Sena, T. Ramaraj, R. Takeshita, G. D. Mayer, and F. Schilkey. 2017. Crude oil impairs immune function and increases susceptibility to pathogenic bacteria in southern flounder. PLoS One **12**:e0176559.

Benson, B. B., and D. Krause. 1984. The concentration and isotopic fractionation of oxygen dissolved in freshwater and seawater in equilibrium with the atmosphere. Limnology and Oceanography **29**:620-632.

Berschick, P., C. Bridges, and M. Grieshaber. 1987. The influence of hyperoxia, hypoxia and temperature on the respiratory physiology of the intertidal rockpool fish *Gobius cobitis Pallas*. Journal of Experimental Biology **130**:368-387.

Blanchet, H. 2010. Assessment of Southern Flounder in Louisiana waters. Louisiana Department of Wildlife and Fisheries, Office of Marine Fisheries, Baton Rouge, LA, 70895.

Boddington, M. 1978. An absolute metabolic scope for activity. Journal of theoretical Biology **75**:443-449.

Bohr, C., K. Hasselbalch, and A. Krogh. 1904. Concerning a biologically important relationship–the influence of the carbon dioxide content of blood on its oxygen binding. Skandinavisches Archiv für Physiologie **16**:402-412.

Bolker, B. M. 2008. Ecological models and data in R. Princeton University Press, Princeton, NJ.

Boltzmann, L. 1886. The second law of thermodynamics. Pages 13-32 *in* B. McGuinness, editor. Theoretical physics and philosophical problems: Selected writings. Springer Netherlands, Dordrecht.

Box, G. E. P. 1979. Robustness in the strategy of scientific model building. Pages 201-236 *in* R. L. Launer and G. N. Wilkinson, editors. Robustness in statistics. Academic Press, New York.

Brady, D. C., and T. E. Targett. 2010. Characterizing the escape response of juvenile summer flounder Paralichthys dentatus to diel-cycling hypoxia. Journal of Fish Biology **77**:137-152.

Brett, J., and T. Groves. 1979. Physiological energetics. Fish physiology **8**:280-352.

Brown-Peterson, N. J., M. Krasnec, R. Takeshita, C. N. Ryan, K. J. Griffitt, C. Lay, G. D. Mayer, K. M. Bayha, W. E. Hawkins, and I. Lipton. 2015. A multiple endpoint analysis of the effects of chronic exposure to sediment contaminated with Deepwater Horizon oil on juvenile Southern flounder and their associated microbiomes. Aquatic Toxicology **165**:197-209.

Burggren, W. W. 1988. Role of the central circulation in regulation of cutaneous gas exchange. American Zoologist **28**:985-998.

Burke, B. J., and J. A. Rice. 2002. A linked foraging and bioenergetics model for southern flounder. Transactions of the American Fisheries Society **131**:120-131.

Burton, D., and M. Burton. 1989. Individual variability in the epidermis of prespawning inshore winter flounder, *Pseudopleuronectes americanus*. Journal of Fish Biology **35**:845-853.

Burton, D., M. Burton, and D. Idler. 1984. Epidermal condition in post-spawned winter flounder, *Pseudopleuronectes americanus* (Walbaum), maintained in the laboratory and after exposure to crude petroleum. Journal of Fish Biology **25**:593-606.

Calder, W. A. 1984. Size, function, and life history. Harvard University Press, Cambridge, MA.

Cameron, J. N. 1989. The respiratory physiology of animals. Oxford University Press, New York, NY.

Capossela, K. M., R. W. Brill, M. C. Fabrizio, and P. G. Bushnell. 2012. Metabolic and cardiorespiratory responses of summer flounder *Paralichthys dentatus* to hypoxia at two temperatures. Journal of Fish Biology **81**:1043-1058.

Cason, P. personal communication, October 21, 2020. Flounder fingerlings reared at SCT ponds.

Casterlin, M. E., and W. W. Reynolds. 1982. Thermoregulatory behavior and diel activity of yearling winter flounder, *Pseudopleuronectes americanus* (Walbaum). Environmental Biology of Fishes **7**:177-180.

Caswell, H. 2001. Matrix population models: construction, analysis, and interpretation. Sinauer Associates, Sunderland, MA.

Cech, J. J., D. M. Rowell, and J. S. Glasgow. 1977. Cardiovascular responses of the winter flounder *Pseudopleuronectes americanus* to hypoxia. Comparative Biochemistry and Physiology Part A: Physiology **57**:123-125.

Chabot, D., J. F. Steffensen, and A. P. Farrell. 2016. The determination of standard metabolic rate in fishes. Journal of Fish Biology **88**:81-121.

Chipps, S. R., and D. H. Wahl. 2008. Bioenergetics modeling in the 21st century: reviewing new insights and revisiting old constraints. Transactions of the American Fisheries Society **137**:298-313.

Claireaux, G., and D. Chabot. 2016. Responses by fishes to environmental hypoxia: integration through Fry's concept of aerobic metabolic scope. Journal of Fish Biology **88**:232-251.

Claireaux, G., and C. Lefrancois. 2007. Linking environmental variability and fish performance: integration through the concept of scope for activity. Philosophical Transactions of the Royal Society B: Biological Sciences **362**:2031-2041.

Clarke, A., and N. M. Johnston. 1999. Scaling of metabolic rate with body mass and temperature in teleost fish. Journal of Animal Ecology **68**:893-905.

Corey, M. M., R. T. Leaf, N. J. Brown-Peterson, M. S. Peterson, S. D. Clardy, and D. A. Dippold. 2017. Growth and spawning dynamics of Southern Flounder in the north-central Gulf of Mexico. Marine and Coastal Fisheries **9**:231-243.

D'Aoust, B. G. 1969. Hyperbaric oxygen: toxicity to fish at pressures present in their swimbladders. Science **163**:576-578.

Dalla Via, J., G. Van den Thillart, O. Cattani, and P. Cortesi. 1997. Environmental versus functional hypoxia/anoxia in sole *Solea solea*: the lactate paradox revisited. MARINE ECOLOGY PROGRESS SERIES **154**:79-90.

Daniels, H., D. Berlinsky, R. Hodson, and C. Sullivan. 1996. Effects of stocking density, salinity, and light intensity on growth and survival of southern flounder *Paralichthys lethostigma* larvae. Journal of the World aquaculture society **27**:153-159.

Davidson, M. I., T. E. Targett, and P. A. Grecay. 2016. Evaluating the effects of diel-cycling hypoxia and pH on growth and survival of juvenile summer flounder *Paralichthys dentatus*. MARINE ECOLOGY PROGRESS SERIES **556**:223-235.

Dejours, P. 1979. Oxygen demand and gas exchange. Pages 1-44 *in* S. Wood and C. Lenfant, editors. Evolution of respiratory processes. Marcel Dekker, New York, NY.

Dejours, P. 1981. Principles of comparative respiratory physiology. 2nd edition. Elsevier/North-Holland Biomedical Press, Amsterdam, The Netherlands.

Dejours, P., A. Toulmond, and J. Truchot. 1977. The effect of hyperoxia on the breathing of marine fishes. Comparative Biochemistry and Physiology Part A: Physiology **58**:409-411.

Del Toro-Silva, F. M. 2008. Evaluation of nursery habitat: an ecophysiological approach [Unpublished doctoral dissertation]. PhD Thesis. North Carolina State University, Raleigh, North Carolina.

Del Toro-Silva, F. M., J. M. Miller, J. C. Taylor, and T. A. Ellis. 2008. Influence of oxygen and temperature on growth and metabolic performance of *Paralichthys lethostigma* (Pleuronectiformes: Paralichthyidae). Journal of Experimental Marine Biology and Ecology **358**:113-123.

Deslauriers, D., S. R. Chipps, J. E. Breck, J. A. Rice, and C. P. Madenjian. 2017. Fish bioenergetics 4.0: an R-based modeling application. Fisheries **42**:586-596.

Deubler, E. E., and G. S. Posner. 1963. Response of postlarval flounders, *Paralicthys lethostigma*, to water of low oxygen concentrations. Copeia:312-317.

Duthie, G. G. 1982. The respiratory metabolism of temperature-adapted flatfish at rest and during swimming activity and the use of anaerobic metabolism at moderate swimming speeds. Journal of Experimental Biology **97**:359-373.

Eddy, F. B., and R. D. Handy. 2012. Ecological and environmental physiology of fishes. Oxford University Press, Oxford, UK.

Enberg, K., E. Dunlop, and C. Jørgensen. 2008. Fish growth. Pages 1564–1572 *in* M. Goldstein, editor. Encyclopedia of ecology. Academic Press, Oxford, UK.

Evans, D. H., P. M. Piermarini, and K. P. Choe. 2005. The multifunctional fish gill: dominant site of gas exchange, osmoregulation, acid-base regulation, and excretion of nitrogenous waste. Physiology Review **85**:97-177.

Farrell, A. P. 2016. Pragmatic perspective on aerobic scope: peaking, plummeting, pejus and apportioning. Journal of Fish Biology **88**:322-343.

Feder, M., and W. Burggren. 1985 Feb. Cutaneous gas exchange in vertebrates: designs, patterns, control and implications. Biological Reviews **60**:1-45.

Feder, M., and W. Burggren. 1985 Nov 1. Skin breathing in vertebrates. Scientific American **253**:126-143.

Fick, A. 1995. On liquid diffusion. Journal of Membrane Science **100**:33-38.

Fischer, A. J., and B. A. Thompson. 2004. The age and growth of southern flounder, Paralichthys lethostigma, from Louisiana estuarine and offshore waters. Bulletin of Marine Science **75**:63-77.

Fischkoff, S., and J. Vanderkooi. 1975. Oxygen diffusion in biological and artificial membranes determined by the fluorochrome pyrene. The Journal of general physiology **65**:663-676.

Flowers, A., S. Allen, A. Markwith, and L. Lee. 2019. Stock assessment of Southern Flounder (*Paralichthys lethostigma*) in the South Atlantic, 1989–2017. NCDMF SAP-SAR-2019-01, Joint report of the North Carolina Division of Marine Fisheries, South Carolina Department of Natural Resources, Georgia Coastal Resources Division, Florida Fish and Wildlife Research Institute, University of North Carolina at Wilmington, and Louisiana State University.

Fonseca, V. F., W. H. Neill, J. M. Miller, and H. N. Cabral. 2010. Ecophys.Fish perspectives on growth of juvenile soles, *Solea solea* and *Solea senegalensis*, in the Tagus estuary, Portugal. Journal of Sea Research **64**:118-124.

Ford, F. A. 1999. Modeling the environment: an introduction to system dynamics models of environmental systems. Island Press, Washington, DC.

Friedman, M. 2008. The evolutionary origin of flatfish asymmetry. Nature **454**:209-212.

Froeschke, B. F., B. Sterba-Boatwright, and G. W. Stunz. 2011. Assessing southern flounder (*Paralichthys lethostigma*) long-term population trends in the northern Gulf of Mexico using time series analyses. Fisheries Research **108**:291-298.

Froese, R., and D. Pauly. 2016. Fishbase, accessed June 6, 2016.

Fry, F. 1947. Effects of the environment on animal activity. University of Toronto Press, Toronto, Ontario.

Fry, F. 1958. Temperature compensation. Annual Review of Physiology **20**:207-224.

Fry, F. 1971. The effect of environmental factors on the physiology of fish. Pages 1-98 *in* W. S. Hoar and D. J. Randall, editors. Fish physiology. Academic Press, New York.

Futuyma, D. J. 1998. Evolutionary biology. 3rd edition. Sinauer Associates, Sunderland, MA.

Galileo, G. 1638. Discorsi e dimostrazioni matematiche intorno à due nuove scienze attenenti alla mecanica & i movimenti locali. Elzevier, Leiden.

Glover, C. N., C. Bucking, and C. M. Wood. 2013. The skin of fish as a transport epithelium: a review. Journal of Comparative Physiology B **183**:877-891.

Graham, J. B., T. A. Baird, and W. Stöckmann. 1987. The transition to air breathing in fishes: IV. Impact of branchial specializations for air breathing on the aquatic respiratory mechanisms and ventilatory costs of the Swamp Eel *Synbranchus marmoratus*. Journal of Experimental Biology **129**:83-106.

Grant, W. E., E. K. Pedersen, and S. L. Marín. 1997. Ecology and natural resource management: systems analysis and simulation. John Wiley & Sons.

Gray, I. E. 1954. Comparative study of the gill area of marine fishes. The Biological Bulletin **107**:219-225.

Green, J., and D. Carritt. 1967. New tables for oxygen saturation in seawater. Journal of Marine Research **24**:140-147.

Grimes, B. H., M. T. Huish, J. H. Kerby, and D. Moran. 1989. Species profiles: life histories and environmental requirements of coastal fishes and invertebrates (mid-Atlantic): summer and winter flounder. Fish and Wildlife Service, U.S. Department of the Interior.

Hannon, B., and M. Ruth. 1997. Modeling dynamic biological systems. Springer-Verlag, New York.

Hanson, P. C., T. B. Johnson, D. E. Schindler, and J. F. Kitchell. 1997. Fish bioenergetics model 3. University of Wisconsin, Sea Grant Institute, Madison. WI.

Harrington, R. A., G. C. Matlock, and J. E. Weaver. 1979. Standard-total length, total length-whole weight and dressed-whole weight relationships for selected species from Texas bays. Texas Parks and Wildlife Department, Coastal Fisheries Branch, Austin, Texas.

Hartman, K. J., and J. F. Kitchell. 2008. Bioenergetics modeling: progress since the 1992 symposium. Transactions of the American Fisheries Society **137**:216-223.

Haynie, D. T. 2001. Biological thermodynamics. Cambridge University Press, Cambridge, UK.

Hill, A. V. 1910. The possible effects of the aggregation of the molecules of haemoglobin on its dissociation curves. Proceedings of the Physiological Society **40**:4-7.

Hill, A. V. 1913. The combinations of haemoglobin with oxygen and with carbon monoxide. I. Biochemical Journal **7**:471.

Hochachka, P. 1985. Exercise limitations at high altitude: the metabolic problem and search for its solution. Pages 240-249 *in* R. Gilles, editor. Circulation, respiration, and metabolism. Springer-Verlag, Berlin, Germany.

Hughes, G. M. 1963. Comparative physiology of vertebrate respiration. Harvard University Press, Cambridge, MA.

Hughes, G. M. 1972. Morphometrics of fish gills. Respiration physiology **14**:1-25.

Hughes, G. M., and M. Morgan. 1973. The structure of fish gills in relation to their respiratory function. Biological Reviews **48**:419-475.

Ishibashi, Y., T. Kotaki, Y. Yamada, and H. Ohta. 2007. Ontogenic changes in tolerance to hypoxia and energy metabolism of larval and juvenile Japanese flounder *Paralichthys olivaceus*. Journal of Experimental Marine Biology and Ecology **352**:42-49.

Iwata, N., K. Kikuchi, H. Honda, M. Kiyono, and H. Kurokura. 1994. Effects of temperature on the growth of Japanese flounder. Fisheries science **60**:527-531.

Jensen, F. B., M. Nikinmaa, and R. E. Weber. 1993. Environmental perturbations of oxygen transport in teleost fishes: causes, consequences and compensations.

Pages 161-179 *in* J. C. Rankin and F. B. Jensen, editors. Fish ecophysiology. Chapman & Hall, London.

Joaquim, N., G. N. Wagner, and A. K. Gamperl. 2004. Cardiac function and critical swimming speed of the winter flounder (*Pleuronectes americanus*) at two temperatures. Comparative Biochemistry and Physiology Part A: Molecular & Integrative Physiology **138**:277-285.

Jobling, M. 1994. Fish bioenergetics. Chapman & Hall, London, UK.

Johnson, J. T., and T. L. Hopkins. 1978. Biochemical components of the mysid shrimp *Taphromysis bowmani Bacescu*. Journal of Experimental Marine Biology and Ecology **31**:1-9.

Jones, D., D. Randall, and G. Jarman. 1970. A graphical analysis of oxygen transfer in fish. Respiration physiology **10**:285-298.

Jorgensen, C. 1983. Ecological physiology: background and perspectives. Comparative Biochemistry and Physiology, A **75**:5-7.

Kamiya, A., and K. Yamamoto. 2019. A biomechanically derived minimum work model of the fish gill lamellar system exhibits its exquisite morphological arrangement and perfusate regulation for oxygen uptake from water. Journal of biomechanics **88**:155-163.

Kerkhoff, A. 2012. Modeling metazoan growth and ontogeny.*in* R. M. Sibly, J. H. Brown, and A. Kodric-Brown, editors. Metabolic Ecology: A Scaling Approach. Wiley-Blackwell, West Sussex, UK.

Kerr, S. R. 1990. The Fry paradigm: its significance for contemporary ecology. Transactions of the American Fisheries Society **119**:779-785.

Kerstens, A., J. Lomholt, and K. Johansen. 1979. The ventilation, extraction and uptake of oxygen in undisturbed flounders, *Platichthys flesus*: responses to hypoxia acclimation. The Journal of Experimental Biology **83**:169-179.

Kirsch, R., and G. Nonnotte. 1977. Cutaneous respiration in three freshwater teleosts. Respiration physiology **29**:339-354.

Kleiber, M. 1932. Body size and metabolism. Hilgardia **6**:315-353.

Kleiber, M. 1975. Metabolic turnover rate: a physiological meaning of the metabolic rate per unit body weight. Journal of theoretical Biology **53**:199-204.

Klyszejko, B., R. Dziaman, and G. Hajek. 2003. Effects of temperature and body weight on ventilation volume of common carp [*Cyprinus carpio* L.]. Acta Ichthyologica et Piscatoria **33**.

Kooijman, S. A. L. M. 2010. Dynamic energy budget theory for metabolic organisation. 3rd edition. Cambridge University Press, Cambridge, UK.

Krogh, A. 1904. Some experiments on the cutaneous respiration of vertebrate animals. Skandinavisches Archiv für Physiologie **16**:348-357.

Krogh, A. 1941. The comparative physiology of respiratory mechanisms. University of Pennsylvania Press, Philadelphia, PA.

Kwon, Y. 2007. Handbook of essential pharmacokinetics, pharmacodynamics and drug metabolism for industrial scientists. Springer US.

Latour, R. J., M. J. Brush, and C. F. Bonzek. 2003. Toward ecosystem-based fisheries management. Fisheries **28**:10-22.

Lide, D. R. 2003. Handbook of chemistry and physics. 84th edition. CRC press, Boca Raton, FL.

Lotka, A. J. 1922. Contribution to the energetics of evolution. Proceedings of the National Academy of Sciences **8**:147-151.

Luckenbach, J. A. 2005. Breeding biotechnology, sex determination, and growth in Southern Flounder, *Paralichthys lethostigma* [Unpublished doctoral dissertation]. North Carolina State University at Raleigh, Raleigh, NC.

Luckenbach, J. A., R. Murashige, H. V. Daniels, J. Godwin, and R. J. Borski. 2007. Temperature affects insulin-like growth factor I and growth of juvenile southern flounder, *Paralichthys lethostigma*. Comparative Biochemistry and Physiology Part A: Molecular & Integrative Physiology **146**:95-104.

Luo, Y., Q. Li, X. Zhu, J. Zhou, C. Shen, D. Xia, P. K. Djiba, H. Xie, X. Lv, and J. Jia. 2020. Ventilation frequency reveals the roles of exchange surface areas in metabolic scaling. Physiological and Biochemical Zoology **93**:13-22.

MacDougall, J., and M. McCabe. 1967. Diffusion coefficient of oxygen through tissues. Nature **215**:1173.

Malloy, K. D., and T. E. Targett. 1991. Feeding, growth and survival of juvenile summer flounder *Paralichthys dentatus*: experimental analysis of the effects of temperature and salinity. MARINE ECOLOGY PROGRESS SERIES **72**:213-223.

Malte, H. 1992. Effect of pulsatile flow on gas exchange in the fish gill: Theory and experimental data. Respiration physiology **88**:51-62.

Malte, H., and R. E. Weber. 1985. A mathematical model for gas exchange in the fish gill based on non-linear blood gas equilibrium curves. Respiration physiology **62**:359-374.

Mandic, M., A. E. Todgham, and J. G. Richards. 2009. Mechanisms and evolution of hypoxia tolerance in fish. Proceedings of the Royal Society of London B: Biological Sciences **276**:735-744.

Mangourova, V., J. Ringwood, and B. Van Vliet. 2011. Graphical simulation environments for modelling and simulation of integrative physiology. computer methods and programs in biomedicine **102**:295-304.

Martine, F. 2008. Status of the Southern Flounder population in Texas. Flounder Scoping Meeting. Texas Parks & Wildlife Deptment, Coastal Fisheries Division, Marine Development Center.

Maxime, V., K. Pichavant, G. Boeuf, and G. Nonnotte. 2000. Effects of hypoxia on respiratory physiology of turbot, *Scophthalmus maximus*. Fish Physiology and Biochemistry **22**:51-59.

McCracken, F. D. 1963. Seasonal movements of the Winter Flounder, *Pseudopleuronectes americanus* (Walbaum), on the Atlantic Coast. Journal of the Fisheries Research Board of Canada **20**:551-586.

McDonald, D. L., T. H. Bonner, P. D. Cason, B. W. Bumguardner, and S. Bonnot. 2016. Effects of three cold weather event simulations on early life stages of Southern Flounder (*Paralichthys lethostigma*). Journal of Applied Aquaculture **28**:26-34.

McLellan, S. A., and T. S. Walsh. 2004. Oxygen delivery and haemoglobin. Continuing Education in Anaesthesia, Critical Care & Pain **4**:123-126.

McNab, B. K. 2002. The physiological ecology of vertebrates: a view from energetics. Cornell University Press, Ithaca, NY.

McNab, B. K. 2012. Extreme measures: the ecological energetics of birds and mammals. University of Chicago Press, Chicago, IL.

Meeh, K. v. 1879. Ober flahenmessungen des mensch-lichen kopers. Zeitschrift fur biologie **15**:S. 425-S. 458.

Menasveta, P. 1981. Lethal temperature of marine fishes of the Gulf of Thailand. Journal of Fish Biology **18**:603-607.

Mendonca, P. C., and A. K. Gamperl. 2010. The effects of acute changes in temperature and oxygen availability on cardiac performance in winter flounder (*Pseudopleuronectes americanus*). Comparative Biochemistry and Physiology Part A: Molecular & Integrative Physiology **155**:245-252.

Mendonca, P. C., A. G. Genge, E. J. Deitch, and A. K. Gamperl. 2007. Mechanisms responsible for the enhanced pumping capacity of the in situ winter flounder heart (*Pseudopleuronectes americanus*). American Journal of Physiology - Regulatory, Integrative and Comparative Physiology **293**:R2112-2119.

Meredith, A. S., P. S. Davie, and M. E. Forster. 1982. Oxygen uptake by the skin of the Canterbury mudfish, *Neochanna burrowsius*. New Zealand Journal of Zoology **9**:387-390.

Miller, D., S. Poucher, and L. Coiro. 2002. Determination of lethal dissolved oxygen levels for selected marine and estuarine fishes, crustaceans, and a bivalve. Marine Biology **140**:287-296.

Miller, D. S. 1987. Aquatic models for the study of renal transport function and pollutant toxicity. Environmental Health Perspectives **71**:59-68.

Milligan, C. L., and C. M. Wood. 1987. Regulation of blood oxygen transport and red cell pHi after exhaustive activity in rainbow trout (*Salmo gairdneri*) and starry flounder (*Platichthys stellatus*). Journal of Experimental Biology **133**:263-282.

Monod, J., J. Wyman, and J.-P. Changeux. 1965. On the nature of allosteric transitions: A plausible model. Journal of Molecular Biology **12**:88-118.

Moore, R. H. 1976. Observations on fishes killed by cold at Port Aransas, Texas, 11-12 January 1973. The Southwestern Naturalist **20**:461-466.

Munroe, T. 2015. Paralichthys lethostigma. The IUCN Red List of Threatened Species. Version 2020-2. https://dx.doi.org/10.2305/IUCN.UK.2015-4.RLTS.T202632A46958684.en. Downloaded on 19 October 2020.

Music, J. L., and J. M. Pafford. 1984. Population dynamics and life history aspects of major marine sportfishes in Georgia's coastal waters. Georgia Department of Natural Resources, Coastal Resources Division.

Nall, L. E. 1979. Age and growth of the southern flounder, *Paralichthys lethostigma*, in the northern Gulf of Mexico with notes on *Paralichthys albigutta*. Florida State University.

Neill, W. H., T. S. Brandes, B. J. Burke, S. R. Craig, L. V. Dimichele, K. Duchon, R. E. Edwards, L. P. Fontaine, D. M. Gatlin III, C. Hutchins, J. M. Miller, B. J.

Ponwith, C. J. Stahl, J. R. Tomasso, and R. R. Vega. 2004. Ecophys.Fish: a simulation model of fish growth in time-varying environmental regimes. Reviews in Fisheries Science **12**:233-288.

Neill, W. H., and J. D. Bryan. 1991. Responses of fish to temperature and oxygen, and response integration through metabolic scope. Aquaculture and water quality **3**:30-57.

Neill, W. H., R. H. Kamps, S. J. Walker, H.-i. Wu, T. S. Brandes, D. M. Gatlin III, T. L. Hopper, and R. R. Vega. 2018. Consilience: a holistic measure of goodness-of-fit. arXiv preprint arXiv:1710.08054.

Neill, W. H., J. M. Miller, H. W. Van Der Veer, and K. O. Winemiller. 1994. Ecophysiology of marine fish recruitment: a conceptual framework for understanding interannual variability. Netherlands Journal of Sea Research **32**:135-152.

Ney, J. J. 1993. Bioenergetics modeling today: growing pains on the cutting edge. Transactions of the American Fisheries Society **122**:736-748.

Nilsson, G. E. 2010. Respiratory physiology of vertebrates: life with and without oxygen. Cambridge University Press, Cambridge, UK.

NOAA. 2020. Water temperature table of the Western Gulf of Mexico. National Centers for Environmental Information. Accessed Aug 30, 2020. https://www.ncei.noaa.gov/access/data/coastal-water-temperature-guide/wgof.html.

Nonnotte, G., and R. Kirsch. 1978. Cutaneous respiration in seven sea-water teleosts. Respiration physiology **35**:111-118.

Ohlberger, J., G. Staaks, P. L. van Dijk, and F. Holker. 2005. Modelling energetic costs of fish swimming. Journal of Experimental Zoology Part A Comparative Experimental Biology **303**:657-664.

Oikawa, S., and Y. Itazawa. 1985. Gill and body surface areas of the carp in relation to body mass, with special reference to the metabolism-size relationship. Journal of Experimental Biology **117**:1-14.

Ospina-Alvarez, N., and F. Piferrer. 2008. Temperature-dependent sex determination in fish revisited: prevalence, a single sex ratio response pattern, and possible effects of climate change. PLoS One **3**:e2837.

Ostadal, B. 2014. Hypoxia and the heart of poikilotherms. Current Research: Cardiology **1**:28-32.

Park, I. S., J. W. Hur, and J. W. Choi. 2012. Hematological responses, survival, and respiratory exchange in the Olive Flounder, *Paralichthys olivaceus*, during starvation. Asian-Australasian Journal of Animal Sciences **25**:1276-1284.

Park, J., H. V. Daniels, and S. H. Cho. 2013. Nitrite toxicity and methemoglobin changes in southern flounder, *Paralichthys lethostigma*, in brackish water. Journal of the World aquaculture society **44**:726-734.

Perry, S. 1986. Carbon dioxide excretion in fishes. Canadian Journal of Zoology **64**:565-572.

Perry, S., and K. Gilmour. 2010. Oxygen uptake and transport in water breathers. Pages 49-94 *in* G. E. Nilsson, editor. Respiratory physiology of vertebrates: Life with and without oxygen. Cambridge University Press, New York.

Piiper, J. 1982. Respiratory gas exchange at lungs, gills and tissues: mechanisms and adjustments. Journal of Experimental Biology **100**:5-22.

Poupa, O. 1991. The artist. Physiological Adaptations in Vertebrates: Respiration: Circulation, and Metabolism **56**:1.

Prentice, J. A. 1989. Low-temperature tolerance of southern flounder in Texas. Transactions of the American Fisheries Society **118**:30-35.

Putter, A. 1920. Studies on the physiological similarity. VI. Similarities in growth. Pflugers Archiv für die Gesamte Physiologie des Menschen und der Tiere **180**:280.

Quinn, G. P., and M. J. Keough. 2002. Experimental design and data analysis for biologists. Cambridge University Press, Cambridge, UK.

R Core Team. 2017. R: a language and environment for statistical computing. R Foundation for Statistical Computing, Vienna, Austria.

Randall, D. 1970. Gas exchange in fish. Pages 253-292 *in* W. S. Hoar and D. J. Randall, editors. Fish physiology. Academic Press, New York,NY.

Reagan, R. E., and W. M. Wingo. 1985. Species profiles: life histories and environmental requirements of coastal fishes and invertebrates (Gulf of Mexico)-southern flounder [*Paralichtys lethostigma*]. Mississippi State Univ., Mississippi State (USA). Dept. of Wildlife and Fisheries.

Riggs, D. S. 1963. The mathematical approach to physiological problems: a critical primer. Williams & Wilkins, Baltimore, MD.

Roff, D., E. Heibo, and L. Vøllestad. 2006. The importance of growth and mortality costs in the evolution of the optimal life history. Journal of evolutionary biology **19**:1920-1930.

Roff, D. A. 1983. An allocation model of growth and reproduction in fish. Canadian Journal of Fisheries and Aquatic Sciences **40**:1395-1404.

Rombough, P., and B. Moroz. 1997. The scaling and potential importance of cutaneous and branchial surfaces in respiratory gas exchange in larval and juvenile walleye. Journal of Experimental Biology **200**:2459-2468.

Rombough, P. J. 1998. Partitioning of oxygen uptake between the gills and skin in fish larvae: a novel method for estimating cutaneous oxygen uptake. Journal of Experimental Biology **201**:1763-1769.

Root, R. 1931. The respiratory function of the blood of marine fishes. The Biological Bulletin **61**:427-456.

Santer, R., M. G. Walker, L. Emerson, and P. Witthames. 1983. On the morphology of the heart ventricle in marine teleost fish (Teleostei). Comparative Biochemistry Physiology Part A: Physiology **76**:453-457.

Satchell, G. H. 1991. Physiology and form of fish circulation. Cambridge University Press, Cambridge, UK.

Scheid, P., and J. Piiper. 1971. Theoretical analysis of respiratory gas equilibration in water passing through fish gills. Respiration physiology **13**:305-318.

Schmidt-Nielsen, K. 1984. Scaling: why is animal size so important? Cambridge University Press, Cambridge, UK.

Schmidt-Nielsen, K. 1997. Animal physiology: adaptation and environment. 5th edition. Cambridge University Press, New York, NY.

Scott, J. 1982. Depth, temperature and salinity preferences of common fishes of the Scotian Shelf. Journal of Northwest Atlantic Fishery Science **3**:29-39.

Seikai, T., T. Takeuchi, and G. S. Park. 1997. Comparison of growth, feed efficiency, and chemical composition of juvenile flounder fed live mysids and formula feed under laboratory conditions. Fisheries science **63**:520-526.

Shelton, G. 1992. Model applications in respiratory physiology. Pages 1-44 *in* S. Egginton and H. F. Ross, editors. Oxygen transport in biological systems: Modelling of pathways from environment to cell. Cambridge University Press, Cambridge, UK.

Sherwood, J., F. Stagnitti, M. Kokkinn, and W. Williams. 1991. Dissolved oxygen concentrations in hypersaline waters. Limnology and Oceanography **36**:235-250.

Sidell, B. D. 1998. Intracellular oxygen diffusion: the roles of myoglobin and lipid at cold body temperature. Journal of Experimental Biology **201**:1119-1128.

Soengas, J. L., S. Sangiao-Alvarellos, R. Laiz-Carrión, and J. M. Mancera. 2007. Energy metabolism and osmotic acclimation in teleost fish. Fish osmoregulation:277-307.

Soldatov, A. 2003. Effects of temperature, pH, and organic phosphates on fish hemoglobins. Journal of Evolutionary Biochemistry and Physiology **39**:159-168.

Springer, T. A., and W. H. Neill. 1988. Automated determination of critical oxygen concentration for routinely active fish. Environmental Biology of Fishes **23**:233-240.

Steffensen, J., and J. Lomholt. 1985. Cutaneous oxygen uptake and its relation to skin blood perfusion and ambient salinity in the plaice, *Pleuronectes platessa*. Comparative Biochemistry and Physiology--Part A: Physiology **81**:373-375.

Steffensen, J. F., J. P. Lomholt, and K. Johansen. 1981. The relative importance of skin oxygen uptake in the naturally buried plaice, *Pleuronectes platessa*, exposed to graded hypoxia. Respiration physiology **44**:269-275.

Steffensen, J. F., J. P. Lomholt, and K. Johansen. 1982. Gill ventilation and O2 extraction during graded hypoxia in two ecologically distinct species of flatfish, the flounder (*Platichthys flesus*) and the plaice (*Pleuronectes platessa*). Environmental Biology of Fishes **7**:157-163.

Stevens, M., J. Maes, and F. Ollevier. 2006. A bioenergetics model for juvenile flounder *Platichthys flesus*. Journal of applied ichthyology **22**:79-84.

Stierhoff, K. L., T. E. Targett, and K. Miller. 2006. Ecophysiological responses of juvenile summer and winter flounder to hypoxia: experimental and modeling analyses of effects on estuarine nursery quality. MARINE ECOLOGY PROGRESS SERIES **325**:255-266.

Stryer, L. 1981. Biochemistry. 2d edition. W. H. Freeman, San Francisco, CA.

Stunz, G. W., T. L. Linton, and R. L. Colura. 2000. Age and growth of southern flounder in Texas waters, with emphasis on Matagorda Bay. Transactions of the American Fisheries Society **129**:119-125.

Subczynski, W. K., L. E. Hopwood, and J. S. Hyde. 1992. Is the mammalian cell plasma membrane a barrier to oxygen transport? The Journal of general physiology **100**:69-87.

Subczynski, W. K., J. S. Hyde, and A. Kusumi. 1989. Oxygen permeability of phosphatidylcholine--cholesterol membranes. Proceedings of the National Academy of Sciences **86**:4474-4478.

Subczynski, W. K., and A. Wisniewska. 2000. Physical properties of lipid bilayer membranes: relevance to membrane biological functions. ACTA Biochimica Polonica-English Edition **47**:613-626.

Tallqvist, M., E. Sandberg-Kilpi, and E. Bonsdorff. 1999. Juvenile flounder, *Platichthys flesus* (L.), under hypoxia: effects on tolerance, ventilation rate and predation efficiency. Journal of Experimental Marine Biology and Ecology **242**:75-93.

Tansey, M. R., and T. D. Brock. 1972. The upper temperature limit for eukaryotic organisms. Proceedings of the National Academy of Sciences **69**:2426-2428.

Taylor, J. C., and J. M. Miller. 2001. Physiological performance of juvenile southern flounder, *Paralichthys lethostigma* (Jordan and Gilbert, 1884), in chronic and episodic hypoxia. Journal of Experimental Marine Biology and Ecology **258**:195-214.

Taylor, W., A. Houston, and J. Horgan. 1968. Development of a computer model simulating some aspects of the cardiovascular-respiratory dynamics of the salmonid fish. Journal of Experimental Biology **49**:477-493.

Thompson, D. A. W. 1942. On growth and form. Dover Publications, Mineola, NY.

Tipsmark, C. K., J. A. Luckenbach, S. S. Madsen, P. Kiilerich, and R. J. Borski. 2008. Osmoregulation and expression of ion transport proteins and putative claudins in the gill of southern flounder (*Paralichthys lethostigma*). Comparative Biochemistry and Physiology Part A: Molecular & Integrative Physiology **150**:265-273.

Tous, P., A. Sidibe, E. Mbye, L. de Morais, Y. H. Camara, T. A. Adeofe, T. Monroe, K. Camara, K. Cissoko, R. Djiman, A. Sagna, and M. Sylla. 2015. Solea solea. The IUCN Red List of Threatened Species 2015: e.T198739A15595369. http://dx.doi.org/10.2305/IUCN.UK.2015-4.RLTS.T198739A15595369.en.

Tseng, Y.-C., and P.-P. Hwang. 2008. Some insights into energy metabolism for osmoregulation in fish. Comparative Biochemistry and Physiology Part C: Toxicology & Pharmacology **148**:419-429.

Van den Berg, H. 2011. Mathematical models of biological systems. Oxford University Press, Oxford, UK.

van der Veer, H. W., S. A. Kooijman, and J. van der Meer. 2001. Intra-and interspecies comparison of energy flow in North Atlantic flatfish species by means of dynamic energy budgets. Journal of Sea Research **45**:303-320.

van Maaren, C. C., J. Kita, and H. V. Daniels. 2000. Temperature tolerance and oxygen consumption rates for juvenile Southern Flounder *Paralichthys lethostigma* acclimated for five different temperature. UJNR Technical Report **28**:135-140.

Van Rooij, J., and J. Videler. 1996. Estimating oxygen uptake rate from ventilation frequency in the reef fish *Sparisoma viride*. MARINE ECOLOGY PROGRESS SERIES **132**:31-41.

VanderKooy, S. J. 2015. Management Profile for the Gulf and Southern Flounder Fishery in the Gulf of Mexico. Pub No. 247, Gulf States Marine Fisheries Commission.

von Bertalanffy, L. 1934. Untersuchungen über die Gesetzlichkeit des Wachstums. Development Genes and Evolution **131**:613-652.

von Bertalanffy, L. 1938. A quantitative theory of organic growth (inquiries on growth laws. II). Human biology **10**:181-213.

von Bertalanffy, L. 1950. The theory of open systems in physics and biology. Science **111**:23-29.

von Bertalanffy, L. 1957. Quantitative laws in metabolism and growth. The quarterly review of biology **32**:217-231.

Vornanen, M., J. A. Stecyk, and G. E. Nilsson. 2009. The anoxia-tolerant crucian carp (*Carassius carassius* L.). Fish physiology **27**:397-441.

Walker, S. J. 2009. Ecophysiology of growth in the Pacific white shrimp (*Litopenaeus vannamei*) [Unpublished doctoral dissertation]. Texas A&M University.

Walker, S. J., W. H. Neill, A. L. Lawrence, and D. M. Gatlin III. 2011. Effects of temperature and starvation on ecophysiological performance of the Pacific white shrimp (*Litopenaeus vannamei*). Aquaculture **319**:439-445.

Watters, K., and L. Smith. 1973. Respiratory dynamics of the Starry Flounder Platichthys stellatus in response to low oxygen and high temperature. Marine Biology **19**:133-148.

Weber, R. E. 2000. Adaptations for oxygen transport: lessons from fish hemoglobins. Pages 23-37 *in* G. Di Prisco, B. Giardina, and R. E. Weber, editors. Hemoglobin function in vertebrates. Springer.

Weber, R. E., and J. A. de Wilde. 1975. Oxygenation properties of haemoglobins from the flatfish plaice (*Pleuronectes platessa*) and flounder (*Platichthys flesus*). Journal of Comparative Physiology B: Biochemical, Systemic, and Environmental Physiology **101**:99-110.

Weber, R. E., and J. A. de Wilde. 1976. Multiple haemoglobins in plaice and flounder and their functional properties. Comparative Biochemistry and Physiology Part B: Comparative Biochemistry **54**:433-437.

Weibel, E. R. 1984. The pathway for oxygen: structure and function in the mammalian respiratory system. Harvard University Press, Cambridge, MA.

Weiss, J. N. 1997. The Hill equation revisited: uses and misuses. The FASEB Journal **11**:835-841.

Welch, B. 1985. The biosphere. Pages 63-71 *in* R. DeHart, editor. Fundamentals of aerospace medicine. Lea & Febiger, Philadelphia, PA.

Wenner, C., and J. Archambault. 2005. Southern Flounder: natural history and fishing techniques in South Carolina. Marine Resources Research Institute, South Carolina Department of Natural Resources.

Wenner, C., W. Roumillat, J. Moran Jr, M. Maddox, L. Daniel III, and J. Smith. 1990. Investigations on the life history and population dynamics of marine recreational fishes in South Carolina: part 1. Report to Fish Restoration Act under Project F-37. South Carolina Department of Natural Resources, Marine Resources Division, Charleston, South Carolina.

West, G. B., and J. H. Brown. 2005. The origin of allometric scaling laws in biology from genomes to ecosystems: towards a quantitative unifying theory of biological structure and organization. Journal of Experimental Biology **208**:1575-1592.

West, G. B., J. H. Brown, and B. J. Enquist. 2000. The origin of universal scaling laws in biology. Pages 87-112 *in* J. H. Brown and G. B. West, editors. Scaling in biology. Oxford University Press, New York, NY.

Willmer, P., G. Stone, and I. Johnston. 2005. Environmental physiology of animals. 2nd edition. Blackwell Publishing, Malden, MA.

Winberg, G. 1960. Rate of metabolism and food requirement of fishes. Fisheries Research Board of Canada, Translation Series 194.

Windrem, D. A., and W. Z. Plachy. 1980. The diffusion-solubility of oxygen in lipid bilayers. Biochimica et Biophysica Acta (BBA)-Biomembranes **600**:655-665.

Wood, C. M., B. McMahon, and D. McDonald. 1979a. Respiratory gas exchange in the resting Starry Flounder, *Platichthys stellatus*: a comparison with other teleosts. Journal of Experimental Biology **78**:167-179.

Wood, C. M., B. McMahon, and D. McDonald. 1979b. Respiratory, ventilatory, and cardiovascular responses to experimental anaemia in the Starry Flounder, *Platichthys stellatus*. Journal of Experimental Biology **82**:139-162.

Wood, C. M., B. R. McMahon, and D. G. McDonald. 1977. An analysis of changes in blood pH following exhausting activity in the Starry Flounder, *Platichthys stellatus*. The Journal of Experimental Biology **69**:173-185.

Wood, S., K. Johansen, and R. Weber. 1975. Effects of ambient PO2 on hemoglobin-oxygen affinity and red cell ATP concentrations in a benthic fish, Pleuronectes platessa. Respiration physiology **25**:259.

Yamamoto, K.-I. 1991. Relationship of respiration to body weight in the carp *Cyprinus carpio* under resting and normoxic condition. Comparative Biochemistry and Physiology Part A: Physiology **100**:113-116.

Yamamoto, K.-I. 1992. Relationship of respiration to body weight in the tilapia *Oreochromis niloticus* under resting and normoxic conditions. Comparative Biochemistry and Physiology Part A: Physiology **103**:81-83.

Yamashita, Y., Y. Kurita, H. Yamada, J. M. Miller, and T. Tomiyama. 2017. A simulation model for estimating optimum stocking density of cultured juvenile flounder *Paralichthys olivaceus* in relation to prey productivity. Fisheries Research **186**:572-578.

Yamashita, Y., M. Tanaka, and J. M. Miller. 2001. Ecophysiology of juvenile flatfish in nursery grounds. Journal of Sea Research **45**:205-218.

Yazdani, G., and R. M. Alexander. 1967. Respiratory currents of flatfish. Nature **213**:96.

Zhu, J., X. Zhang, and T. Gao. 2005. Histological study on the skin of Japanese Flounder *Paralichthys olivaceus*. Journal of Ocean University of China **4**:145-151.

APPENDIX A

TEMPERATURE AND OXYGEN LIMITS FOR PLUERONECTIFORMES

Table A - 1. Temperature and Oxygen Limits for Plueronectiformes

Source Authors	Species	Common Name	Notes	Ta acclimated (°C)	Ta optimal (°C)	Ta Upper (°C)	Ta Lower (°C)	DO Limit (mg O2/L water)
McCracken (1963)	*Pseudopleuronectes americanus*	Winter Flounder				26		
Malloy and Targett (1991)	*Paralichthys dentatus*	Summer Flounder	Juvenile				3	
Stierhoff et al. (2006)	*Paralichthys dentatus*	Summer Flounder	LC_{50}	25	22	30		1.1
	Paralichthys dentatus	Summer Flounder	LC_{50}	25	22	30		1.6
	Pseudopleuronectes americanus	Winter Flounder	LC_{50}	25	18	27		1.4
Miller et al. (2002)	*Paralichthys dentatus*	Summer Flounder	Juvenile					
	Pseudopleuronectes americanus	Winter Flounder	Juvenile, LC_{50}	20				1.4
	Pseudopleuronectes americanus	Winter Flounder	Juvenile, LC_{90}	20				1.1
	Scophthalmus aquosus	Windowpane Flounder	Juvenile, LC_{50}	24				1.6
	Scophthalmus aquosus	Windowpane Flounder	Juvenile, LC_{90}	24				1.8
	Scophthalmus aquosus	Windowpane Flounder	Juvenile, LC_{50}	20				1.1
	Scophthalmus aquosus	Windowpane Flounder	Juvenile, LC_{90}	20				1.3

Table A – 1 Continued

Menasveta (1981)	*Pseudorhombus elevatus*	Deep Flounder	Mean critical thermal max	27.3		37.2		
	Solea ovata	Ovate Sole	Mean critical thermal max	27.3		37.9		
van Maaren et al. (2000)	*Paralichthys lethostigma*	Southern Flounder	Juvenile, mean lethal temp.	13		32.88		
	Paralichthys lethostigma	Southern Flounder	Juvenile, mean lethal temp.	13		33.14		
	Paralichthys lethostigma	Southern Flounder	Juvenile, mean lethal temp.	13		34.08		
	Paralichthys lethostigma	Southern Flounder	Juvenile, mean lethal temp.	17		34.98		
	Paralichthys lethostigma	Southern Flounder	Juvenile, mean lethal temp.	17		35.84		
	Paralichthys lethostigma	Southern Flounder	Juvenile, mean lethal temp.	17		36.1		
	Paralichthys lethostigma	Southern Flounder	Juvenile, mean lethal temp.	21		36.8		
	Paralichthys lethostigma	Southern Flounder	Juvenile, mean lethal temp.	21		37.16		
	Paralichthys lethostigma	Southern Flounder	Juvenile, mean lethal temp.	21		37.22		
	Paralichthys lethostigma	Southern Flounder	Juvenile, mean lethal temp.	25		37.98		
	Paralichthys lethostigma	Southern Flounder	Juvenile, mean lethal temp.	25		38.12		
	Paralichthys lethostigma	Southern Flounder	Juvenile, mean lethal temp.	25		38.18		
	Paralichthys lethostigma	Southern Flounder	Juvenile, mean lethal temp.	29		38.7		

Table A – 1 Continued

van Maaren et al. (2000)	*Paralichthys lethostigma*	Southern Flounder	Juvenile, mean lethal temp.	29		38.94		
	Paralichthys lethostigma	Southern Flounder	Juvenile, mean lethal temp.	29		38.96		
Prentice (1989)	*Paralichthys lethostigma*	Southern Flounder	Juvenile	20			9.3	
	Paralichthys lethostigma	Southern Flounder	Juvenile	20			4.1	
	Paralichthys lethostigma	Southern Flounder	Adult	20			8.7	
	Paralichthys lethostigma	Southern Flounder	Adult	20			6.6	
Tallqvist et al. (1999)	*Platichthys flesus*	European Flounder	Juvenile, LC_{50} at 2000 min (33 h)					2
	Platichthys flesus	European Flounder	Juvenile, LC_{50} at 250 min (4.2 h)					1
	Platichthys flesus	European Flounder	Juvenile, LC_{50} at ~100 min (1.7 h)					0.6

Table A – 1 Continued

Deubler and Posner (1963)	*Paralichthys lethostigma*	Southern Flounder	Post larval, 100% self-withdrawal from hypoxic water after 23 min	6.1				1.09
	Paralichthys lethostigma	Southern Flounder	Post larval, 100% self-withdrawal (kinesis) from hypoxic water after 13 min	14.4				0.68
	Paralichthys lethostigma	Southern Flounder	Post larval, 100% self-withdrawal (kinesis) from hypoxic water after 7 min	25.3				1.03
Daniels et al. (1996)	*Paralichthys lethostigma*	Southern Flounder	Larvae, salinity survival sig. decline < 20 ppt					

Table A – 1 Continued

Grimes et al. (1989)	*Pseudopleuronectes americanus*	Winter Flounder	Larvae, 100% mortality in 4 minutes	5	18.5	30		
	Pseudopleuronectes americanus	Winter Flounder	10 cm, incipient lethal temp.	22		29		
	Pseudopleuronectes americanus	Winter Flounder	10 cm, incipient lethal temp.	4		19		
	Pseudopleuronectes americanus	Winter Flounder	10 cm, incipient lethal temp.	20		26.5		
	Pseudopleuronectes americanus	Winter Flounder	10 cm, incipient lethal temp.	28			5.4	
	Pseudopleuronectes americanus	Winter Flounder	10 cm, incipient lethal temp.	21			1	

APPENDIX B

RESPIRATORY MODEL, DYNAMIC PROCESSES

Blood O2 Capacity

```
CaO2 = Max_Hb__O2_Sat+CplaO2
CplaO2 = DOa*0.0007
CvO2 = (Hb_g_per_ml*Hbs*SvO2)
Hbs = 1.12
Hb_g_per_ml = 0.15
Max_Hb__O2_Sat = Hb_g_per_ml*Hbs*Y
```

Cardiac Output

```
HR = HR_PO2_f*HR_Ta
HR_PO2_f = MIN(1, (0.0054 * PO2 + 0.68))
HR_Ta = MAX(0, ((-0.2*Ta^2+9*Ta-31) * 60))
Q = HR*SV
SV = (Vvol*Wfish/1000)*SV_Ta_f*SV_PO2_f
SV_PO2_f = MAX(1, (1+(0.4-0.4*(PO2/60))))
SV_Ta_f = MIN((EXP(0.0135*Ta)),1.4)
Vvol = (0.506*(Wfish/1000)^1.026)/(Wfish/1000)
```

Environmental Oxygen

```
DOa = (EXP((-7.424+(4417/(Ta+273.16))+(-
2.927*LOGN(Ta+273.16))+(0.04238*(Ta+273.16)))-((Sal-0.03)/1.805)*((-
0.1288+(53.44/(273.16+Ta))+(-
0.0444*LOGN(273.16+Ta))+(0.00071*(273.16+Ta)))))/22.414*32/760*PO2)
FO2 = 0.209
PO2 = 760*FO2
```

Environmental Parameters

```
Sal = 5
Ta = 30
```

Gill Ventilation

```
Ext_Eff = (PO2-PvO2)/PO2
```

fR = (((-0.08*Ta^2+6*Ta)*fR_con)* 160/PO2) * MIN(1, PO2/30) * MIN(1, PO2/20)
fR_con = 25
Topt = 25
VsR = MAX(0.008 *Ta/Topt, MIN(0.008*20/PO2,0.014))
Vw = fR*VsR

Hb Saturation

n = (-0.264*pH_blood+3.7)
P50 = MAX(0.1, -16.786*pH_blood+140)
pH_blood = IF pH_Switch = 1 THEN (T_Slope*Ta+pH_Ta_zero) ELSE pH_Set
pH_Set = 7.8
pH_Switch = 1
pH_Ta_zero = 8
T_Slope = -0.019
Y = PO2^n/(P50^n+PO2^n)

Oxygen Supply

cal_g = mg_O2_g*oxycal
cal_kg = mg_O2_kg*oxycal
mg_O2_g = ml_O2_g*1.4286
mg_O2_kg = mg_O2_g*1000
ml_O2_g = VO2/Wfish
ml_O2_kg = ml_O2_g*1000
oxycal = 3.4
Percent_Skin = IF Q = 0 THEN 0 ELSE ((Skin_mg_O2/mg_O2_g)*100)
Skin_mg_O2 = (VO2_Skin/Wfish)*1.4286

PvO2 Derivation

PvO2 = ((SvO2*P50^n)/(1-SvO2))^(1/n)
SvO2 = Y * (n/(4-n))

VO2 Derivation

VO2_gill = Krogh*(Gill_SA/dX)*(PO2-PvO2)
VO2_Q = Q*(CaO2/PO2)*(PO2-PvO2)
VO2_Skin = ((Krogh*((Skin_SA/2)/upper_Skin_dX)*(PO2-PvO2)) +
(Krogh*((Skin_SA/2)/lower_Skin_dX)*(PO2-PvO2)))*Skin_eff_f
VO2 = VO2_Q+VO2_Skin
VO2_w = (Vw*Wfish)*(BwO2/1000)*(PO2-PvO2)
VO2_gill = Krogh*(Gill_SA/dX)*(PO2-PvO2)
BwO2 = (DOa*0.7)/PO2

dX = 0.0005
Gill_SA = 2.42 *Wfish
Krogh = O2_Diff*(BwO2/1000)
lower_Skin_dX = (0.04886*Wfish+45)/10000
O2_Diff = (0.0064*EXP(0.04*Ta))
Skin_eff_f = IF Q = 0 THEN 0 ELSE 1
Skin_SA = 10*Wfish^0.7
upper_Skin_dX = (0.0198*Wfish+36)/10000

Weight

Wfish = 1